

UNIVERSITY OF GLASGOW

CHEMISTRY DEPARTMENT

RADICAL AND PHOTOCHEMICAL REACTIONS  
OF THE NITROSITES  
OF HUMULENE AND CARYOPHYLLENE

being

A thesis submitted in part fulfilment of the  
requirements for the

DEGREE OF DOCTOR OF PHILOSOPHY

by

DEREK KENNETH MACALPINE

November 1977

ProQuest Number: 13804139

All rights reserved

INFORMATION TO ALL USERS

The quality of this reproduction is dependent upon the quality of the copy submitted.

In the unlikely event that the author did not send a complete manuscript and there are missing pages, these will be noted. Also, if material had to be removed, a note will indicate the deletion.



ProQuest 13804139

Published by ProQuest LLC (2018). Copyright of the Dissertation is held by the Author.

All rights reserved.

This work is protected against unauthorized copying under Title 17, United States Code  
Microform Edition © ProQuest LLC.

ProQuest LLC.  
789 East Eisenhower Parkway  
P.O. Box 1346  
Ann Arbor, MI 48106 – 1346

## ACKNOWLEDGEMENTS

I would like to express my sincere thanks to Dr. A.L. Porte for the guidance, constructive criticism, and encouragement provided during the course of this work.

I thank Professor G.A. Sim in whose laboratories this work was carried out.

I would also like to thank Dr. S.T.R.S. Mitchell for the gift of a sample of humulene nitrosite, and Mr. D.S.J. Gardner and Mr. J.M. Fincher, of White Stevenson Limited, North Albert Road, Reigate, Surrey, for a gift of 500 gm of the higher boiling fractions of hop oil, from which humulene was extracted.

My thanks are also extended to the many people in the Chemistry Department of the University of Glasgow, whom it would be impossible to mention by name here, whose assistance and advice were of value to me in the course of this work.

I should also like to record my gratitude to my mother-in-law, Mrs. Janette Kempton for the typing of this thesis.

Finally I would like to acknowledge with gratitude the award of a Carnegie Research Scholarship, during the tenure of which this work was carried out.

Derek K. MacAlpine.

## SUMMARY

The Thesis is concerned with the following two main topics;

- 1) First the reactions of chloroform solutions of humulene (14) and humulene nitrosite (17) with the oxides of nitrogen were investigated.
- 2) In conjunction with the first topic a study was made of the products obtained when,
  - a) crystalline samples of humulene nitrosite (17) and,
  - b) solutions of humulene nitrosite in the aprotic solvents chloroform, toluene, and benzene, and
  - c) solid solutions of humulene nitrosite in dinitro-humulene (24) are irradiated with red light.

The mechanistic flow charts contained in S.1 and S.2 explain the formation of the products observed during these studies. The products obtained were characterised in the manner described below.

- 1) All derivatives marked with a single asterisk were isolated using chromatographic techniques, obtained where possible in a pure crystalline state, and characterised using a combination of elemental analysis, and  $^1\text{H}$  n.m.r.,  $^{13}\text{C}$  n.m.r., infra-red and mass spectroscopy.
- 2) Derivatives marked with a double asterisk, were isolated as mixtures of similar isomeric compounds which could not be separated by chromatographic or other means. The structures postulated are consistent with the available spectroscopic data.
- 3) Those nitroxide radicals which were not isolated and character-



ised, were detected using e.p.r. spectroscopy, and the spin Hamiltonian parameters were obtained. The photochemical reactions shown in figure S.2, were also monitored in an infra-red spectrometer, and the changes observed in the spectra, were shown to be consistent with the structures postulated for the nitroxide radicals.

- 4) The remaining species shown in figures S.1 and S.2 are transient intermediates, which were not detected, but previous workers investigating the chemistry of C-nitroso compounds, and of humulene derivatives, have postulated intermediates of similar structure.

Topic one: The reactions of humulene and humulene nitrosite with the oxides of nitrogen

Three main products are obtained from the reaction of humulene with the oxides of nitrogen, humulene nitrosite (17), dinitro-humulene (24), and nitro-nitrato-humulene (26), each forming by the addition of the relevant oxides of nitrogen, over the double bond of humulene indicated in figure S.1.

When humulene nitrosite is reacted with  $N_2O_3$ , the initial stages of the reaction involve the addition of two molecules of nitric oxide to the nitroso group of humulene nitrosite, forming the diazonium nitrate complex (37), as shown in figure S.1. This complex subsequently decomposes with the evolution of nitrogen, forming an aliphatic radical (18). By studying the reaction products, this aliphatic radical (18), is deduced to stabilise in the following four ways.

- 1) The first option is for the radical (18), to add  $\dot{NO}_2$  forming dinitro-humulene (24).

- 2) Second, an  $\dot{\text{O}}\text{NO}_2$  radical can abstract a proton, forming the isomeric species (41), (42), and (43).
- 3) Third, the radical can react with humulene nitrosite, forming nitroxide radical (19).
- 4) In its final mode of behaviour, (18) undergoes a transannular cyclisation, as shown in figure S.1 forming the tricyclic species (50), (52), and (53) and (48), which contain a cyclopropyl ring. These species have not been detected. However, species (44), (45), (46), and (40), which form by the further reaction of the cyclopropyl based intermediates with the oxides of nitrogen, have been isolated and characterised.

Three nitroxide radicals are detected when humulene nitrosite is reacted with  $\text{N}_2\text{O}_3$ . These radicals are postulated to form as shown in figure S.1. It has been demonstrated, that nitroxide radicals are not formed by the direct attack of  $\dot{\text{NO}}_2$  at the  $\pi$  system of humulene nitrosite, as shown in figure 5.1, but instead  $\dot{\text{NO}}_2$  can replace the nitroso group of humulene nitrosite forming the cis and trans isomers of dinitro-humulene (24), with a subsequent addition of  $\dot{\text{NO}}_2$  over the remaining double bonds, forming (38) and (39).

Topic two: The photolysis reactions of humulene nitrosite when irradiated with red light

Humulene nitrosite exists in two crystalline forms, which consist of needles or platelets, and both forms produce the same paramagnetic species when irradiated with red light. In all, six different nitroxide radicals have been generated photochemically from humulene nitrosite. Four nitroxide radicals (19a), (19b), (20), and (21) are obtained when crystalline humulene nitrosite, or solutions of the nitrosite in the aprotic solvents chloroform, toluene,

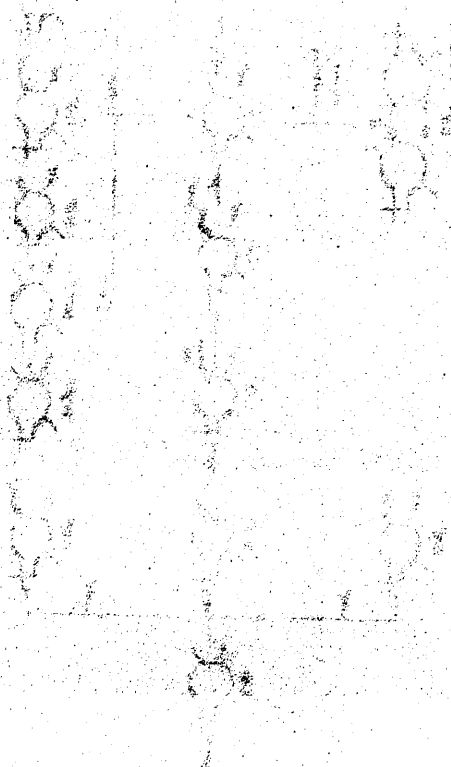
and benzene are irradiated with red light. A fifth nitroxide radical (29) is generated by irradiating solid solutions of humulene nitrosite (17) in dinitro-humulene (24) with red light. The two mechanisms described below are involved in the formation of these radicals.

- 1) In the first mechanism the nitroso group absorbs a quantum of red light inducing an  $n \rightarrow \pi^*$  transition, which results in the cleavage of the C-N bond, forming the aliphatic radical (18) and  $\dot{\text{NO}}$ . This aliphatic radical (18) reacts with humulene nitrosite forming nitroxide radicals (19a) and (19b).
- 2) The second mechanism involves the displacement of  $\dot{\text{NO}}$  and  $\dot{\text{NO}}_2$  from molecules of humulene nitrosite or dinitro-humulene (24), by the red excited nitroso group of a neighbouring molecule of humulene nitrosite, forming nitroxide radicals (19a), (19b), (20), (21), and (29).

The nitroxide radical (21), when irradiated with white light can rearrange to a further nitroxide radical (33), shown in figure S.2. The initial photochemical step for this reaction is believed to involve an  $n \rightarrow \pi^*$  transition in the nitroxide group.

The diamagnetic species observed when humulene nitrosite is irradiated with red light, form by the interaction of the nitrosite with the  $\dot{\text{NO}}$  and  $\dot{\text{NO}}_2$  liberated in forming the nitroxide radicals. The mechanism involved is virtually identical to that described previously for the reaction of humulene nitrosite, dissolved in an aprotic solvent, with the oxides of nitrogen. Products (54-59), and (61-66) formed by a process of transannular cyclisation, are observed only when the platelet crystals of humulene nitrosite are irradiated. The conformation of the nitrosite molecules in the needle crystals appears to be unsuitable for such cyclisations.

The photochemistry of caryophyllene nitrosite has in part been studied by previous workers. In this present investigation the photochemistry of caryophyllene nitrosite, was shown to proceed via mechanisms analogous to those described for humulene nitrosite.







## TABLE OF CONTENTS

### CHAPTER 1

#### INTRODUCTION

		<u>PAGE</u>
1.1	Free radicals	... 1
1.2	The generation of nitroxide radicals from C-nitroso compounds	... 2
1.3	The photochemistry of caryophyllene nitrosite (2)	... 4
1.4	The radical and photochemical reactions of humulene nitrosite	... 11

### CHAPTER 2

#### INITIAL STUDIES OF THE PRODUCTS OBTAINED FROM THE PHOTOLYSIS REACTIONS OF HUMULENE NITROSITE IRRADIATED WITH RED LIGHT

2.1	Determination of the structure of humulene nitrosite	... 15
2.2	Radicals obtained when humulene nitrosite (19), and solutions of humulene nitrosite are irradiated with red light	... 23
2.2.1	The irradiation of a crystalline sample of humulene nitrosite with red light	... 23
2.2.2	Radicals obtained when solutions of humulene nitrosite in chloroform, toluene and benzene are irradiated with red light	... 27
2.2.3	Monitoring the irradiation of crystalline humulene nitrosite with red light, as a function of time, in an e.p.r. spectrometer	... 32

2.3	Initial attempts at using chromatographic techniques to isolate the products formed on irradiating humulene nitrosite with red light	...	40
2.3.1	Detection of the impurities present in humulene nitrosite and its subsequent purification	...	41
2.3.2	Isolation of the products formed when chromatographically purified humulene nitrosite is irradiated with red light	...	41

## APPENDIX 2

2'.1'	Determination of the structure of humulene nitrosite	...	56
2'.2'	Initial attempts at using chromatographic techniques to isolate the products formed when humulene nitrosite is irradiated with red light	...	67
2'.2'.1'	The preparation of a sample of pure humulene nitrosite	...	67
2'.2'.2'	Isolation of the products formed when chromatographically purified humulene nitrosite is irradiated with red light	...	68

## CHAPTER 3

### REACTIONS OF HUMULENE AND CARYOPHYLLENE WITH THE OXIDES OF NITROGEN

3.1	The extraction of a sample of pure humulene from technical grade caryophyllene	...	83
-----	--	-----	----



		<u>PAGE</u>
3.2	The reactions of humulene with the oxides of nitrogen	... 85
3.3	The reactions of caryophyllene with the oxides of nitrogen	... 96

### APPENDIX 3

3'.1'	The extraction of a pure sample of humulene from technical grade caryophyllene	... 102
3'.2'	The preparation of a pure sample of humulene nitrosite	... 107
3'.3'	The preparation of a pure sample of caryophyllene nitrosite	... 115

### CHAPTER 4

#### AN EXAMINATION OF THE MECHANISMS GOVERNING THE PRODUCTION OF THE PARAMAGNETIC SPECIES OBSERVED WHEN HUMULENE NITROSITE IS IRRADIATED WITH RED LIGHT

4.1	Monitoring by means of infra-red spectro- scopy, the irradiation of humulene nitrosite with red light	... 124
4.2	The irradiation, with red light, of a solid solution of caryophyllene nitrosite (2) in dinitro-caryophyllene (27)	... 126
4.2.1	Monitoring by means of e.p.r. spectroscopy the irradiation, with red light, of a solid solution of caryophyllene nitrosite (2) in dinitro-caryophyllene (27)	... 127

4.2.2	Monitoring by means of infra-red spectroscopy the irradiation with red light, of a solid solution of caryophyllene nitrosite (2) in dinitro-caryophyllene (27)	... 131
4.3	The irradiation, with red light, of a solid solution of humulene nitrosite (17) in dinitro-humulene (24)	... 132
4.3.1	Monitoring by means of e.p.r. spectroscopy the irradiation with red light of a solid solution of humulene nitrosite (17) in dinitro-humulene (24)	... 132
4.3.2	Monitoring by means of infra-red spectroscopy, the irradiation with red light, of a solid solution of humulene nitrosite (17) in dinitro-humulene (24)	... 137
4.4	The irradiation, with red light, of dilute solutions of humulene nitrosite or caryophyllene nitrosite, in chloroform, or toluene, at 77°K	... 138
4.5	The irradiation, with white light of solutions of nitroxide radicals $I_A$ , and $I_B$ , (19) and II (21) in chloroform	... 143

#### APPENDIX 4

4'.1'	Monitoring by means of infra-red spectroscopy the irradiation of humulene nitrosite with red light	... 150
-------	--	---------

4'.2'	Following by means of infra-red spectroscopy the irradiation with red light, of a solid solution of caryophyllene nitrosite (2) in dinitro-caryophyllene (27)	... 154
4'.3'	Following by means of infra-red spectroscopy the irradiation with red light, of a solid solution of humulene nitrosite (17) in dinitro- humulene (24) (30:70)	... 157
4'.4'	The irradiation, with red light of a dilute solution of humulene nitrosite in chloroform, or toluene, at 77°K	... 160
4'.5'	The irradiation, with red light, of a dilute solution of caryophyllene nitrosite in chloro- form, or toluene, at 77°K	... 161

## CHAPTER 5

### THE REACTIONS OF HUMULENE NITROSITE WITH THE OXIDES OF NITROGEN

5.1	Investigation of the paramagnetic species formed during the reaction of humulene nitrosite with $N_2O_3$	... 163
5.2	The reaction of humulene nitrosite with nitrogen dioxide	... 169
5.3	Investigation of the diamagnetic species formed during the reaction of humulene nitrosite with $N_2O_3$	... 170
5.4	The mechanism by which humulene nitrosite reacts with $N_2O_3$	... 178

5.5	The paramagnetic species formed during the reaction of caryophyllene nitrosite with $N_2O_3$	... 180
-----	--	---------

#### APPENDIX 5

5'.1'	The reaction of humulene nitrosite with nitrogen dioxide	... 183
5'.2'	Spectroscopic data obtained from the compounds (41), (40) and (44-46)	... 200

#### CHAPTER 6

#### AN EXAMINATION OF THE MECHANISMS GOVERNING THE PRODUCTION OF THE DIAMAGNETIC SPECIES OBSERVED WHEN HUMULENE NITROSITE IS IRRADIATED WITH RED LIGHT

6.1	Characterisation of the diamagnetic species formed on irradiating humulene nitrosite with red light	... 214
6.1.1	The diamagnetic species observed on irradiating needle shaped crystals of humulene nitrosite with red light	... 214
6.1.2	The mechanism involved in the production of the diamagnetic species observed when needle like crystals of humulene nitrosite are irradiated with red light	... 217
6.1.3	The diamagnetic species observed on irradiating platelets of humulene nitrosite with red light..	219

## APPENDIX 6

### PAGE

6'.1'	Interpretation of the spectroscopic data for the components of $R_{f.} = 0.8$ , obtained by irradiating the needle like crystals of humulene nitrosite with red light	... 227
6'.2'	Interpretation of the spectroscopic data for the fractions of $R_{f.} = 0.15, 0.2$ , and 0.3, obtained by irradiating the platelets of humulene nitrosite with red light	... 231

## APPENDIX 7

7'.1'	Introduction	... 236
7'.2'	The Zeeman interaction	... 237
7'.3'	The spin Hamiltonian	... 239
7'.4'	The hyperfine interaction	... 242
7'.5'	The quadrupolar interaction	... 244
7'.6'	Solution of the spin Hamiltonian	... 245
7'.7'	Spin relaxation and line shapes	... 249
7'.8'	Sources of line broadening	... 252
7'.9'	Line shapes of electron paramagnetic resonance spectra of dilute glasses or polycrystalline samples	... 253

FiguresChapter 1PAGE

1.1	.....	5
1.2	.....	7
1.3	.....	9
1.4	.....	10

Chapter 2

2.1	.....	17
2.2	.....	18
2.3	.....	21
2.4	.....	25
2.5	.....	26
2.6	.....	28
2.7	.....	30
2.8	.....	31
2.9	.....	33
2.10	.....	34
2.11	.....	36
2.12	.....	38
2.13	.....	43
2.14	.....	45
2.15	.....	47
2.16	.....	48
2.17	.....	51
2.18	.....	53

Chapter 3

3.1	.....	84
3.2	.....	87
3.3	.....	92
3.4	.....	93
3.5	.....	97
3.6	.....	101

FiguresChapter 4PAGE

4.1	.....	128
4.2	.....	130
4.3	.....	134
4.4	.....	136
4.5	.....	139
4.6	.....	141
4.7	.....	144
4.8	.....	146
4.9	.....	148

Chapter 5

5.1	.....	164
5.2	.....	166
5.3	.....	184
5.4	.....	192
5.5	.....	193
5.6	.....	172
5.7	.....	174
5.8	.....	176
5.9	.....	181

Chapter 6

6.1	.....	218
6.2	.....	220
6.3	.....	222
6.4	.....	223
6.5	.....	224

Appendix 7

7.1	.....	257
7.2	.....	258

## CHAPTER 1

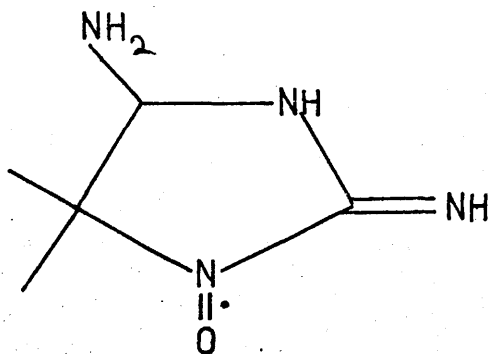
### INTRODUCTION

#### 1.1 Free radicals

The first authenticated organic free radical triphenylmethyl, was discovered by Gomberg in 1900.<sup>1</sup> Since this initial discovery, many "stable" free radicals have been isolated and purified, and the existence of radicals as short lived transients formed during the course of chemical reactions has become a commonly accepted concept. The presence of a free valence tends to make most radicals highly reactive, many having lifetimes of the order of micro-, or milli-seconds, unless they are trapped within an inert matrix.

The most characteristic property of any free radical is the paramagnetism arising from the spin and orbital motions of the free electrons. The development of electron paramagnetic resonance spectroscopy proved to be a very powerful tool in the examination of free radicals, being able to detect even short lived transients, by the application of flow systems.

One group of radicals which were extensively studied as a result of the development of e.p.r. spectroscopy, were the nitroxides. The first organic nitroxide to be prepared, was porphyrexide,<sup>2</sup> a heterocyclic free radical.



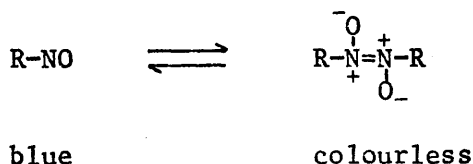
Porphyrexide

Many organic nitroxide radicals have now been prepared, and they appear to have an inherently stable electronic arrangement around the nitrogen and oxygen atoms, the bond order being 1.5, with the unpaired electron in a  $\pi^*$  orbital. The organic nitroxide radicals show no tendency to dimerise at the  $\text{NO}^\bullet$  centre,<sup>3</sup> however their stability is affected by the groups attached to the nitrogen, the presence of a proton on the carbon  $\alpha$  to the nitrogen resulting in a disproportionation,<sup>4</sup> and groups which allow delocalisation of the valence electron may cause dimerisation at some other centre in the molecule.

## 1.2. The generation of nitroxide radicals from C-nitroso compounds

The work outlined in this thesis involves a general study of the photolysis and radical reactions of humulene nitrosite, and the following is a brief review of the methods involved in generating nitroxide radicals from C-nitroso compounds of relevance to this work.

Organic nitroso compounds are known to exist in either the monomeric, or dimeric forms, often forming an equilibrium in solution.<sup>5-9</sup>

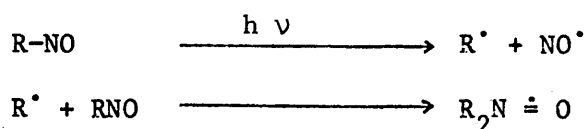


In early studies of the photolysis and pyrolysis reactions of organic nitroso compounds using e.p.r. techniques, free radicals were observed, which after some initial disagreement,<sup>7,8,10,11</sup> were confirmed to be nitroxide radicals. It was initially unclear whether the nitroso monomer,<sup>7,8</sup> or dimer,<sup>10,11</sup> was the source of the radicals. The nitroso monomer was eventually confirmed to be the precursor,<sup>12</sup>

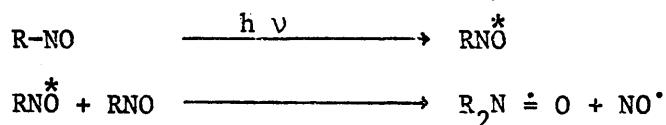


the irradiation of aliphatic nitroso compounds with red light, and aromatic nitroso compounds with ultra-violet light,<sup>6,13-15</sup> stimulating an  $n \rightarrow \pi^*$  transition<sup>16</sup> in the nitroso group, which was then postulated to lead to the production of nitroxide radicals in either of the two following ways.

1. The excited nitroso species may undergo C-N bond cleavage producing alkyl or aryl radicals, which attack a second molecule of the nitroso compound forming the nitroxide radical.



2. The excited nitroso species, could displace nitric oxide from a neighbouring unexcited molecule of the nitroso compound, as shown below.



The pyrolysis of C-nitroso compounds forms nitroxide radicals by a process involving the cleavage of the C-N bond.<sup>7,12,17,18</sup>

The reaction of C-nitroso compounds with alkyl and aryl radicals forming nitroxide radicals, has been well established,<sup>7,19,20</sup> C-nitroso compounds being frequently used as radical scavengers.<sup>19,21-23</sup> Current literature suggests, that C-N bond cleavage, with the formation of nitroxides is general to the photolysis of C-nitroso compounds.<sup>24-28</sup> No definite evidence as to whether mechanism 2 does or does not operate is available, and although there is some suggestion that in the specific case of 1-cyclopropyl-1-nitroethane it does not,<sup>29</sup> there is no reason to assume that this applies generally.

The dimeric forms of C-nitroso compounds can only indirectly undergo photolysis reactions to form nitroxide radicals, having first to be dissociated to the monomer, either by heating<sup>7,12</sup> or by irradiating in ultra-violet light.<sup>12</sup>

### 1.3. The photochemistry of caryophyllene nitrosite

The increased knowledge of the photochemistry of C-nitroso compounds discussed above, and the compilation of the magnetic characteristics of nitroxide radicals, which had resulted from the advent of e.p.r spectroscopy,<sup>30-47</sup> coincided with a renewal in interest in the photochemistry of caryophyllene and its derivatives.<sup>48-50</sup> This prompted McConnell, Porte et.al., to re-examine the properties of caryophyllene nitrosite using e.p.r. spectroscopy.

An excellent review of the chemistry and crystallography of caryophyllene and its derivatives has been written by J.Monteith Robertson.<sup>51</sup> The structure of caryophyllene (1) was determined by Barton<sup>52-56</sup> and Šorm,<sup>57,58</sup> using methods of chemical degradation. However, X-ray crystallography was used to great effect by among others Robertson to elucidate the structures of caryophyllene derivatives,<sup>59,60</sup> demonstrating the remarkable ease with which caryophyllene undergoes cyclisations and molecular rearrangements.<sup>59-63</sup>

The crystalline nitrosite of caryophyllene was one of the first derivatives used by Chapman to characterise caryophyllene.<sup>64,65</sup> This compound is a brilliant blue solid, the nitroso group absorbing red light of wavelength  $6,700\text{\AA}$ , which induces an  $n \rightarrow \pi^*$  transition. Caryophyllene nitrosite is known to have structure (2),<sup>51</sup> the stereochemistry having been deduced from the structure of the iodonitrosite, formed by the reaction of the nitrosite with iodine, as shown in figure 1.1.<sup>66</sup> The iodonitrosite (3) has been obtained in a pure crystalline form and crystallography has demonstrated that it has the stereochemistry shown.<sup>67,68</sup> E.p.r. studies have confirmed

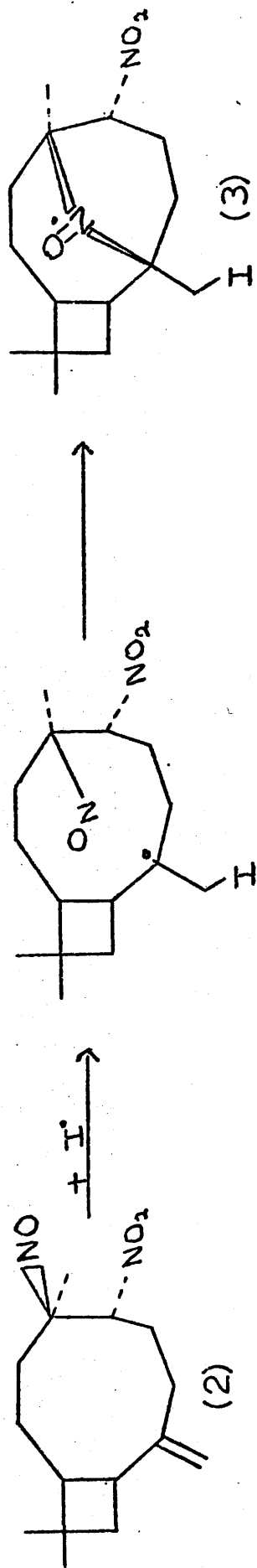


Figure 1.1 The reaction of dilute chloroform solutions of caryophyllene nitrosite (2) with iodine forming the iodonitrosite (3).

that the iodonitrosite is a nitroxide radical.<sup>69</sup> Caryophyllene nitrosite is known to form a bromonitrosite (4)<sup>70</sup> by an exactly analogous mechanism.

Prior to the investigations of McConnell, Porte et.al., various attempts had been made to study the effect of light on caryophyllene nitrosite,<sup>71-77</sup> but many of the results were inconclusive, only the gaseous products having been identified as 86.1% N<sub>2</sub> and 13.9% N<sub>2</sub>O<sub>3</sub>.<sup>76</sup> McConnell, Porte et.al., monitored the irradiation of caryophyllene nitrosite in red light and u.v. light using an e.p.r. spectrometer,<sup>70</sup> and demonstrated, that it was a versatile source of nitroxide radicals. The irradiation of caryophyllene nitrosite in u.v. light produces the nitroxide radical (5). However, the initial photochemical step involves the nitro group and not the nitroso group. The following important observations were made about the nitroxide radicals formed when solid caryophyllene nitrosite, or solutions of the nitrosite, were irradiated in red light.

1. The nitroxide radicals observed appeared to form by mechanisms, which with slight modifications, were in agreement with those postulated by previous workers studying the photolysis of C-nitroso compounds, and in particular it was demonstrated, that a transannular addition to the exomethylene group of caryophyllene nitrosite in the manner shown in figure 1.2. did not take place.
2. The paramagnetic species observed, when solutions of caryophyllene nitrosite were irradiated in red light, were dependent on whether a protic or an aprotic solvent was used. When the nitrosite was irradiated in solution

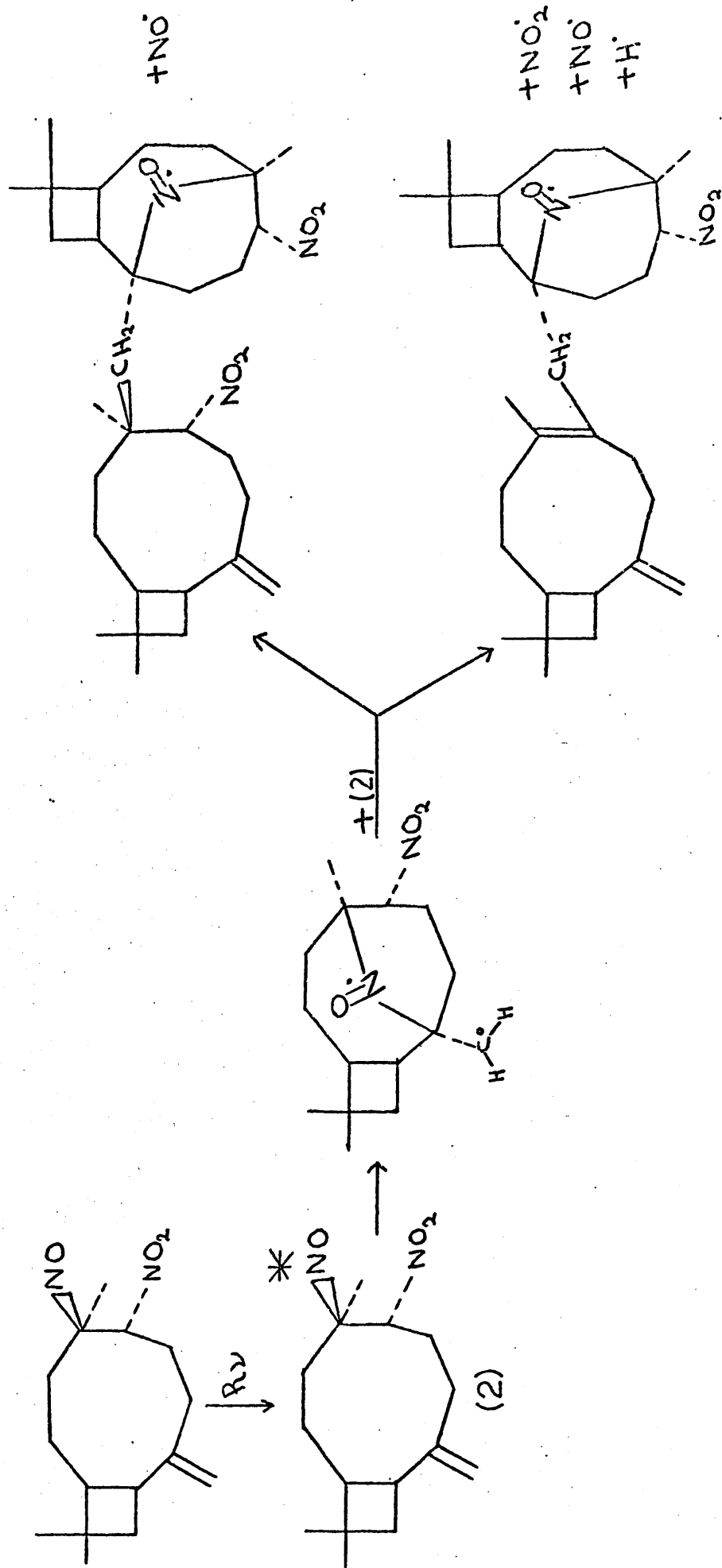


Figure 1.2 A mechanism involving a transannular cyclisation of caryophyllene nitrosite (2), which was shown by McConnell, Porte, et.al., not to operate when caryophyllene nitrosite is irradiated with red light.

in ethanol, the red excited nitroso species appeared to interact with the solvent molecules, forming the diamagnetic hydroxylamines (6) and (7), which on standing in air oxidised to the nitroxide radicals (8) and (9), as shown in figure 1.3.

3. Two nitroxide radicals, which for the purposes of this thesis are called I' and II', were observed when solid caryophyllene nitrosite and solutions of caryophyllene nitrosite in aprotic solvents such as benzene, or toluene, were irradiated in red light. Figure 1.4. illustrates the mechanism postulated to explain the formation of these two radicals I' (10) and II' (11).

Nitroxide radical I' (10) can clearly form by either of the two mechanisms discussed earlier to explain the formation of nitroxide radicals observed, when C-nitroso species are irradiated in red light. The red excited nitroso group either undergoes a C-N bond cleavage, forming the aliphatic radical (12) which interacts with caryophyllene nitrosite to form nitroxide radical I' (10), or displaces nitric oxide from a neighbouring unexcited molecules of caryophyllene nitrosite.

The formation of nitroxide radical II' (11), is of more interest, in that its presence indicates, that one of the following two mechanisms is in operation.

1. The photolytic cleavage of the C-N bond of the nitroso group, is followed by the loss of  $\text{NO}_2^{\cdot}$  resulting in the formation of an isomer of caryophyllene, which can interact with a red excited molecule of caryophyllene nitrosite, to form nitroxide radical II' (11).

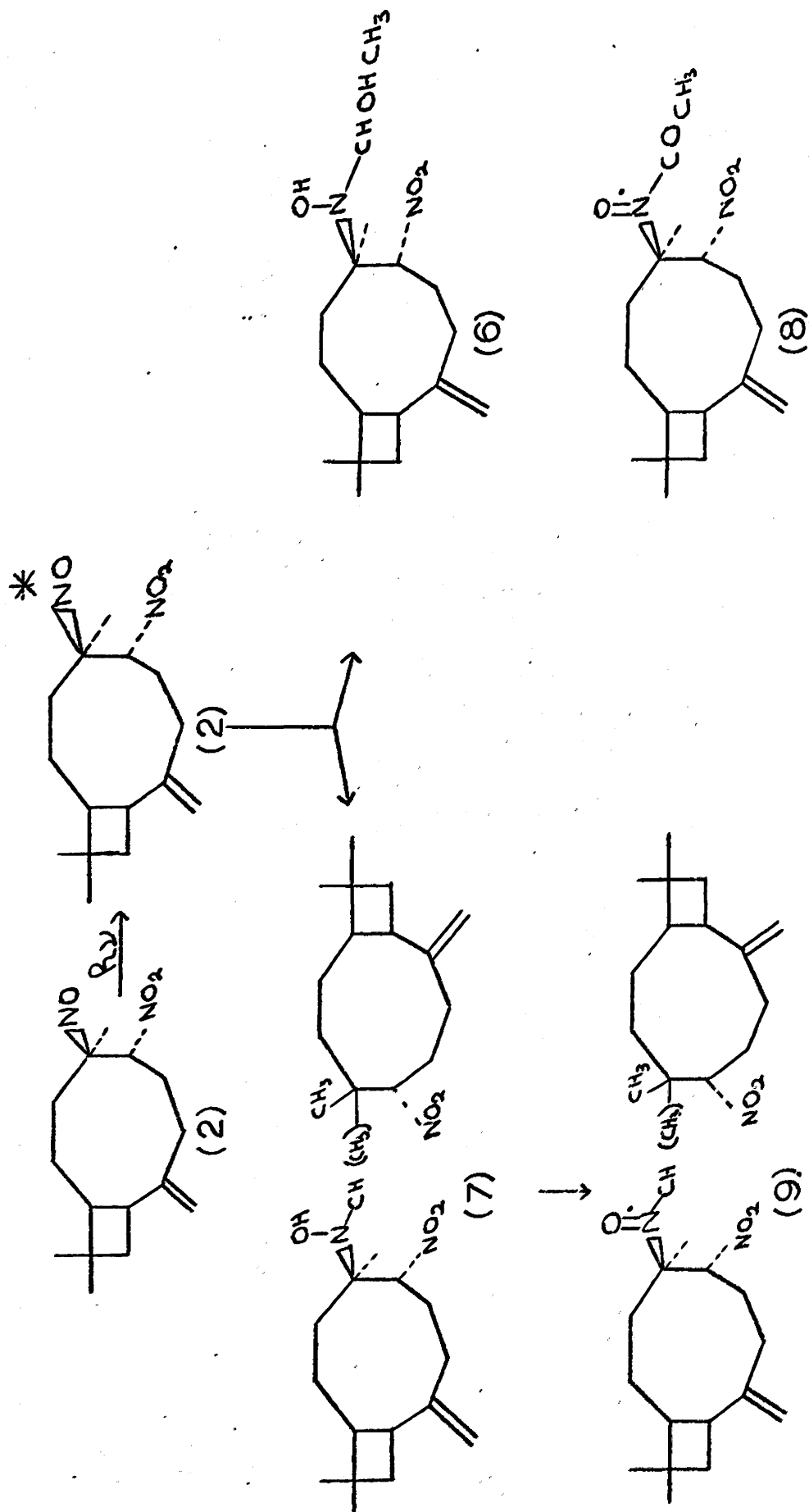


Figure 1.3 The formation of the nitroxide radicals observed when solutions of caryophyllene nitrosite (2) in ethanol are irradiated with red light.

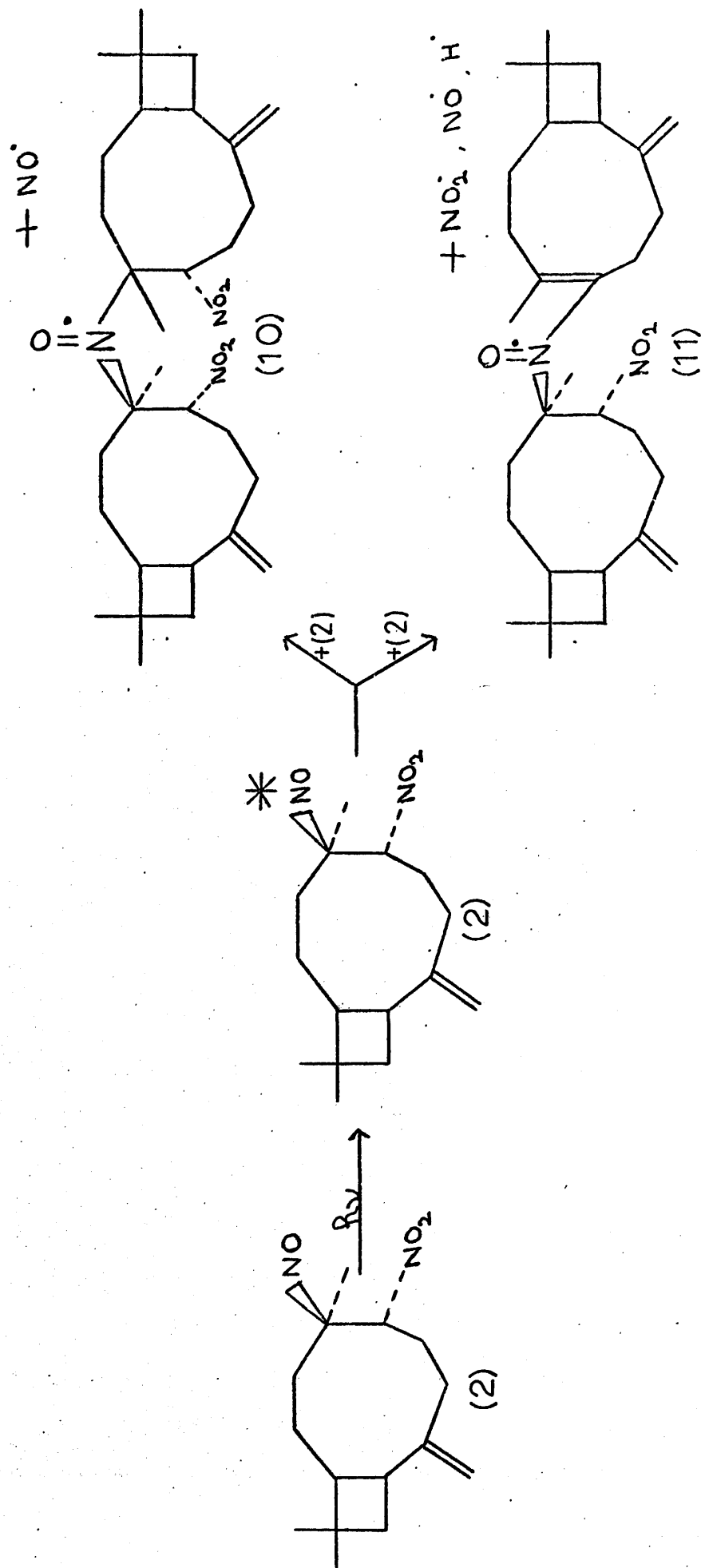
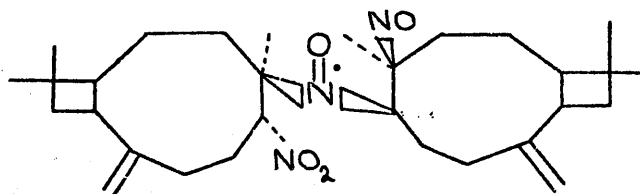


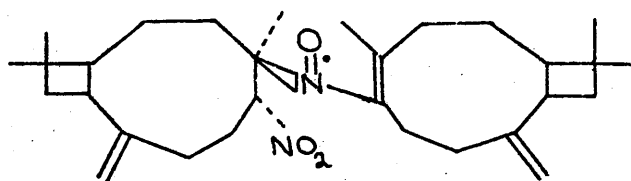
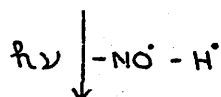
Figure 1.4 The mechanism postulated by McConnell, Porte, et.al., to account for the nitroxide radicals observed when crystalline caryophyllene nitrosite (2) or its solutions in aprotic solvents are irradiated with red light.



2. Alternatively the red excited nitroso group can displace the nitro group of a neighbouring molecule of caryophyllene nitrosite, forming a nitroxide intermediate III' (13), shown below, which retains a nitroso chromophore, and which on further irradiation in red light, would rearrange to nitroxide radical II' (11).



Nitroxide radical III' (13)



Nitroxide radical II' (11)

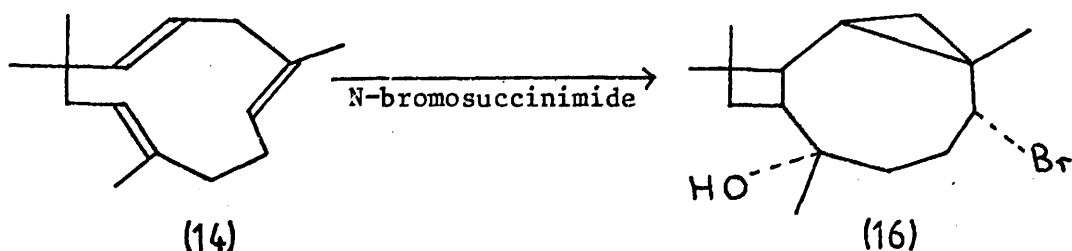
This work by McConnell, Porte, et.al., thus left mechanistic problems still to be answered, and also the nitroxide radicals I' and II' were not extracted, purified, and unambiguously characterised and shown to have the structures (10) and (11).

#### 1.4. The radical and photochemical reactions of humulene nitrosite

The investigations reported in this thesis involved a study of the photochemical, and radical reactions of humulene nitrosite.

The structure of the sesquiterpene humulene (14), was established by a combination of organic chemical degradation studies on humulene,<sup>78-90</sup> and X-ray work on its silver nitrate complex by

Sim and others,<sup>91-93</sup> which provided its absolute stereochemistry and an insight into its preferred conformation in the liquid. Like caryophyllene, humulene readily undergoes interesting transannular reactions, the eleven membered triene ring allowing cyclisations to tricyclic compounds e.g; when reacted with sulphuric acid it produces  $\alpha$  caryophyllene alcohol (15),<sup>94-96</sup> and treatment with N-bromosuccinimide produces the cyclisation shown below, forming humulene bromohydrin (16).<sup>97,98</sup>



The blue crystalline nitrosite of humulene was prepared by Chapman for use in characterising humulene. No extensive studies had been carried out into the products formed when humulene nitrosite was irradiated with red light, and indeed the structure of the nitrosite itself, had not been determined. The initial objectives of the research described in this thesis can thus be summarised under three headings.

1. The first objective was to determine the structure, and absolute stereochemistry of humulene nitrosite, by comparing its <sup>1</sup>H n.m.r., <sup>13</sup>C n.m.r., infra-red, and mass spectra, with the corresponding spectra of caryophyllene nitrosite, the structure and stereochemistry of which are known. In particular it was to be determined whether N<sub>2</sub>O<sub>3</sub> added directly over one of the double bonds, or

whether the products had cyclised in a manner similar to humulene bromohydrin (16).

2. The second objective was to follow the irradiation of solid humulene nitrosite, and its solutions in the aprotic solvents chloroform, benzene, and toluene, in red light, in order to achieve the following two objectives.
  - a. First it was hoped to determine whether humulene nitrosite forms nitroxide radicals in a manner analogous to caryophyllene nitrosite, and if so, to devise experiments to check the exact details of the mechanisms involved.
  - b. Second to relate any differences observed in the mechanisms involved in the photolysis of humulene nitrosite and caryophyllene nitrosite, to structural differences in the parent molecules.

If humulene nitrosite did not itself have a cyclised structure, having formed by the addition of  $N_2O_3$  over one of the double bonds, then the photolysis reaction might produce the types of species discussed below.

- b<sub>1</sub>. Products might form by transannular cyclisation of the aliphatic radicals formed by the C-N bond cleavage of the red excited nitroso group.
  - b<sub>2</sub>. Alternatively the red excited nitroso group might undergo a transannular addition to the carbon to carbon bonds in the ring.
3. The third objective was to isolate, and characterise, using all relevant spectroscopic techniques, the paramagnetic species produced.

The more recent literature concerning the photochemistry of C-nitroso species, has involved extensive studies of the diamagnetic species formed during the secondary dark reactions, which follow the

initial photochemical step of C-N bond cleavage of the nitroso group.

This work is discussed in later chapters of this thesis.

## CHAPTER 2

### INITIAL STUDIES OF THE PRODUCTS OBTAINED FROM THE

#### PHOTOLYSIS REACTIONS OF HUMULENE NITROSITE

#### IRRADIATED WITH RED LIGHT

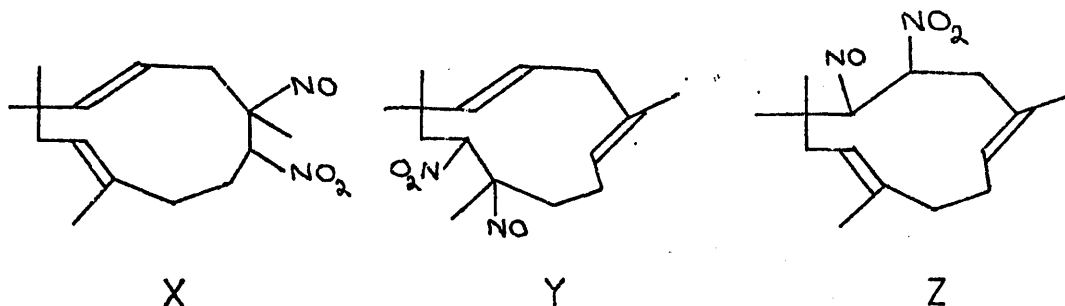
#### 2.1. Determination of the structure of humulene nitrosite

The small amount of humulene nitrosite used in the initial studies described in this chapter was kindly donated by Dr. S.T.R.S. Mitchell, who in the 1930's, had used the substance in early work on the Cotton effect<sup>71</sup> and in studies of asymmetrical photochemical reactions, involving circularly polarised light.<sup>72</sup> Mitchell prepared the nitrosite according to the method described by Chapman,<sup>64,65</sup> which allows for one equivalent of  $\text{NO}_2^\cdot + \text{NO}^\cdot$  reacting with one equivalent of humulene (14). An elemental analysis for the elements C, H, and N has confirmed, that the sample of nitrosite has the empirical formula  $\text{C}_{15}\text{H}_{24}\text{N}_2\text{O}_3$  based on the results shown in appendix 2, table 2.1.

In determining the structure of humulene nitrosite a careful consideration must be given to the manner in which one equivalent of  $\text{N}_2\text{O}_3$  can react with humulene (14). The following points need to be cleared up.

1. Does the  $\text{NO}_2^\cdot$  attach through the oxygen as a nitrite, or through the nitrogen as a nitro grouping?
2. In forming the nitrosite, does the eleven membered triene ring of humulene undergo the type of transannular reaction involved in the formation of humulene bromohydrin (16)<sup>97,98</sup> as was discussed in chapter 1?
3. Does the  $\text{N}_2\text{O}_3$  add directly, across one of the humulene double bonds, giving a nitrosite of structure x, y, or z

as shown below, or one of the structural isomers obtained by interchanging the nitroso, and nitro groups?

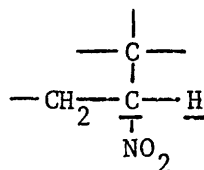


4. Finally what is the precise structural configuration of the isomers and what are their preferred conformations?

To determine the above points, use was made of the similarity in structure of humulene (14), and the sesquiterpene caryophyllene (1), the structure of whose nitrosite derivative is accurately known. A comparison was undertaken of the <sup>1</sup>H n.m.r., <sup>13</sup>C n.m.r., infra-red, and mass spectra of caryophyllene nitrosite (2), and humulene nitrosite. The pertinent data obtained from these spectroscopic techniques, are summarised in tables 2.2, 2.3, 2.4, and 2.5, respectively in appendix 2. Figures 2.1, and 2.2, compare the <sup>1</sup>H n.m.r. spectra in the  $\tau$  ranges 3 to 10 and 4 to 5 respectively.

From the above comparisons the following points emerged.

1. The NO<sub>2</sub> adds through the nitrogen as a nitro grouping, the <sup>1</sup>H n.m.r., and <sup>13</sup>C n.m.r., showing multiplets at  $\tau = 3.86$ , and 88.9 p.p.m. respectively, which are consistent with the following structure.



The infra-red spectrum of humulene nitrosite clearly shows the asymmetric and symmetric stretching absorptions of a nitro group attached to a secondary carbon atom at 1560 cm<sup>-1</sup>, 1360 cm<sup>-1</sup>, respectively, and no absorptions

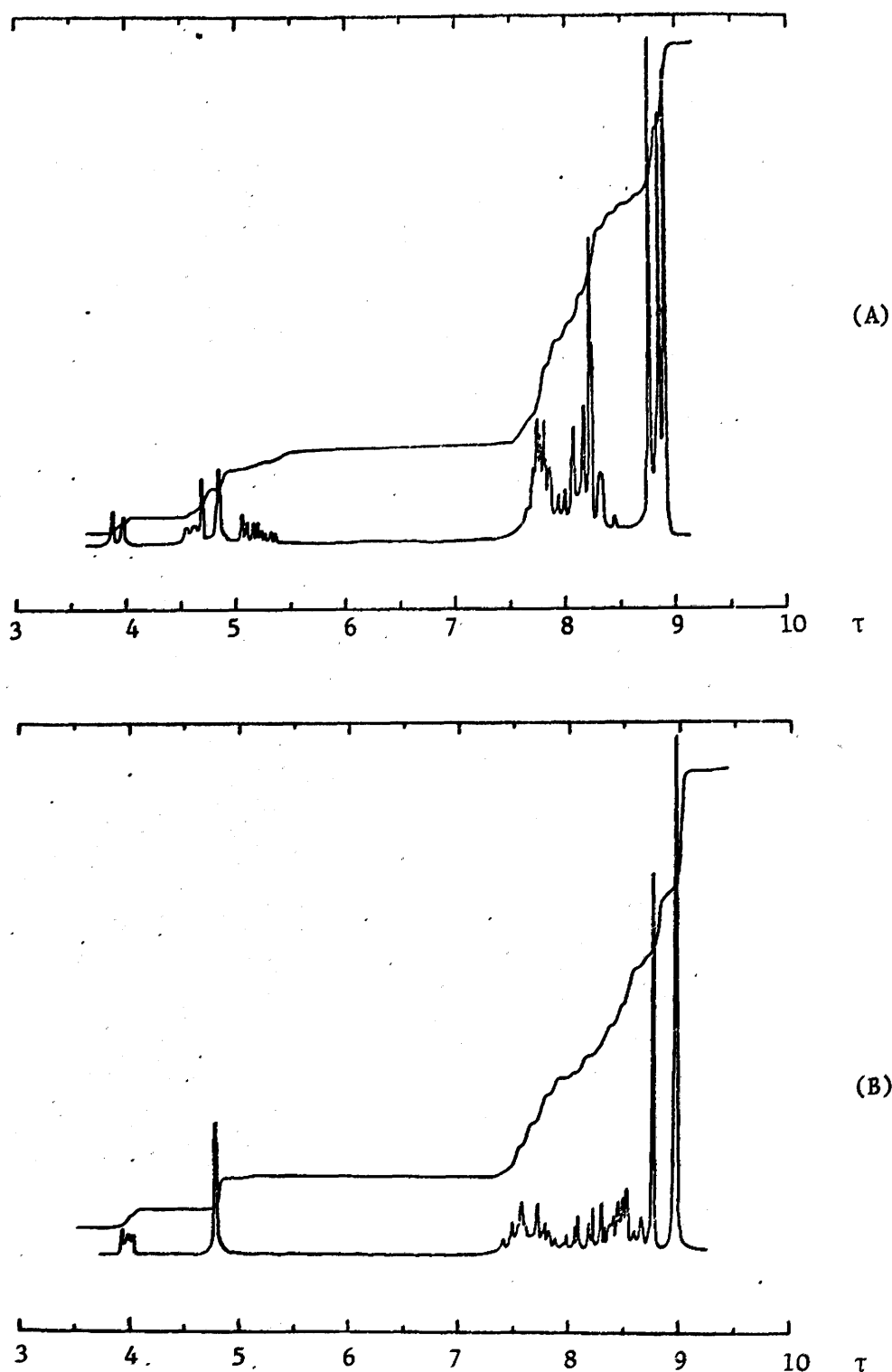


Figure 2.1 The  $^1\text{H}$  n.m.r. spectra of solutions of (A) humulene nitrosite and (B) caryophyllene nitrosite (2) in  $\text{CDCl}_3$  recorded in the  $\tau$  range 3 to 10.

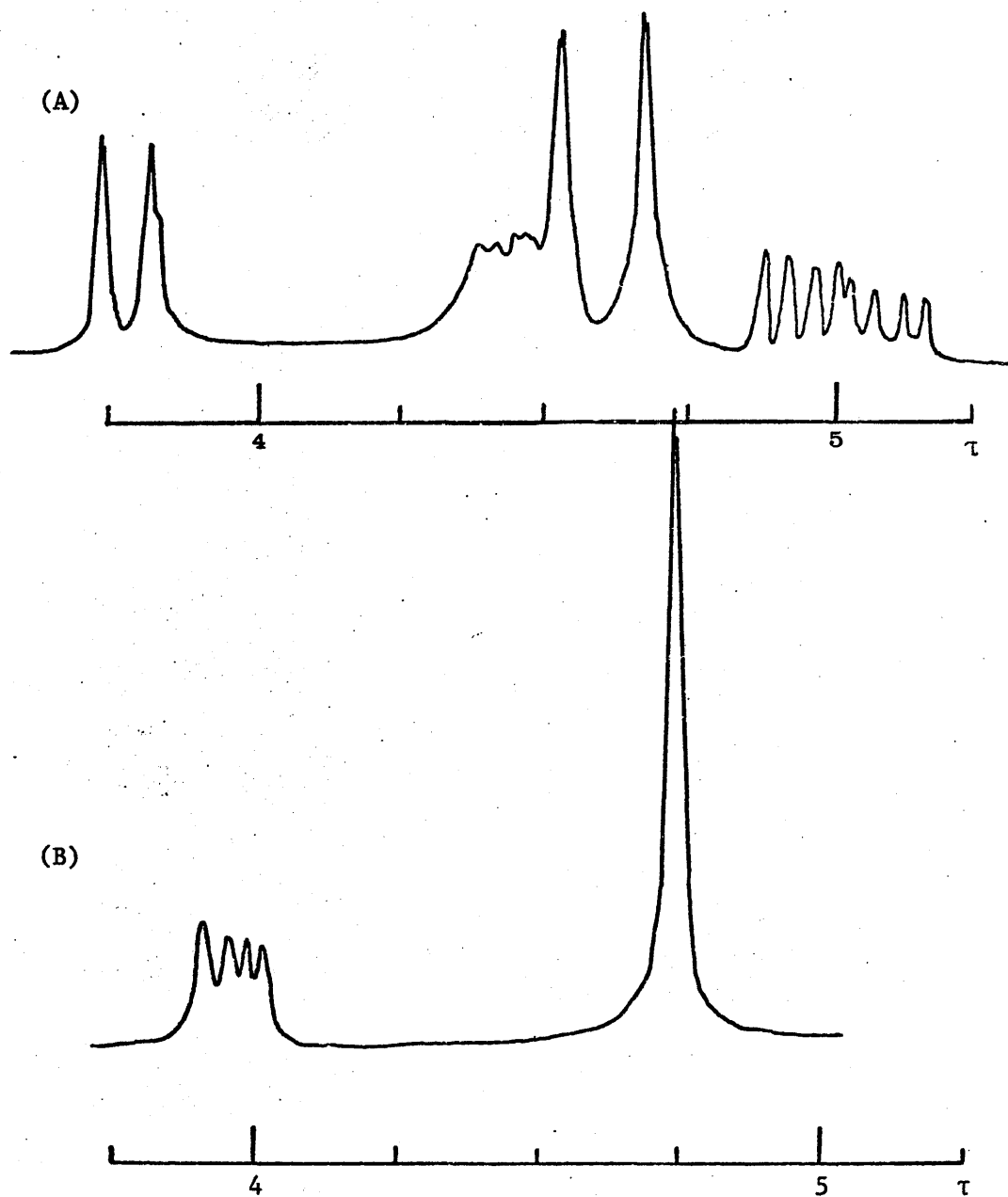
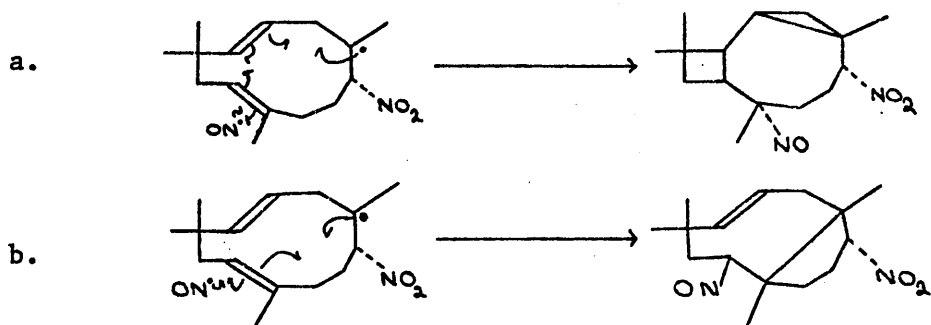


Figure 2.2 The  $^1\text{H}$  n.m.r. spectra in the  $\tau$  range 4 to 5 of (A) humulene nitrosite and (B) caryophyllene nitrosite in  $\text{CDCl}_3$  solution.

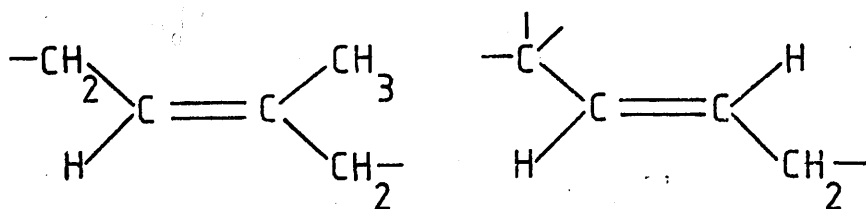


compatible with the presence of a nitrite are observed.

2. On addition of  $N_2O_3$  to humulene, no transannular cyclisations take place. Such rearrangement reactions would remove as shown below, two or three of the double bonds, and produce a cyclopropyl ring structure



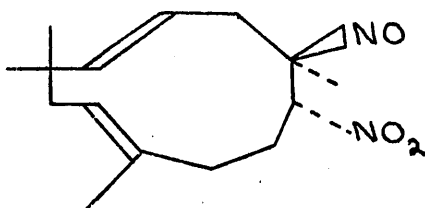
The  $^1H$  n.m.r.,  $^{13}C$  n.m.r., and infra-red spectra, clearly show the retention of the following structures



and no evidence for cyclopropyl protons at  $\tau > 9.0$  is found in the  $^1H$  n.m.r. spectrum. The ethylenic region of the humulene nitrosite  $^1H$  n.m.r. spectrum integrates for four protons.

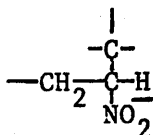
3. The  $N_2O_3$  obviously adds directly over one of the double bonds of humulene. As the trans double bond is retained, structure Z can be discounted, and  $^1H$  n.m.r. helps to distinguish between structures X and Y by showing the presence of nine allylic protons, which is only consistent with structure X. Furthermore structure Y contains the structural unit  $C=C-\underline{CH_2}-C=C$ , which would have been expected to give proton resonance signals at  $\tau \sim 7.1$ , and no resonances are observed in this region of the spectrum.

Humulene nitrosite has structure X with the  $\text{NO}_2^*$  and  $\text{NO}^*$  having added in the order shown below.



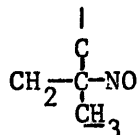
Humulene nitrosite (17)

The  $^1\text{H}$  n.m.r. and  $^{13}\text{C}$  n.m.r. show the presence of the following groupings,



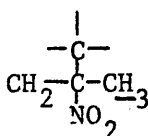
$^1\text{H}$  n.m.r. multiplet  $\tau=3.86$

$^{13}\text{C}$  n.m.r. 88.9 p.p.m.



$^1\text{H}$  n.m.r. singlet  $\tau=8.75$

$^{13}\text{C}$  n.m.r. 102.1 p.p.m.

but show no resonances attributable to the grouping  which would arise at  $\tau \sim 8.0$  in the  $^1\text{H}$  n.m.r. spectrum.

This attachment of the nitroso group to the tertiary carbon is chemically sound, as a secondary nitroso grouping would rearrange to an oxime<sup>99</sup> and the nitrosite would lose its characteristic blue colour. The infra-red spectrum showed no absorptions consistent with the presence of oximes.

Early studies by Mitchell<sup>72</sup> showed humulene nitrosite to be a racemic mixture of enantiomers. The  $^1\text{H}$  n.m.r. of humulene nitrosite shows no duplication of signals for protons on the asymmetric carbon atoms, or on the adjacent carbon atoms, of the type which might indicate the presence of diastereomers. It would thus appear that the addition of  $\text{N}_2\text{O}_3$  across the double bond of humulene is stereospecific, the most likely product being an

an entirely trans configuration, the cis configuration leading to a sterically congested product.

Sim has suggested, that humulene could have the preferred conformation shown in figure 2.3.<sup>100</sup>

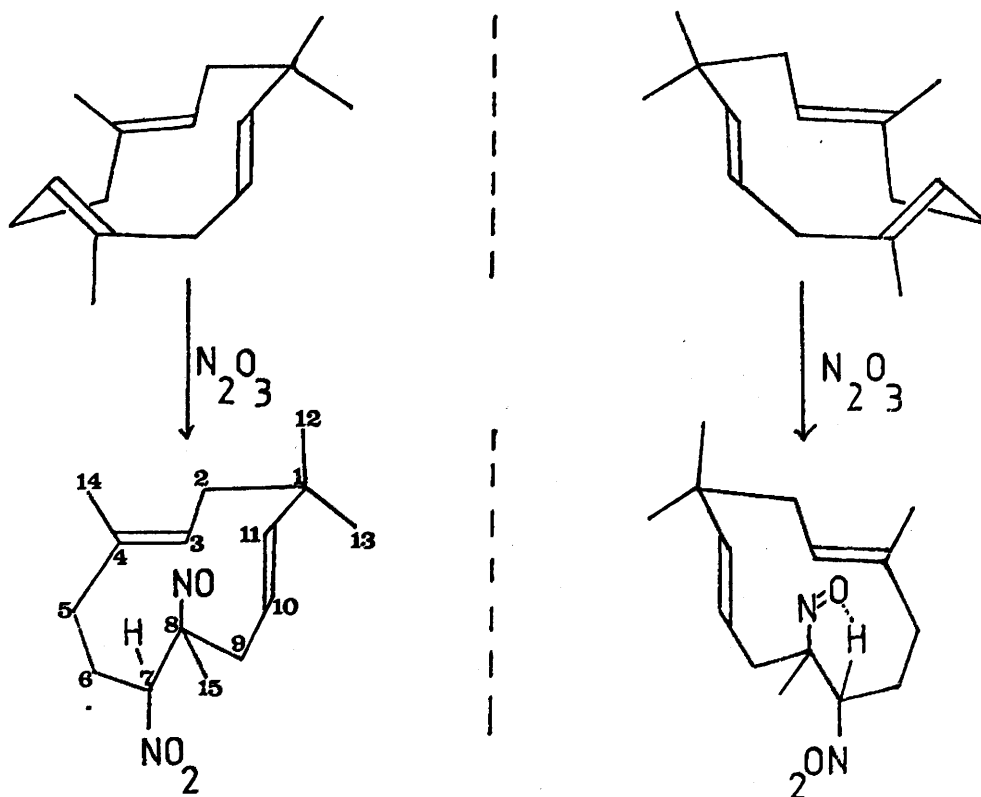


Figure 2.3 The reaction of humulene in its preferred conformation with  $N_2O_3$

Humulene in solution is conformationally mobile and readily interconverts between the two mirror image forms of the preferred conformation. Figure 2.3 shows the racemic mixture of enantiomers of humulene nitrosite, formed by a trans diaxial addition of  $N_2O_3$ , on these preferred conformations of humulene initiated by a frontal attack of  $NO_2^+$ . The conformation of humulene nitrosite shown in figure 2.3. is in good agreement with the experimental coupling constants found in the  $^1H$  n.m.r. spectrum for three key positions of the molecule, which are discussed below.

1. In the unit   $H_X$  is the

X part of an ABXY spectrum  $J_{AX} = 9.0$  Hz. and  $J_{BX} = 4.0$  Hz.

These coupling constants are in accord with the dihedral angles of  $\sim 180^\circ$  and  $\sim 65^\circ$  found in the above conformation.

2. In the unit  the underlined

proton is the X part of an ABX system with  $J_{AX} = 9$  Hz. and  $J_{BX} = 3.5$  Hz. These coupling constants are in accord with the dihedral angles of approximately  $180^\circ$  and  $60^\circ$  found for the above conformation.

3. For the unit  the dihedral angles are

$\sim 90^\circ$  and  $150^\circ$ . The underlined proton gives a signal at  $\tau = 3.86$ , which is split into a doublet  $J = 8$  Hz. The dihedral angle of  $90^\circ$  would explain the zero coupling to one of the neighbouring protons, however the conformational mobility of the molecule results in considerable broadening of the resonances. Some of this broadening may also be due to hydrogen bonding, since in figure 2.3. the acidic proton on  $C_7$  lies adjacent to the nitroso group.  $C_7$  is detected in the partially proton decoupled  $^{13}\text{C}$  n.m.r. spectrum as a doublet at 88.9 p.p.m.

## 2.2. Radicals obtained when humulene nitrosite and solutions of humulene nitrosite, are irradiated with red light

The intense blue colour associated with humulene nitrosite (17), is the result of an absorption in the visible spectrum at  $6,700\text{\AA}^0$  arising from an  $n \rightarrow \pi^*$  transition in the nitroso group. In the case of caryophyllene nitrosite, the excitation of the nitroso grouping brought about by irradiating in red light, leads to the production of nitroxide radicals.<sup>70</sup> Figure 1.4. shows the mechanism postulated by McConnell, Porte, et.al., to explain the formation of the two nitroxide radicals I' (10) and II' (11), which are observed, when solid caryophyllene nitrosite, or its solutions in the aprotic solvents benzene and toluene are irradiated with red light. The mechanism involves either a cleavage of the C-N bond of the red excited nitroso group, or the attack of the electron in the  $\sigma$  - framework of the red excited nitroso group at a neighbouring molecule of caryophyllene nitrosite, forming the two nitroxide radicals I' (10) and II' (11), and liberating  $\text{NO}^\bullet$  and  $\text{NO}^\bullet_2$  plus  $\text{H}_2$ . The composition of the nitrogen containing gaseous products has been shown to be 13.9%  $\text{N}_2\text{O}_3$  and 86.1%  $\text{N}_2$ .<sup>76</sup>

The irradiation of humulene nitrosite in red light was investigated using e.p.r. spectroscopy, to determine if it also was a versatile source of nitroxide radicals and whether the basic mechanism of the photolysis was similar to that observed for caryophyllene nitrosite or if differences arising from the differences in structure of humulene nitrosite and caryophyllene nitrosite could be detected.

### 2.2.1. The irradiation of a crystalline sample of humulene nitrosite with red light.

A solid crystalline sample of humulene nitrosite was

irradiated in a sealed quartz tube in the absence of air, using light from a tungsten lamp in conjunction with a red filter transmitting in the range 6,250 - 6,750 Å°. The nitrosite was observed to slowly decompose to a viscous yellow oil, with the evolution of gaseous products. The e.p.r. spectrum of the yellow oil recorded at 295°K, is shown in figure 2.4. The conclusions listed below were made from an analysis of the line shape of this spectrum.

1. The line shape is consistent with that predicted for a polycrystalline sample of nitroxide radicals, which have a single unpaired electron ( $S = \frac{1}{2}$ ) in an environment of ortho-rhombic symmetry, and with coupling to  $^{14}\text{N}$  ( $I = 1$ ). The line widths are broad, and it is possible, that more than one type of nitroxide radical is present, with possibly additional couplings, such as hydrogen ( $I = \frac{1}{2}$ ), which are not resolved.
2. Within this viscous material the tumbling motions of the radicals are of too low a frequency to average out magnetic anisotropies. This suggests, that the nitroxide radicals have a high molecular weight.
3. The sample appears to be magnetically dilute, indicating, either that the molecules are sufficiently large to screen the nitroxide groupings, or that other diamagnetic species are present.

The spectrum shown in figure 2.5. is obtained at 295°K from a dilute solution of the yellow viscous photolysis product in chloroform, which has been thoroughly degassed. Two nitroxide radicals appear to be present.

Radical I The paramagnetic resonance spectrum of radical I consists of 1:1:1 triplet [isotropic  $\langle g \rangle = 2.0058 \pm 0.0003$ ;

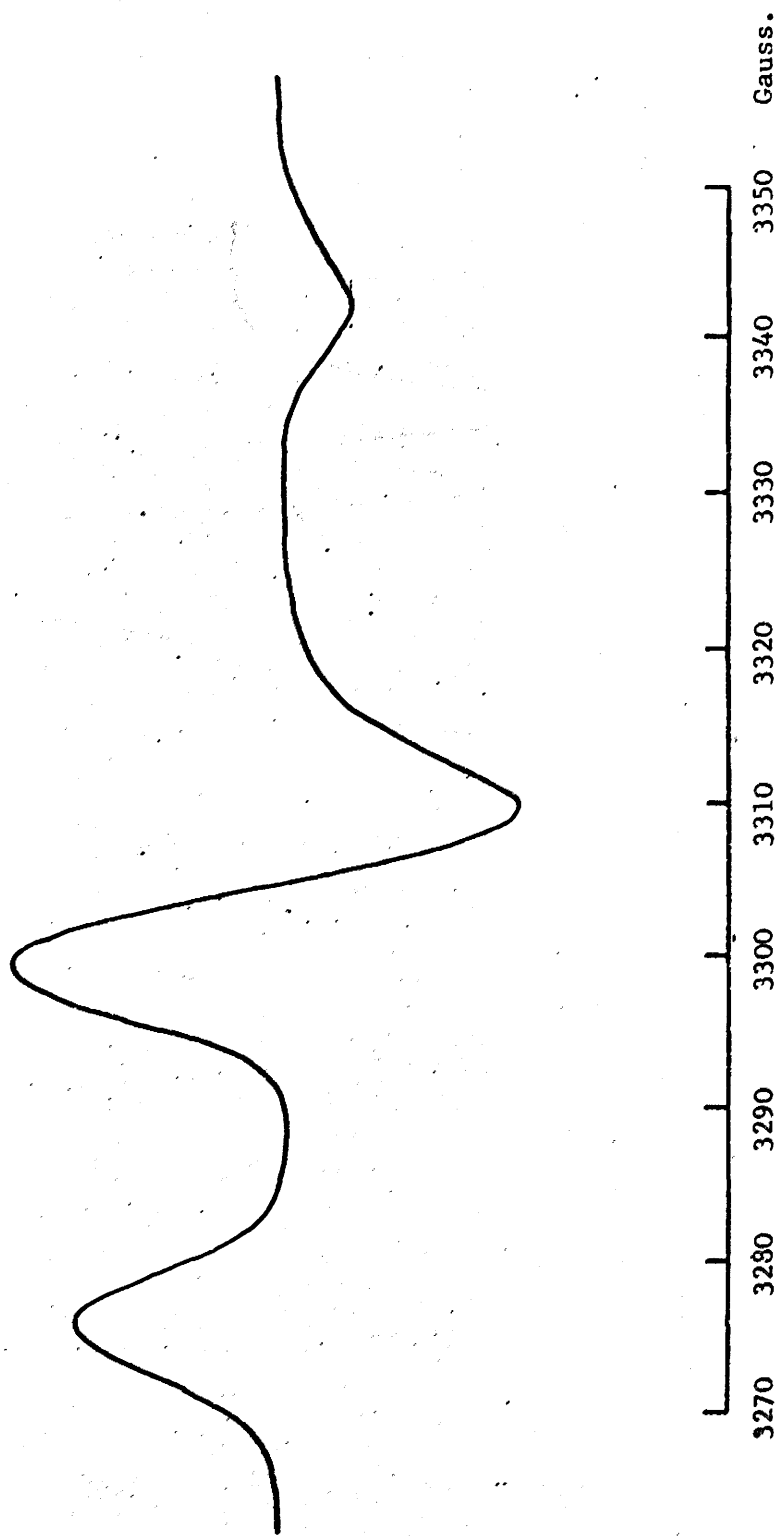


Figure 2.4 The e.p.r. spectrum of the viscous yellow oil obtained at 295°K by irradiating humulene nitrosite (17) with red light until it completely decomposes.

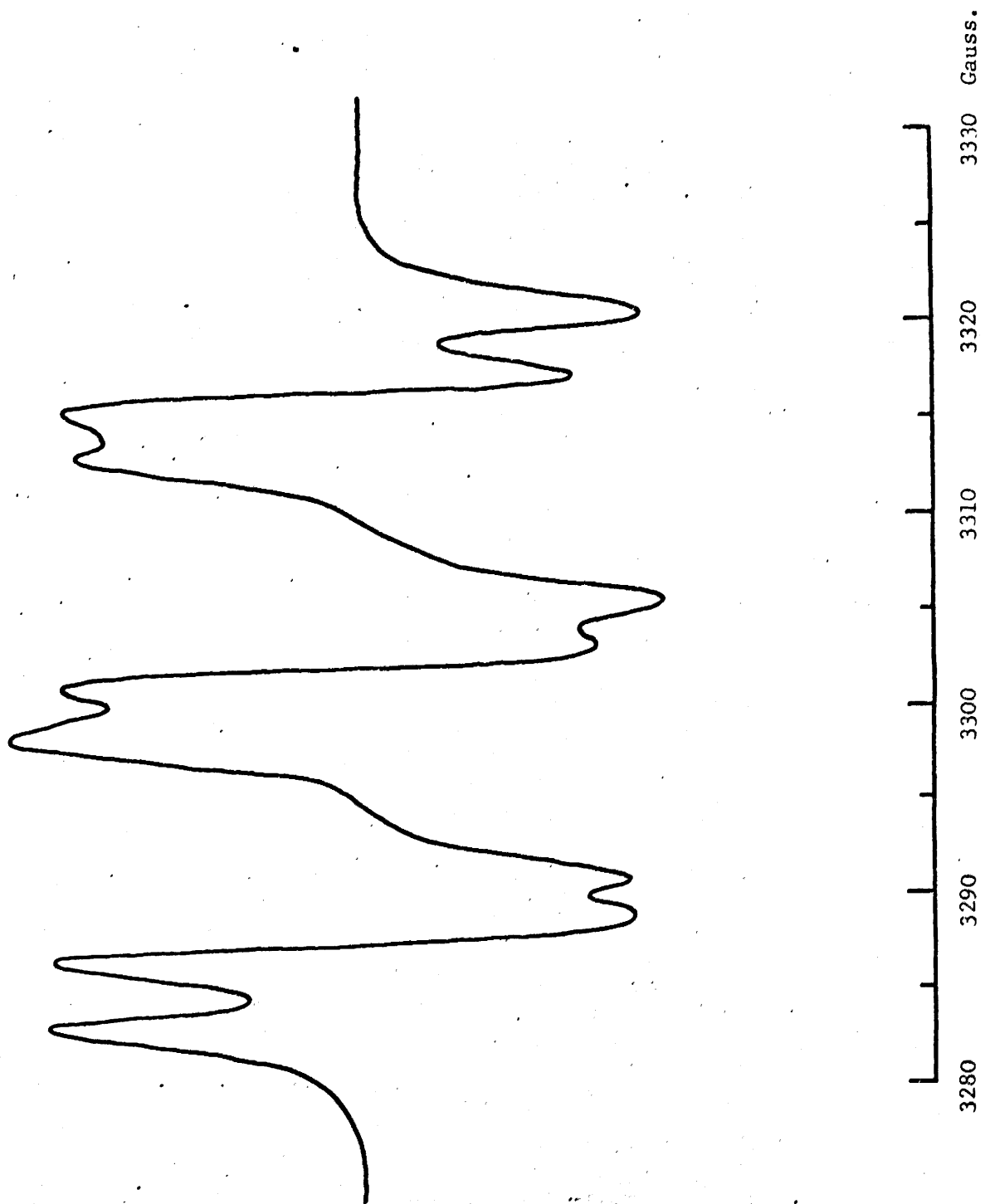


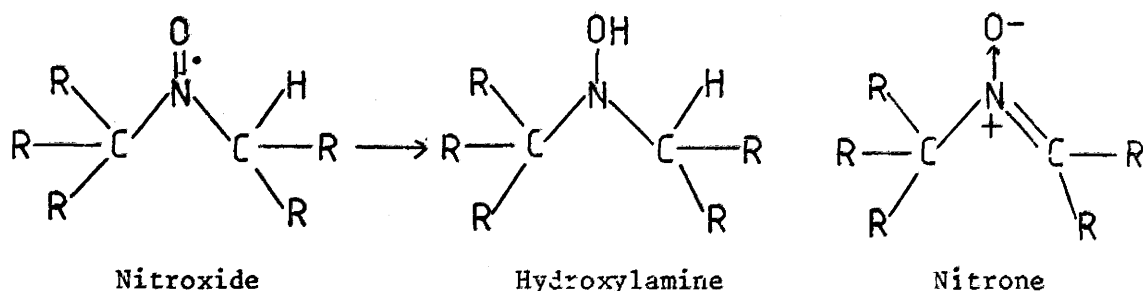
Figure 2.5 The e.p.r. spectrum of a dilute solution in chloroform of the viscous yellow oil obtained by irradiating humulene nitrosite (17) with red light. The spectrum was recorded at 295°K.



isotropic  $a(^{14}\text{N}) = 14.6 \pm 0.2\text{G}$ ]. This radical contains the molecular fragment  $\text{R}_1\text{R}_2\text{R}_3\text{C}-\dot{\text{N}}\text{O}-\text{CR}_4\text{R}_5\text{R}_6$ .

Radical II The paramagnetic resonance spectrum, of radical II consists of a 1:1:1 triplet, further split into doublets, by the interaction with a  $\beta$  proton [isotropic  $\langle g \rangle = 2.0058 \pm 0.0003$ ; isotropic  $a(^{14}\text{N}) = 14.8 \pm 0.2\text{G}$ ; isotropic  $a(^1\text{H}) = 5.5 \pm 0.5\text{G}$ ]. This radical contains the molecular fragment  $\text{R}_1\text{R}_2\text{R}_3\text{C}-\dot{\text{N}}\text{O}-\text{CHR}_4\text{R}_5$ .

If the solution is left standing, nitroxide radical II decomposes, most probably undergoing a disproportionation reaction of the type shown below.



### 2.2.2 Radicals obtained when solutions of humulene nitrosite, in chloroform, toluene, and benzene are irradiated with red light

When a 0.2M solution of humulene nitrosite in ethanol-free chloroform is thoroughly degassed and irradiated with red light, then the e.p.r. spectrum shown in figure 2.6 is obtained from the products. Two nitroxide radicals appear to be present and within the limits of experimental error, their isotropic  $\langle g \rangle$  factors and isotropic coupling constants, are consistent with the formation of radicals I and II. Nitroxide radical II of course slowly decomposes to diamagnetic species, as it is formed. Similar results are obtained if benzene, or toluene, rather than chloroform are used as solvent in this experiment.

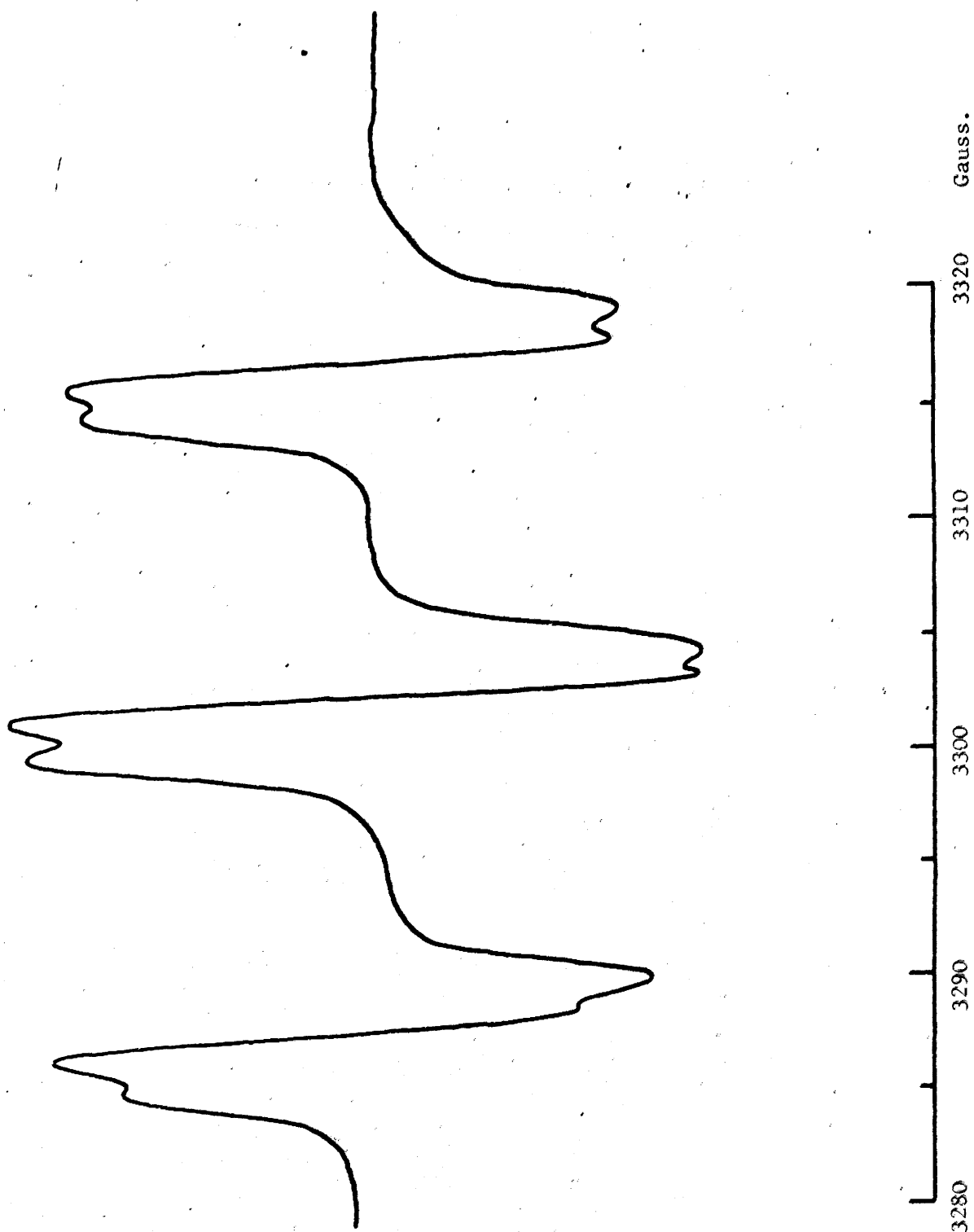


Figure 2.6 The e.p.r. spectrum of the radicals obtained by irradiating a dilute degassed solution of humulene nitrosite (17) in chloroform with red light. The spectrum was recorded at 295°K.

The following two postulated photolysis schemes appear to be consistent with the observations made in sections 2.2.1. and 2.2.2.

1. Scheme I, shown in figure 2.7 is based on the mechanism proposed by McConnell, Porte, et. al., for the irradiation of caryophyllene nitrosite under similar circumstances. Two processes are considered.

a) Photolytic cleavage of the C-N bond of the nitroso group, produces an aliphatic radical (18), which reacts with humulene nitrosite forming a nitroxide radical (19), containing the structural unit  $R_1R_2R_3C-\dot{N}O-CR_4R_5R_6$ .

b) Alternatively the radicals may form due to the attack of the unpaired electron in the  $\sigma$  framework of a red excited nitroso group, at a neighbouring molecule of humulene nitrosite, displacement of  $NO^*$  producing nitroxide radical (19) containing the structural unit  $R_1R_2R_3C-\dot{N}O-CR_4R_5R_6$ , and displacement of  $\dot{N}O_2$  producing an intermediate nitroxide radical (20), which would retain a nitroso chromophore. Further irradiation in red light would cause the intermediate radical (20) to lose  $\dot{N}O$ , with a subsequent rearrangement to a nitroxide radical (21), containing the structural unit  $R_1R_2R_3C-\dot{N}O-CHR_4R_5$ .

The mechanism proposed by McConnell, Porte, et. al., for the irradiation of caryophyllene nitrosite with red light, can be extended as shown in figure 2.8 to include an intermediate radical III' (13), containing a nitroso grouping. In the studies of the photolysis reactions of caryophyllene nitrosite recorded in the literature, no attempt was made to detect such an intermediate radical.

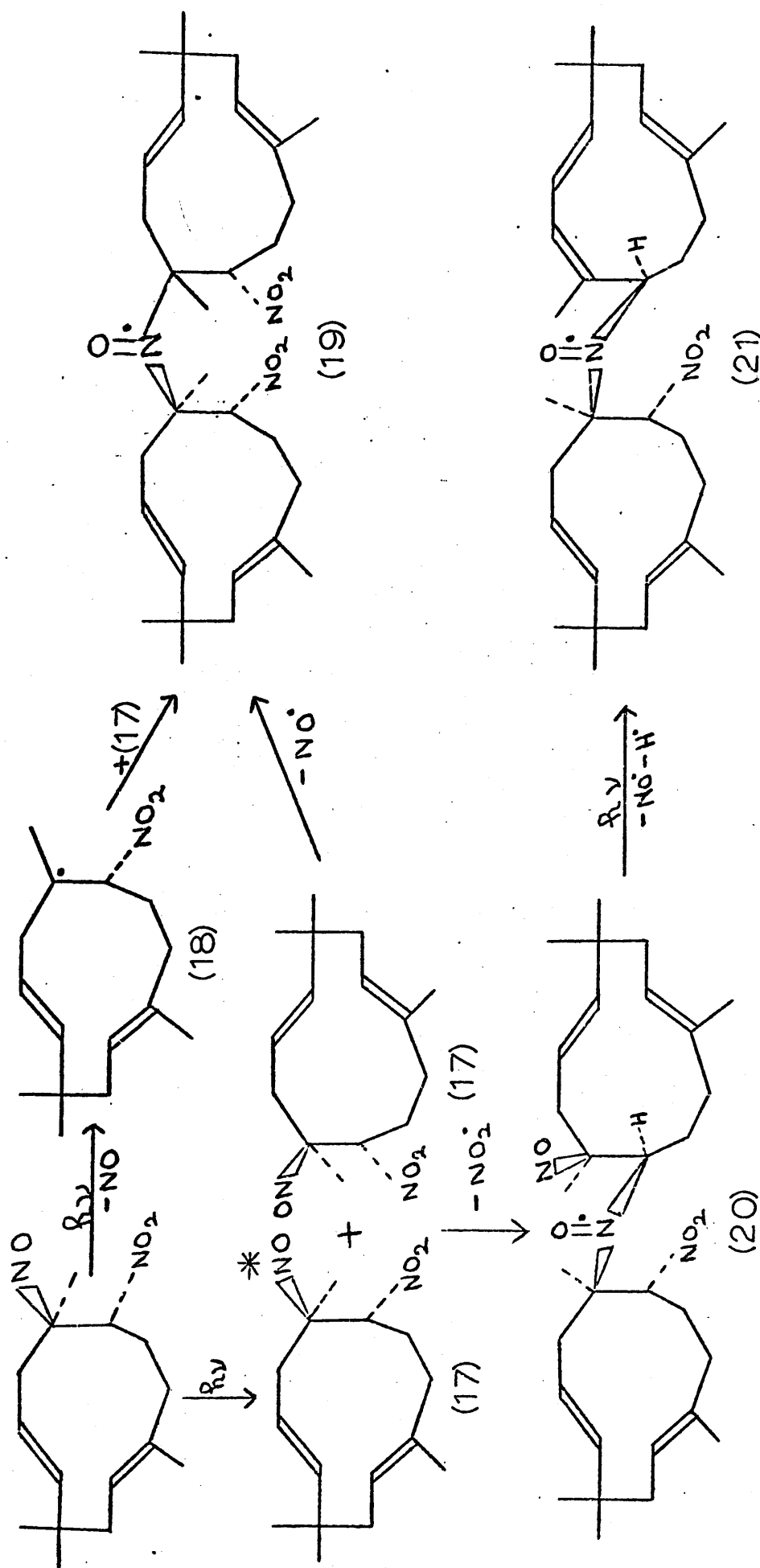


Figure 2.7 Photolysis scheme I, a mechanism postulated to explain the formation of the paramagnetic species

observed when humulene nitrosite or its solutions in aprotic solvents are irradiated with red light.

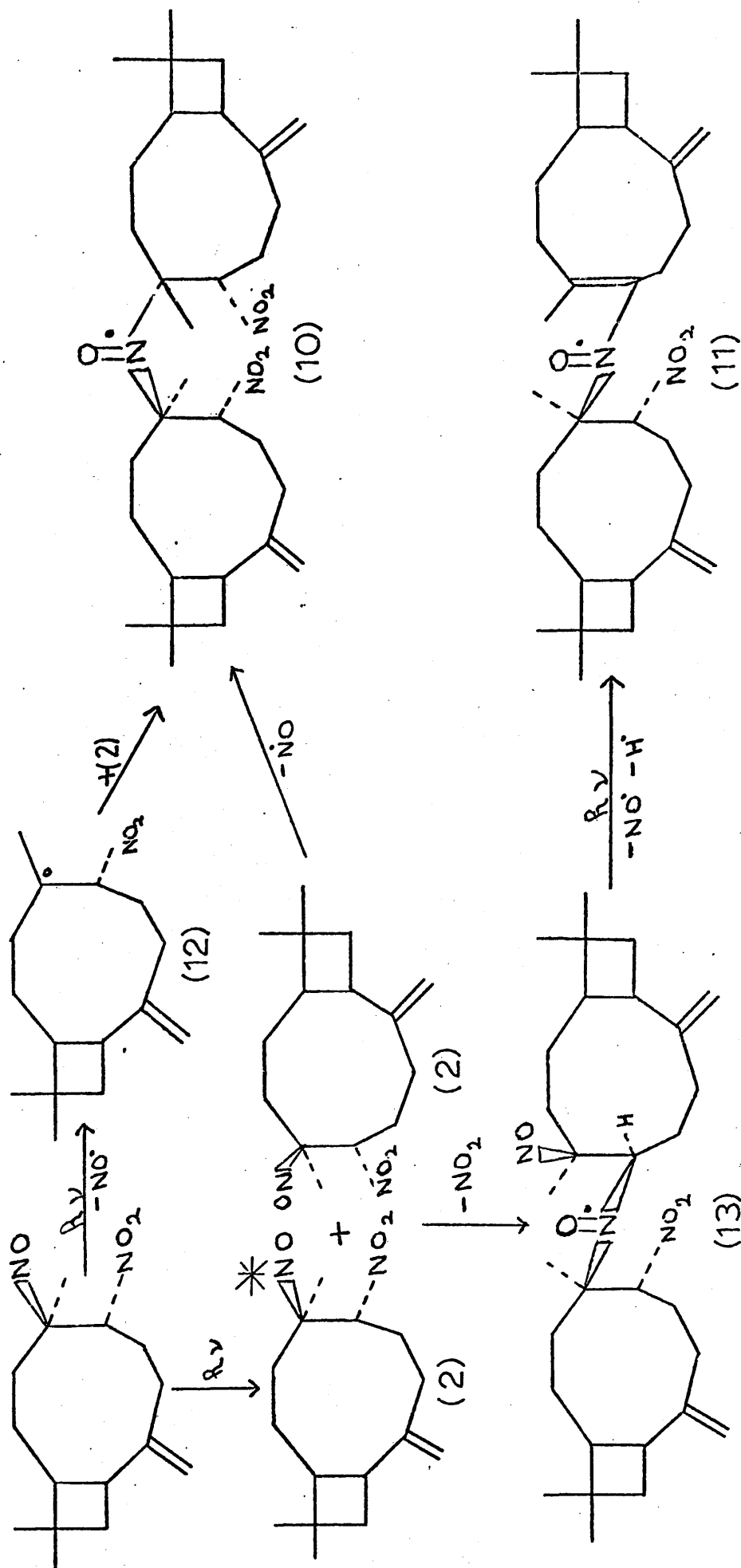


Figure 2.8 The mechanism postulated to explain the formation of the paramagnetic species observed when caryophyllene nitrosite or its solutions in aprotic solvents are irradiated with red light.

2. Scheme II is shown in figure 2.9, and involves a transannular addition of the red excited nitroso group, to either of the carbon to carbon  $\pi$  bonds present in the humulene nitrosite structure, producing intermediates, which are immediately stabilised, either by the loss of a proton, or by some further intermolecular reaction to the  $\pi$  systems of neighbouring molecules. The aliphatic radicals, or triplet states, which might be associated with the intermediates, could not be detected using e.p.r. spectroscopy. Scheme II would however produce two nitroxide radicals (22) and (23), containing the requisite structural units to be compatible with the experimental results. This second scheme has no direct precedent in the literature.

In an attempt to distinguish between the two mechanisms postulated above, the irradiation of solid humulene nitrosite with red light was followed in an e.p.r. spectrometer, to determine if an intermediate radical of the type predicted by scheme I, formed.

#### 2.2.3 Monitoring the irradiation of crystalline humulene nitrosite with red light as a function of time in an e.p.r. spectrometer

Figure 2.10, shows the spectra, recorded at periodic intervals during the irradiation of the polycrystalline samples of humulene nitrosite. In the initial stages of the irradiation the spectra show a greater complexity than the spectrum of radicals I + II shown in figure 2.5. These spectra were re-recorded after pumping for one hour at less than 0.1 mm Hg pressure, to remove any gaseous products, and the form of the spectra did not change, demonstrating, that the extra structure was not due to trapped  $\text{NO}^\bullet$  or  $\text{NO}_2^\bullet$ . The e.p.r. spectra are in fact composed of a

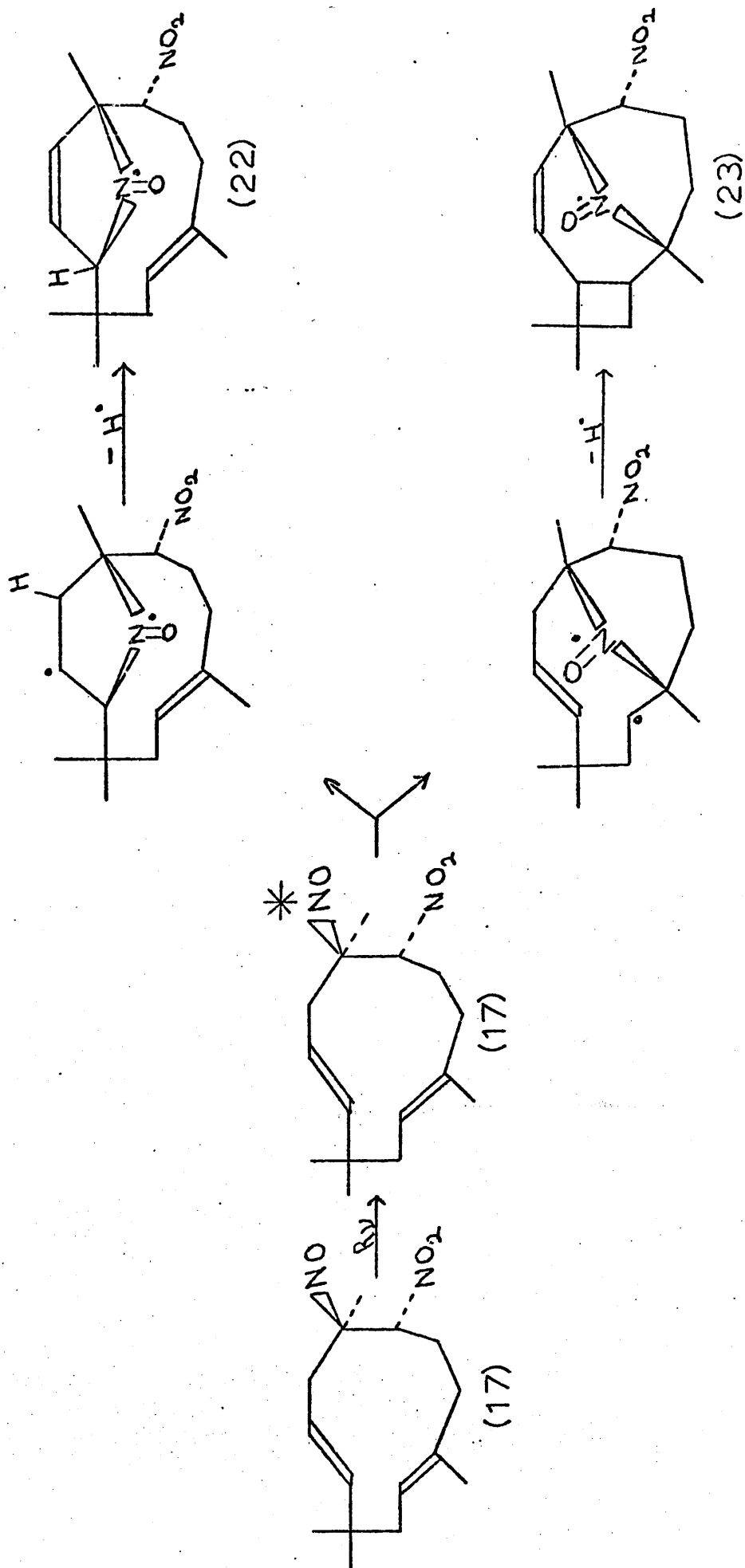


Figure 2.9 Photolysis scheme II, a mechanism postulated to explain the formation of the paramagnetic species observed when humulene nitrosite or its solutions in aprotic solvents are irradiated with red light.

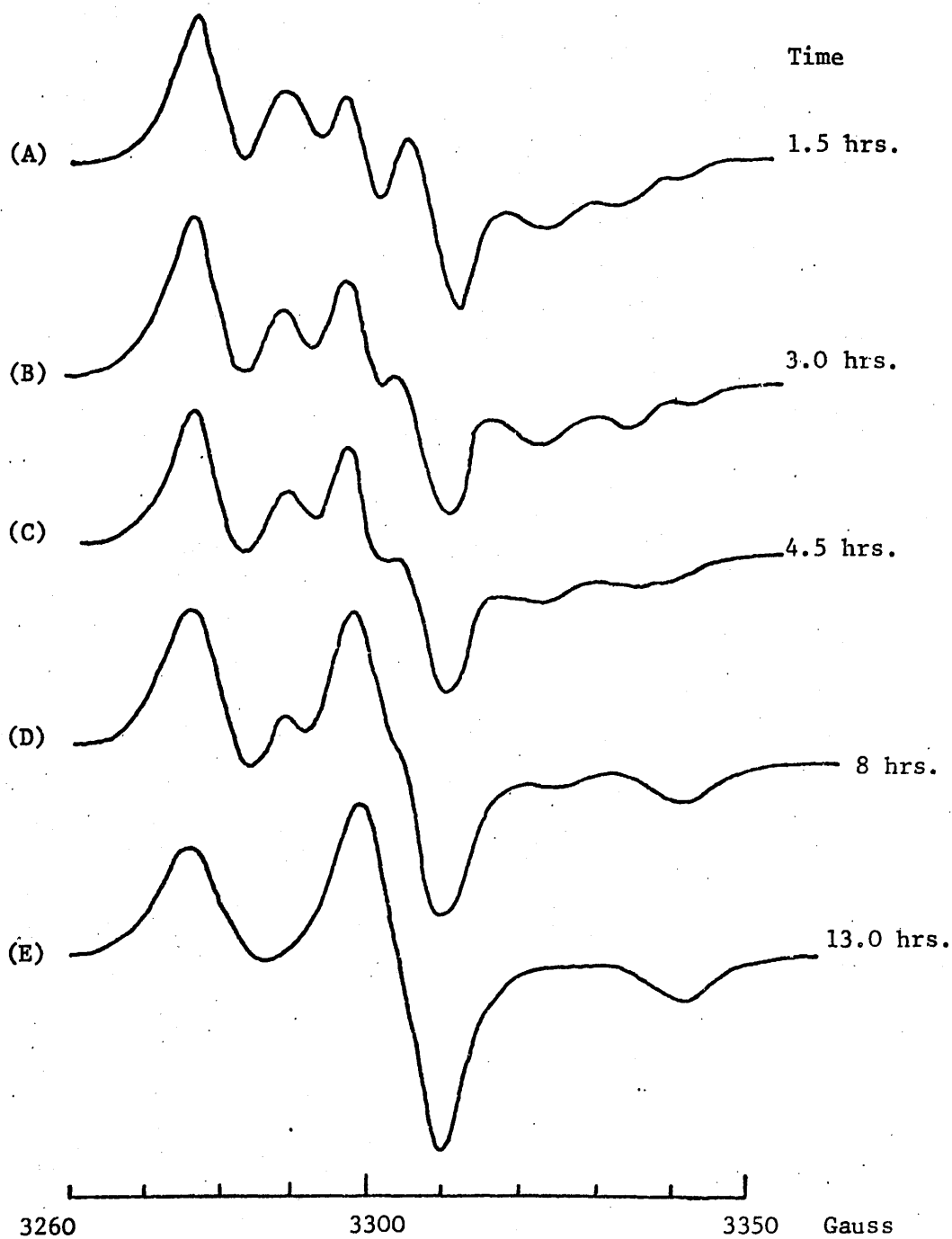


Figure 2.10 The e.p.r. spectra of polycrystalline samples of humulene nitrosite which have been irradiated with red light for respectively, (A) 1.5 hrs., (B) 3.0 hrs., (C) 4.5 hrs., (D) 8.0 hrs., and (E) 13.0 hrs.



super-position of the following spectra.

- 1) The polycrystalline e.p.r. spectrum of nitroxide radicals I plus II.
- 2) A spectrum, which arises from a transient paramagnetic species.

The relative amounts of radicals I plus II, and the transient species present at any stage of the irradiation, can be determined by comparing the areas of their respective integrated peaks. The e.p.r. spectrum shown in figure 2.11, is that of the transient species, and is obtained by subtracting a suitably scaled spectrum of radicals I plus II, from the observed spectrum after 1.5 hrs. irradiation. If the spin Hamiltonian for the nitroxide radical is written in the form,

$$\mathcal{H} = \beta_e \underline{H} \cdot \underline{g} \cdot \underline{S} + \sum_{\text{over the nuclei}} \underline{S} \cdot \underline{A} \cdot \underline{I}$$

then the spectrum shown in figure 2.11, can be analysed in terms of a superposition of six curves of the type described by Kneubühl (see appendix 7 section 7'.9'.), and the principal components of the  $g$  tensor, and the hyperfine tensor  $A$ , along with the line-broadening parameter,  $\beta$  can be obtained from it. The analysis of the spectrum in figure 2.11. shows that it arises from the interaction of an unpaired electron with one  $^{14}\text{N}$  nucleus and one proton. The transient species, is thus a nitroxide radical, which contains the molecular fragment  $\text{R}_1\text{R}_2\text{R}_3\text{C}\cdot\text{NO}-\text{CHR}_4\text{R}_5$ . The spin Hamiltonian parameters of this radical, radical III, are shown in table 2.6.

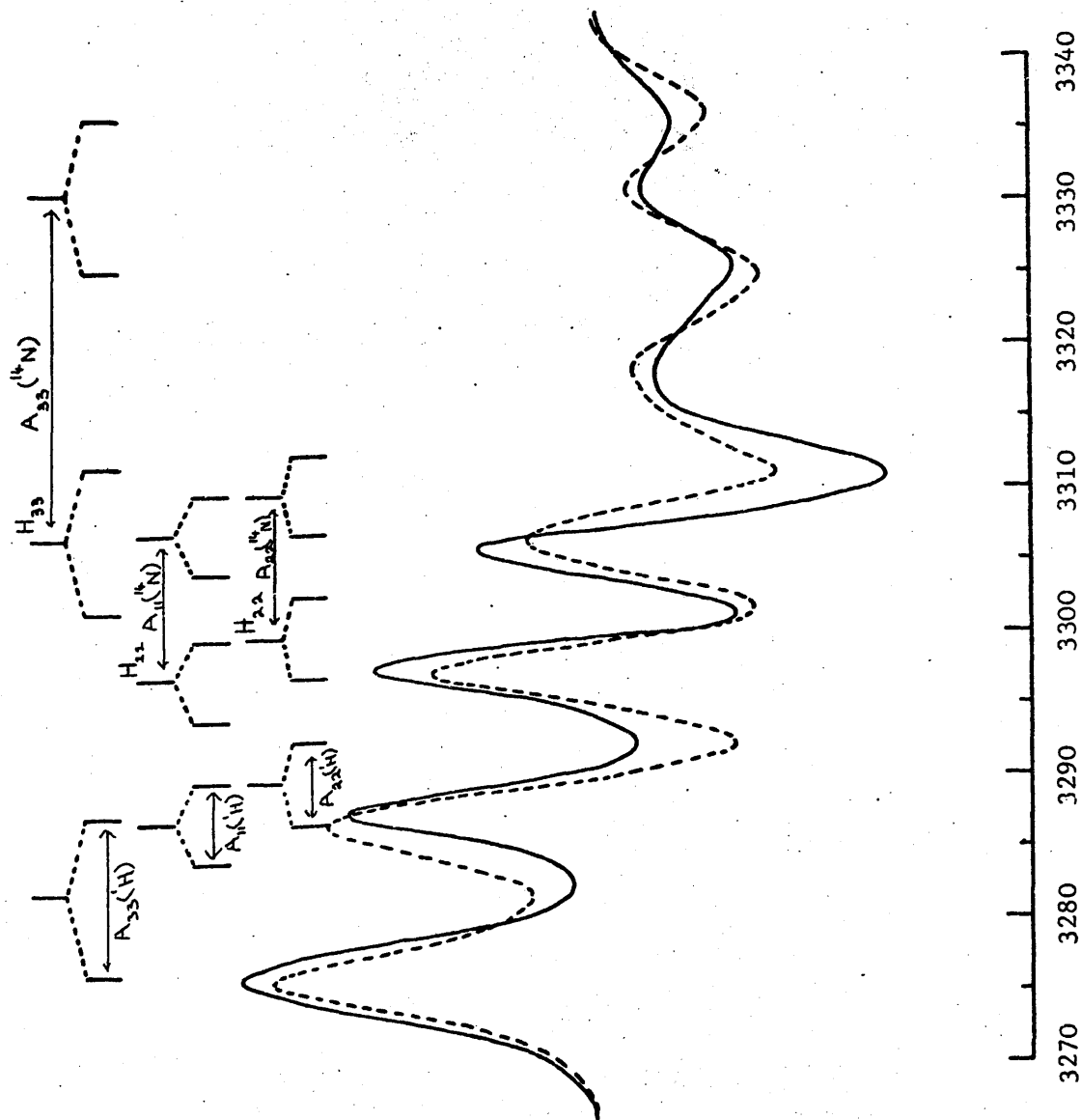


Figure 2.11 The e.p.r. spectrum of a dilute polycrystalline sample of the transient nitroxide radical III observed when humulene nitrosite is irradiated with red light. The dotted line represents the calculated spectrum for nitroxide radical III.

Table 2.6

The spin Hamiltonian parameters for nitroxide radical III

$g_{11}$	$g_{22}$	$g_{33}$	$\langle g \rangle$	
2.0091	2.0073	2.0034	2.0066	
$A_{11}(^{14}\text{N})$	$A_{22}(^{14}\text{N})$	$A_{33}(^{14}\text{N})$	$a(^{14}\text{N})$	
10.0G	10.0G	24.6G	14.9G	
$A_{11}(^1\text{H})$	$A_{22}(^1\text{H})$	$A_{33}(^1\text{H})$	$a(^1\text{H})$	$\beta$
5.4G	5.4G	10.5G	7.1G	4.0G

Broadening functions are assumed to have the Gaussian form  $\left[ (2\pi)^{-1/2} \beta^{-1} \exp \left[ -\frac{(H-H')^2}{2\beta^2} \right] \right]$ . The limits of error for  $g_{11}$ ,  $g_{22}$ ,  $g_{33}$ ,  $\langle g \rangle$ ,  $A_{11}(^{14}\text{N})$ ,  $A_{22}(^{14}\text{N})$ ,  $A_{33}(^{14}\text{N})$ ,  $a(^{14}\text{N})$ ,  $A_{11}(^1\text{H})$ ,  $A_{22}(^1\text{H})$ ,  $A_{33}(^1\text{H})$ ,  $a(^1\text{H})$  are respectively  $\pm 0.0003$ ,  $\pm 0.0003$ ,  $\pm 0.0002$ ,  $\pm 0.0003$ ,  $\pm 0.5\text{G}$ ,  $\pm 0.5\text{G}$ ,  $\pm 0.1\text{G}$ ,  $\pm 0.5\text{G}$ ,  $\pm 0.5\text{G}$ ,  $\pm 0.1\text{G}$ , and  $\pm 0.5\text{G}$ .

If at any stage of the irradiation the products are dissolved in chloroform, then radical III immediately disproportionates to diamagnetic species and the e.p.r. spectrum decreases greatly in intensity and is identical to the spectrum of nitroxide radicals I plus II shown in figure 2.5. If the e.p.r. spectrum of this solution is recorded at 77°K in the glass, all the structure associated with radical III is seen to have gone. Nitroxide radical III is only stable when stored in the dark in the solid state.

This discovery of a transient nitroxide radical III, containing the molecular unit  $\text{R}_1\text{R}_2\text{R}_3\text{C}-\dot{\text{N}}\text{O}-\text{CHR}_4\text{R}_5$ , and which is stable when stored in the solid state in the dark, is in very good agreement with photolysis scheme I. The kinetics associated with scheme I, also agree well with those determined experimentally. Figure 2.12 is a graphical representation of how the relative concentrations of

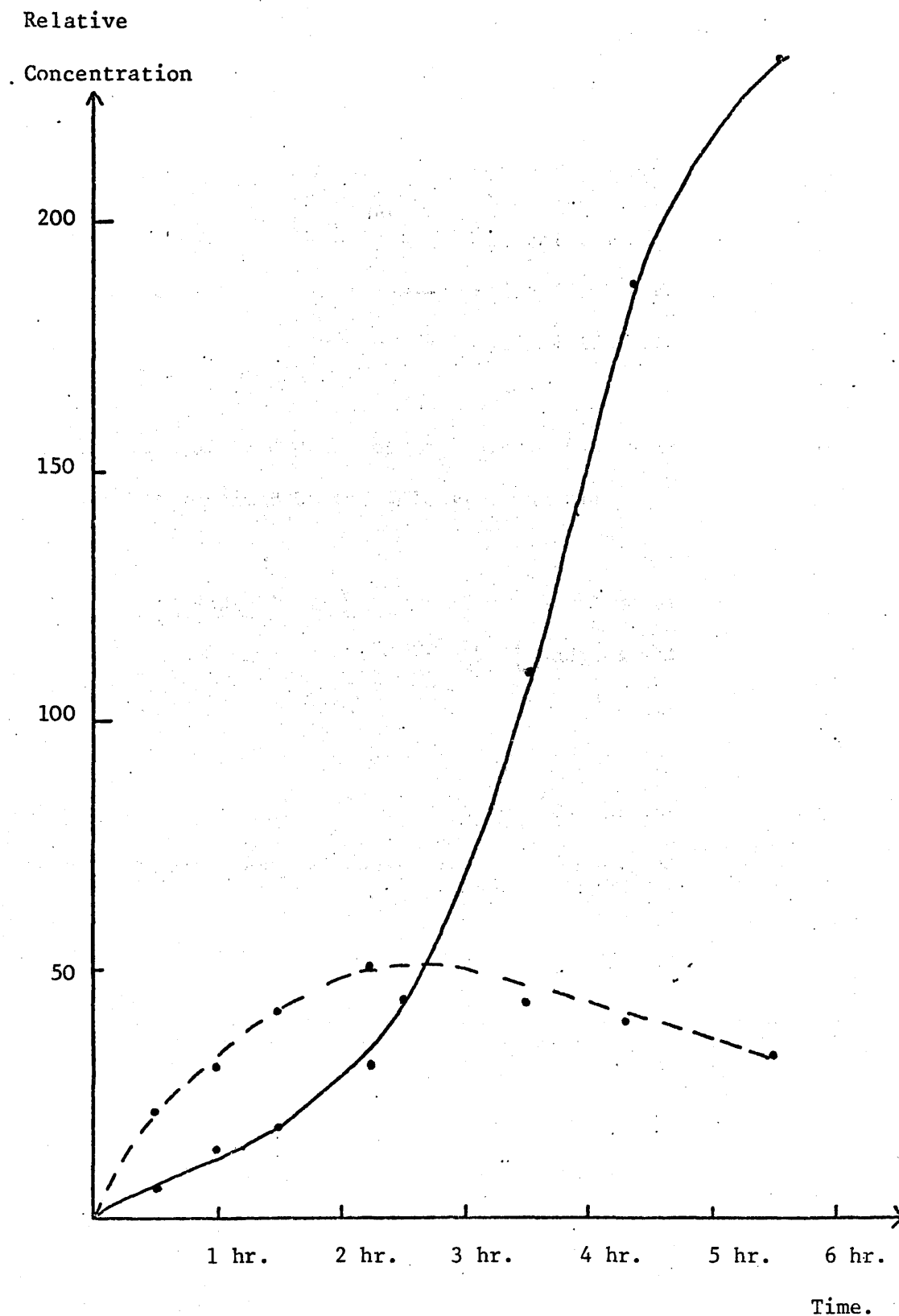
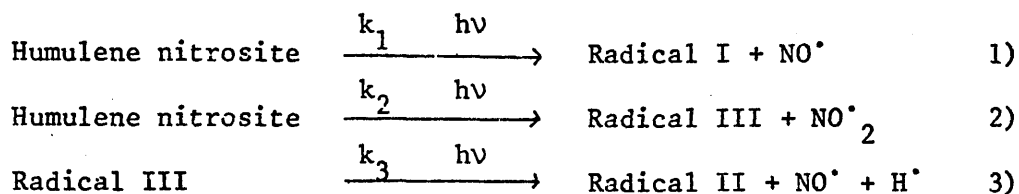


Figure 2.12 The irradiation of a polycrystalline sample of humulene nitrosite with red light. The relative concentrations of radicals I + II, (—) and radical III, (---), are plotted as a function of the irradiation time.

radicals I plus II and radical III are found to vary with time. If photolysis scheme I is represented by the following three equations.



then the rate of production of the intermediate nitroxide radical III, will be governed by the following equation,

$$\frac{d [\text{Radical III}]}{dt} = k_2 I [\text{humulene nitrosite}]^2 - k_3 I [\text{Radical III}]$$

where I is the light intensity. In the initial stages of the reaction the first term of this equation must dominate and the concentration of radical III increases. However, as the concentration of radical III increases, so does the rate of its photochemical decomposition to nitroxide radical II, and eventually the two terms will produce a steady state situation, with the concentration of radical III remaining constant. Towards the end of the photolysis the concentration of radical III falls to zero. The rate of production of nitroxide radical II, is dependent on the concentration of radical III, and will increase up to the point where radical III achieves a steady state concentration, whereupon it will remain almost constant.

Photolysis scheme II can not adequately account for the three nitroxide radicals found experimentally, as it postulates the formation

of only two nitroxide radicals (22) and (23). The radical (22), which contains the molecular unit  $R_1R_2R_3C-\dot{N}O-CHR_4R_5$ , is capable of disproportionation to diamagnetic species, and thus might have been considered as a possible transient intermediate. This is however, unlikely, since the transient radical experimentally is found to reach a steady state concentration, when the reaction is approximately one eighth complete. It does not seem reasonable, that in the solid state with restricted movement, that radicals at this level of concentration could be sufficiently close for disproportionation to be substantial.

The experimental results obtained in this section are consistent with photolysis scheme I, but they can not exclude the possibility, that both schemes I and II are concurrently in operation. Moreover on completing the irradiation, the products are magnetically dilute, indicating that diamagnetic species may also be present.

When caryophyllene nitrosite is irradiated in red light 86% of the gaseous products evolved is nitrogen,<sup>76</sup> which is not produced in the mechanism shown in figure 2.8 by which the nitroxide radicals form. This nitrogen may be evolved during secondary reactions, which follow the initial photochemical steps. If this is the case, then the diamagnetic species formed during these secondary reactions would predominate. Attempts were made to use chromatographic techniques to isolate the products formed when humulene nitrosite was irradiated with red light, in order to, characterise the individual nitroxide radicals formed, and determine if any diamagnetic species are also present.

2.3. Initial attempts at using chromatographic techniques to isolate the products formed on irradiating humulene nitrosite in red light

### 2.3.1 Detection of the impurities present in humulene nitrosite and its subsequent purification

During a series of preliminary chromatographic experiments on humulene nitrosite and its photolysis products, it was observed that the humulene nitrosite obtained from Mitchell, contained two clear crystalline impurities. These two impurities were removed using silica column chromatography, the purity of the humulene nitrosite being monitored using infra-red and  $^1\text{H}$  n.m.r. spectroscopy. Full details of this purification are contained in appendix 2 section 2.2.1'. The two impurities were obtained as pure crystalline solids and elemental analyses, and  $^1\text{H}$  n.m.r., infra-red, and mass spectra were obtained for both species. As the origin of these impurities was unknown, no attempt was made at this stage to characterise them.

Having thus obtained a sample of pure humulene nitrosite free of any contaminants all the experiments described in section 2.2, were repeated, using this purified material. In every case the nitroxide radicals observed by irradiating humulene nitrosite and its solutions, were identical in structure and behaviour to those described previously. Attempts were now resumed to isolate the individual products of the photolysis reaction using chromatographically purified humulene nitrosite as the starting material.

### 2.3.2 Isolation of the products formed when chromatographically purified humulene nitrosite is irradiated with red light

The products formed when pure humulene nitrosite is irradiated with red light, were separated into three components by using silica t.l.c. with ether: pet. ether, (50:50) as solvent. The details of this separation are outlined in appendix 2 section 2.2.2' (a). These products can be classified into two groups,

since all the paramagnetic species were found at  $R_{f.} = 0$ , all the components of  $R_{f.} > 0$ , being diamagnetic.

1) The characterisation of the paramagnetic species

A yellow solid was extracted from the region of  $R_{f.} = 0$ , which accounted for approximately 10% by weight of the total products. The e.p.r. spectrum of a dilute degassed solution of this yellow solid in chloroform, is shown in figure 2.13. Two nitroxide radicals, which contain the structural unit  $R_1R_2R_3C-\dot{N}O-CR_4R_5R_6$  are present. They have similar isotropic  $\langle g \rangle$  factors and isotropic coupling constants  $a(^{14}N)$ .

Radical I<sub>A</sub>      [ isotropic  $\langle g \rangle = 2.0058 \pm 0.0002$ ;  
isotropic  $a(^{14}N) = 14.6 \pm 0.2G$  ]

Radical I<sub>B</sub>      [ isotropic  $\langle g \rangle = 2.0062 \pm 0.0002$ ;  
isotropic  $a(^{14}N) = 14.9 \pm 0.2G$  ]

Nitroxide radical II was not observed in this mixture since it decomposes on the silica surface.

To determine if both radicals I<sub>A</sub> and I<sub>B</sub> are produced in the photolysis reaction, or if one forms due to reactions on the activated silica surface, the e.p.r. spectra obtained from the photolysis products prior to their being chromatographed were re-examined. The e.p.r. spectrum obtained from a degassed chloroform solution at 295°K, containing nitroxide radicals I and II, which had been allowed to stand until nitroxide radical II had completely disproportionated, was identical to the spectrum shown in figure 2.13 and contained both nitroxide radicals I<sub>A</sub> and I<sub>B</sub>.

The line shape of the polycrystalline e.p.r. spectrum, obtained from the yellow solid of  $R_{f.} = 0$  suggested that the



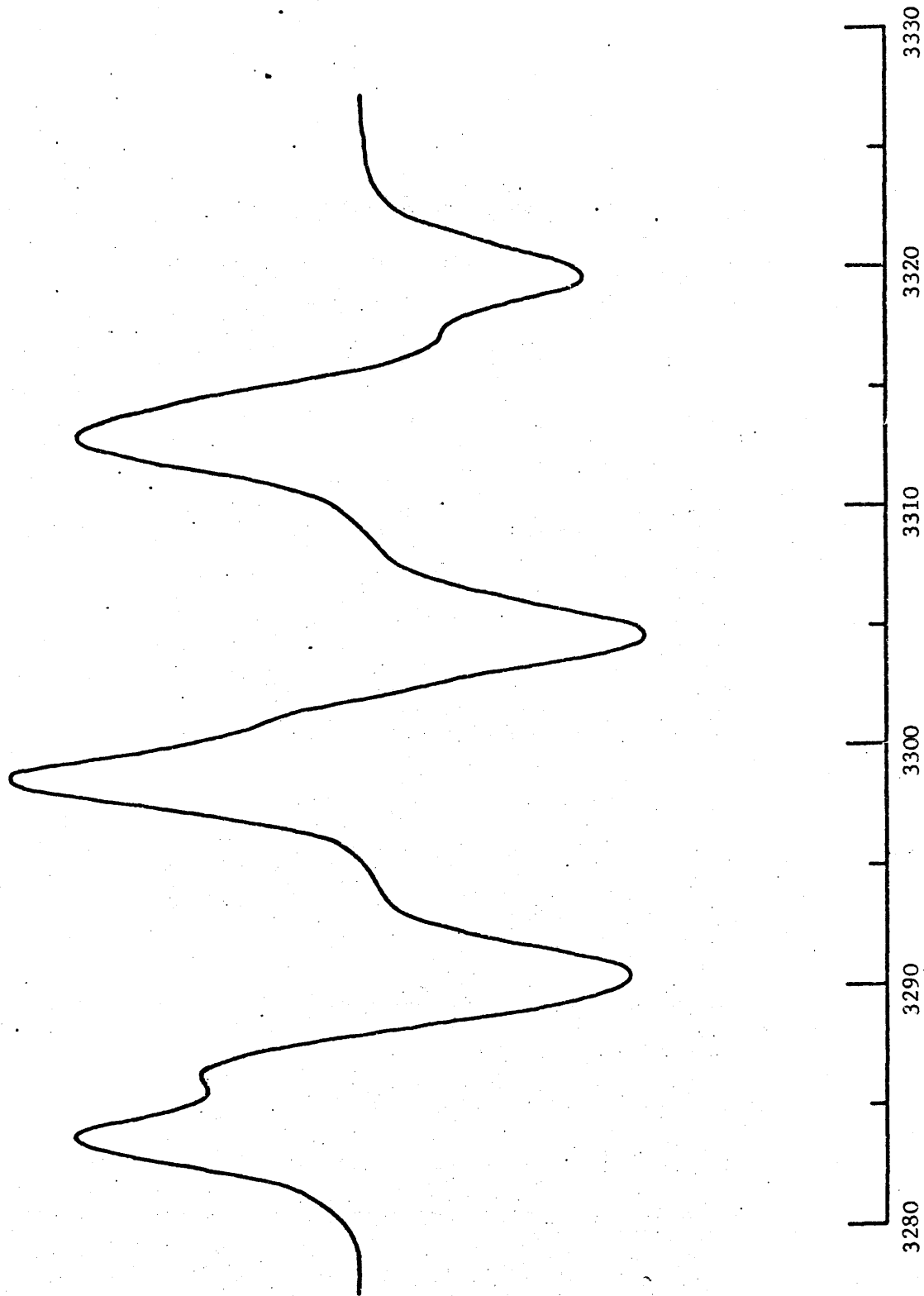


Figure 2.13 The e.p.r. spectrum of a dilute degassed solution in chloroform of the components of  $R_f = 0$ , Gauss. namely radicals  $I_A$  and  $I_B$  isolated chromatographically from the product of humulene nitrosite (17) irradiated with red light.

sample was magnetically dilute, indicating that the sample might contain some diamagnetic species as well as nitroxide radicals  $I_A$  and  $I_B$ .

This solid was further chromatographed using silica plates with ether: pet.ether (80:20) as solvent, an extended run of approximately two hours, producing a broad yellow band. The regions of this band of higher  $R_f$  value contained a yellow solid enriched in nitroxide radicals  $I_A$  and  $I_B$ . In the regions of lower  $R_f$  value, mainly diamagnetic species were present. The material enriched in nitroxide radicals  $I_A$  and  $I_B$  could not be crystallised, and attempts were made to separate radicals  $I_A$  and  $I_B$  as follows.

- 1) The period of chromatographic separation was extended.
- 2) Silica column chromatography was used with various different solvents being tried.
- 3) Finally alumina and cellulose t.l.c. techniques were used.

All such attempts were however, unsuccessful, and the longer the nitroxide radicals were kept on the activated silica surface, the more impure they became due to decomposition.

Figure 2.14 shows the infra-red spectrum of the solid enriched in nitroxide radicals  $I_A$  and  $I_B$ . A comparison of the pertinent data obtained from this spectrum and the infra-red spectrum of humulene nitrosite are summarised in appendix 2, table 2.7. This comparison clearly shows, that the radicals retain all the structural units present in humulene nitrosite, with the exception of the nitroso group. This is consistent with the nitroxide radicals present having the structure shown below, which is the radical postulated in scheme I.

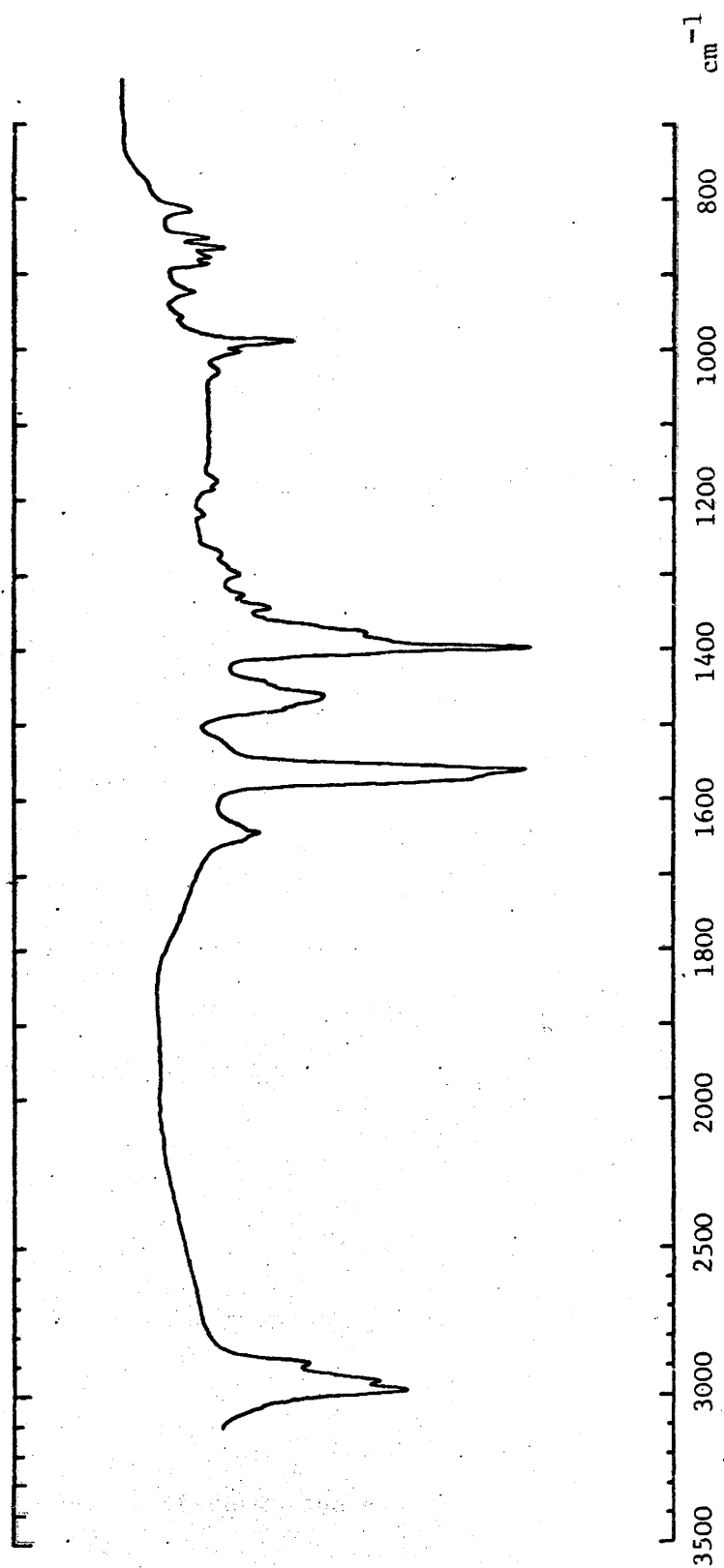
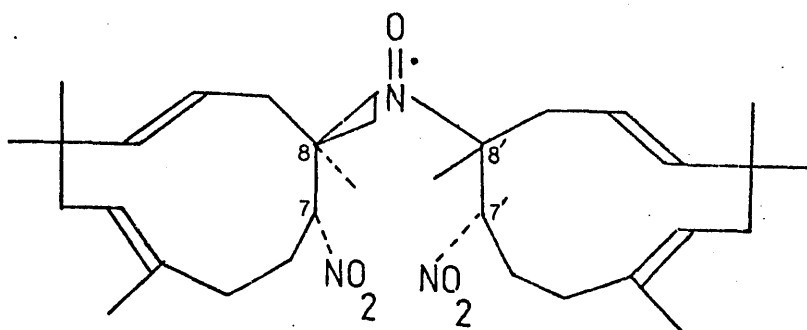


Figure 2.14 The infra-red spectrum recorded in a KBr disc in the range  $3,500 - 800 \text{ cm}^{-1}$  of a component enriched in nitroxide radicals  $I_A$  and  $I_B$  (19) obtained chromatographically from the product of humulene nitrosite irradiated with red light.



Nitroxide radical I (19)

The structure shown above could exist in various diastereomeric forms. Humulene nitrosite itself is a racemic mixture of the two enantiomers shown in figure 2.3. Figure 2.15 illustrates the two diastereomeric forms of radical I, which arise when the ( $\pm$ ) enantiomers of humulene nitrosite combine in such a way that the nitroxide grouping on carbons 8 and 8' lies trans to both the nitro groups attached to carbons 7 and 7'. The geometry at carbon 8' can of course vary, as the initial photochemical cleavage of the C-N bond of the nitroso group at this position, produces a planar aliphatic radical to which the nitroso group of a neighbouring molecule of humulene nitrosite can approach in either direction. There are in total therefore four possible diastereomeric forms of radical I, and in each the nitroxide grouping would experience a different chemical environment. Nitroxide radicals  $I_A$  and  $I_B$  would thus appear to represent two of the diastereomeric forms of structure (19).

Figure 2.16 shows the e.p.r. spectrum obtained from a solid sample of the material enriched in nitroxide radicals  $I_A$  and  $I_B$ . The line shape of this spectrum, indicates that the sample is still magnetically dilute, however the large bulk of the molecule may be shielding the nitroxide group from further interaction. The spin Hamiltonian parameters obtained from an analysis of this spectrum are contained in table 2.8.

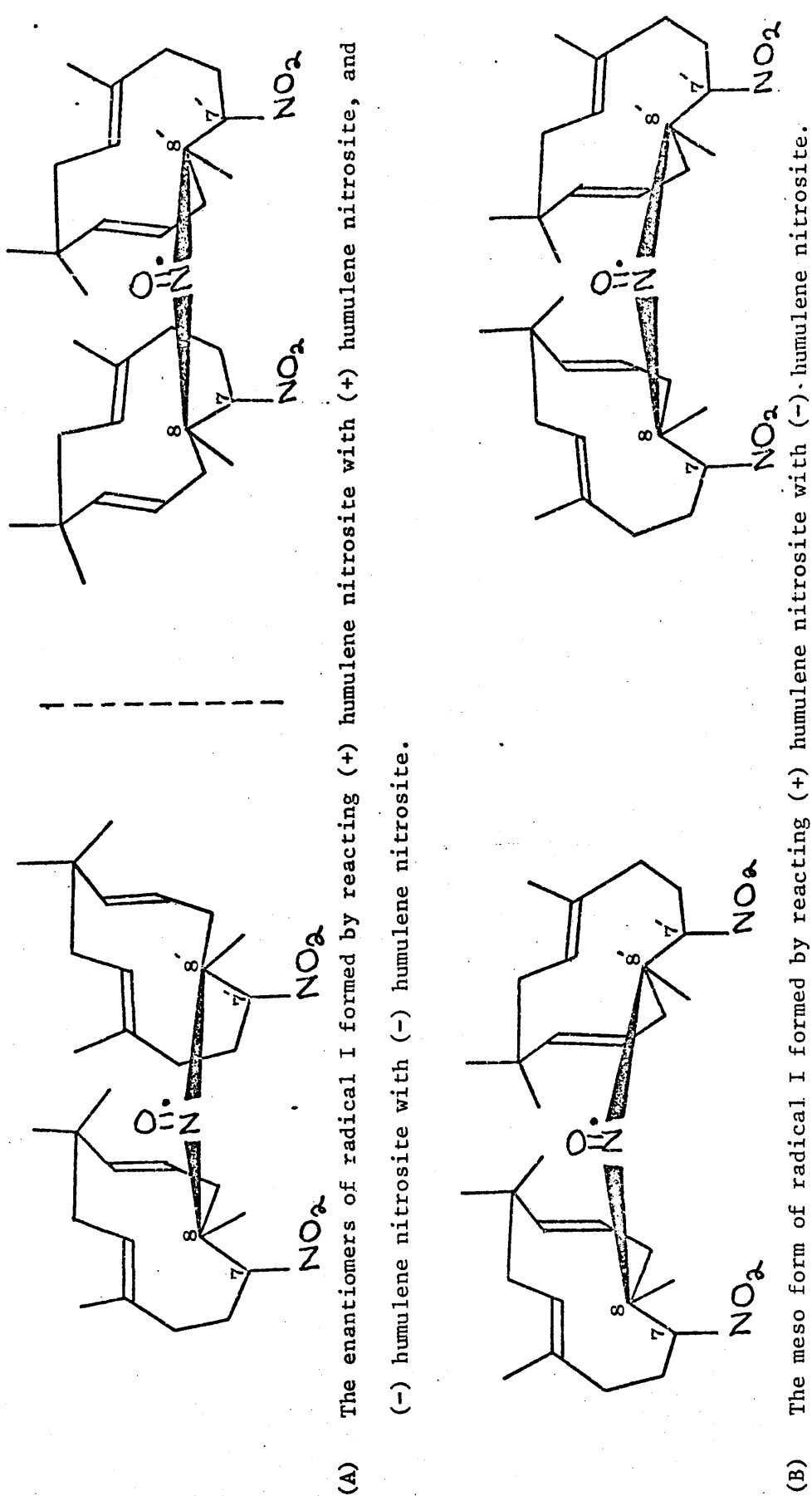


Figure 2.15 The diastereomeric forms of nitroxide radical I (19), for the specific case in which the nitroxide grouping attached to C<sub>8</sub> and C<sub>8</sub>, has a trans geometry to the nitro group on C<sub>7</sub> and the nitro group on C<sub>7</sub>.

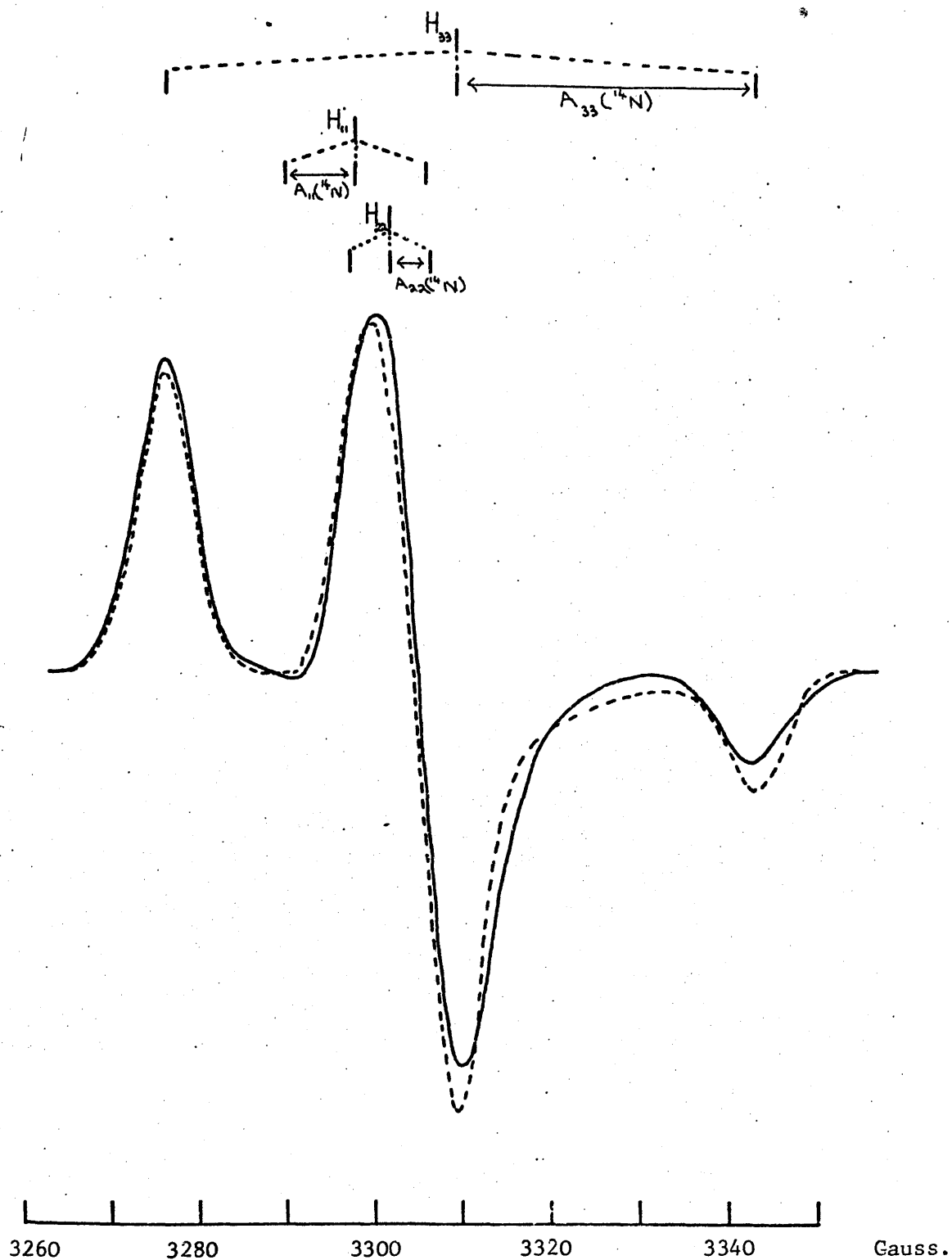


Figure 2.16 The e.p.r. spectrum of a polycrystalline sample of the solid enriched in nitroxide radicals  $I_A$  and  $I_B$ , isolated from the product of the irradiation of humulene nitrosite (17) with red light. The dotted line represents the calculated spectrum.

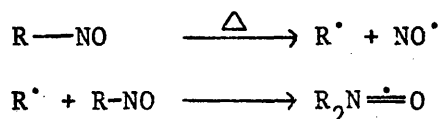
Table 2.8

The spin Hamiltonian parameters for nitroxide radicals I<sub>A</sub> and I<sub>B</sub>

$g_{11}$	$g_{22}$	$g_{33}$	$\langle g \rangle$	
2.0089	2.0065	2.0019	2.0058	
$A_{11}(^{14}\text{N})$	$A_{22}(^{14}\text{N})$	$A_{33}(^{14}\text{N})$	$a(^{14}\text{N})$	$\beta$
8.0G	4.5G	33.1G	15.2G	2.5G

The limits of error for  $g_{11}$ ,  $g_{22}$ ,  $g_{33}$ ,  $\langle g \rangle$ ,  $A_{11}(^{14}\text{N})$ ,  $A_{22}(^{14}\text{N})$ ,  $A_{33}(^{14}\text{N})$ , and  $a(^{14}\text{N})$  are respectively,  $\pm 0.0003$ ,  $\pm 0.0003$ ,  $\pm 0.0002$ ,  $\pm 0.0003$ ,  $\pm 0.5\text{G}$ ,  $\pm 0.5\text{G}$ ,  $\pm 0.2\text{G}$ ,  $\pm 0.5\text{G}$ .

To test the hypothesis that nitroxide radicals I<sub>A</sub> and I<sub>B</sub> are diastereomeric forms of structure (19), a sample of (19) was prepared by heating humulene nitrosite in an oil bath at  $\sim 112^\circ\text{C}$ , until the sample decomposed to a yellow oil. The application of heat to C-Nitroso compounds, produces nitroxide radicals by the process of C-N bond cleavage shown below.<sup>7,12,17,18</sup>



Thus on heating humulene nitrosite the diastereomeric forms of nitroxide radical I should form. The e.p.r. spectrum of a dilute degassed chloroform solution, of the oil obtained by heating humulene nitrosite, is identical to the spectrum shown in figure 2.13, and both radicals I<sub>A</sub> and I<sub>B</sub> are present.

The mechanisms proposed for the photolysis reactions of humulene nitrosite, and caryophyllene nitrosite shown in figures 2.7 and 2.8 respectively are completely analogous.

When caryophyllene nitrosite is irradiated with red light or heated only one nitroxide radical, containing the structural unit  $R_1R_2R_3C-\dot{N}O-CR_4R_5R_6$ , is produced and this radical is based on structure (10). Caryophyllene nitrosite exists as a single enantiomer and not a racemic mixture of enantiomers and hence only two diastereomeric forms of (10) were possible, of which one appears to form stereospecifically.

2) Attempts to characterise the diamagnetic species formed when humulene nitrosite is irradiated with red light

The diamagnetic species abstracted from the region of  $R_f > 0$  accounted for approximately 90% of the products by weight. Two major components were isolated from the regions of  $R_f = 0.37$  and  $R_f = 0.8$  and these are discussed below.

a) The components of  $R_f = 0.37$

The components extracted from the band of  $R_f = 0.37$  constituted a mixture from which a pure, clear crystalline product was extracted after rechromatographing using ether: pet. ether (70:30) as solvent and recrystallising from ethanol. An elemental analysis of this crystalline product yielded the empirical formula  $C_{15}H_{24}N_2O_4$  based on the results contained in table 2.9. of appendix 2. A comparison was undertaken of the  $^1H$  n.m.r. and infra-red spectra of this clear crystalline derivative, with the corresponding spectra of humulene nitrosite, and the pertinent data obtained are summarised in tables 2.10, and 2.11, respectively. Figure 2.17 shows the  $^1H$  n.m.r. spectra of the clear crystals of  $R_f = 0.37$  and of humulene nitrosite in the  $\tau$  range 4 to 10.

The comparisons described above enabled the crystalline product of  $R_f = 0.37$  to be characterised as the di-nitro derivative of



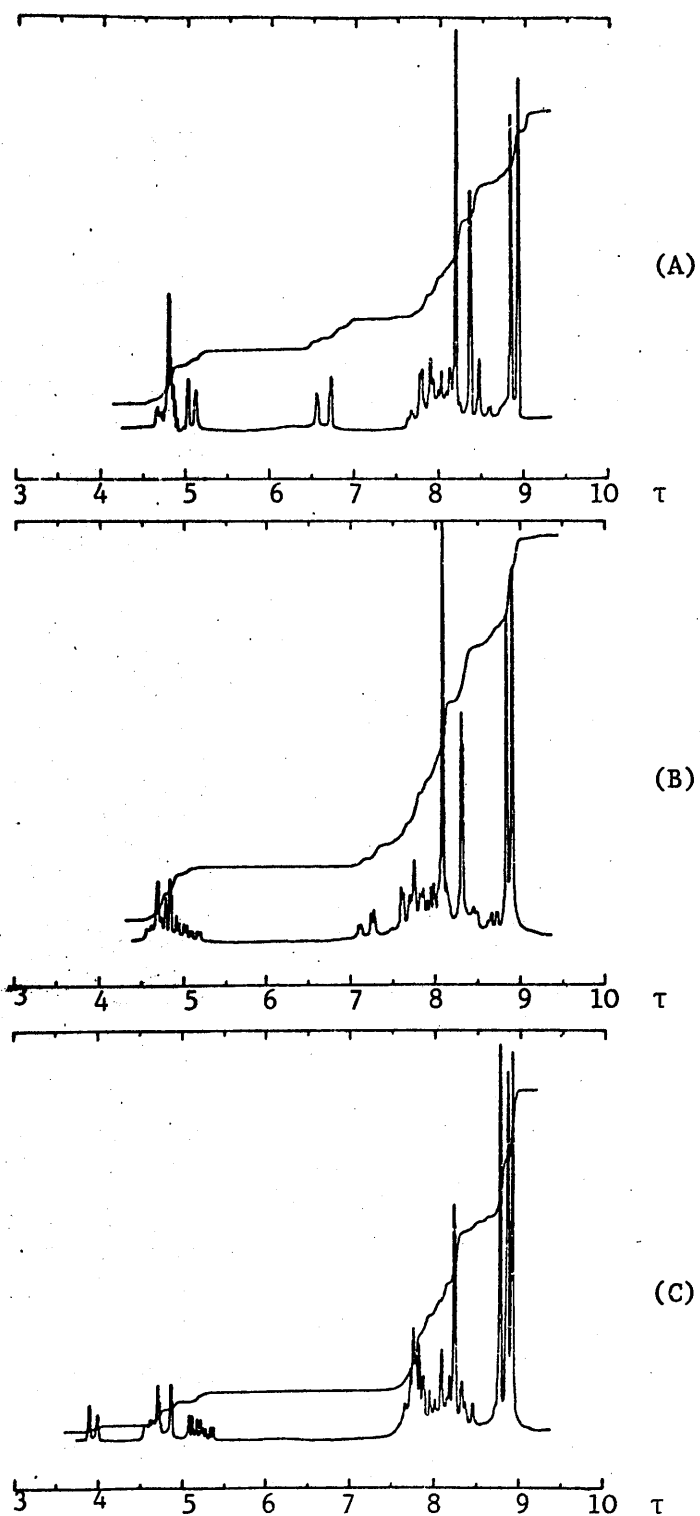
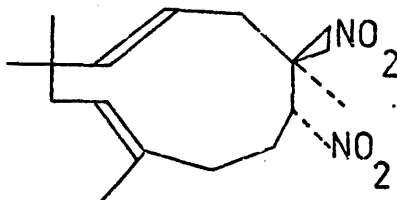


Figure 2.17 The  $^1\text{H}$  n.m.r. spectra of dilute solutions of (A) nitro-nitrato-humulene (26), (B) dinitro-humulene (24), and (C) humulene nitrosite (17), in  $\text{CDCl}_3$ , recorded in the  $\tau$  range 3 to 10.

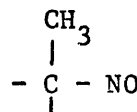
humulene shown below.



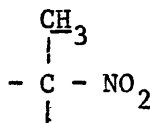
Dinitro - humulene (24)

The characterisation is based on the following observations.

- 1) The infra-red and  $^1\text{H}$  n.m.r. spectra of the clear crystals show that the following group is not present



- 2) A singlet methyl resonance is present in the  $^1\text{H}$  n.m.r. spectrum of the clear crystals at  $\tau = 8.08$  and is assigned to the following grouping.



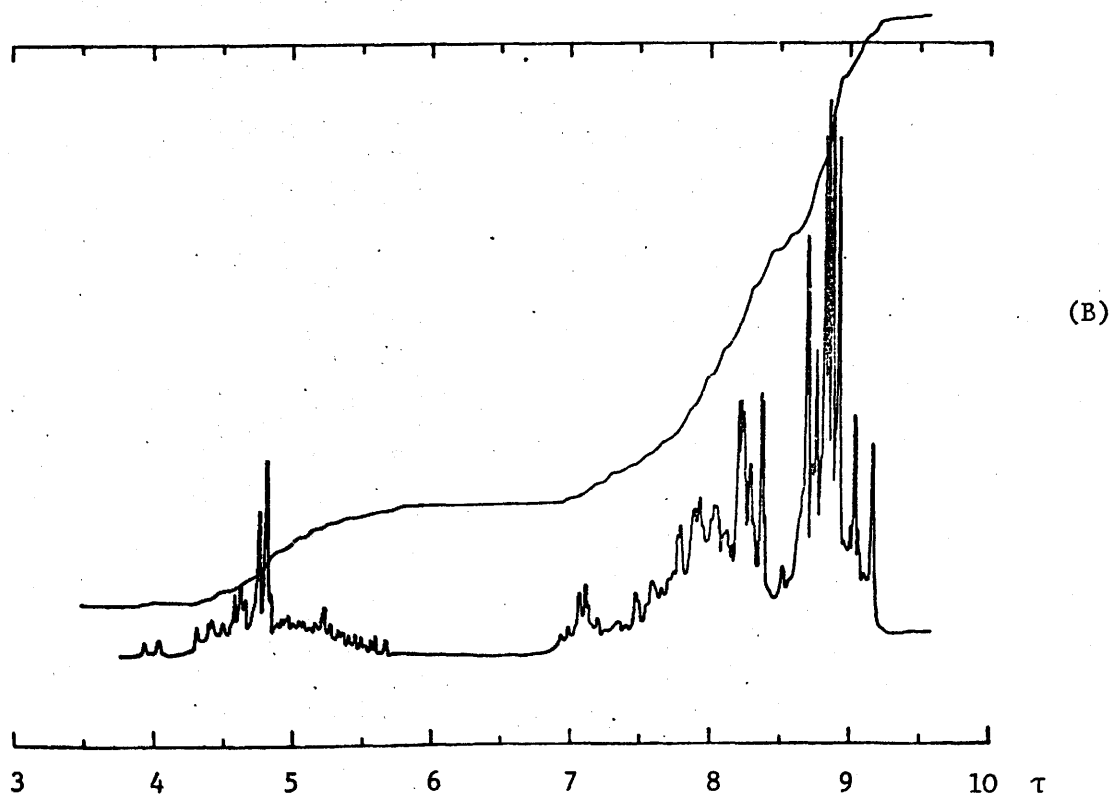
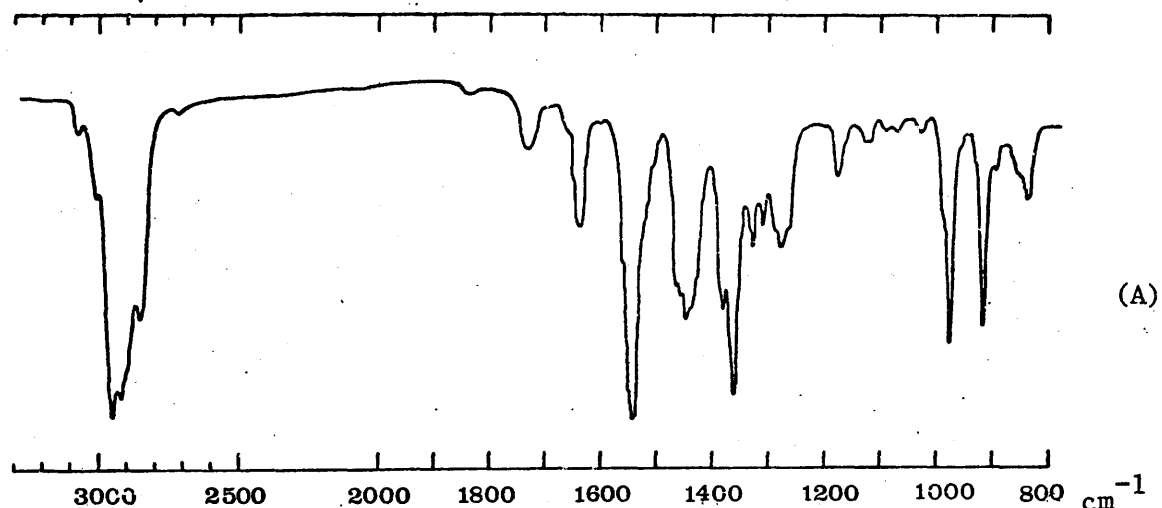
The infra-red spectrum also shows absorptions at  $1545\text{ cm}^{-1}$  and  $1355\text{ cm}^{-1}$ , which are consistent with the asymmetric and symmetric stretching vibrations of a nitro group attached to a tertiary carbon atom.

- 3) The spectroscopic evidence is consistent with the retention of all the other structures present in humulene nitrosite.
- 4) The mass spectra of humulene nitrosite and this crystalline photolysis derivative, are identical in every major peak, other than that of the parent ion.

b) The components of  $R_f = 0.8$

The material extracted from the band of  $R_f = 0.8$  was an oil and no crystalline derivatives could be obtained on work up. The  $^1\text{H}$  n.m.r. and infra-red spectra of this oil, are shown in figure 2.18. It is apparent from the complexity of these spectra, that more than

Figure 2.18 (A) The infra-red spectrum recorded in a  $\text{CCl}_4$  solution in the range  $3,300 - 800 \text{ cm}^{-1}$ , and (B) the  $^1\text{H}$  n.m.r. spectrum recorded in a  $\text{CDCl}_3$  solution in the  $\tau$  range 3 to 10, of the components of  $R_f = 0.8$  namely (41), (42) and (43), isolated from the product of needle crystals of humulene nitrosite (17) irradiated with red light.



one humulene based structure is present, however further attempts to isolate the components of the mixture using chromatography were unsuccessful. Appendix 2, section 2'.2'.2'(d), contains a summary of the pertinent data, which can be abstracted from a comparison of these spectra with the corresponding spectra of humulene nitrosite. From these comparisons, the oil is shown to contain a mixture of compounds, perhaps isomeric, which are based either on a humulene structure or a rearrangement of it, and have a single nitro group as the only functional group attached.

At this stage in the investigation, the components of the oil of  $R_f = 0.8$  could not be fully characterised. Moreover the nature of the mechanism by which this oil and the other diamagnetic component, dinitro-humulene (24), formed was not understood at this stage. It is worth pointing out however, that the irradiations were performed in the absence of air, and molecular oxygen was not involved in the formation of dinitro-humulene (24).

It was observed that the diamagnetic species of  $R_f > 0$  produced small traces of nitroxide radicals, if they were allowed to stand in contact with the atmosphere. If these same diamagnetic species were stored under a  $N_2$  atmosphere, then no nitroxide radicals formed. The infra-red and  $^1H$  n.m.r. spectra of the major diamagnetic components at  $R_f = 0.37$ , and  $R_f = 0.8$ , showed no change when recorded before and after this oxidation process, and the e.p.r. spectra showed that only minute traces of nitroxide radicals were forming. It appears that the oxidation of some minor photolysis product is responsible for the formation of the nitroxides, and the major diamagnetic components at  $R_f = 0.37$  and  $R_f = 0.8$  are not involved. Table 2.12 of appendix 2 section 2'.2'.2'(e), shows the distribution of the nitroxide radicals as a function of the  $R_f$ .

value of the diamagnetic precursor from which they were oxidised.

Two of the nitroxide radicals formed when humulene nitrosite is irradiated in red light, radicals II and III, contain the structural unit  $R_1R_2R_3\dot{C}-NO-CHR_4R_5$ , and could disproportionate forming hydroxylamines and nitrones. To determine if these hydroxylamines were the precursors of the nitroxide radicals formed on standing in air, the isotropic spin Hamiltonian parameters of these radicals were compared with the isotropic spin Hamiltonian parameters of radicals I, II, and III from which the hydroxylamines originated. The two sets of isotropic spin Hamiltonian parameters were clearly not identical. The diamagnetic precursors of these nitroxide radicals formed on standing were never isolated and characterised.

Attempts were made to isolate hydroxylamines from the photolysis products as their isolation would enable the regeneration of the nitroxide radicals from which they were derived. The infra-red spectra of the bulk photolysis products, prior to chromatographing show a small absorption at  $3,620\text{ cm}^{-1}$ , which may arise from the O-H stretching vibration of hydroxylamines. Various chromatographic techniques were employed in the attempted isolation of the hydroxylamines, however no hydroxylamines could be detected, and it seems probable that they oxidise on the activated silica surface.

At this stage of the investigations, the supply of humulene nitrosite donated by Mitchell was exhausted.

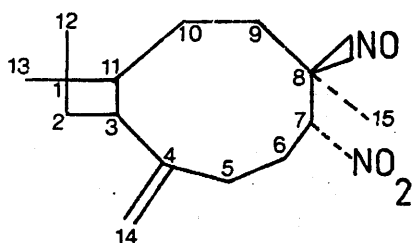
APPENDIX 22'.1' Determination of the structure of humulene nitrositeTable 2.1The elemental analysis of humulene nitrosite

Experimental content C 64.32%, H 8.37%, N 10.45%, O 16.86%.

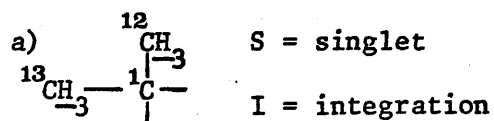
Theoretical content C 64.28%, H 8.57%, N 10.0%, O 17.15%.

Table 2.2

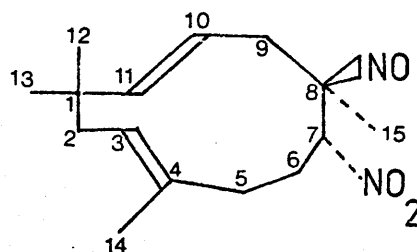
The comparison of the data obtained from the  $^1\text{H}$  n.m.r. spectra of caryophyllene nitrosite and humulene nitrosite



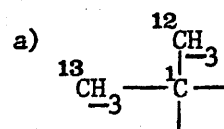
Caryophyllene nitrosite (2)



S  $\tau$  = 8.96, I = 6H.



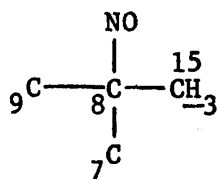
Humulene nitrosite (17)



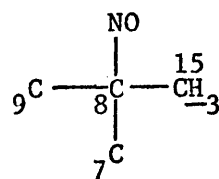
S  $\tau$  = 8.89, I = 3H.

S  $\tau$  = 8.84, I = 3H.

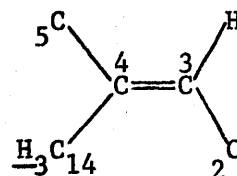
b)

S  $\tau$  = 8.76 , I = 3H.

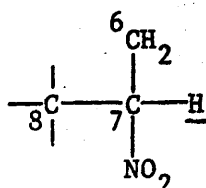
b)

S  $\tau$  = 8.75 , I = 3H.

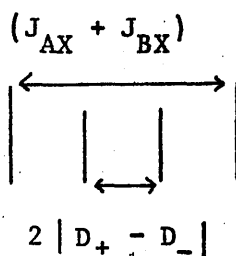
c)

S  $\tau$  = 8.22, I = 3H.small coupling  $J < 1\text{Hz}$ .

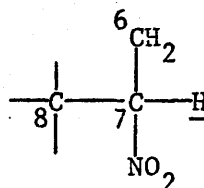
d)

Multiplet  $\tau$  = 3.97.

This proton is the X part of an ABX system. The two outermost combination transitions are very weak and the spectrum has the following appearance



d)



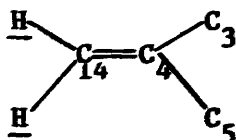
The underlined proton is the X part of an ABX system and its spectrum should consist of 6 lines. In fact the observed spectrum shows a doublet at  $\tau$  = 3.86 and  $J$  = 8 Hz. Only one proton appears to be coupling.

$$2D_+ = \sqrt{\left[\delta_{AB} + \frac{1}{2}(J_{AX} - J_{BX})\right]^2 + J_{AB}^2}$$

$$2D_- = \sqrt{\left[\delta_{AB} - \frac{1}{2}(J_{AX} - J_{BX})\right]^2 + J_{AB}^2}$$

$$J_{AX} = 5.5\text{Hz.}, \quad J_{BX} = 4.5\text{Hz.}$$

e) Ethylenic protons.



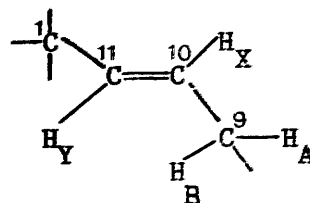
Doublet  $\tau = 4.77$ ,  $I = 2H$ .

Small coupling  $J < 1\text{Hz}$ .

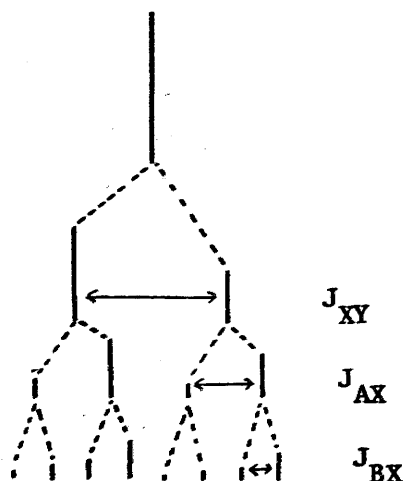
e) Ethylenic protons.

Range  $\tau = 4.4 - 5.4$ .

Total  $I = 3H$ .



1)  $H_X$  is the X part of an ABXY system. It couples to the trans proton to give a doublet of separation 16.0Hz. and then interacts further with  $H_A$  and  $H_B$  to give eight peaks with the following intensity distribution.





$$\tau = 5.2, \quad I = 1H.$$

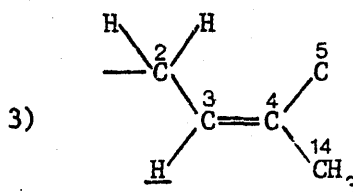
$$J_{XY} = 16.0 \text{ Hz.}, \quad J_{AX} = 9.0 \text{ Hz.},$$

$$J_{BX} = 4.0 \text{ Hz.}$$

2)  $H_Y$

Doublet  $\tau = 4.69, I = 1H.$

Trans coupling  $J = 16.0 \text{ Hz.}$



The underlined proton is the X part of an ABX system.

Multiplet  $\tau = 4.56, I = 1H.$

$J = 3.5 \text{ Hz.},$  and  $J = 9 \text{ Hz.}$

f) Allylic protons.

The  $CH_2$  region of the spectrum is difficult to analyse, however, there appear to be two main groups of resonances.

$$\tau 8.38 - 8.96, \quad I = 4H.$$

This region probably contains the allylic protons and the 2 protons attached to tertiary carbons.

$$\tau = 8.96 - 9.71, \quad I = 8H.$$

contains the remaining 4  $CH_2$  groups.

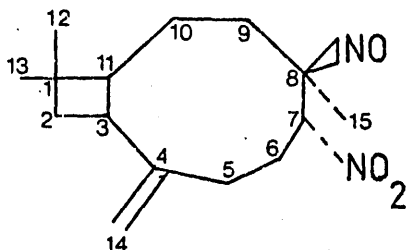
f) Allylic protons.

The  $CH_2$  region of the spectrum is difficult to analyse. The region there appears to be two main groups of resonances.  $\tau = 7.4 - 8.4$  integrates as 14 protons - 4  $CH_2$ 's and an allylic methyl.

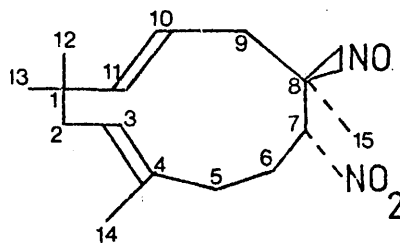
The region  $\tau = 7.4 - 8.1$  integrates as nine protons. These latter 9 protons could be the 9 allylic protons.

Table 2.3

A comparison of the data obtained from the  $^{13}\text{C}$  n.m.r. spectra of caryophyllene nitrosite and humulene nitrosite



Caryophyllene nitrosite (2)



Humulene nitrosite (17)

Resonances quoted in p.p.m.  
downfield from T.M.S.

D. - decoupled

P.D. - partially decoupled

a) $\text{C}_4$	148.5 p.p.m.
$\text{C}_8$	100.9 p.p.m.
$\text{C}_1$	34.9 p.p.m.

In each case  $^1\text{H}(\text{D})$  - 1 peak  
 $^1\text{H}(\text{P.D.})$  - 1 peak.

No protons are attached.

The relaxation times were  
measured using a  $180^\circ - \tau - 90^\circ$   
pulse sequence with  $\tau = 2$   
seconds.

$\text{C}_1$  has the longest relaxation  
time of all the carbons present.

a) $\text{C}_4$	135.8 p.p.m.
$\text{C}_8$	102.1 p.p.m.
$\text{C}_1$	38.3 p.p.m.

In each case  $^1\text{H}(\text{D.})$  - 1 peak  
 $^1\text{H}(\text{P.D.})$  - 1 peak.

No protons are attached

b) $C_7$	88.1 p.p.m.
$C_3$	59.3 p.p.m.
$C_{11}$	42.7 p.p.m.

In each case  $^1H(D.) - 1$   
peak.  $^1H(P.D.) - 2$  peaks.  
One proton is attached.

$C_3$  is to lower field than  $C_{11}$   
being adjacent to a  $C = C$ . In  
the partially decoupled spectrum  
the extra structure due to  
coupling with  $\beta$  protons  
decreases as follows

$$C_3, C_{11} - 3\beta^1H > C_7 - 2\beta^1H.$$

b) $C_3$	145.8 p.p.m.
$C_{11}$	125.1 p.p.m.
$C_{10}$	117.6 p.p.m.
$C_7$	88.9 p.p.m.

In each case  $^1H(D.) - 1$  peak  
 $^1H(P.D.) - 2$  peaks.

One proton is attached.

The assignment of the olefinic  
carbons  $C_{11}$ ,  $C_3$  and  $C_{10}$ , was based  
on the extra structure, which  
appears in the partially de-  
coupled spectrum, due to coupling  
with  $\beta$  protons. This extra  
structure decreases as follows

$$C_{10} - 3\beta^1H > C_3 - 2\beta^1H > C_{11} - 1\beta^1H.$$

c) $C_{14}$	113.2 p.p.m.
$C_5$	37.0 p.p.m.
$C_6$	36.2 p.p.m.
$C_9$	35.2 p.p.m.
$C_{10}$	28.3 p.p.m.
$C_2$	23.3 p.p.m.

In each case  $^1H(D.) - 1$  peak  
 $^1H(P.D.) - 3$  peaks. Two protons  
are attached  $C_6$  with 2  $\beta$  protons  
shows greater structure in the  
partially decoupled spectrum than  
does  $C_9$  with 2  $\beta$  protons.

c) $C_9$	44.4 p.p.m.
$C_2$	40.6 p.p.m.
$C_5$	35.4 p.p.m.
$C_6$	25.2 p.p.m.

In each case  $^1H(P.D.) - 3$  peaks.

Two protons are attached.

$C_5$  with 3  $\beta$  protons shows more  
structure in the partially  
decoupled spectrum than does  $C_2$   
with 2  $\beta$  protons.

d)  $C_{15}$  29.6 p.p.m.  
 $C_{12}$  21.6 p.p.m.  
 $C_{13}$  13.8 p.p.m.

In each case  $^1H(P.D.) - 4$

peaks. Three protons are attached.  $C_{12}$  is surrounded by a greater proton density when caryophyllene nitrosite is in its preferred conformation, and was assigned to the resonance of shorter relaxation time.

d)  $C_{15}/C_{14}$  29.9 p.p.m.  
 28.7 p.p.m.  
 $C_{12}/C_{13}$  17.6 p.p.m.  
 15.5 p.p.m.

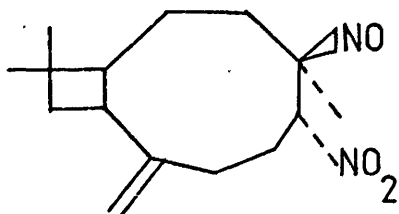
In each case  $^1H(P.D.) - 4$  peaks.

Three protons are attached.

---

Table 2.4

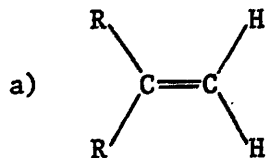
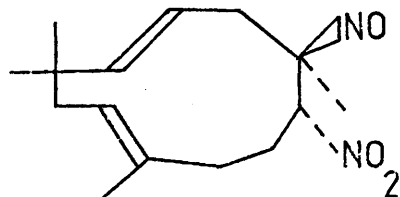
Pertinent data from the infra-red spectra of caryophyllene  
nitrosite and humulene nitrosite



Caryophyllene nitrosite (2)

o.o.p. - out of plane

def. - deformation

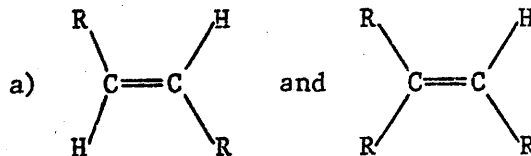
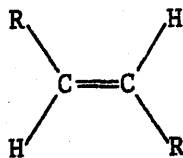

 $\nu_{C-H}$  str.  $3,085\text{ cm}^{-1}$ 
 $\nu_{C=C}$  str.  $1,640\text{ cm}^{-1}$ 
 $\nu_{o.o.p.}$  def.  $900\text{ cm}^{-1}$ 


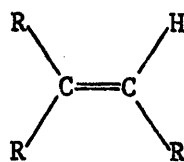
Humulene nitrosite (17)

str. - stretch

sym. - symmetric

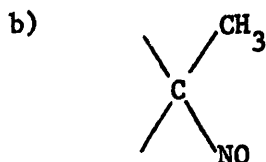
asym. - asymmetric


 $\nu_{C-H}$  str.  $3,015\text{ cm}^{-1}$ 
 $\nu_{C=C}$  str.  $3,010\text{ cm}^{-1}$ 
 $\nu_{C=C}$  str.  $1,660\text{ cm}^{-1}$ 
 $\nu_{C=C}$  str.  $1,665\text{ cm}^{-1}$ 

 $\nu_{o.o.p.}$  def.  $980\text{ cm}^{-1}$



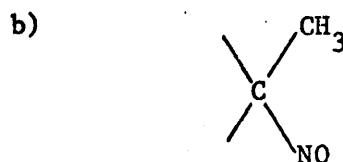
vo.o.p. def.

840  $\text{cm}^{-1}$



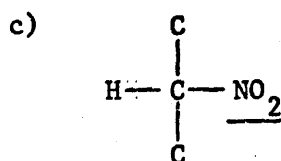
$\nu\text{N}=\text{O}$  str.

1570  $\text{cm}^{-1}$



$\nu\text{N}=\text{O}$  str.

1570  $\text{cm}^{-1}$



$\nu_{\text{asym.}}$

1550  $\text{cm}^{-1}$

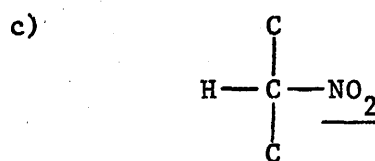
$\nu_{\text{sym.}}$

1360  $\text{cm}^{-1}$

$\nu\text{C}-\text{N}$  bend

870  $\text{cm}^{-1}$

These wavenumbers are characteristic of NO<sub>2</sub> attached to a secondary carbon atoms.



$\nu_{\text{asym.}}$

1560  $\text{cm}^{-1}$

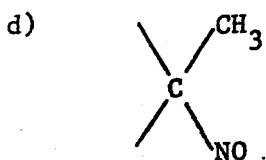
$\nu_{\text{sym.}}$

1360  $\text{cm}^{-1}$

$\nu\text{C}-\text{N}$  bend

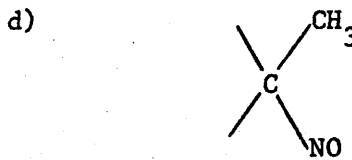
872  $\text{cm}^{-1}$

These wavenumbers are characteristic of NO<sub>2</sub> attached to a secondary carbon atoms.



$\nu\text{CH}_3$  str. asym.

2960  $\text{cm}^{-1}$



$\nu\text{CH}_3$  str. asym.

2965  $\text{cm}^{-1}$

$\nu\text{CH}_3$  str. sym.  $2875\text{ cm}^{-1}$

$\nu\text{def. (1470-1435)}\text{ cm}^{-1}$

unidentified

$\nu\text{def. } 1385\text{ cm}^{-1}$

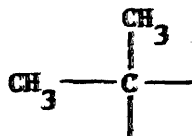
$\nu\text{CH}_3$  str. sym.  $2865\text{ cm}^{-1}$

$\nu\text{def. (1470-1435)}\text{ cm}^{-1}$

unidentified

$\nu\text{def. } 1385\text{ cm}^{-1}$

e)



$\nu\text{asym. str. } 2960\text{ cm}^{-1}$

$\nu\text{sym. str. } 2870\text{ cm}^{-1}$

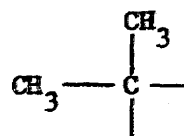
$\nu\text{sym. def. } 1385\text{ cm}^{-1}$

$\nu\text{skeletal } 1365\text{ cm}^{-1}$

$\nu\text{skeletal } 1170\text{ cm}^{-1}$

$\nu\text{skeletal } 805\text{ cm}^{-1}$

e)



$\nu\text{asym. str. } 2960\text{ cm}^{-1}$

$\nu\text{sym. str. } 2860\text{ cm}^{-1}$

$\nu\text{sym. def. } 1380\text{ cm}^{-1}$

$\nu\text{skeletal } 1365\text{ cm}^{-1}$

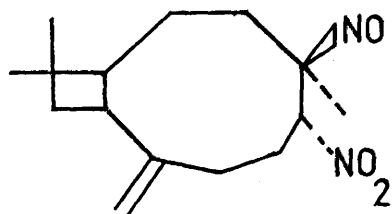
$\nu\text{skeletal } 1170\text{ cm}^{-1}$

$\nu\text{skeletal } 810\text{ cm}^{-1}$

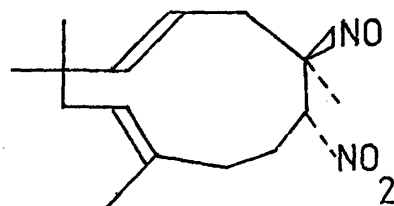
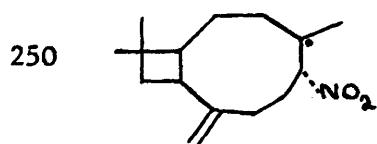
Table 2.5

A comparison of the main peaks in the mass spectra of caryophyllene  
nitrosite and humulene nitrosite

(The mass of the parent molecule = 280 in each case.)



Caryophyllene nitrosite (2)



Humulene nitrosite (17)

250	
220	loss of - (2 x NO)
203	loss of - (N <sub>2</sub> O <sub>3</sub> + H <sup>+</sup> )
189	
175	
161	
147	
133	
119	
105	
93	
81	
67	
53	
39	

250	
220	loss of - (N <sub>2</sub> O <sub>2</sub> )
203	loss of - (N <sub>2</sub> O <sub>3</sub> + H <sup>+</sup> )
189	
175, 177	
161	
147	
133, 135	
121	
105, 107	
93, 91	
77, 79	
65	
53	
41	



2'.2' Initial attempts at using chromatographic techniques to isolate the products formed when humulene nitrosite is irradiated with red light

2'.2'.1' The preparation of a sample of pure humulene nitrosite

Humulene nitrosite was chromatographed using one metre plates of 1 m.m. depth silica, with the solvent ether: pet. ether (50:50) which was found to give an optimum separation. Three bands were present at  $R_f = 0.37$ ,  $R_f = 0.58$ , and  $R_f = 0.66$ , however the bands of  $R_f = 0.66$  and  $R_f = 0.58$  overlapped slightly, and had to be selectively cut near to their centre. A better separation was achieved by using silica column chromatography, with columns 1.5 metres long and the same solvent. When 300 mg of humulene nitrosite were passed through such a column, and 25 fractions each of 10 ml collected, the following results were obtained.

Fraction	$R_f$ value	content	% by weight
1 - 6	0.66	Blue needle shaped crystals, crystallised from EtOH. M.pt. = $118 \pm 1^\circ\text{C}$	83.3.
8 - 12	0.58	Clear needle shaped crystals crystallised from EtOH. M.pt. = $136.8 \pm 0.5^\circ\text{C}$	7.1
15 - 19	0.37	Clear needle shaped crystals crystallised from EtOH. M.pt. = $168.5 \pm 0.5^\circ\text{C}$	6.2

Infra-red,  $^1\text{H}$  n.m.r., and mass spectra, were obtained for each species, and by a detailed comparison of these spectra, humulene nitrosite, was seen to be free of any contamination by the components of  $R_{f.} = 0.37$  and  $R_{f.} = 0.58$ .

2'.2'.2' Isolation of the products formed when chromatographically purified humulene nitrosite is irradiated with red light

a) The use of silica t.l.c. to separate the products formed when humulene nitrosite is irradiated with red light

When the products of the irradiation of humulene nitrosite with red light were chromatographed using one metre plates of 1 mm depth silica, with a solvent of ether: pet.ether, (50:50) three main bands were observed at  $R_{f.} = 0$ ,  $R_{f.} = 0.37$  and  $R_{f.} = 0.8$ . The components of  $R_{f.} > 0$ , were extracted from the silica, using analar chloroform, which was first passed through a silica column and then distilled, thereby removing phthalate impurities, which would heavily contaminate the photolysis products during the extraction process. Acetone was the only suitable solvent found to extract the products of  $R_{f.} = 0$ . The e.p.r. spectra of dilute chloroform solutions, of each component, were recorded immediately after their extraction. The components of  $R_{f.} > 0$  were all diamagnetic, all the paramagnetic species being located in the material of  $R_{f.} = 0$ .

b) Attempts at isolating and characterising the paramagnetic components present in the photolysis products of humulene nitrosite

The yellow solid of  $R_{f.} = 0$  accounted for approximately 10%, by weight, of the total product. Figure 2.13 shows the e.p.r. spectrum of a dilute degassed solution of this yellow solid in chloroform. Two nitroxide radicals,  $I_A$  and  $I_B$ , containing the

structural unit  $R_1R_2R_3C-\dot{N}O-CR_4R_5R_6$  are present. Nitroxide radical II, is not observed, as it decomposes on the silica. The line shape of the polycrystalline e.p.r. spectrum of this solid indicates that it is magnetically dilute, a finding confirmed by the infra-red spectrum, which indicated that only small amounts of the nitroxide radicals were present.

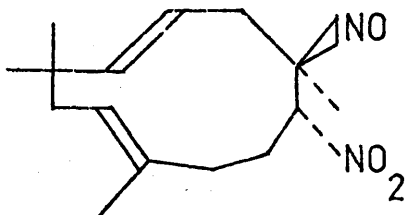
In order to isolate pure samples of nitroxide radicals  $I_A$  and  $I_B$ , the solid of  $R_f = 0$  was chromatographed for a second time. No solvent could be found which gave clearly separated bands containing pure samples of nitroxide radicals  $I_A$  and  $I_B$  but by using a combination of ether: pet.ether (80:20) and allowing an extended run over several hours on silica plates, a broadened yellow band was obtained. A series of cuts taken over this yellow band allowed two main regions to be identified, and these are discussed below.

- 1) In the regions of the band of higher  $R_f$  value a yellow solid was extracted, which was enriched in nitroxide radicals  $I_A$  and  $I_B$ . All attempts to crystallise this material were unsuccessful, despite triturating the solid using chloroform, and ethyl acetate. The radicals could not be further purified chromatographically, as they slowly decomposed on the silica surface.

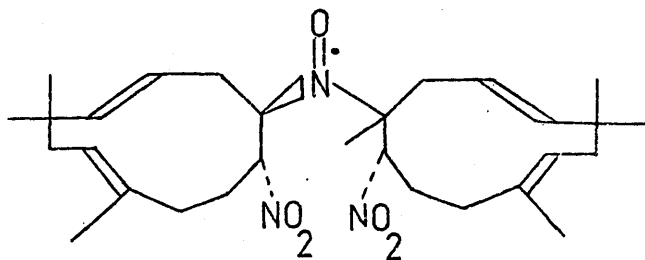
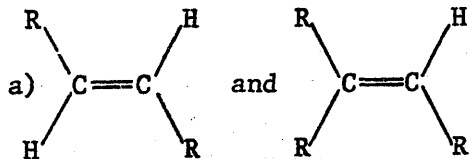
A comparison of the infra-red spectrum of this solid enriched in nitroxide radicals  $I_A$  and  $I_B$  with that of humulene nitrosite enabled the radicals to be characterised as diastereomeric forms of structure (19). Table 2.7. summarises the pertinent data obtained from this comparison.

Table 2.7

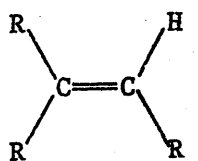
Pertinent data from the infra-red spectra of humulene  
nitrosite and the sample containing radicals  $I_A$   
and  $I_B$  as its sole paramagnetic products



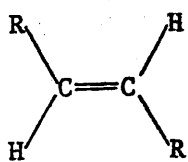
Humulene nitrosite (17)

Product containing radicals  $I_A$   
and  $I_B$  (19)

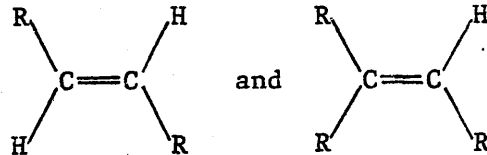
νC-H str.  $3,015\text{ cm}^{-1}$   
 $3,010\text{ cm}^{-1}$   
 νC=C str.  $1,660\text{ cm}^{-1}$   
 $1,665\text{ cm}^{-1}$



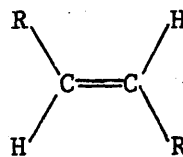
νo.o.p. def.  $840\text{ cm}^{-1}$



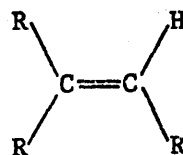
νo.o.p. def.  $980\text{ cm}^{-1}$



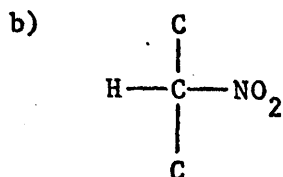
νC-H str.  $(3,010-3,015)\text{ cm}^{-1}$  shows  
 a broadening of the absorptions.  
 νC=C str.  $(1,665-1,640)\text{ cm}^{-1}$   
 shows a broadening of the  
 absorptions.



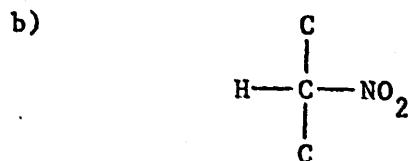
νo.o.p. def.  $975\text{ cm}^{-1}$



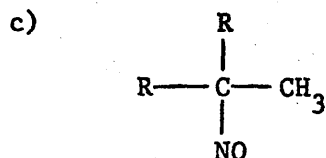
νo.o.p. def.  $850\text{ cm}^{-1}$



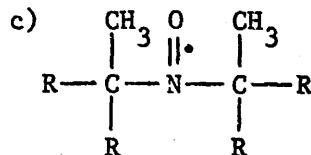
$\nu\text{NO}_2$ asym.	$1,560 \text{ cm}^{-1}$
$\nu\text{NO}_2$ sym.	$1,360 \text{ cm}^{-1}$
$\nu\text{C-N}$ bend	$872 \text{ cm}^{-1}$



$\nu\text{NO}_2$ asym.	$1,560 \text{ cm}^{-1}$
$\nu\text{NO}_2$ sym.	$1,550 \text{ cm}^{-1}$
$\nu\text{NO}_2$ sym.	$1,360 \text{ cm}^{-1}$
	$1,355 \text{ cm}^{-1}$
$\nu\text{C-N}$ bend	$870 \text{ cm}^{-1}$
	$875 \text{ cm}^{-1}$



$\nu\text{N=O}$ str.	$1570 \text{ cm}^{-1}$
----------------------	------------------------



$\nu\text{N=O}$ str.	$(1380-1385) \text{ cm}^{-1}$
----------------------	-------------------------------

2) The regions of the broadened yellow band of lower  $R_f$  value contained diamagnetic species.

c) Attempts to separate nitroxide radicals I<sub>A</sub>, I<sub>B</sub>, and II using alumina and cellulose t.l.c.

All attempts to isolate the nitroxide radicals present in the photolysis products, using cellulose t.l.c. plates were unsuccessful. Using alumina t.l.c. plates with ether as solvent, the material separated into two bands, the lower band being yellow, and the upper band orange-red in colour. This separation required a long continuous run, and the materials constituting the bands could not

be extracted using any of the common laboratory solvents. The  $\alpha$ -alumina used in the above experiment is insoluble in acid, and the possibility of repeating the experiment using  $\delta$ -alumina, which is acid soluble was considered as a possible method of extracting the materials from the alumina surface. In the time taken to achieve separation, it was considered likely that radical II would have decomposed and it was also felt unwise to subject the nitroxide radicals to acid on the alumina surface, which might lead to isomerisation reactions, and the formation of hydroxylamines and oxoammonium salts, which hydrolyse to nitroxides +  $\text{OH}^{\cdot}$ .<sup>101</sup>

d) Characterisation of the diamagnetic components present in the photolysis products of humulene nitrosite

1) The components of  $R_f = 0.37$

An oil was extracted from the region of  $R_f = 0.37$ . This oil contained more than one humulene based derivative, and the infra-red spectra showed the presence of nitro and nitrate groups. The oil was rechromatographed using ether: pet.ether (30:70) on silica plates, an extended run producing a broadened band, from the lower  $R_f$  regions of which a pure material was extracted, which crystallised from hot ethanol as clear needle shaped crystals of M.pt. =  $168.0 \pm 0.5^\circ\text{C}$ . This material has the empirical formula  $\text{C}_{15}\text{H}_{24}\text{N}_2\text{O}_4$  and a comparison of its  $^1\text{H}$  n.m.r. and infra-red spectra, with the corresponding spectra of humulene nitrosite, enabled it to be characterised as a dinitro derivative of humulene (24).

Table 2.9

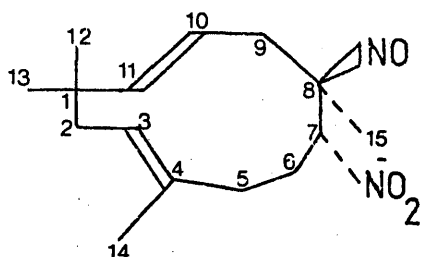
The elemental analysis of dinitro-humulene (24)

Experimental content C 61.4%, H 7.9%, N 10.0%, O 20.7%.

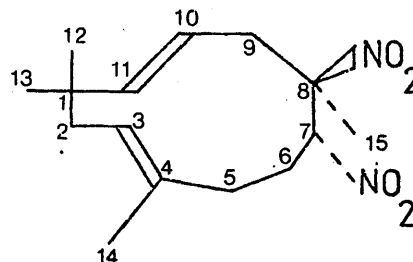
Theoretical content C 60.9%, H 8.1%, N 9.5%, O 21.5%.

Table 2.10

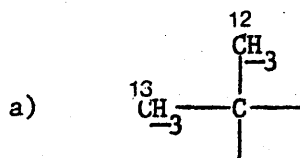
Pertinent data from the  $^1\text{H}$  n.m.r. spectra of humulene nitrosite  
and dinitro-humulene



Humulene nitrosite (17)

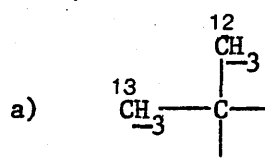


Dinitro-humulene (24)



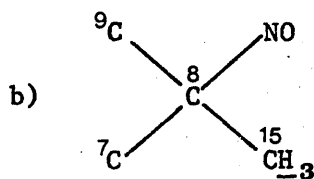
$S \tau = 8.89, \quad I = 3H.$

$S \tau = 8.84, \quad I = 3H.$

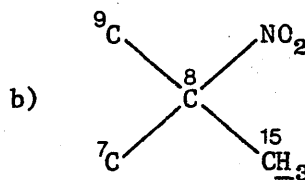


$S \tau = 8.89, \quad I = 3H.$

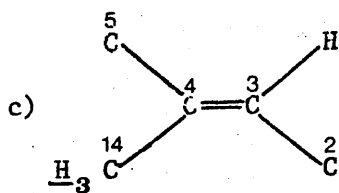
$S \tau = 8.84, \quad I = 3H.$



$S \tau = 8.75, \quad I = 3H.$

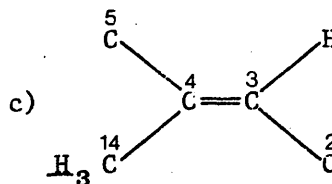


$S \tau = 8.08, \quad I = 3H.$



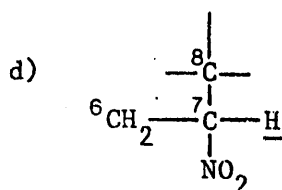
$S \tau = 8.22, \quad I = 3H.$

small coupling  $J < 1\text{Hz}.$

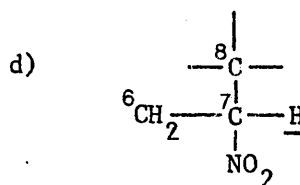


$S \tau = 8.29, \quad I = 3H.$

small coupling  $J < 1\text{Hz}.$



The underlined proton is the X part of an ABX system. The observed spectrum however, shows a doublet  $\tau = 3.86$ ,  $J = 8\text{Hz}$ . Only one proton appears to be coupling.



The underlined proton is the X part of an ABX system. The two outermost combination transitions are not observed, and the spectrum appears as a doublet

COUPLING IS ONLY OBSERVED WITH ONE PROTON.

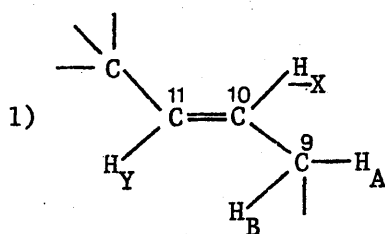
$$\tau = 4.74, \quad I = 1H.$$

$$J = 0 \text{ Hz.} \quad J = 8.8\text{Hz.}$$

e) Ethylenic protons

Total  $I = 3H$ .

Range  $\tau = 4.4 - 5.4$ .

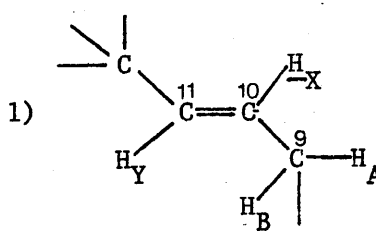


$H_X$  is the X part of an ABXY system. This is an ABXY system and  $H_X$  gives a spectrum with 8 peaks with the following intensity distribution.

e) Ethylenic protons

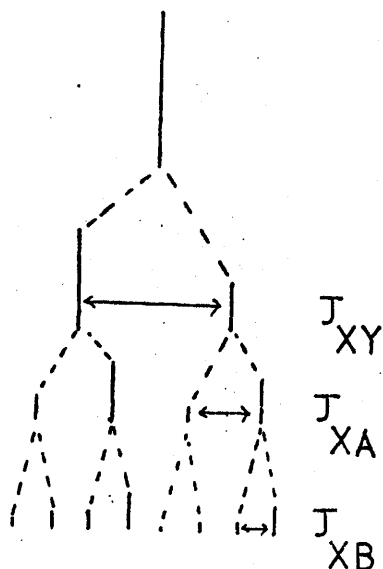
Total  $I = 3H$ .

Range  $\tau = 4.5 - 5.2$ .



$H_X$  gives a spectrum with 8 peaks with the following intensity distribution.



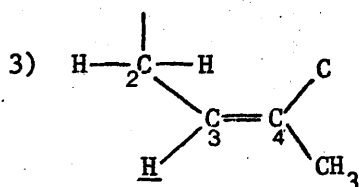


$$J_{XY} = 16.0 \text{ Hz.}, J_{XA} = 9 \text{ Hz.},$$

$$J_{XB} = 4 \text{ Hz.}, \quad \tau = 5.2, I = 1 \text{ H.}$$

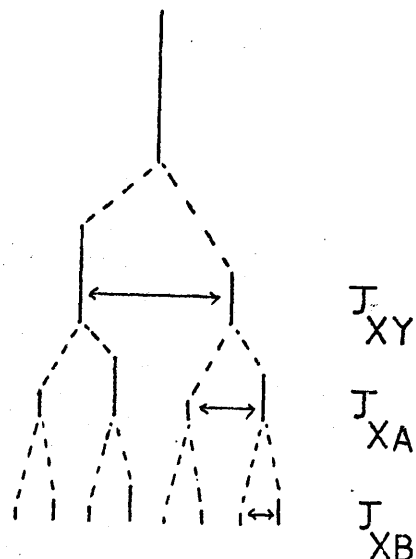
2)  $H_Y$

Doublet  $\tau = 4.69, J = 16 \text{ Hz.}$



The underlined proton is the X part of an ABX system.

Multiplet  $\tau = 4.56, I = 1 \text{ H.}$   
 $J = 3.5 \text{ Hz. and } J = 9 \text{ Hz.}$



$$J_{XY} = 15.9 \text{ Hz.}, J_{XA} = 8.8 \text{ Hz.},$$

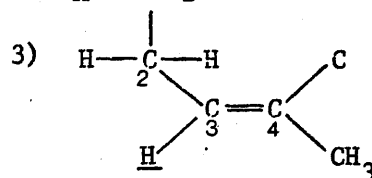
$$J_{XB} = 3 \text{ Hz.}, \quad \tau = 5.04, I = 1 \text{ H.}$$

2)  $H_Y$

Doublet  $\tau = 4.68, J = 15.9 \text{ Hz.}$

shows a small coupling of  $\sim 1 \text{ Hz.}$

to  $H_A$  and  $H_B$

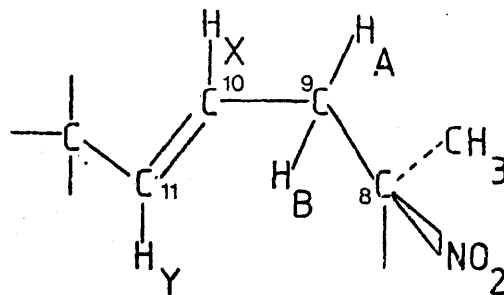


The underlined proton is the X part of an ABX system.

Multiplet  $\tau = 4.64, I = 1 \text{ H.}$   
 $J = 5.0 \text{ Hz. and } J = 9.0 \text{ Hz.}$

f)

f)



8 peaks are observed for  $H_A$

$\tau = 7.28$ ,  $I = 1H$ .  $J_{AB} = 15Hz$ .

$J_{AX} = 3Hz$ . and  $J_{AY} = 1Hz$ .

8 peaks are also observed for

$H_B$   $\tau = 7.72$ ,  $I = 1H$ .  $J_{AB} = 15Hz$ .

$J_{BX} = 8.8Hz$ .  $J_{BY} = 2Hz$ .

g) Allylic protons

The region  $\tau = 7.4 - 8.4$

integrates as 11 protons, namely  
4  $CH_2$ 's and an allylic methyl.

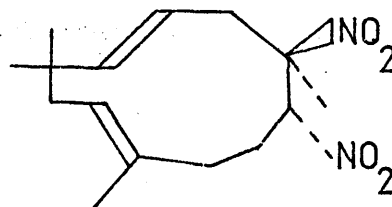
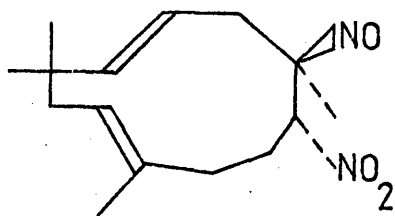
The  $\tau$  region 7.4. - 8.1 integrates  
as 9 protons. These could be the  
nine allylic protons.

g) Allylic protons

The  $\tau$  region 7.06 - 8.52 contains  
14 protons, namely the 4  $CH_2$ 's,  
the allylic methyl and the methyl  
on the carbon adjacent to the  
nitro group.

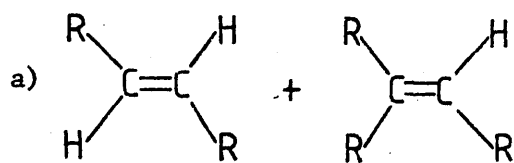
Table 2.11

Pertinent data from the infra-red spectra of humulene nitrosite  
and dinitro-humulene



Humulene nitrosite (17)

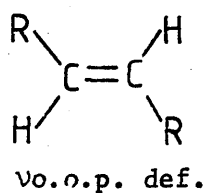
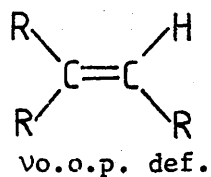
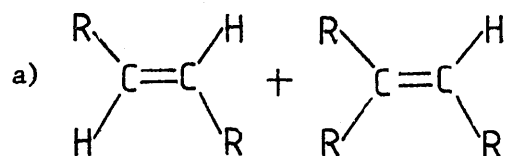
Dinitro-humulene (24)



vC-H str.

3,015 cm<sup>-1</sup>3,010 cm<sup>-1</sup>

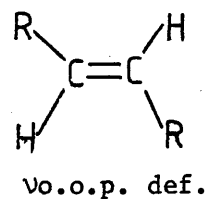
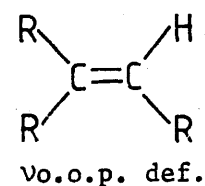
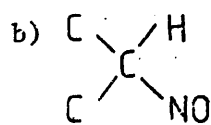
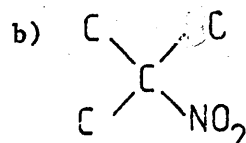
vC=C str.

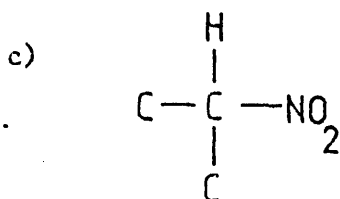
1,660 cm<sup>-1</sup>1,665 cm<sup>-1</sup>980 cm<sup>-1</sup>840 cm<sup>-1</sup>

vC-H str.

3,015 cm<sup>-1</sup>3,010 cm<sup>-1</sup>

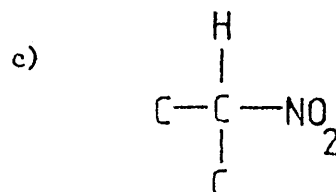
vC=C str.

1,660 cm<sup>-1</sup>1,665 cm<sup>-1</sup>980 cm<sup>-1</sup>840 cm<sup>-1</sup>1,570 cm<sup>-1</sup>1,545 cm<sup>-1</sup>vNO<sub>2</sub> sym. str.1,355 cm<sup>-1</sup>vCH<sub>3</sub> asym. str.2,965 cm<sup>-1</sup>vCH<sub>3</sub> sym. str.2,865 cm<sup>-1</sup>vCH<sub>3</sub> sym. def.1,385 cm<sup>-1</sup>vCH<sub>3</sub> asym. str.2,965 cm<sup>-1</sup>vCH<sub>3</sub> sym. str.2,860 cm<sup>-1</sup>vCH<sub>3</sub> sym. def.1,390 cm<sup>-1</sup>



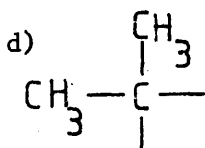
$\nu\text{NO}_2$ asym.	$1,560 \text{ cm}^{-1}$
$\nu\text{NO}_2$ sym.	$1,360 \text{ cm}^{-1}$
$\nu\text{C-N}$ bend	$872 \text{ cm}^{-1}$

These wavenumbers are characteristic of  $\text{NO}_2$  attached to a secondary carbon atom.

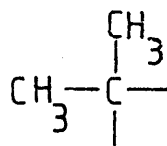


$\nu\text{NO}_2$ asym.	$1,550 \text{ cm}^{-1}$
$\nu\text{NO}_2$ sym.	$1,360 \text{ cm}^{-1}$
$\nu\text{C-N}$ bend	$872 \text{ cm}^{-1}$

These wavenumbers are characteristic of  $\text{NO}_2$  attached to a secondary carbon atom.



$\nu$ asym. str.	$2,960 \text{ cm}^{-1}$
$\nu$ sym. str.	$2,860 \text{ cm}^{-1}$
$\nu$ asym. def.	$\sim 1,440 \text{ cm}^{-1}$
$\nu$ sym. def.	$\sim 1,380 \text{ cm}^{-1}$
$\nu$ skeletal	$1,365 \text{ cm}^{-1}$
$\nu$ skeletal	$\sim 1,170 \text{ cm}^{-1}$
$\nu$ skeletal	$810 \text{ cm}^{-1}$



$\nu$ asym. str.	$2,960 \text{ cm}^{-1}$
$\nu$ sym. str.	$2,860 \text{ cm}^{-1}$
$\nu$ asym. def.	$\sim 1,440 \text{ cm}^{-1}$
$\nu$ sym. def.	$\sim 1,390 \text{ cm}^{-1}$
$\nu$ skeletal	$1,375 \text{ cm}^{-1}$
$\nu$ skeletal	$\sim 1,165 \text{ cm}^{-1}$
$\nu$ skeletal	$805 \text{ cm}^{-1}$

## 2) The components of $R_f = 0.8$

Figure 2.18 shows the  $^1\text{H}$  n.m.r. and infra-red spectra of the oil extracted from the region of  $R_f = 0.8$ . The spectra are complex and several humulene based derivatives are present. All attempts to isolate the individual compounds present using chromatography were unsuccessful and at this stage the individual components of this oil could not be characterised. The following observations

were however made.

1) Interpretation of the infra-red spectrum

a) Nitro groups.

An average of one nitro group was present per molecule and they were comprised of the following two types.

1) Nitro groups attached to a secondary carbon atom.

The absorptions were broad, several being present and they were centred at

$$\nu \text{ asym. } 1,550 \text{ cm}^{-1}, \quad \nu \text{ sym. } 1,360 \text{ cm}^{-1}$$

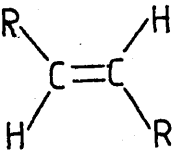
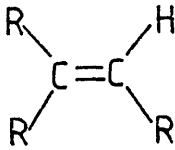
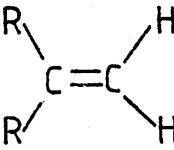
2) Conjugated nitro groups  $\text{>C=C<NO}_2$

$$\nu \text{ asym. } 1,520 \text{ cm}^{-1}, \quad \nu \text{ sym. } 1,330 \text{ cm}^{-1}.$$

b) Nitroso groups

Nitroso absorptions were not observed

c) Olefinic absorptions

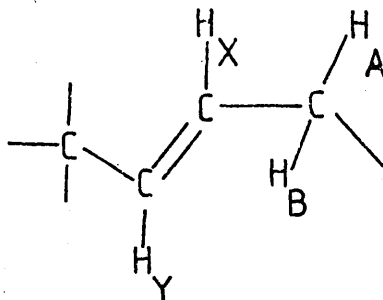
			
$\nu\text{C-H str.}$	$3,015 \text{ cm}^{-1}$	$3010 \text{ cm}^{-1}$	$3,080 \text{ cm}^{-1}$
$\nu\text{C=C str.}$	$1,650 \text{ cm}^{-1}$	$1,640 \text{ cm}^{-1}$	$1,640 \text{ cm}^{-1}$
$\nu\text{o.o.p. def.}$	$975 \text{ cm}^{-1}$	$840 \text{ cm}^{-1}$	$915 \text{ cm}^{-1}$

In each case more than one absorption was present.

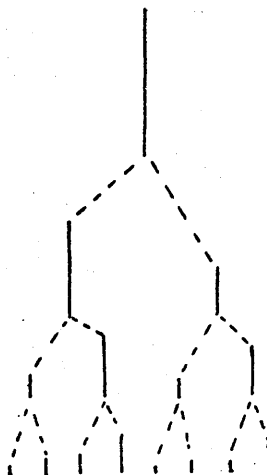
2) Interpretation of the main resonances found in the  $^1\text{H}$  n.m.r. spectrum

- a)  $\tau = 8.6 - 8.88$  This region contains a large number of methyl resonances, attributed to gem-di-methyl structures.

- b)  $\tau = 8.2 - 8.4$  This region contains 6 allylic methyls.
- c)  $\tau = 4.72 - 5.69$  This region contains resonances compatible with the following structure.



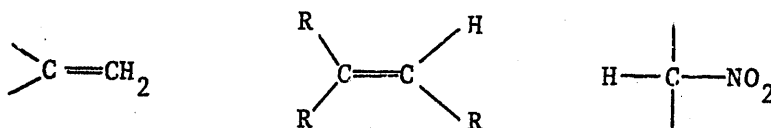
- 1)  $H_Y$  - A minimum of three doublets having the correct coupling constant of  $\sim 16\text{Hz.}$ , and the correct weighting to be  $H_Y$  coupling to an upfield  $H_X$ , are observed in this region.
- 2)  $H_X$  is the X part of an ABXY spectrum,  $J_{XY} \approx 16\text{Hz.}$  being the strongest coupling, and the overall resonance consisting of 8 lines with the following intensity distribution.



The  $^1\text{H}$  n.m.r spectrum of the oil contains approximately 32 peaks in the  $\tau$  region 4.72 to 5.69, and at least two groups of resonances are present, which consist of 8 peaks with the correct intensity distribution, to be

attributed to a proton of type  $H_X$ .

- 3) In the  $\tau$  region 3.92 to 5.69 various resonances are present which are consistent with the following structures



The oil of  $R_f = 0.8$  would appear to be a series of humulene based derivatives containing a single nitro group. The structures may be isomeric, and probably involve simple rearrangements of the humulene structure.

- e) Monitoring the production of the nitroxide radicals formed when the diamagnetic photolysis products of humulene nitrosite are allowed to stand in air

Table 2.12 illustrates the distribution of the nitroxide radicals as a function of the  $R_f$  value of the diamagnetic precursors from which they were oxidised.

Table 2.12

Distribution of the nitroxide radicals formed when the  
diamagnetic photolysis products of humulene  
nitrosite are oxidised in air

$R_f$ value of precursor	Paramagnetic species observed
a)	The nitroxide radical formed, when dissolved in chloroform, gives an e.p.r spectrum, which consists of a 1:1:1 triplet [isotropic $\langle g \rangle = 2.0064 \pm 0.0003$ ; isotropic $a(^{14}\text{N}) = 15.4 \pm 0.3\text{G}$ ].
$0.8 > R_f > 0.6$	
b)	Two nitroxide radicals are present, the e.p.r. spectrum consisting of two 1:1:1 triplets [isotropic $\langle g \rangle = 2.0064 \pm 0.0003$ ; isotropic $a(^{14}\text{N}) = 15.7 \pm 0.3\text{G}$ ], and [isotropic $\langle g \rangle = 2.0058 \pm 0.0003$ ; isotropic $a(^{14}\text{N}) = 15.0 \pm 0.5\text{G}$ ].
$0.6 > R_f > 0.45$	
c)	Two nitroxide radicals are present. One contains the structural unit $\text{R}_1\text{R}_2\text{R}_3\text{C}\dot{\text{N}}\text{O}-\text{CR}_4\text{R}_5\text{R}_6$ [isotropic $\langle g \rangle = 2.0058 \pm 0.0003$ ; isotropic $a(^{14}\text{N}) = 14.3 \pm 0.3\text{G}$ ]. The second radical contains the structural unit $\text{R}_1\text{R}_2\text{R}_3\text{C}\dot{\text{N}}\text{O}-\text{CHR}_4\text{R}_5$ [isotropic $\langle g \rangle = 2.0058 \pm 0.0003$ ; isotropic $a(^{14}\text{N}) = 14.3 \pm 0.3\text{G}$ ; isotropic $a(^1\text{H}) = 5.8 \pm 0.3\text{G}$ ].
$0.45 > R_f > 0.3$	



CHAPTER 3REACTIONS OF HUMULENE AND CARYOPHYLLENE WITH  
THE OXIDES OF NITROGEN3.1. The extraction of a sample of pure humulene from  
technical grade caryophyllene

A source of pure humulene was required to replenish the stock of humulene nitrosite which was now exhausted. Technical grade caryophyllene is reported in the literature to contain approximately 13% humulene (14)<sup>102</sup> and a  $^1\text{H}$  n.m.r. spectrum of the mixture confirmed this. The method employed to extract pure humulene from this mixture, is based on a technique developed by M.D. Sutherland and R.P. Hildebrand<sup>102</sup> which makes use of the differential solubilities of the silver nitrate adducts of humulene and caryophyllene, in the solvents water, and ethanol. The exact experimental procedures involved are described in appendix 3, section 3'.1' and they include details of several innovations, which were introduced to increase the yield. In the later stages of this investigation, humulene was also extracted from hop oil. The hop oil was first distilled, and the fraction of b.pt. 90-100°C/ 1mm was subjected to procedures completely analogous to those described in appendix 3, section 3'.1'.

At all stages of its extraction, the purity of the humulene enriched samples was monitored using  $^1\text{H}$  n.m.r. spectroscopy. Figure 3.1 shows the  $^1\text{H}$  n.m.r. spectrum of the pure humulene, and the pertinent data extracted from this spectrum are summarised in Table 3.2, appendix 3. S. Dev, et.al.<sup>103</sup> have studied the temper-

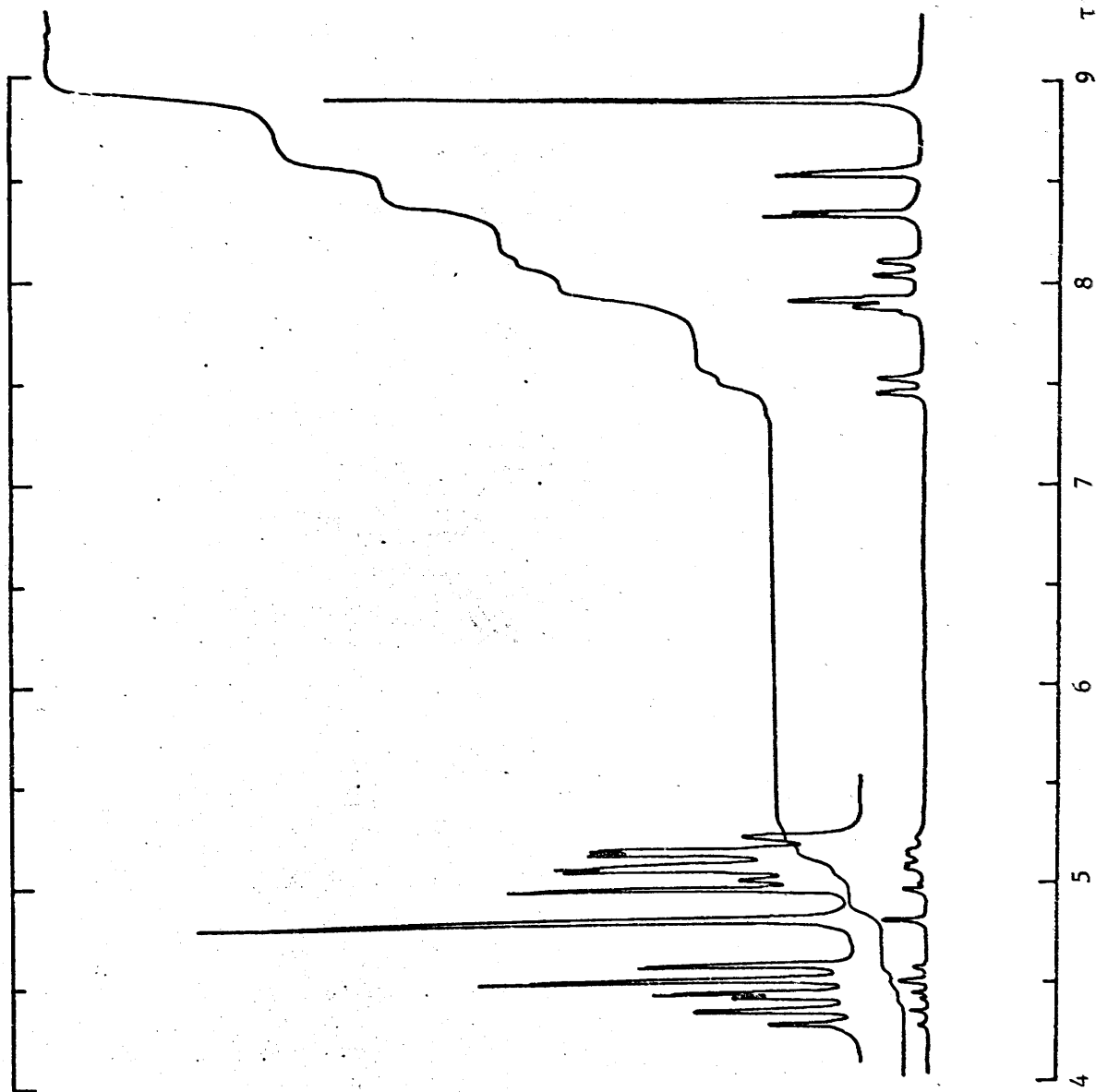
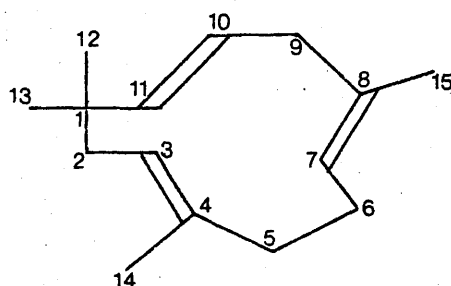


Figure 3.1 The  $^1\text{H}$  n.m.r. spectrum of a solution of humulene (14) in  $\text{CDCl}_3$  in the  $\tau$  range 4 to 9.

ature dependence of the  $^1\text{H}$  n.m.r. spectrum of pure humulene and although they do not give a complete analysis of all the resonances, they demonstrate that humulene has a very flexible structure at room temperature, and that the main barrier to inversion involves a flipping of the double bond over carbons 3 and 4. The spectrum shown in figure 3.1 was recorded at  $+30^\circ\text{C}$  and the conformational mobility is such, that the protons on  $\text{C}_9$ ,  $\text{C}_{10}$  and  $\text{C}_{11}$  constitute an  $\text{A}_2\text{XY}$  system, on  $\text{C}_5$ ,  $\text{C}_6$ , and  $\text{C}_7$  an  $\text{A}_2\text{B}_2\text{X}$  system, and on  $\text{C}_2$ ,  $\text{C}_3$  an  $\text{A}_2\text{X}$  system.



Humulene (14)

### 3.2 The reactions of humulene with the oxides of nitrogen

In preparing a sample of humulene nitrosite, care was taken to follow as closely as possible the procedures employed by S. Mitchell.<sup>72</sup> The basis of the method is to allow humulene to react with an equivalent amount of  $\text{N}_2\text{O}_3$ , generated by adding a drop of glacial acetic acid, to a saturated aqueous solution of  $\text{NaNO}_2$ . The reaction products were then to be carefully monitored for evidence of the formation of the following types of species.

- 1) In appendix 2 section 2'.2'.1' it was demonstrated that the sample of humulene nitrosite prepared by Mitchell contained two clear crystalline impurities which were removed chromato-

graphically. These species may have their origins in the reaction of humulene with the oxides of nitrogen.

- 2) It was demonstrated in Chapter 2 that humulene nitrosite did not form by a process involving a transannular cyclisation of the humulene ring, however when humulene is allowed to come into contact with the oxides of nitrogen in the presence of an acidic medium, other species may form via such a mechanism.

The experimental details involved in reacting humulene with  $N_2O_3$ , are discussed in appendix 3 section 3'.2' (a). The products obtained from the reaction yield on crystallisation, from ethanol, a mixture of crystalline derivatives and a yellow oil.

- a) The crystalline derivatives formed when humulene reacts with the oxides of nitrogen

Figure 3.2 illustrates the crystalline derivatives which form when humulene is reacted with the oxides of nitrogen. The three pure derivatives were isolated using silica column chromatography and full details of the separation techniques used are contained in appendix 3 section 3'.2' (b). The three derivatives were characterised by an analysis and comparison of their  $^1H$  n.m.r., infra-red, and mass spectra and an elemental analysis was obtained in each case. Figure 2.17 shows a comparison of the  $^1H$  n.m.r. spectra of the three species, humulene nitrosite (17), dinitro-humulene (24), and nitro-nitrato-humulene (26).

#### Humulene nitrosite (17)

Humulene nitrosite was the major product isolated, and

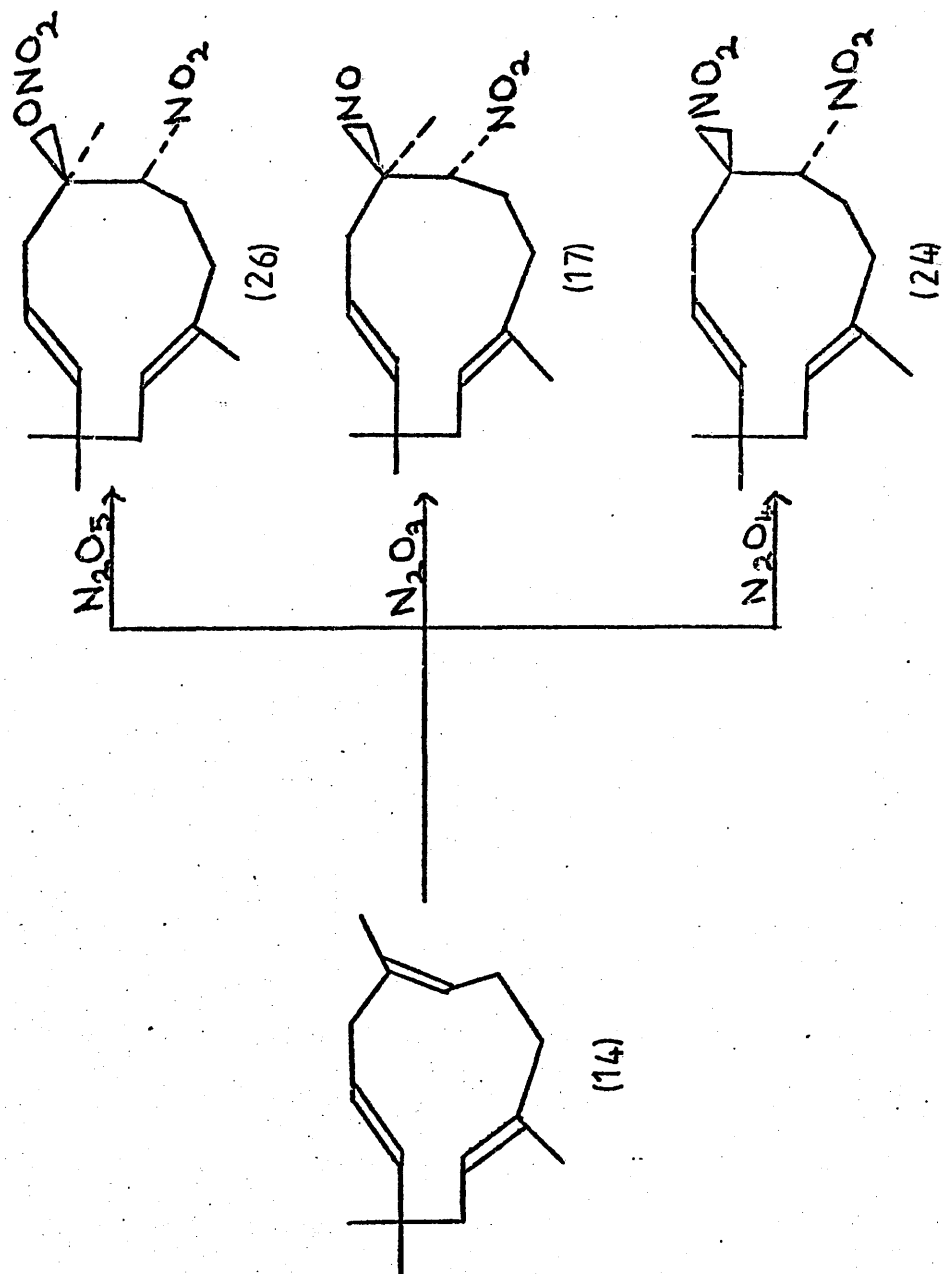


Figure 3.2 The crystalline products which form when a solution of humulene (14) in an aprotic solvent is reacted with the oxides of nitrogen.

the spectroscopic evidence indicated that all the contaminants had been removed.

The remaining two crystalline species accounted for less than 18% by weight of the total product and were identified as the two impurities present in the humulene nitrosite donated by Mitchell.

#### Dinitro-humulene (24)

One of the clear crystalline derivatives was immediately characterised as dinitro-humulene (24), having an empirical formula  $C_{15}H_{24}N_2O_4$ , and identical  $^1H$  n.m.r., infra-red, and mass spectra, to those of a pure sample of dinitro-humulene, which had been previously isolated and fully characterised as one of the products formed on irradiating humulene nitrosite in red light. The pertinent data from the  $^1H$  n.m.r. and infra-red spectra of dinitro-humulene (24) have been previously summarised in tables 2.10, and 2.11, respectively.

It should be noted that all the experimental work, including the chromatographic separations, involved in extracting the products formed when humulene is reacted with  $N_2O_3$ , were performed in the absence of light. The dinitro-humulene obtained is thus a product of the reaction of humulene with  $N_2O_3$  and its presence is not due to the photolytic decomposition of humulene nitrosite.

#### Nitro-nitrato-humulene (26)

The third crystalline derivative has the empirical formula  $C_{15}H_{24}N_2O_5$  based on the results of an elemental analysis shown in table 3.3 appendix 3. A detailed comparison of the  $^1H$  n.m.r.

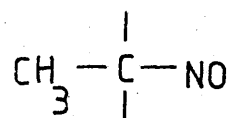
and infra-red spectra of this derivative with those of humulene nitrosite (17), and dinitro-humulene (24), revealed the following points.

- 1) The spectroscopic evidence is consistent with all three compounds having an identical structure, except for the nature of the group attached to  $C_8$ .
- 2) The infra-red spectra indicate the presence of the following groups on  $C_8$ .

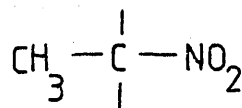
Humulene nitrosite (17)	Dinitro-humulene (24)	Third crystalline derivative.
nitroso	nitro	nitrate
$\nu N = O$ str. $1,570\text{ cm}^{-1}$	$\nu NO_2$ asym. $1,545\text{ cm}^{-1}$	$\nu ONO_2$ sym.str. $1,632\text{ cm}^{-1}$
	$\nu NO_2$ sym. $1,355\text{ cm}^{-1}$	$\nu ONO_2$ asym.str. $1,287\text{ cm}^{-1}$
		$\nu N-O$ str. $852\text{ cm}^{-1}$

- 3) The  $^1H$  n.m.r. spectra have methyl resonances consistent with the following structures.

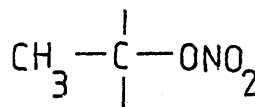
Humulene nitrosite (17) S. $\tau$  = 8.75



Dinitro-humulene (24) S. $\tau$  = 8.08



Third crystalline derivative S. $\tau$  = 8.35



This third derivative was thus characterised as the nitro-nitrato derivative of humulene, of structure (26), and the pertinent data from its  $^1H$  n.m.r., and infra-red spectra are summarised in appendix 3, tables 3.4 and 3.5 respectively.

The  $^1\text{H}$  n.m.r. spectra of humulene nitrosite (17), dinitro-humulene (24), and nitro-nitrato-humulene (26), shows no duplication of resonances for the protons on the asymmetric carbon atoms  $\text{C}_7$  and  $\text{C}_8$ , or on the adjacent carbon atoms  $\text{C}_6$  and  $\text{C}_9$ , of the type which might indicate the presence of diastereoisomers. The addition of the appropriate oxides of nitrogen, over the double bond of humulene, is thus stereospecific, the most probable products being the trans configurations, the cis configurations being sterically congested. The experimentally observed proton coupling constants, for dinitro-humulene (24), and nitro-nitrato-humulene (26) are consistent with their having a preferred conformation similar to that postulated for humulene nitrosite (17), which is illustrated in figure 2.3, and is based on a diaxial addition of  $\text{N}_2\text{O}_3$  to the preferred conformation of humulene.

No products formed by a transannular cyclisation of the humulene ring were observed.

2) The nature of the yellow oil formed when humulene reacts with the oxides of nitrogen

When humulene reacts with the oxides of nitrogen, the products consist of the three crystalline derivatives discussed above and a yellow oil. The yields of humulene nitrosite obtained in the reaction were small, approximately 15%. Attempts were made to increase the yield by recycling unreacted humulene and adding a large excess of  $\text{N}_2\text{O}_3$ . Each cycle produced a crude product which was becoming greener in colour, and when these products were kept in contact with  $\text{N}_2\text{O}_3$ , the humulene nitrosite reacted leaving a yellow oil. It was thus uncertain as to whether the yellow oil formed from the reaction of humulene with the oxides of nitrogen,



or the reaction of humulene nitrosite with the oxides of nitrogen.

Figure 3.3 shows the e.p.r. spectrum at 295°K, of a dilute degassed solution in chloroform of the yellow oil formed when humulene reacts with  $N_2O_3$ . Two nitroxide radicals appear to be present:-

Radical A The e.p.r. spectrum of radical A consists of a 1:1:1 triplet [isotropic  $\langle g \rangle = 2.0059 \pm 0.0002$ ; isotropic  $a(^{14}N) = 14.6 \pm 0.2G$ ]. This radical contains the molecular fragment  $R_1R_2R_3\dot{C}-NO-CR_4R_5R_6$ .

Radical B The e.p.r. spectrum of radical B, consists of a 1:1:1 triplet, further split into doublets by the interaction with a  $\beta$  proton [isotropic  $\langle g \rangle = 2.0062 \pm 0.0002$ ; isotropic  $a(^{14}N) = 14.8 \pm 0.2G$ ; isotropic  $a(^1H) = 3.5 \pm 0.5G$ ]. This radical contains the molecular fragment  $R_1R_2R_3\dot{C}-NO-CHR_4R_5$ .

If the solution containing nitroxide radicals A and B is allowed to stand, then radical B disproportionates to diamagnetic species and the e.p.r. spectrum which remains is shown in figure 3.4. Two nitroxide radicals containing the structural unit  $R_1R_2R_3\dot{C}-NO-CR_4R_5R_6$ , are now seen to be present.

Radical A<sub>1</sub> [isotropic  $\langle g \rangle = 2.0059 \pm 0.0002$ ; isotropic  $a(^{14}N) = 14.6 \pm 0.2G$ ].

Radical A<sub>2</sub> [isotropic  $\langle g \rangle = 2.0062 \pm 0.0002$ ; isotropic  $a(^{14}N) = 15.0 \pm 0.2G$ ].

When a pure sample of humulene nitrosite is reacted with the oxides of nitrogen, the product consists of a yellow oil, whose e.p.r. spectrum in solution, is exactly the same as that shown in figure 3.3. The paramagnetic species thus appear to form from the reaction of humulene nitrosite with the oxides of nitrogen. Quantitative silica t.l.c. has also enabled the isolation of

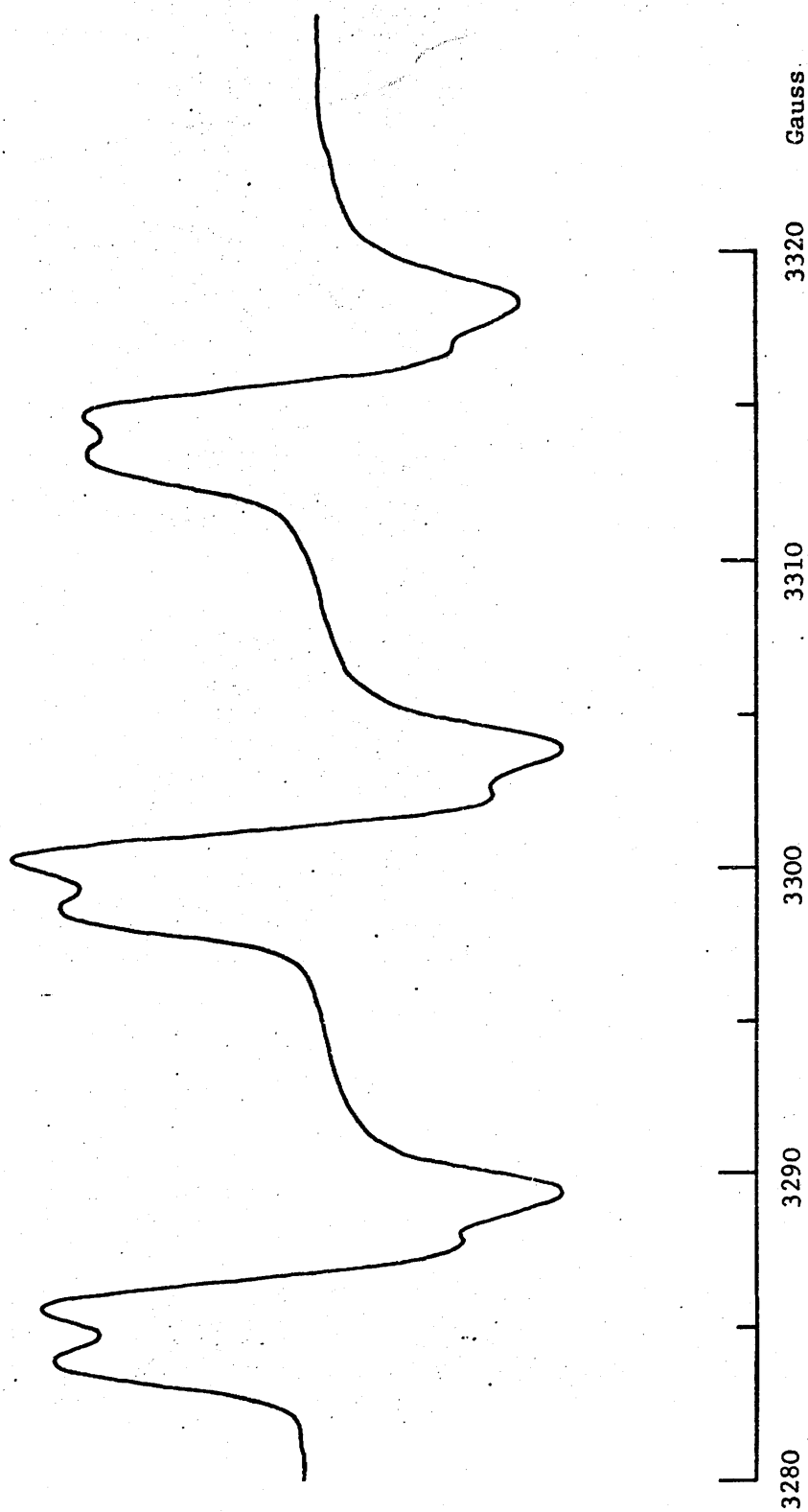


Figure 3.3 The e.p.r. spectrum of a dilute degassed solution in chloroform, of the yellow oil formed when humulene (14) reacts with  $\text{N}_2\text{O}_3$ . The spectrum was recorded at  $295^\circ\text{K}$ .

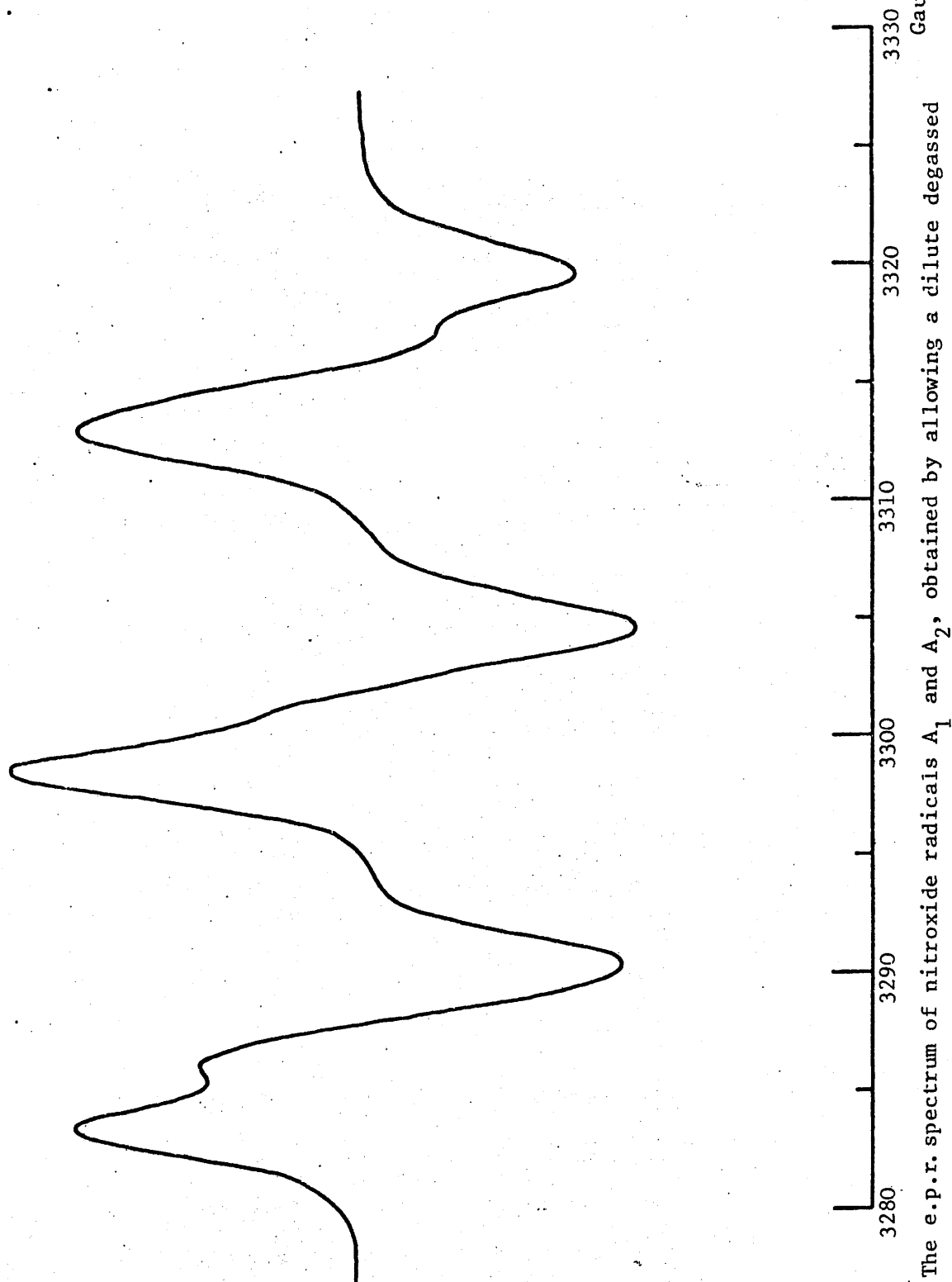


Figure 3.4 The e.p.r. spectrum of nitroxide radicals  $A_1$  and  $A_2$ , obtained by allowing a dilute degassed solution in chloroform, of the yellow oil formed when humulene (14) reacts with  $N_2O_3$  to stand until nitroxide radical B disproportionates.

several diamagnetic compounds from both the oil formed when humulene reacts with  $N_2O_3$  and the oil formed when humulene nitrosite reacts with  $N_2O_3$ .

It was decided to investigate further. this interesting reaction of humulene nitrosite with the oxides of nitrogen in order to clear up the following points.

- 1) What is the nature of the paramagnetic species and by what mechanism do they form?
- 2) What is the nature of the diamagnetic species, and which of these are formed by the reaction of humulene nitrosite with  $N_2O_3$  and which by the reaction of humulene with  $N_2O_3$ ?
- 3) Finally do any of the diamagnetic products form by a transannular cyclisation of the humulene ring?

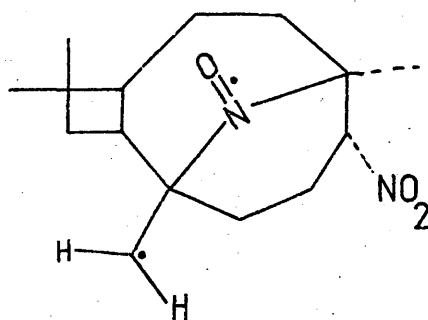
These studies of the reaction of humulene nitrosite with  $N_2O_3$  are discussed fully in chapter 5, however before this investigation was undertaken, experiments aimed at determining the mechanisms involved in the formation of the paramagnetic species observed, when humulene nitrosite is irradiated with red light were resumed.

### 3) Solid solutions of humulene nitrosite (17) in dinitro-humulene (24) and nitro-nitrato-humulene (26)

The discovery of dinitro-humulene (24), and nitro-nitrato-humulene (26) was fortuitous, as both readily formed solid solutions with humulene nitrosite, and this provided a method of isolating molecules of humulene nitrosite within a host lattice. If the red excited nitroso group of such an isolated molecule of humulene nitrosite did not react with the host molecules, then nitroxide radicals could only form by transannular cyclisations ,

of the type postulated by scheme II shown in figure 2.9. Thus by monitoring the irradiation of dilute solid solutions of humulene nitrosite in dinitro-humulene, it was hoped to determine if photolysis scheme II operated.

A control experiment was however required to determine if the red excited nitroso group did or did not react with the lattice molecules. Caryophyllene nitrosite (2) does not appear to form nitroxide radicals by cyclisation reactions analogous to those postulated for humulene nitrosite under scheme II. Such a cyclisation in caryophyllene nitrosite would produce the following intermediate



This intermediate can not be stabilised by the loss of a proton from the carbon adjacent to the radical site, nor can the aliphatic radical further interact with neighbouring molecules, this latter possibility having been discounted by McConnell, Porte, et.al.<sup>70</sup> Thus if a dilute solution of caryophyllene nitrosite (2) in dinitro-caryophyllene (27) were to be irradiated in red light, then nitroxide radicals could only form by the interaction of the red excited nitroso group with neighbouring lattice molecules of dinitro-caryophyllene. Samples of caryophyllene nitrosite (2) and dinitro-caryophyllene (27) were thus prepared, using a completely analogous procedure to that just described for preparing the corresponding humulene derivatives.

### 3.3 The reaction of caryophyllene with the oxides of nitrogen

When caryophyllene reacts with the oxides of nitrogen using the procedures described in appendix 3 section 3'.3', the products consist of a mixture of crystalline derivatives or caryophyllene and a yellow oil.

#### a) The crystalline derivatives formed when caryophyllene reacts with the oxides of nitrogen

Two pure crystalline derivatives namely caryophyllene nitrosite (2), and dinitro-caryophyllene (27), form when caryophyllene is reacted with the oxides of nitrogen. The two products were isolated using silica column chromatography, and full details of the separation techniques used are contained in appendix 3, section 3'.3'. Both products were characterised by an analysis and comparison of their  $^1\text{H}$  n.m.r., infra-red, and mass spectra, and an elemental analysis was obtained in each case. Figure 3.5 shows a comparison of the  $^1\text{H}$  n.m.r. spectra of caryophyllene nitrosite (2) and dinitro-caryophyllene (27).

#### Caryophyllene nitrosite (2)

Caryophyllene nitrosite was the major product isolated and spectroscopic evidence indicated that all the contaminants had been removed.

#### Dinitro-caryophyllene (27)

A clear crystalline derivative which had the empirical formula  $\text{C}_{15}\text{H}_{24}\text{N}_2\text{O}_4$  based on the results of the elemental analysis shown in table 3.6. appendix 3 was isolated. A detailed comparison of the  $^1\text{H}$  n.m.r., and infra-red spectra of this derivative, with those of caryophyllene nitrosite (2), enabled it to be characterised,

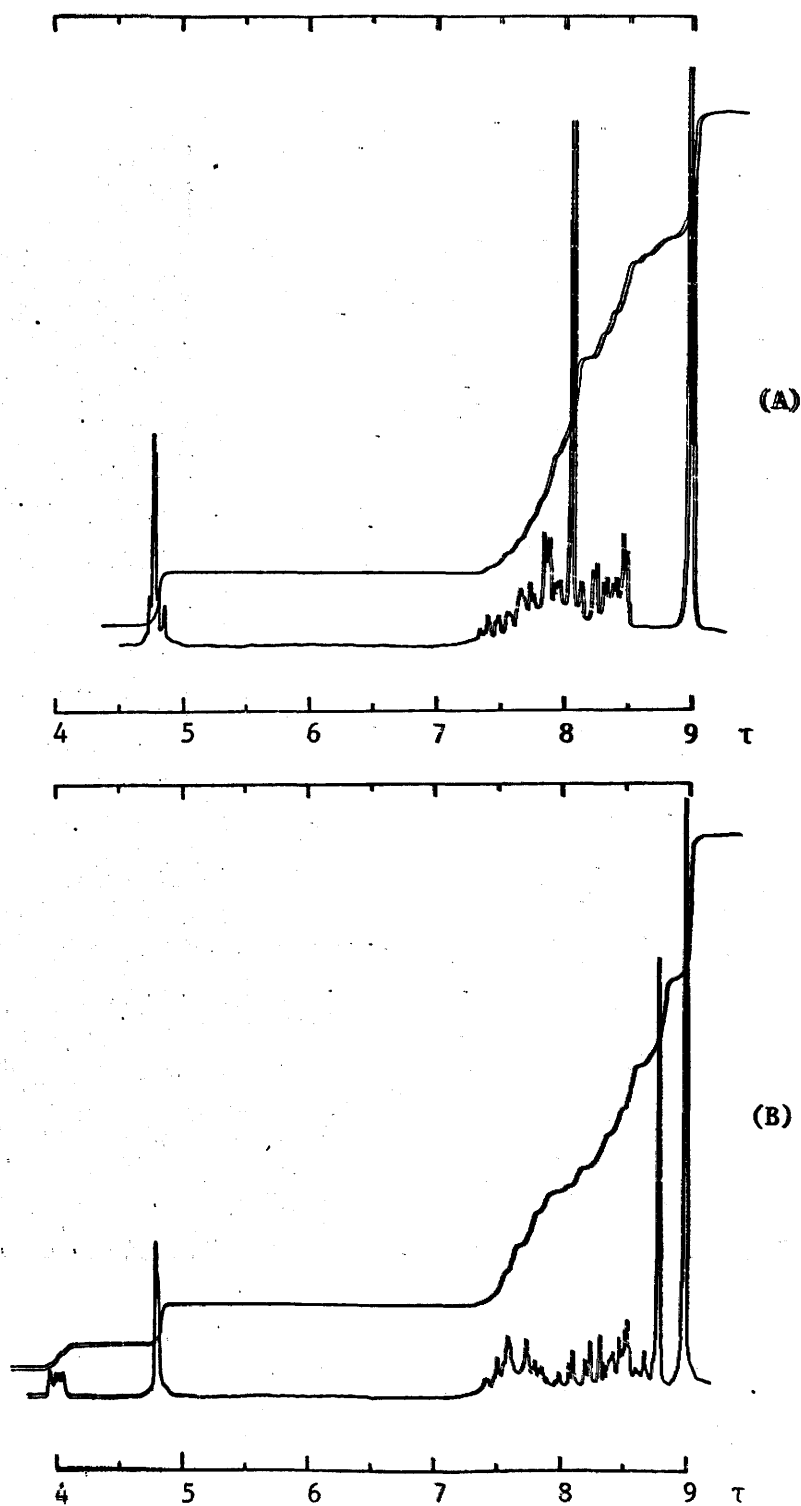
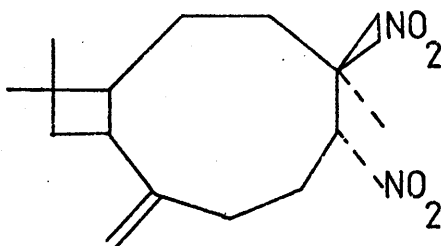


Figure 3.5 The  $^1\text{H}$  n.m.r. spectra of solutions of (A) dinitrocaryophyllene (27) and (B) caryophyllene nitrosite (2) in  $\text{CDCl}_3$ , recorded in the  $\tau$  range 4 to 9.

as the dinitro derivative of caryophyllene shown below.



Dinitro-caryophyllene (27)

The pertinent data from the  $^1\text{H}$  n.m.r. and infra-red spectra of dinitro-caryophyllene (27) are summarised in tables 3.7, and 3.8 respectively.

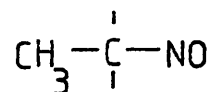
The characterisation of structure (27) was based primarily on the following observations.

- 1) The spectroscopic evidence indicates that the structure of the clear crystals and of caryophyllene nitrosite (2) differs only in the nature of the group attached to  $\text{C}_8$ .
- 2) The infra-red spectra indicate the presence of the following groups on  $\text{C}_8$ .

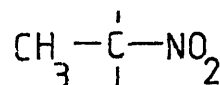
Caryophyllene nitrosite		Clear crystalline derivative	
nitroso		nitro	
$\nu\text{N} = 0$	$1,570\text{ cm}^{-1}$	$\nu\text{NO}_2$ asym.	$1,550\text{ cm}^{-1}$
		$\nu\text{NO}_2$ sym.	$1,340\text{ cm}^{-1}$

- 3) The  $^1\text{H}$  n.m.r. spectra have methyl resonances consistent with the following structures

Caryophyllene nitrosite (2)  $\text{S}\tau = 8.76$



Clear crystalline derivative  $\text{S}\tau = 8.05$





- 4) The mass spectra obtained from the clear crystals and from caryophyllene nitrosite differ only in the position of the parent molecular ion.

The crystalline derivatives of humulene and caryophyllene, namely humulene nitrosite (17), dinitro-humulene (24), nitro-nitrato-humulene (26), caryophyllene nitrosite (2), and dinitro-caryophyllene (27), provided a set of  $^1\text{H}$  n.m.r. and infra-red spectra, which were very useful in helping to characterise other products obtained as the investigations continued.

- b) The nature of the yellow oil formed when caryophyllene reacts with the oxides of nitrogen

The yellow oil formed when caryophyllene is reacted with the oxides of nitrogen has been shown by t.l.c. to consist of several components. Figure 3.6 shows the e.p.r. spectrum at  $295^\circ\text{K}$  of a dilute degassed solution of this yellow oil in chloroform. A single nitroxide radical is present, and the e.p.r. spectrum consists of a 1:1:1 triplet  $\left[ \text{isotropic } \langle g \rangle = 2.0059 \pm 0.0002; \text{isotropic } a(^{14}\text{N}) = 15.9 \pm 0.1\text{G} \right]$ . This radical, radical C, contains the molecular fragment  $\text{R}_1\text{R}_2\text{R}_3\text{C}-\dot{\text{N}}\text{O}-\text{CR}_4\text{R}_5\text{R}_6$ .

When a pure sample of caryophyllene nitrosite reacts with the oxides of nitrogen, the product obtained is also a yellow oil; in solution this has an e.p.r. spectrum, which is the same as that shown in figure 3.6. Thus caryophyllene nitrosite, like humulene nitrosite, can react with the oxides of nitrogen to provide paramagnetic species. This reaction of the nitrosites with the oxides of nitrogen, is fully investigated at a later stage, and is discussed in chapter 5.

Having prepared both humulene nitrosite (17) and

caryophyllene nitrosite (2), and their corresponding dinitro-derivatives (24) and (27), investigations into the mechanisms involved in the photolysis reacts of humulene nitrosite, were resumed.

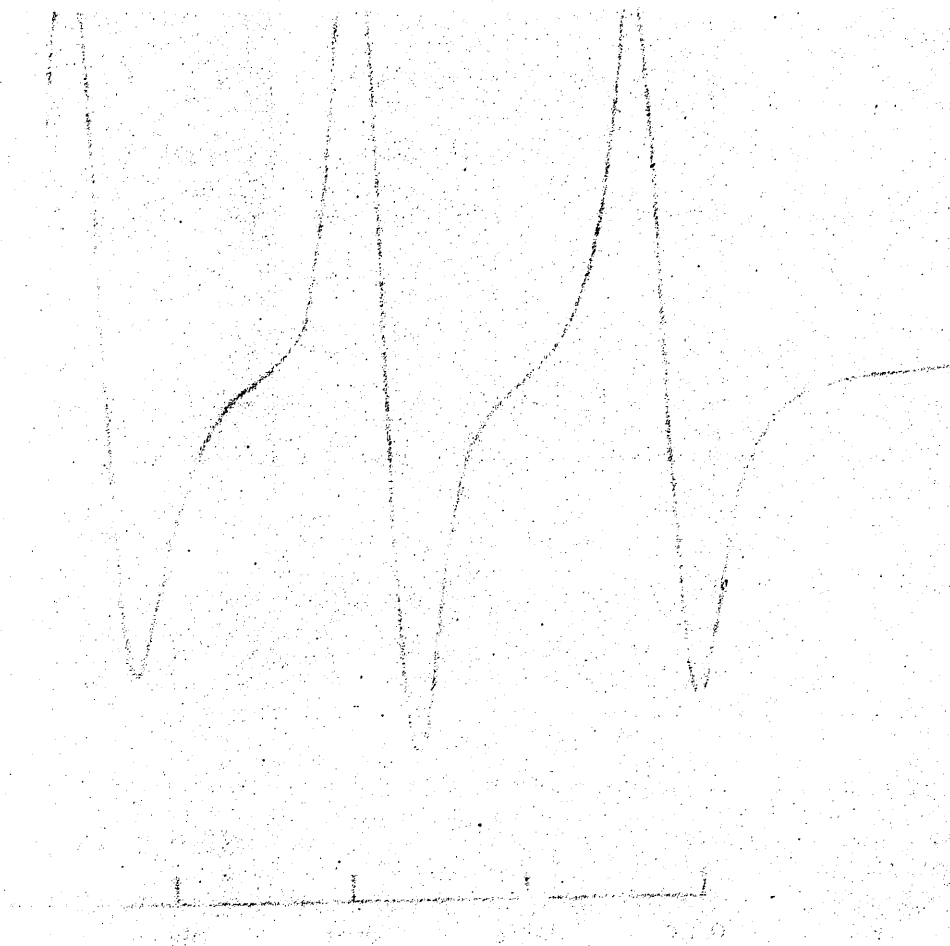


Fig. 1. The photolysis reaction of humulene nitrosite (2) in the laboratory, at the wavelength of 313 nm. The reaction was followed by measuring the absorbance of the solution at 313 nm.

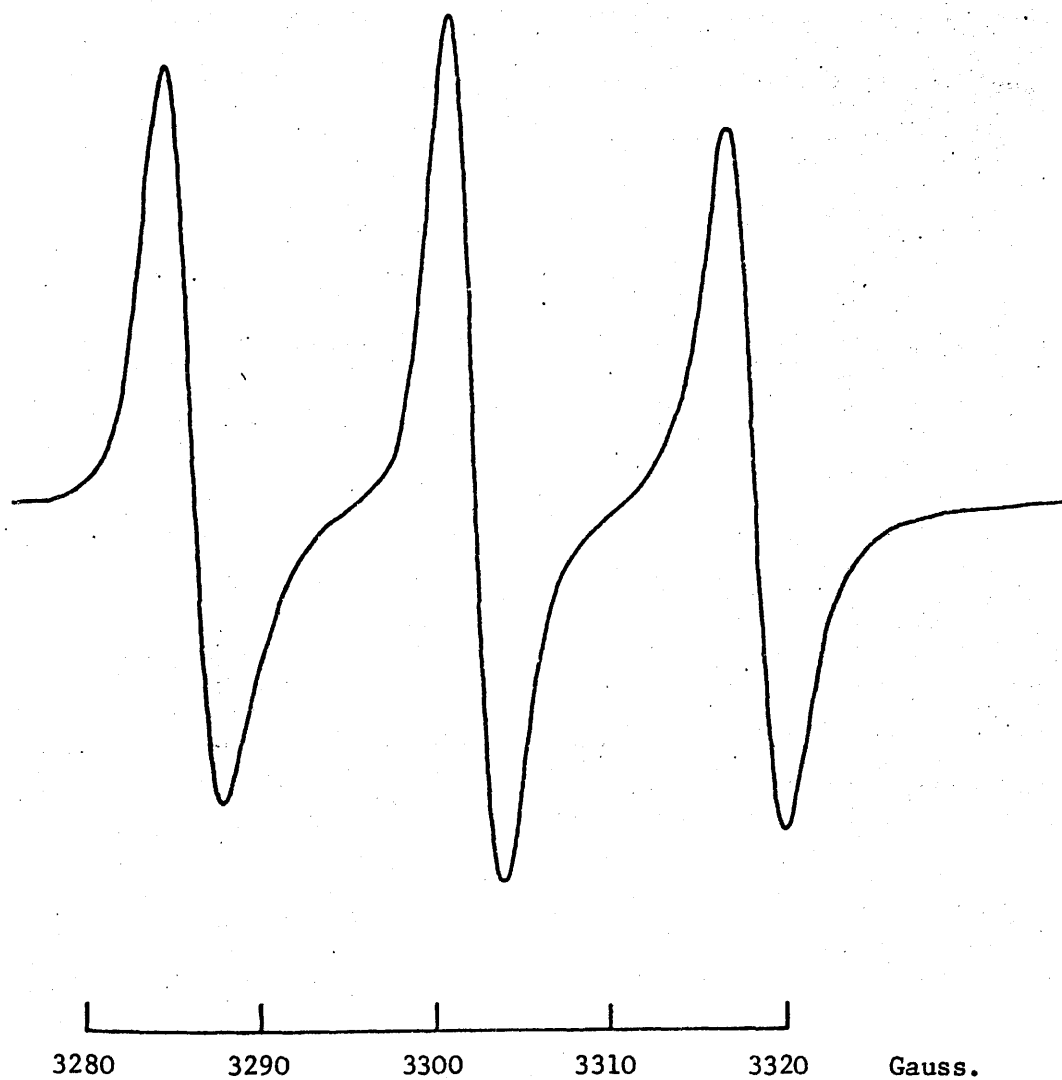


Figure 3.6 The e.p.r. spectrum of a dilute degassed solution in chloroform, of the yellow oil formed when caryophyllene (1) reacts with  $\text{N}_2\text{O}_3$ . The spectrum was recorded at  $295^\circ\text{K}$ .

APPENDIX 3

3'.1' The extraction of a sample of pure humulene from  
technical grade caryophyllene

The method used for the extraction of humulene from technical grade caryophyllene is based on the method employed by R.P. Hildebrand, and M.D. Sutherland<sup>102</sup> with some innovations incorporated.

a) The extraction of a sample enriched in humulene from  
technical grade caryophyllene

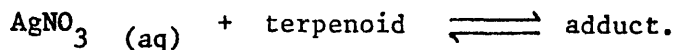
The  $^1\text{H}$  n.m.r. spectrum of technical grade caryophyllene was recorded and a comparison of the relative intensities of the gem-dimethyl peak of humulene (14) singlet at  $\tau = 8.90$  with the gem-dimethyl resonances of caryophyllene (1) at  $\tau = 8.97$ , and  $\tau = 8.99$  showed the mixture to contain 12% humulene and 88% caryophyllene.

Procedure as adopted by R.P. Hildebrand and M.D. Sutherland

Technical grade caryophyllene, 50 gm was shaken with the theoretical amount (for adduct formation) of silver nitrate in a 50% W/W aqueous solution 130 ml. A viscous oil formed over the aqueous layer, and after several hours this oil solidified to a white solid. This white solid which is predominantly caryophyllene:  $\text{AgNO}_3$  adduct, was removed by filtration and the aqueous layer, when steam distilled, yielded 2.4 gm of product a 40% yield. The  $^1\text{H}$  n.m.r. spectrum of this product showed it to consist of 80% humulene, and 20% caryophyllene. Using the procedures described above, Hildebrand, and Sutherland achieved a 50% yield of product of composition, 12% caryophyllene, and 88% humulene.

Innovations made to increase the yield of humulene

- 1) In practice excess  $\text{AgNO}_3$  must be added, as the adduct formation involves an equilibrium process.



- 2) By increasing the volume of the 50% W/W  $\text{AgNO}_3$  solution added, the yield of product is improved, without significantly altering the composition of the product. This is illustrated below in table 3.1.

Table 3.1

Variation in the yield of humulene enriched product on changing the volume of the 50% W/W  $\text{AgNO}_3$  solution added

Concentration of $\text{AgNO}_3$	Volume of $\text{AgNO}_3$ solution	Yield of product	Composition of product
50% W/W	130 ml	2.4 gm	~ 80% humulene
50% W/W	650 ml	3.2 gm	~ 80% humulene

- 3) If the aqueous phase is allowed to stand for 24 hours prior to steam distillation, then clear needles of caryophyllene:  $\text{AgNO}_3$  form. These needles can be removed by filtration, and steam distillation of the filtrate yields a product of composition 16% caryophyllene and 84% humulene.
- 4) If all the solid caryophyllene:  $\text{AgNO}_3$  adduct is rewashed, and the above procedure repeated, a further 1.3 gm of product are obtained. An aqueous solution of 50% W/W  $\text{AgNO}_3$  must

be used for this washing process otherwise the caryophyllene:  
 $\text{AgNO}_3$  adduct dissociates.

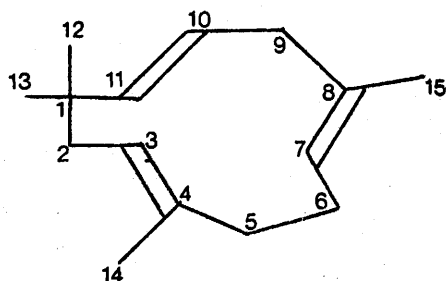
- b) The extraction of pure humulene from the mixture of composition  
 84% humulene and 16% caryophyllene

The 4.5 gm of sample enriched in humulene was dissolved in 10 ml of light petroleum, and the requisite amount of 50% W/W aq. —  $\text{AgNO}_3$  solution added. On standing clear white crystalline needles of humulene:  $(\text{AgNO}_3)_2$  (25) formed in the light petroleum layer. These crystals were dried, and crystallised several times from hot ethanol, yielding 7.0 gm of humulene:  $(\text{AgNO}_3)_2$  of m.pt. =  $176 \pm 0.5^\circ\text{C}$ . Steam distillation of these white crystals allowed the recovery of 2.6 gm of pure humulene. The pertinent data from the  $^1\text{H}$  n.m.r. spectrum of this sample of pure humulene are summarised in table 3.2. The aqueous layer was also steam distilled, and was found to contain 1.3 gm of a mixture of composition 93% humulene, 7% caryophyllene.

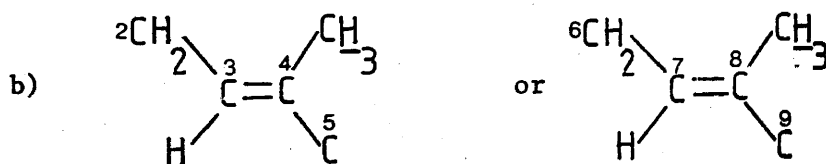
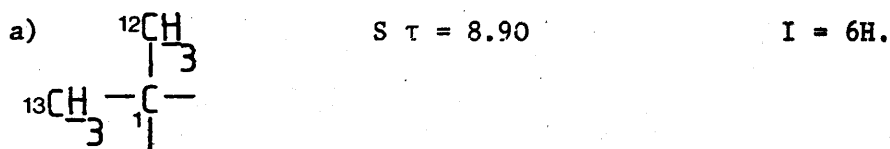
The eventual yield of humulene was 3.6 gm, which is 60% of the humulene present in 50 gm of technical grade caryophyllene.

Table 3.2

Pertinent data from the  $^1\text{H}$  n.m.r. spectrum of humulene



Humulene (14)

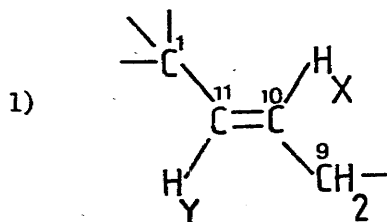


$S \tau = 8.55$  shows a small coupling  $J < 1\text{Hz}.$

$S \tau = 8.35$  shows a small coupling  $J < 1\text{Hz}.$

---

c) Ethylenic protons

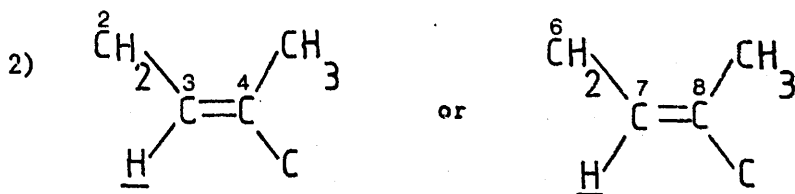


$\text{H}^Y$  doublet  $\tau = 4.88, J_Y = 16.0\text{Hz}.$   $I = 1\text{H}.$

$\text{H}^X$  multiplet  $\tau = 4.42, I = 1\text{H}.$

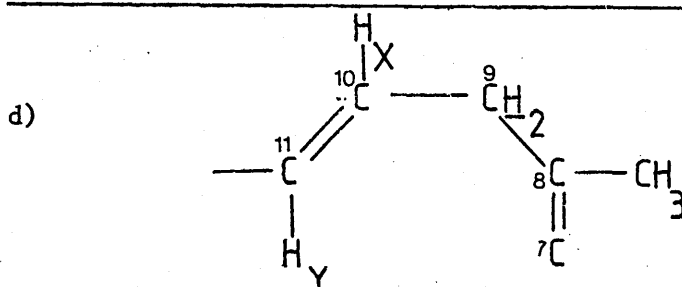
$\text{H}^X$  is the part of an  $\text{XY}$  quartet of  $J_{\text{XY}} = 16.0\text{Hz}.$  due to trans

coupling with  $H_Y$ . Each line is split further into 1:2:1 triplets, through interaction with the  $CH_2$  of  $C_9$ ,  $J = 7\text{Hz}$ .

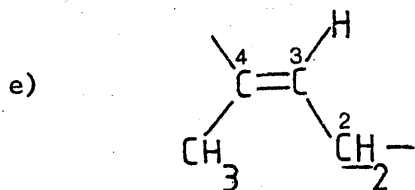


1:2:1 triplet  $\tau = 5.01$ ,  $I = 1H$ ,  $J = 7\text{Hz}$ .

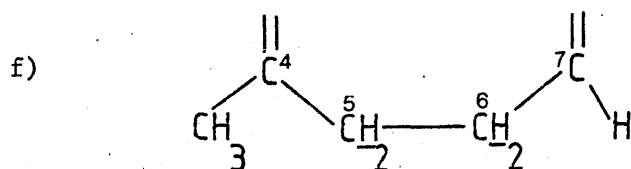
1:2:1 triplet  $\tau = 5.09$ ,  $I = 1H$ ,  $J = 7\text{Hz}$ .



Doublet  $\tau = 7.49$ ,  $I = 2H$ ,  $J = 7\text{Hz}$ , appears as the  $A_2$  part of an  $A_2X$  spectrum.



The underlined protons are the  $A_2$  part of an  $A_2X$  spectrum. Doublet  $\tau = 8.07$ ,  $I = 2H$ , and  $J = 7.5\text{Hz}$ .



Multiplet  $\tau = 7.90$ ,  $I = 4H$ .



### 3.2' The preparation of a pure sample of humulene nitrosite

The method used to prepare humulene nitrosite from humulene does not differ significantly from that employed by S. Mitchell.<sup>72</sup> This was based on work originally carried out by Chapman.<sup>64,65</sup> Several interesting observations which were not detected in the earlier work were however made.

#### a) Repetition of the procedure used by Mitchell to prepare humulene nitrosite

The following procedure was designed to allow one equivalent of humulene to react with one equivalent of  $N_2O_3$ . 3 gm of humulene are dissolved in 7.5 ml of petroleum ether (40-60°C) and cooled to  $\sim 10^\circ C$ . A saturated aqueous solution of  $NaNO_2$  (2 gm), is also cooled to  $10^\circ C$  and the two solutions are mixed. 1.2 ml of glacial acetic acid are added dropwise with continual stirring, over a period of one hour. The petroleum ether layer turns a blue green colour, and when left for thirty minutes at  $0^\circ C$  in an ice bath, a blue solid precipitates out. This solid is filtered and recrystallised from ethanol yielding blue needle shaped, crystals of M.pt =  $112 \pm 2^\circ C$ , yield = 0.45 gm  $\approx$  15%. The above procedure was carried out in total darkness to avoid any photolysis reactions.

#### Innovations made to improve the yield of humulene nitrosite

The blue precipitate from the petroleum ether layer was oily. Washing with petroleum ether removed this oil which was characterised using  $^1H$  n.m.r. spectroscopy as unreacted humulene. This humulene was recycled and when excess  $N_2O_3$  was generated in the petroleum ether layer, the solution became

a dark green colour. On allowing this dark green solution to stand at  $0^{\circ}\text{C}$ , more blue crystals precipitated out. By repeating the above procedure several times, the yield of humulene nitrosite could be increased to approximately 45%. It was noted that each cycle produced a crude product before re-crystallisation which was becoming greener in colour, and eventually a yellow oil was the sole product. Crystallisation of the green material from ethanol gave blue crystals and a yellow solution remained.

b) Isolation of the crystalline derivatives formed when humulene reacts with  $\text{N}_2\text{O}_3$

A qualitative silica t.l.c. of the crystalline products of the reaction of humulene with  $\text{N}_2\text{O}_3$  using ether: pet.ether (50:50) as solvent, showed the presence of three components at  $R_f = 0.36$ ,  $R_f = 0.58$ , and  $R_f = 0.66$ . These  $R_f$  values coincide exactly with those obtained for the impurities, which were found to be present in the humulene nitrosite donated by Mitchell. A quantitative separation of these components was achieved by using silica column chromatography, with columns 1.5 m long, with ether: pet.ether (50:50) as solvent. When 400 mg of humulene nitrosite were chromatographed and 25 fractions each 10 ml collected, then the following results were obtained:

Fraction	$R_f$	Content	% by weight
1 - 6	0.66	Blue needle shaped crystals crystallised from EtOH. M.pt. = $118 \pm 1^{\circ}\text{C}$ .	79.3
7 - 12	0.57	Clear needle shaped crystals crystallised from EtOH. M.pt. = $136.8 \pm 0.5^{\circ}\text{C}$ .	8.5

15.- 20    0.36    Clear needle shaped crystals cryst-    9.6  
allised from EtOH. M.pt. =  $169 \pm 0.5^{\circ}\text{C}$

---

The  $^1\text{H}$ .n.m.r., infra-red, and mass spectra, and an elemental analysis were obtained for each species. All three components have been fully characterised, the component of  $R_f = 0.36$  being dinitro-humulene (24), the component of  $R_f = 0.57$  being nitro-nitrato-humulene (26), and the component of  $R_f = 0.66$  is humulene nitrosite (17). Figure 2.17 shows a comparison of the  $^1\text{H}$  n.m.r. spectra of the three species, and the pertinent data from the  $^1\text{H}$  n.m.r. and infra-red spectra of dinitro-humulene (24) and humulene nitrosite (17) have been previously summarised in tables 2.10 and 2.11.

The following tables 3.3, 3.4, and 3.5, summarise respectively the pertinent data from the elemental analysis,  $^1\text{H}$  n.m.r. spectrum, and infra-red spectrum of nitro-nitrato-humulene (26).

Table 3.3

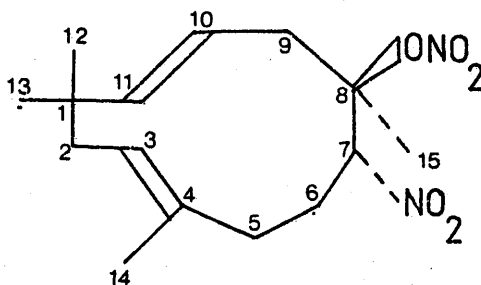
The elemental analysis of nitro-nitrato- humulene (26)

Experimental content    C 57.84%,    H 7.87%,    N 8.99%,    O 25.3%.

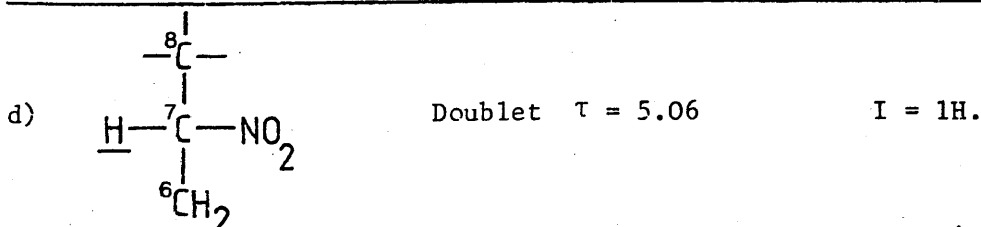
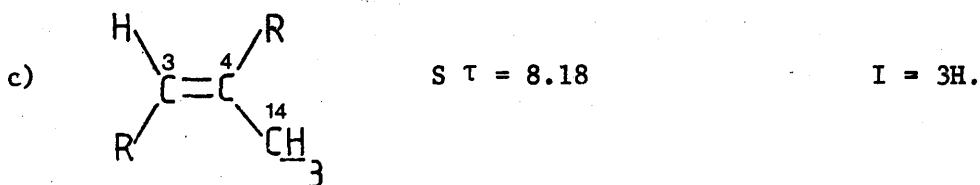
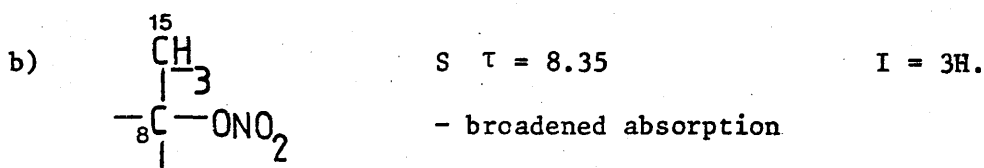
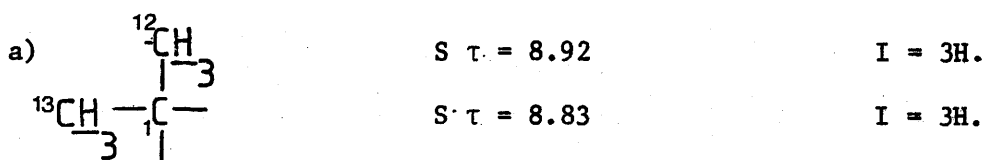
Theoretical content    C 57.68%,    H 7.68%.    N 8.97%.    O 25.65%.

Table 3.4

Pertinent data from the  $^1\text{H}$  n.m.r. spectrum of  
nitro-nitrato-humulene (26)



Nitro-nitrato-humulene (26)

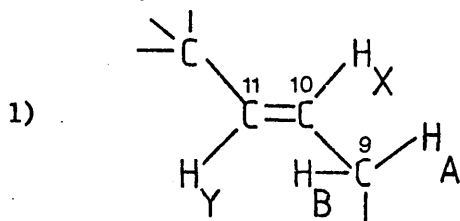


The underlined proton is the X part of an ABX system, and its spectrum should consist of six lines. The observed spectrum, is a doublet, and only one proton appears to be coupling. For humulene nitrosite, the proton on  $\text{C}_7$  also gives a doublet.

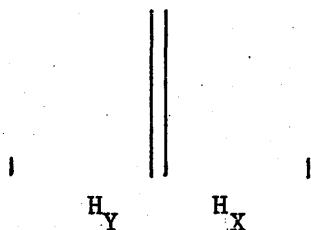
## e) Ethylenic protons

Range  $\tau = 4.53 - 4.91$ .

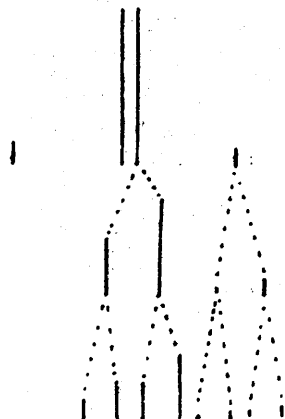
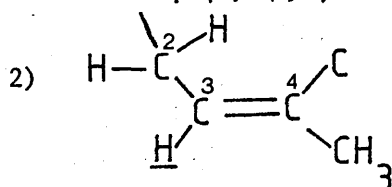
Total I = 3H.



$H_X$  should be the X part of an ABXY system with a trans coupling to  $H_Y$  of  $\sim 16\text{Hz}$ , and then further interaction with  $H_A$  and  $H_B$  to give eight peaks. In this case however, the chemical shifts of  $H_X$  and  $H_Y$  are almost identical and hence the outer lines of their quartet have greatly decreased in intensity.

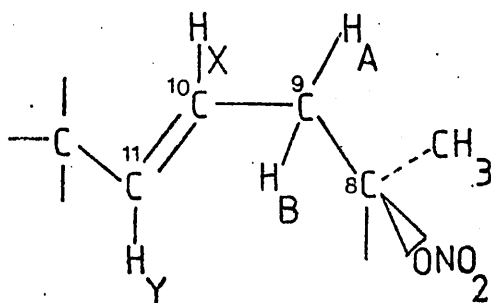


$H_X$  further interacts with  $H_A$  and  $H_B$  as follows.

For  $H_X$   $\tau = 4.83$ For  $H_Y$   $\tau = 4.79$  $J_{AX} = 9 \text{ Hz.}$   $J_{BX} = 2 \text{ Hz.}$  $J_{XY} = 16 \text{ Hz.}$ 

The underlined proton is the X part of an ABX system. Multiplet  $\tau = 4.83, I = 1H, J = 9.5\text{Hz.}$  and  $J = 5\text{Hz.}$  with small additional couplings of  $J < 1\text{Hz.}$

f)



Four peaks are observed for  $H_A$   $\tau = 6.62$ ,  $I = 1H$ ,  $J_{AB} = 17 \text{ Hz.}$ ,  
 $J_{AX} = 2 \text{ Hz.}$  Coupling to  $H_Y$  is less than  $1\text{Hz.}$

Four peaks are observed for  $H_B$   $\tau = 7.89$ ,  $I = 1H$ ,  $J_{AB} = 17\text{Hz.}$ ,  
 $J_{BX} = 9.5 \text{ Hz.}$  Coupling to  $H_Y$  is less than  $1\text{Hz.}$

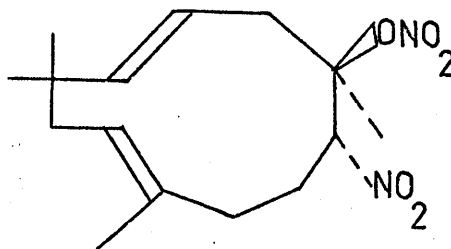
g) Allylic protons

The  $\tau$  region 6.50 to 8.28 contains 9 allylic protons, namely the three allylic  $\text{CH}_2$ 's and the allylic methyl.

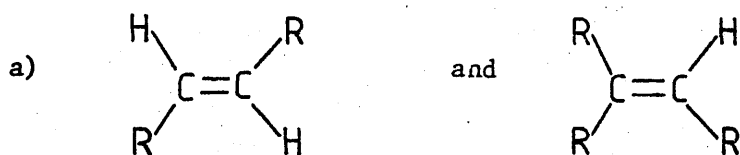
The  $\tau$  region 8.28 to 8.62 contains five protons namely the methyl on the carbon attached to the nitrate and the remaining  $\text{CH}_2$ .

Table 3.5

Pertinent data from the infra-red spectrum of nitro-nitrato-  
-humulene (26)

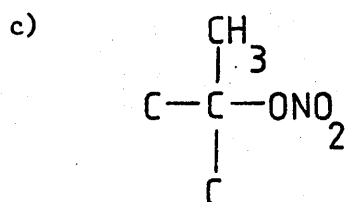
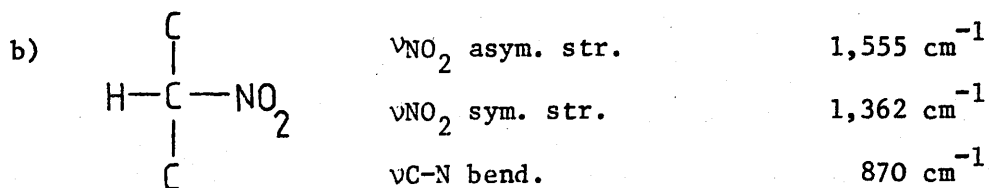
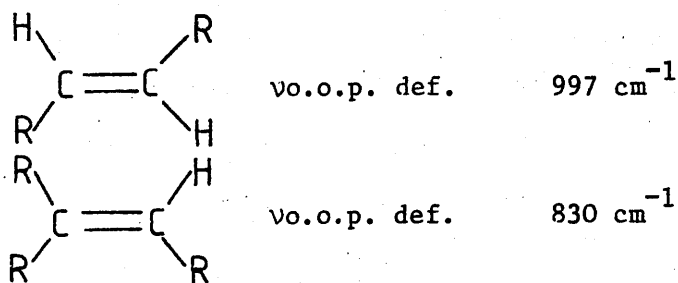


Nitro-nitrato-humulene (26)

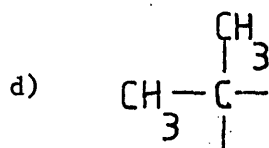


$\nu\text{C} - \text{H}$  str.  $3,015 \text{ cm}^{-1}$ ,  $3,010 \text{ cm}^{-1}$

$\nu\text{C} = \text{C}$  str.  $1,660 \text{ cm}^{-1}$ ,  $1,665 \text{ cm}^{-1}$



Nitrate grouping		Attached methyl	
$\nu$ asym. $\text{NO}_2$ str.	$1,632 \text{ cm}^{-1}$	$\nu$ $\text{CH}_3$ asym. str.	$2,965 \text{ cm}^{-1}$
$\nu$ sym. $\text{NO}_2$ str.	$1,287 \text{ cm}^{-1}$	$\nu$ $\text{CH}_3$ sym. str.	$2,865 \text{ cm}^{-1}$
$\nu$ N-O str.	$852 \text{ cm}^{-1}$	$\nu$ $\text{CH}_3$ sym. def.	$1,387 \text{ cm}^{-1}$
$\nu$ o.o.p. def.	$730 \text{ cm}^{-1}$		
$\nu$ $\text{NO}_2$ def.	$695 \text{ cm}^{-1}$		



$\nu$ asym. str.	$2,960 \text{ cm}^{-1}$	$\nu$ skeletal	$1,374 \text{ cm}^{-1}$
$\nu$ sym. str.	$2,860 \text{ cm}^{-1}$	$\nu$ skeletal	$1,160 \text{ cm}^{-1}$
$\nu$ asym. def. $\sim$	$1,440 \text{ cm}^{-1}$	$\nu$ skeletal	$800 \text{ cm}^{-1}$
$\nu$ sym. def.	$1,387 \text{ cm}^{-1}$		

c) Nature of the yellow oil obtained when humulene reacts with the oxides of nitrogen

Figure 3.3 is the e.p.r. spectrum of a dilute solution in chloroform of the yellow oil formed when humulene reacts with  $\text{N}_2\text{O}_3$ . This oil was chromatographed using silica plates with ether:pet.ether (50:50) as solvent, and four diamagnetic compounds were abstracted. Their  $R_f$  values were 0.1, 0.3, 0.4, and 0.8, respectively. The  $^1\text{H}$  n.m.r. and infra-red spectra were recorded for each species.

d) The reaction of pure humulene nitrosite with the oxides of nitrogen

This reaction is completely analogous to the reaction described in appendix 3, section 3'.2' (a) except that instead of



a sample of humulene dissolved in petroleum ether being used as the reactant, a sample of pure humulene nitrosite dissolved in "ethanol free" chloroform was used. The product of the reaction is a yellow oil, and the e.p.r. spectrum of this yellow oil, in a dilute chloroform solution, is exactly the same as the spectrum shown in figure 3.3.

### 3'.3' The preparation of a pure sample of caryophyllene nitrosite (2)

The procedures used to prepare caryophyllene nitrosite from caryophyllene are completely analogous to those used to prepare humulene nitrosite from humulene, which are described in appendix 3, section 3'.2'.

The yield of caryophyllene nitrosite obtained by allowing one equivalent of caryophyllene, to react with one equivalent of  $N_2O_3$ , has been reported in the literature as  $\sim 14\%$ . This yield was increased to 35% by first performing the reaction at  $10^\circ C$ , instead of the  $0^\circ C$  used by Chapman,<sup>64,65</sup> and second by recycling unreacted caryophyllene whilst allowing excess  $N_2O_3$  into the system. Each cycle produced a crude product which was becoming greener in colour and eventually, a yellow oil was the sole product. Crystallisation of the green material from ethanol, gave blue needle shaped crystals of M.pt. =  $113 \pm 1^\circ C$  and a yellow solution remained.

A qualitative silica t.l.c. of the crystalline products of the reaction of caryophyllene with  $N_2O_3$  with ether: pet.ether (50:50) as solvent, showed the presence of two components at  $R_f = 0.59$  and  $R_f = 0.64$ . A quantitative separation of these components was achieved using silica column chromatography with columns 1.5 m long, and ether: pet.ether (50:50) as solvent.

The component of  $R_f = 0.64$

The component of  $R_f = 0.64$ , when crystallised from hot

ethanol gave blue needle crystals of M.pt. =  $116 \pm 1^{\circ}\text{C}$ . An analysis of the  $^1\text{H}$  n.m.r. and infra-red spectra confirmed that these crystals are caryophyllene nitrosite (2).

The component of  $R_f$  = 0.59

The component of  $R_f$  = 0.59 when crystallised from ethanol, produces clear needle shaped crystals of M.pt. =  $127 \pm 0.5^{\circ}\text{C}$ . This material has been characterised as the dinitro-derivative of caryophyllene (27). Table 3.6 shows the results of an elemental analysis of dinitro-caryophyllene (27). The pertinent data obtained from a comparison of the  $^1\text{H}$  n.m.r. spectra, and the infra-red spectra of dinitro-caryophyllene (27), and caryophyllene nitrosite (2), are summarised in tables 3.7, and 3.8, respectively.

Table 3.6

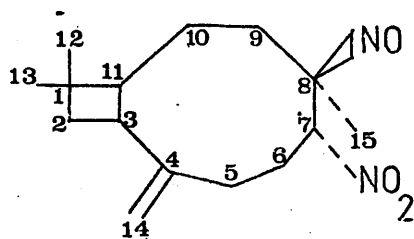
The elemental analysis of dinitro-caryophyllene (27)

Experimental content C 60.62%, H 7.89%, N 9.6%, O 21.9%.

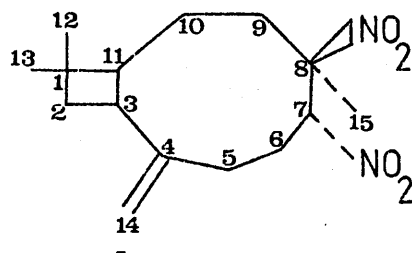
Theoretical content C 60.9%, H 8.1%, N 9.5%, O 21.5%.

Table 3.7

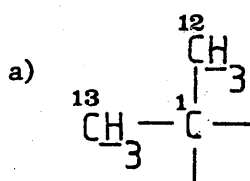
Pertinent data from the  $^1\text{H}$  n.m.r. spectra of caryophyllene nitrosite (2) and dinitro-caryophyllene (27)



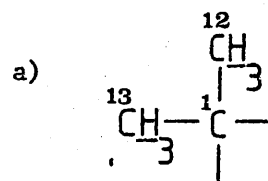
Caryophyllene nitrosite (2)



Dinitro-caryophyllene (27)

S  $\tau = 8.96$ 

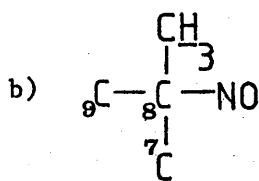
I = 6H.

S  $\tau = 8.99$ 

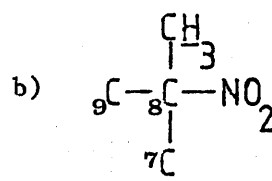
I = 3H.

 $\tau = 8.96$ 

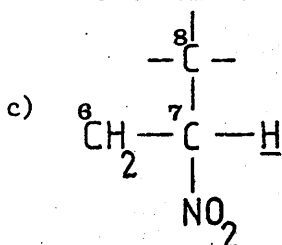
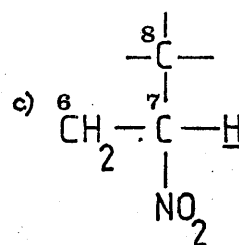
I = 3H.

S  $\tau = 8.76$ 

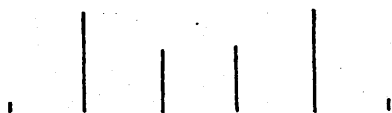
I = 3H.

S  $\tau = 8.05$ 

I = 3H.

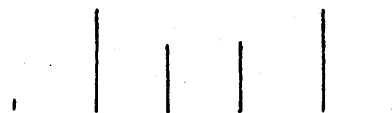
Multiplet  $\tau = 3.97$  I = 1H.Multiplet  $\tau = 4.07$  I = 1H.

This proton is the X part of an ABX system. The two outermost transitions are very weak and the spectrum has the following appearance.



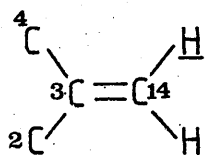
$$J_{AX} = 5.5 \text{ Hz.}, \quad J_{BX} = 4.5 \text{ Hz.}$$

This proton is the X part of an ABX system. The two outermost transitions are very weak and the spectrum has the following appearance.



$$J_{AX} = 5.6 \text{ Hz.}, \quad J_{BX} = 4.5 \text{ Hz.}$$

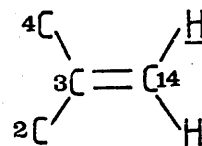
d) Ethylenic protons



Doublet  $\tau = 4.77$   $I = 2H$ .

small coupling  $J < 1\text{Hz}$ .

d) Ethylenic protons



Doublet  $\tau = 4.77$   $I = 2H$ .

small coupling  $J < 1\text{Hz}$ .

e) Allylic protons

The  $\text{CH}_2$  region of the spectrum is difficult to analyse. There are two main groupings of resonances.

1)  $\tau = 8.38 - 8.96$   $I = 4H$ .

This region probably contains the allylic  $\text{CH}_2$  and the protons attached to the tertiary carbons.

2)  $\tau = 8.96 - 9.71$   $I = 8H$ ,

e) Allylic protons

The  $\text{CH}_2$  region of the spectrum is difficult to analyse. There are two main groups of resonances.

1)  $\tau = 8.49 - 8.99$   $I = 6H$ .

This region probably contains the allylic  $\text{CH}_2$  the two protons attached to the tertiary carbons and two

of the four protons on  $\text{CH}_2$  groups

contains the remaining four  $\text{CH}_2$  groups.

$\alpha$  to the carbon attached to a nitro group.

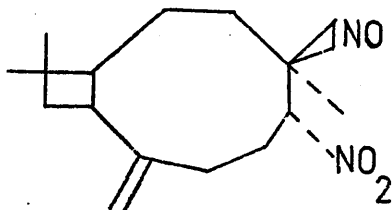
2)  $\tau = 9.10 - 9.84$   $I=6H$

contains the remaining two  $\text{CH}_2$  groups, and two of the protons on the  $\text{CH}_2$  groups  $\alpha$  to the carbons attached to nitro groups.

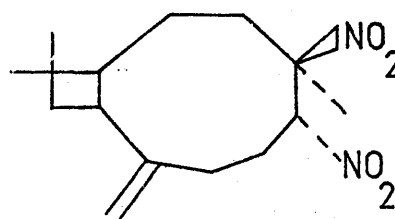
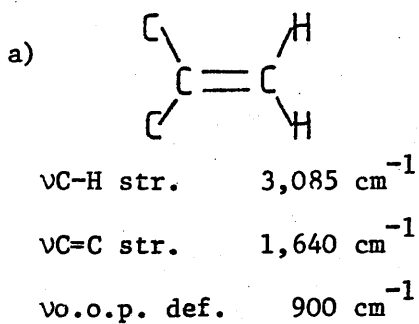
---

Table 3.8

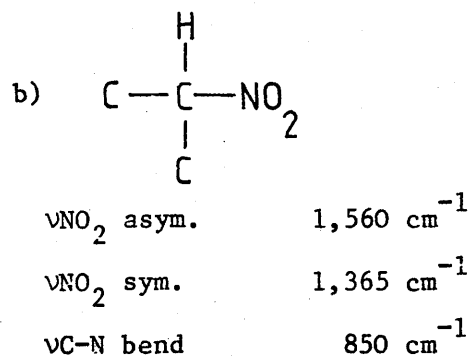
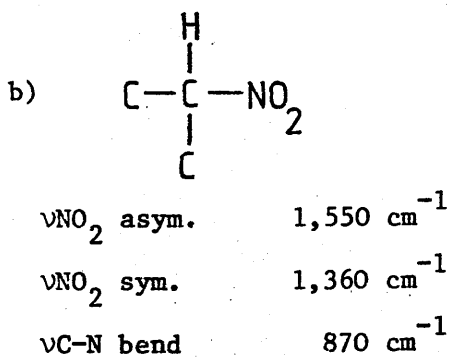
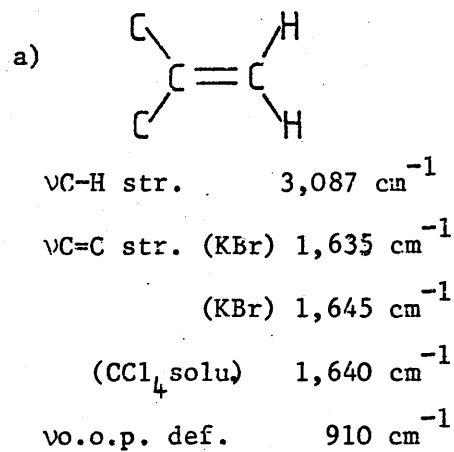
Pertinent data from the infra-red spectra of caryophyllene nitrosite (2) and dinitro-caryophyllene (27)

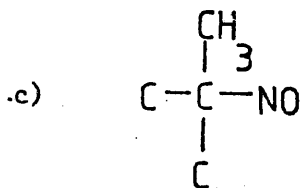


Caryophyllene nitrosite (2)



Dinitro-caryophyllene (27)



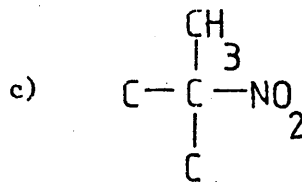


$\nu\text{N}=\text{O}$  str. 1,570  $\text{cm}^{-1}$

$\nu\text{CH}_3$  str. asym. 2,960  $\text{cm}^{-1}$

$\nu\text{CH}_3$  str. sym. 2,875  $\text{cm}^{-1}$

$\nu\text{CH}_3$  def. 1,385  $\text{cm}^{-1}$



$\nu\text{NO}_2$  asym. 1,550  $\text{cm}^{-1}$

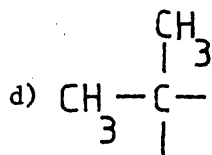
$\nu\text{NO}_2$  sym. 1,340  $\text{cm}^{-1}$

$\nu\text{C}-\text{N}$  bend 850  $\text{cm}^{-1}$

$\nu\text{CH}_3$  str. asym. 2,960  $\text{cm}^{-1}$

$\nu\text{CH}_3$  str. sym. 2,860  $\text{cm}^{-1}$

$\nu\text{CH}_3$  def. 1,395  $\text{cm}^{-1}$



$\nu$  asym str. 2,960  $\text{cm}^{-1}$

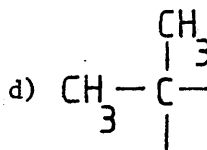
$\nu$  sym. str. 2,870  $\text{cm}^{-1}$

$\nu$  sym. def. 1,385  $\text{cm}^{-1}$

$\nu$  skeletal 1,365  $\text{cm}^{-1}$

$\nu$  skeletal ~ 1,170  $\text{cm}^{-1}$

$\nu$  skeletal 805  $\text{cm}^{-1}$



$\nu$  asym. str. 2,960  $\text{cm}^{-1}$

$\nu$  sym. str. 2,860  $\text{cm}^{-1}$

$\nu$  sym. def. 1,390  $\text{cm}^{-1}$

$\nu$  skeletal 1,375  $\text{cm}^{-1}$

$\nu$  skeletal ~ 1,165  $\text{cm}^{-1}$

$\nu$  skeletal 805  $\text{cm}^{-1}$

b) The yellow oil obtained when caryophyllene reacts with the oxides of nitrogen

Figure 3.6 shows the e.p.r. spectrum recorded at 295°K, of a dilute degassed solution, in chloroform, of the yellow oil obtained by reacting caryophyllene with  $\text{N}_2\text{O}_3$ . A series of qualitative

silica t.l.c. experiments using various solvents, showed the presence of at least four components, within the oil.

c) The reaction of pure caryophyllene nitrosite (2) with the oxides of nitrogen

The experimental procedure used was completely analogous to that described in appendix 3, section 3'.2' (d). The product of the reaction is a yellow oil, and the e.p.r. spectrum of this yellow oil in a dilute chloroform solution, is exactly the same as the spectrum shown in figure 3.6.



## CHAPTER 4

### AN EXAMINATION OF THE MECHANISMS GOVERNING THE PRODUCTION OF THE PARAMAGNETIC SPECIES OBSERVED WHEN HUMULENE NITROSITE IS IRRADIATED WITH RED LIGHT

It was demonstrated in chapter 2 that humulene nitrosite, like caryophyllene nitrosite, was a versatile source of nitroxide radicals when irradiated with red light. When the irradiation of crystalline samples of humulene nitrosite and its solutions in solvents which do not interact with a red excited nitroso group, were monitored in an e.p.r. spectrometer, four different nitroxide radicals were observed. Measurements were made of the kinetics governing the production of these radicals and in the solid state three of the radicals were stable, namely radicals  $I_A$ , and  $I_B$ , both of which contain the structural unit  $R_1R_2R_3C-\dot{N}O-CR_4R_5R_6$  and radical II, which contains the structural unit  $R_1R_2R_3C-\dot{N}O-CHR_4R_5$ . The remaining radical, radical III, contained the structural unit  $R_1R_2R_3C-\dot{N}O-CHR_4R_5$ , and was a transient species, which decomposed as the irradiation proceeded. Two mechanisms were postulated to explain the formation of these radicals. The first of these schemes, scheme I, is shown in figure 2.7. It involves the attack of the electron in the  $\sigma$  framework of a red excited nitroso group, at a neighbouring molecule of humulene nitrosite, displacement of  $\dot{N}O$  producing a stable nitroxide radical, containing the structural unit  $R_1R_2R_3C-\dot{N}O-CR_4R_5R_6$ , and displacement of  $\dot{N}O_2$ , producing a transient radical, containing the structural unit  $R_1R_2R_3C-\dot{N}O-CHR_4R_5$ , which also retains a nitroso chromophore. Further irradiation with red

light would cause this transient intermediate to lose  $\dot{\text{N}}\text{O}$ , with a subsequent rearrangement, to a stable nitroxide radical containing the structural unit  $\text{R}_1\text{R}_2\text{R}_3\text{C}-\dot{\text{N}}\text{O}-\text{CHR}_4\text{R}_5$ . Scheme I, was found to be consistent with all the nitroxide radicals observed, and with the kinetics of their formation, and is analogous to the scheme postulated by McConnell, Porte, et.al.,<sup>70</sup> to explain the production of the nitroxide radicals observed when caryophyllene nitrosite is irradiated with red light.

Scheme II is shown in figure 2.9. and involves an intramolecular cyclisation, the red excited nitroso group undergoing a transannular addition to either of the carbon to carbon  $\pi$  bonds in the humulene nitrosite structure. Scheme II could not adequately explain the formation of the nitroxide radicals observed but the possibility that it operated in conjunction with scheme I could not be discounted.

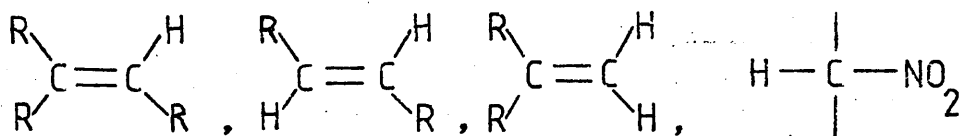
A mixture of nitroxide radicals  $\text{I}_\text{A}$  and  $\text{I}_\text{B}$ , was isolated in a nearly pure state, using chromatographic techniques, and their infra-red spectrum was shown to be consistent with the diastereomeric forms of structure (19), postulated by scheme I. Diamagnetic species were also isolated and accounted for 90% of the product. The nature of these diamagnetic species, and the mechanism by which they formed, were not however understood.

#### 4.1 Monitoring by means of infra-red spectroscopy the irradiation of humulene nitrosite with red light

On replenishing the supply of humulene nitrosite, the irradiation with red light, of a polycrystalline sample of the nitrosite was monitored in an infra-red spectrometer, in an attempt

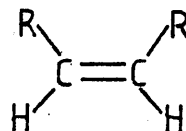
to identify if products of the type postulated by scheme II were present. The experimental details are contained in appendix 4, section 4'.1'. The main changes observed in the spectra as the irradiation proceeds are summarised in table 4.1. appendix 4.

These changes have to be considered in the knowledge that 90% of the products are diamagnetic. Details of the isolation of these diamagnetic species were given in appendix 2, section 2'.2'.2'(d) and their  $^1\text{H}$  n.m.r., and infra-red spectra were discussed. The two main diamagnetic components extracted were dinitro-humulene (24) and an oil, which contained a mixture of isomeric compounds containing a single nitro group attached either to a humulene structure, or to a rearrangement of it. These isomeric compounds were shown by  $^1\text{H}$  n.m.r. and infra-red spectroscopy, to contain the following groupings.



The major changes observed in the infra-red spectra, as the irradiation proceeds, were consistent with the formation of the diamagnetic species discussed above, and as only 10% of the products were paramagnetic, this was not a good technique for monitoring their production. The following observations were however made.

- 1) As the irradiation proceeded, the absorption at  $1,570\text{ cm}^{-1}$  due to the nitroso group slowly disappeared and a new absorption arose at  $1,380\text{ cm}^{-1}$ ; this latter absorption is attributed to a nitroxide group.
- 2) No absorptions attributable to the



- 3) The intensities of the original C=C bonds decreased in a manner consistent with the isomerisation of the C=C positions in the diamagnetic species formed. Overall however there was little, if any reduction in the number of C=C units present.

Photolysis scheme II, shown in figure 2.9 involved the production of cis double bonds, and a substantial removal of the other double bonds present.

4.2 The irradiation, with red light, of a solid solution of caryophyllene nitrosite (2) in dinitro-caryophyllene (27)

Humulene nitrosite (17), was found to readily form solid solutions with dinitro-humulene (24). This provided a method whereby molecules of humulene nitrosite could be isolated within a crystalline lattice of host molecules. If the red excited nitroso group of such an isolated molecule did not react with a host molecule of dinitro-humulene, then nitroxide radicals could only form by the process of transannular cyclisation, postulated in photolysis scheme II.

In order to determine if the red excited nitroso group was likely to interact with the host molecules, a closely analogous control experiment was carried out, which involved the irradiation of dilute solid solutions of caryophyllene nitrosite (2) in dinitro-caryophyllene (27). As was discussed in chapter 3, section 3.2. caryophyllene nitrosite, does not undergo transannular cyclisations of the type postulated for humulene nitrosite under scheme II, and the detection of nitroxide radicals during the irradiation would imply

that the red excited nitroso group could interact with the lattice molecules of dinitro-caryophyllene.

#### 4.2.1 Monitoring by means of e.p.r. spectroscopy the irradiation with red light of a solid solution of caryophyllene nitrosite (2) in dinitro-caryophyllene (27)

The irradiation with red light, of a polycrystalline sample of a solid solution of caryophyllene nitrosite, in dinitro-caryophyllene (10:90), was monitored in an e.p.r. spectrometer. The crystals slowly turned pale yellow, and figure 4.1 shows the e.p.r. spectrum of the irradiated material. The line shape of the spectrum did not change as the irradiation proceeds and the increase in intensity was almost linear with time. The form of this spectrum did not change when the products were pumped for one hour at <0.1 mm Hg pressure, indicating that trapped  $\dot{\text{NO}}$  or  $\dot{\text{NO}}_2$ , was not responsible for any of the structure in the spectrum.

An analysis of the spectrum shown in figure 4.1. shows that it arises because of the presence of a nitroxide radical containing the structural unit  $\text{R}_1\text{R}_2\text{R}_3\text{C}-\dot{\text{N}}\text{O}-\text{CHR}_4\text{R}_5$ . The spin Hamiltonian parameters for this radical, radical IV' are shown in table 4.2.

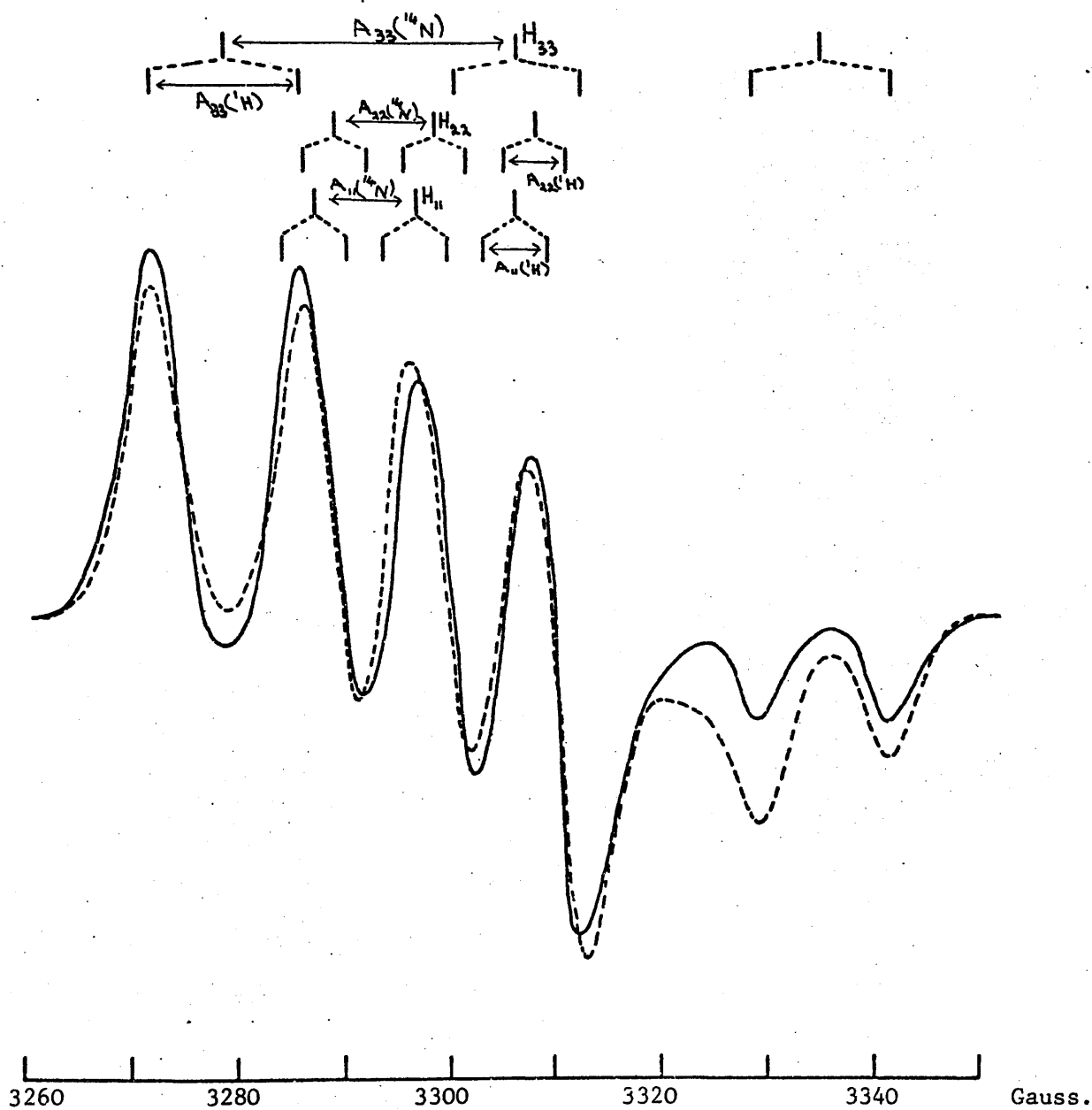


Figure 4.1 The e.p.r. spectrum of a dilute polycrystalline sample of nitroxide radical IV' obtained by irradiating a solid solution of caryophyllene nitrosite (2) in dinitro-caryophyllene (27) (10:90) with red light. The dotted line represents the calculated spectrum of radical IV'.

Table 4.2

The spin Hamiltonian parameters for nitroxide radical  $\overline{\text{IV}}'$

$g_{11}$	$g_{22}$	$g_{33}$	$\langle g \rangle$	
2.0092	2.0079	2.0031	2.0067	
$A_{11}(^{14}\text{N})$	$A_{22}(^{14}\text{N})$	$A_{33}(^{14}\text{N})$	$a(^{14}\text{N})$	
9.5G	9.5G	28.0G	15.7G	
$A_{11}(^1\text{H})$	$A_{22}(^1\text{H})$	$A_{33}(^1\text{H})$	$a(^1\text{H})$	$\beta$
6.0G	6.0G	12.5G	8.2G	2.5G

The limits of error for  $g_{11}$ ,  $g_{22}$ ,  $g_{33}$ ,  $\langle g \rangle$ ,  $A_{11}(^{14}\text{N})$ ,  $A_{22}(^{14}\text{N})$ ,  $A_{33}(^{14}\text{N})$ ,  $a(^{14}\text{N})$ ,  $A_{11}(^1\text{H})$ ,  $A_{22}(^1\text{H})$ ,  $A_{33}(^1\text{H})$ , and  $a(^1\text{H})$ , are respectively,  $\pm 0.0003$ ,  $\pm 0.0003$ ,  $\pm 0.0002$ ,  $\pm 0.0003$ ,  $\pm 0.5\text{G}$ ,  $\pm 0.5\text{G}$ ,  $\pm 0.2\text{G}$ ,  $\pm 0.5\text{G}$ ,  $\pm 0.5\text{G}$ ,  $\pm 0.2\text{G}$ , and  $\pm 0.5\text{G}$ .

If at any stage the products are dissolved in chloroform, then the radical  $\overline{\text{IV}}'$  immediately disproportionates to diamagnetic species, and the e.p.r. spectrum decreased greatly in intensity. This is the behaviour expected of a nitroxide radical containing the molecular fragment  $\text{R}_1\text{R}_2\text{R}_3\text{C}-\dot{\text{N}}\text{O}-\text{CHR}_4\text{R}_5$ . The weak e.p.r. signal which remains after radical  $\overline{\text{IV}}'$  has disproportionated, is attributed to a nitroxide radical containing the molecular fragment  $\text{R}_1\text{R}_2\text{R}_3\text{C}-\dot{\text{N}}\text{O}-\text{CR}_4\text{R}_5\text{R}_6$ .

The mechanism involved in producing nitroxide radical  $\overline{\text{IV}}'$  is probably that shown in figure 4.2, whereby a red excited nitroso group displaces a nitro group from a neighbouring molecule of dinitro-caryophyllene. There are two possible nitro groups which

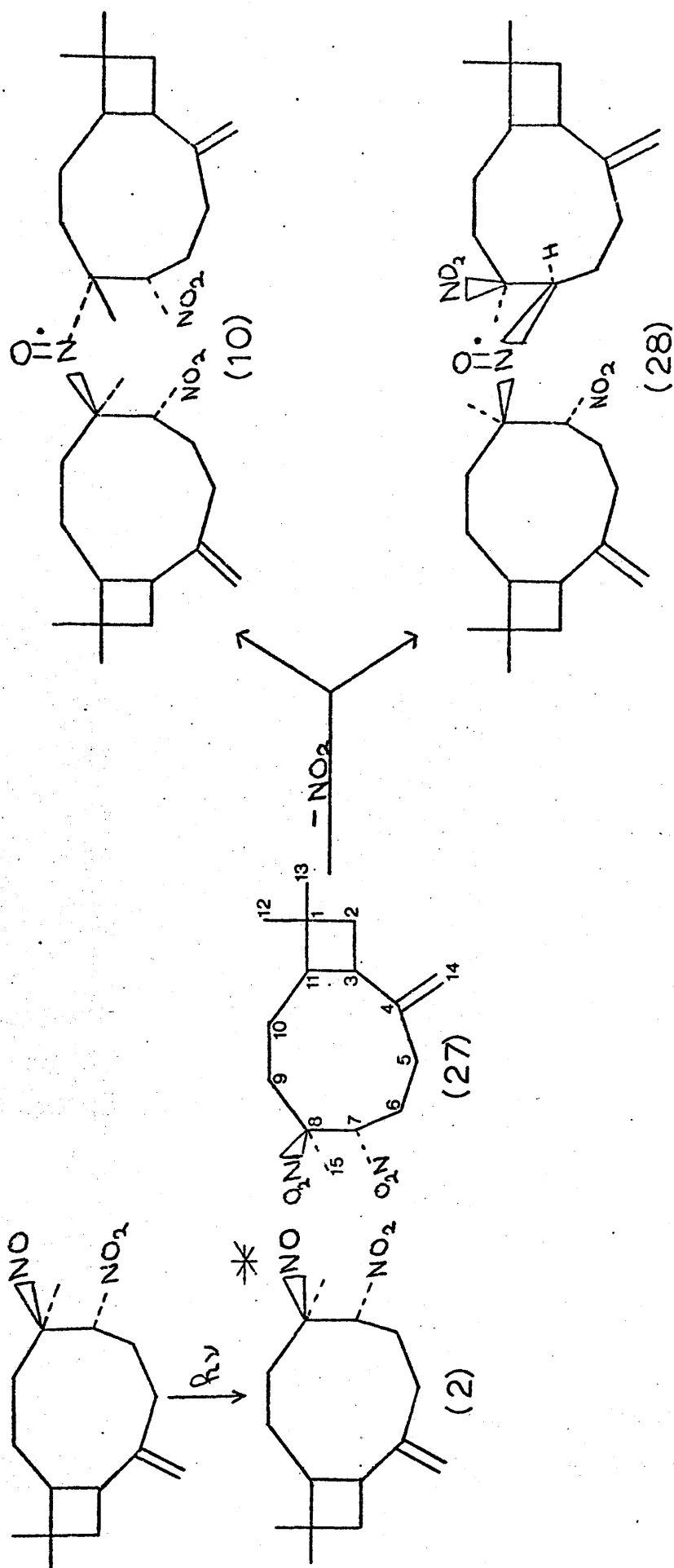


Figure 4.2 The mechanism governing the formation of the paramagnetic species observed when a solid solution of caryophyllene nitrosite (2) in dinitro-caryophyllene (27) (10:90) is irradiated with red light.



could be displaced, and the predominance of the nitroxide radical IV' of structure (28), which forms by displacing the nitro group on C<sub>7</sub> of dinitro-caryophyllene is probably a function of geometric and steric considerations within the crystal structure. Small amounts of a radical containing the structural unit  $R_1R_2R_3C-\dot{N}O-CR_4R_5R_6$  were detected, their origin is however, uncertain, since they could either arise as shown in figure 4.2, or result from a small amount of residual intermolecular reaction, between molecules of caryophyllene nitrosite, which by chance adopted adjacent positions within the lattice.

The only alternative mechanism to that described above would involve the transannular cyclisation of the red excited nitroso group of caryophyllene nitrosite, to the exomethylene group of the molecule. Caryophyllene nitrosite has never previously been observed to undergo such cyclisations, and moreover they could not explain the formation of a nitroxide radical containing the molecular unit  $R_1R_2R_3C-\dot{N}O-CHR_4R_5$ .

#### 4.2.2 Monitoring by means of infra-red spectroscopy the irradiation with red light of a solid solution of caryophyllene nitrosite in dinitro-caryophyllene

In order to confirm that nitroxide radical IV' had structure (28), the irradiation of a solid solution of caryophyllene nitrosite in dinitro-caryophyllene was monitored in an infra-red spectrometer. The experimental details are contained in appendix 4, section 4'.2'. The changes observed in the infra-red spectra, are summarised in table 4.3, appendix 4, and are consistent with the nitroxide radical IV' having structure (28). The main observations

favouring the mechanism shown in figure 4.2. are listed below.

- 1) First it was observed that the nitroso absorption slowly disappears, and is replaced by an absorption at  $1,387\text{ cm}^{-1}$  which has been assigned to a nitroxide stretching frequency.
- 2) Second there is a decrease in intensity of both the symmetric, and asymmetric nitro absorptions. It was difficult to accurately determine the position from which the nitro groups were being lost, but it is probably from  $C_7$  of dinitro-caryophyllene.
- 3) Third all the remaining infra-red absorptions remained unchanged.

4.3. The irradiation, with red light, of a solid solution of humulene nitrosite (17) in dinitro-humulene(24)

In investigating the irradiation of dilute solutions of humulene nitrosite, in dinitro-humulene, with red light, a careful consideration was given to the possible methods by which nitroxide radicals might form. There were two distinct mechanisms which might operate.

- 1) The first mechanism involves the production of radicals by reactions analogous to those involved when dilute solutions of caryophyllene nitrosite in dinitro-caryophyllene are irradiated with red light.
- 2) The second mechanism which might operate is shown in photolysis scheme II, which involves an intra-molecular cyclisation of the humulene nitrosite structure.

4.3.1 Monitoring by means of e.p.r. spectroscopy the irradiation with red light of a solid solution of humulene nitrosite (17) in dinitro-humulene (24)

When solid solutions of humulene nitrosite, in dinitro-humulene (10:90) were irradiated with red light, they behaved in a manner completely analogous to the solid solutions of caryophyllene nitrosite in dinitro-caryophyllene. Figure 4.3 shows the polycrystalline e.p.r. spectrum of the irradiated solid. The line shape of this spectrum did not change as the irradiation proceeded, and the increase in intensity was almost linear with time. An analysis of the spectrum shown in figure 4.3, shows that it arises because of the presence of a nitroxide radical which contains the structural unit  $R_1R_2R_3\dot{C}-NO-CHR_4R_5$ . The spin Hamiltonian parameters for this radical, radical IV, are shown in table 4.4.

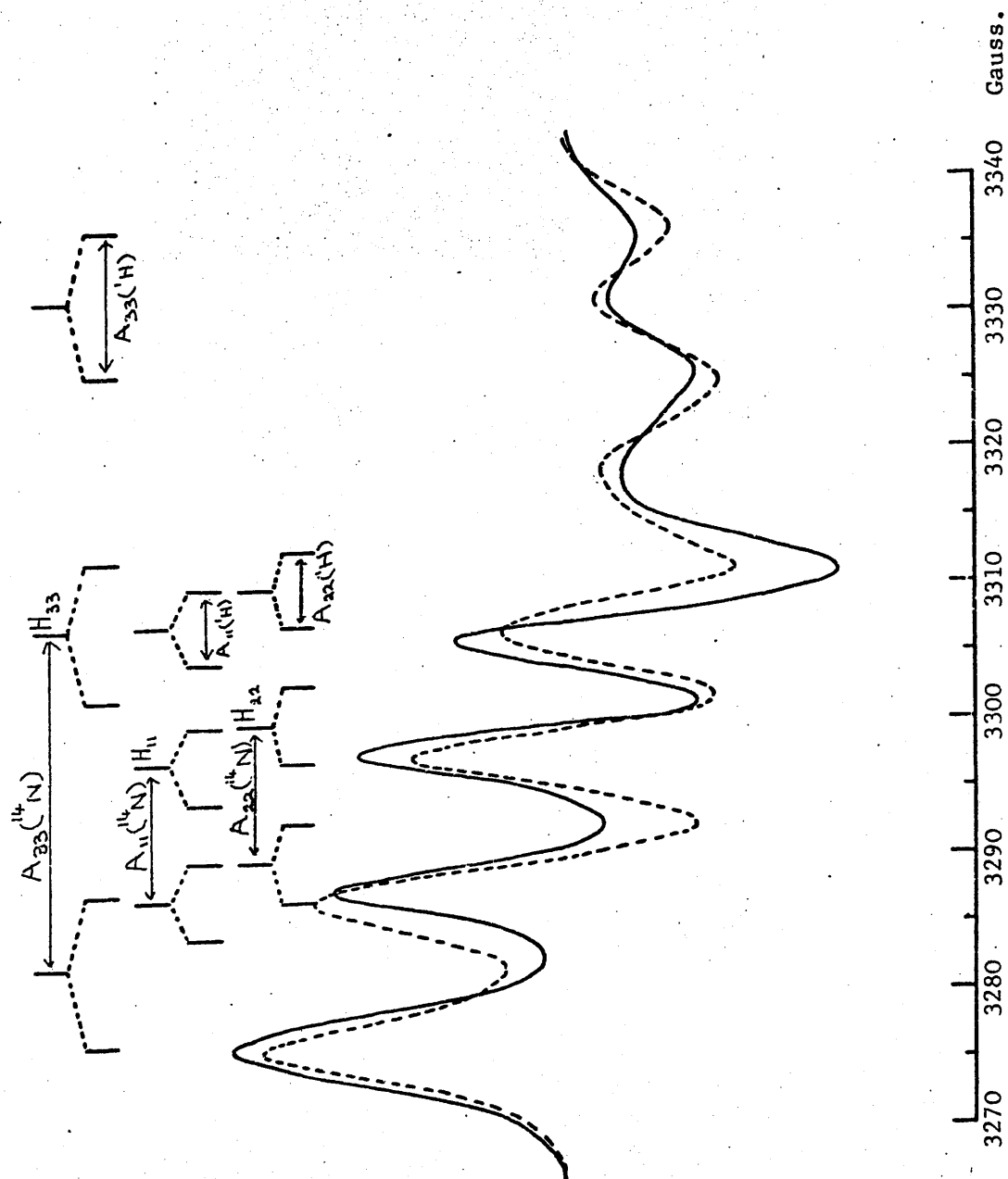


Figure 4.3 The e.p.r. spectrum of a dilute polycrystalline sample of nitroxide radical IV, obtained by irradiating a solid solution of humulene nitrosite (17) in dinitro-humulene (24) (10:90) with red light. The dotted line represents the calculated spectrum of radical IV.

Table 4.4

The spin Hamiltonian parameters for nitroxide radical IV

$g_{11}$	$g_{22}$	$g_{33}$	$\langle g \rangle$	
2.0093	2.0074	2.0035	2.0067	
$A_{11}(^{14}\text{N})$	$A_{22}(^{14}\text{N})$	$A_{33}(^{14}\text{N})$	$a(^{14}\text{N})$	
10.8G	10.8G	22.5G	14.7G	
$A_{11}(^1\text{H})$	$A_{22}(^1\text{H})$	$A_{33}(^1\text{H})$	$a(^1\text{H})$	$\beta$
5.5G	5.5G	11.0G	7.3G	2.5G

The limits of error for  $g_{11}$ ,  $g_{22}$ ,  $g_{33}$ ,  $\langle g \rangle$ ,  $A_{11}(^{14}\text{N})$ ,  $A_{22}(^{14}\text{N})$ ,  $A_{33}(^{14}\text{N})$ ,  $a(^{14}\text{N})$ ,  $A_{11}(^1\text{H})$ ,  $A_{22}(^1\text{H})$ ,  $A_{33}(^1\text{H})$ , and  $a(^1\text{H})$  are respectively,  $\pm 0.0003$ ,  $\pm 0.0003$ ,  $\pm 0.0002$ ,  $\pm 0.0003$ ,  $\pm 0.5\text{G}$ ,  $\pm 0.5\text{G}$ ,  $\pm 0.2\text{G}$ ,  $\pm 0.5\text{G}$ ,  $\pm 0.5\text{G}$ ,  $\pm 0.5\text{G}$ ,  $\pm 0.2\text{G}$ , and  $\pm 0.5\text{G}$ .

If at any stage the products are dissolved in chloroform, then radical IV immediately disproportionates to diamagnetic species, and the e.p.r. spectrum decreases greatly in intensity. The weak e.p.r. signal which remains, is attributed to a nitroxide radical containing the molecular fragment  $\text{R}_1\text{R}_2\text{R}_3\text{C}\dot{\text{N}}\text{O}-\text{CR}_4\text{R}_5\text{R}_6$ .

Nitroxide radical IV appears to form by the mechanism shown in figure 4.4. This mechanism is completely analogous to that employed by caryophyllene nitrosite, when its solid solutions in dinitro-caryophyllene are irradiated. There are two nitro groups on dinitro-humulene, which the red excited nitroso group of humulene nitrosite could displace, however the nitroxide radical IV of structure (29) predominates, indicating that it is either geometrically or sterically easier to displace the nitro group on  $\text{C}_7$ .

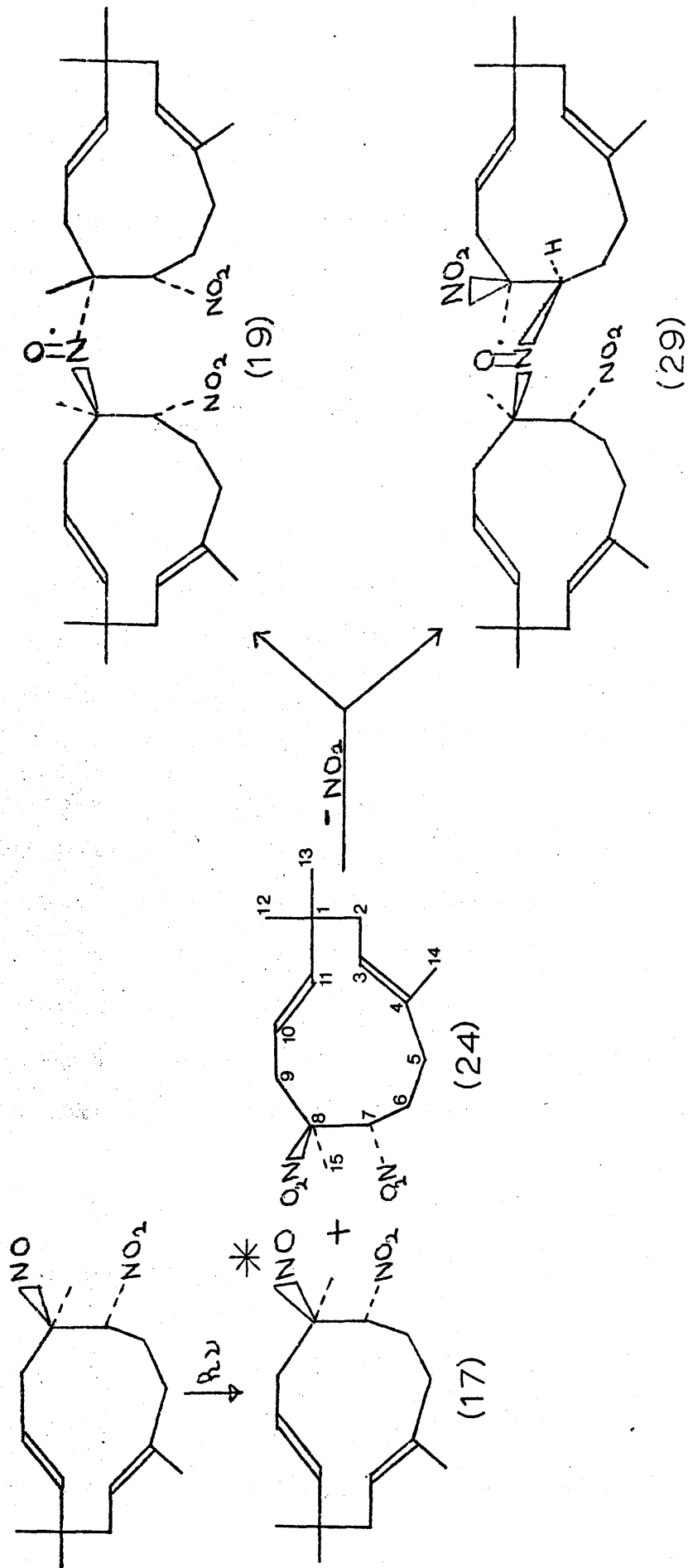


Figure 4.4 The mechanism governing the formation of the paramagnetic species observed when a solid solution of humulene nitrosite (17), in dinitro-humulene (24), (10:90) is irradiated with red light.

At no stage in the irradiation were the nitroxide radicals  $I_A$ ,  $I_B$ , II, or III, which form when pure humulene nitrosite is irradiated with red light, detected. If photolysis scheme II operated in both experiments, then at least some of these latter radicals should have been observed.

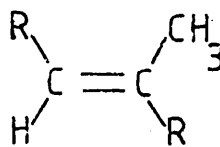
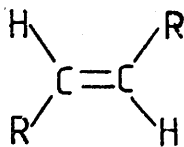
#### 4.3.2 Monitoring by means of infra-red spectroscopy the irradiation with red light of a solid solution of humulene nitrosite (17) in dinitro-humulene (24)

In order to confirm that nitroxide radical  $\overline{IV}$  has structure (29), the irradiation of a solid solution of humulene nitrosite in dinitro-humulene (30:70) was monitored in an infra-red spectrometer. The experimental details are contained in appendix 4, section 4'.3'. The changes observed in the infra-red spectra, are summarised in table 4.5, appendix 4, and are consistent with structure (29) for the nitroxide radical  $\overline{IV}$ . The main observations favouring the mechanism shown in figure 4.4. are listed below.

- 1) As the irradiation proceeds the nitroso absorption slowly disappears and is replaced by an absorption at  $1,380\text{ cm}^{-1}$  which has been assigned to a nitroxide stretching mode.
- 2) The symmetric and asymmetric nitro group absorptions at  $1,360\text{ cm}^{-1}$  and  $1,555\text{ cm}^{-1}$ , of the nitro group attached to  $C_7$  of dinitro-humulene, decrease slightly in intensity, indicating a loss of  $\text{NO}_2$  from this position.
- 3) All the remaining absorptions in the infra-red spectrum remained unchanged.

No changes were observed in the infra-red spectra consistent with the operation of photolysis scheme II. In particular

no cis carbon to carbon double bonds containing the structural unit  $\begin{array}{c} \diagup \\ \text{C} \\ \diagdown \end{array} = \begin{array}{c} \diagdown \\ \text{C} \\ \diagup \end{array}$  could be detected, and the small decrease in intensity of less than 5% of the absorptions associated with the following structures



is probably due to their reaction with the  $\dot{\text{NO}}_2$  liberated.

4.4 The irradiation with red light, of dilute solutions of humulene nitrosite, or caryophyllene nitrosite, in chloroform, or toluene, at 77°K

The experiments described in sections 4.1, 4.2, and 4.3, have all indicated that when humulene nitrosite, or its solid solutions in dinitro-humulene are irradiated with red light, no nitroxide radicals are formed by the processes of intra-molecular cyclisation, postulated in photolysis scheme II. These findings were further confirmed by irradiating dilute solutions of humulene nitrosite in either chloroform or toluene at 77°K. The solvents chloroform and toluene do not interact with a red excited nitroso group, and hence provide an inert host matrix. The full details of these experiments are contained in appendix 4. sections 4'.4' and 4'.5'.

Figure 4.5 shows the e.p.r. spectrum obtained when such a glass, containing humulene nitrosite, is irradiated with red light. The line shape of the spectrum is not consistent with the formation of any of the nitroxide radicals  $\text{I}_\text{A}$ ,  $\text{I}_\text{B}$ , II, and III, which have been previously observed, when humulene nitrosite is irradiated with red light, but appears to arise from a superposition



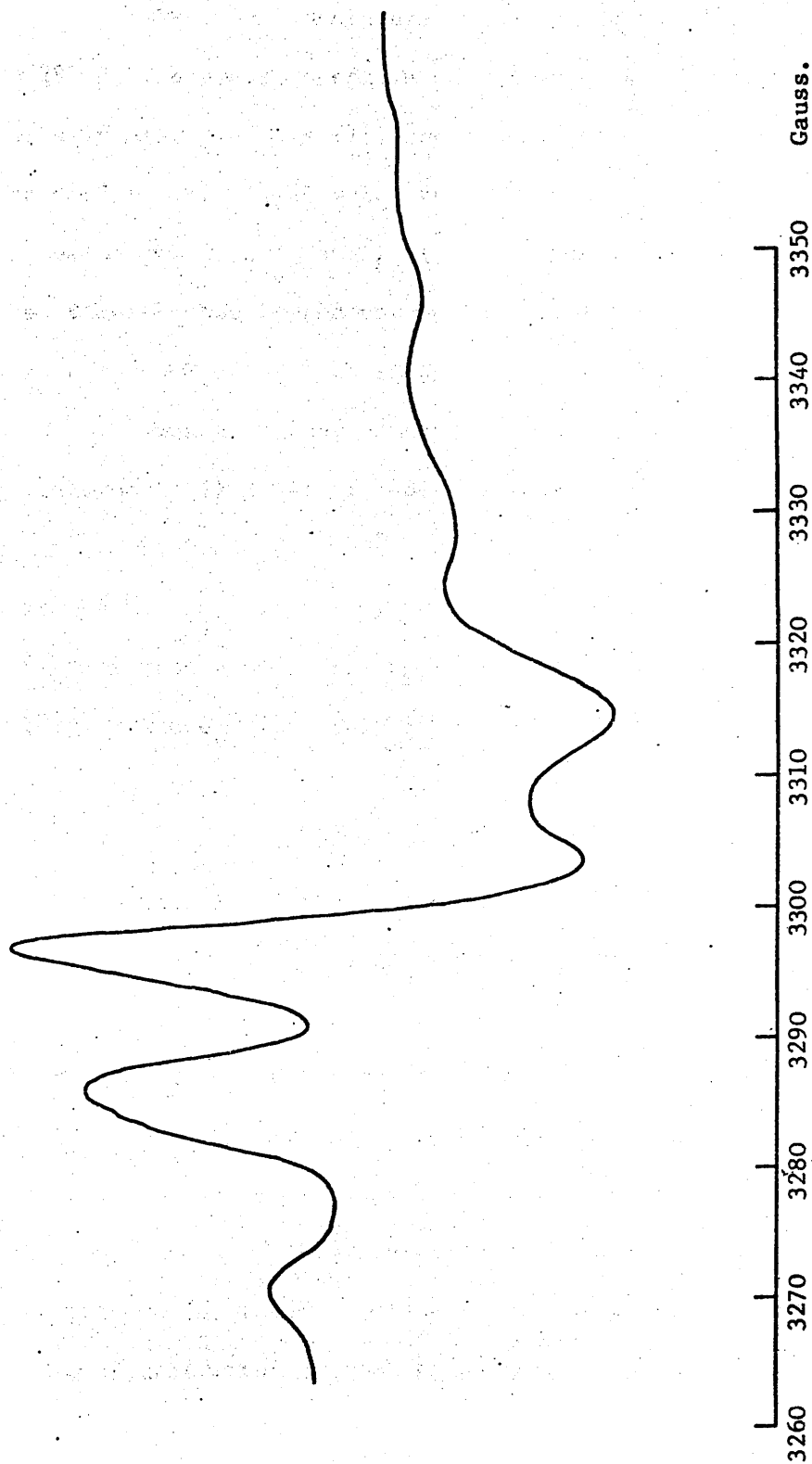


Figure 4.5 The e.p.r. spectrum of the radicals obtained by irradiating a dilute degassed solution of humulene nitrosite (17) in chloroform at 77°K. The spectrum was recorded at 77°K.

of the spectra due to trapped NO, and the aliphatic radical of structure (18). The predominant process during the irradiation is thus a C-N bond fission of the nitroso group, and photolysis scheme II does not operate.

When the temperature of the glass is allowed to rise to 295°K, the e.p.r. spectrum decreases greatly in intensity, as the aliphatic radicals (18) combine to give diamagnetic products. The weak e.p.r. signal which remains, shows the presence of nitroxide radicals  $I_A$  and  $I_B$  (19) formed by the interaction of the nitroso group of the unreacted humulene nitrosite with the aliphatic radical (18) as shown in figure 4.6.

When solutions of caryophyllene nitrosite in chloroform, or toluene at 77°K, are irradiated with red light, the e.p.r. spectrum obtained, is exactly the same as the spectrum shown in figure 4.5, and again the predominant process is C-N bond fission of the nitroso group, forming an aliphatic radical (12). When the temperature of the solution is raised to 295°K, the e.p.r. spectrum decreases greatly in intensity, as the aliphatic radicals combine to give diamagnetic products. The weak e.p.r. spectrum which remains, is of the single nitroxide radical, structure (10), formed by the interaction of unreacted caryophyllene nitrosite, with the aliphatic radicals (12).

All the experimental observations reported in chapters 2, and 4, concerning the irradiation with red light, of crystalline samples of humulene nitrosite, of solid solutions of humulene nitrosite in dinitro-humulene, and lastly, of solutions of humulene nitrosite in chloroform, toluene, and benzene, at 77°K and 295°K, are consistent with the mechanisms shown in figures 2.7, 4.4, and 4.6, respectively. The nitroxide radicals observed, form either

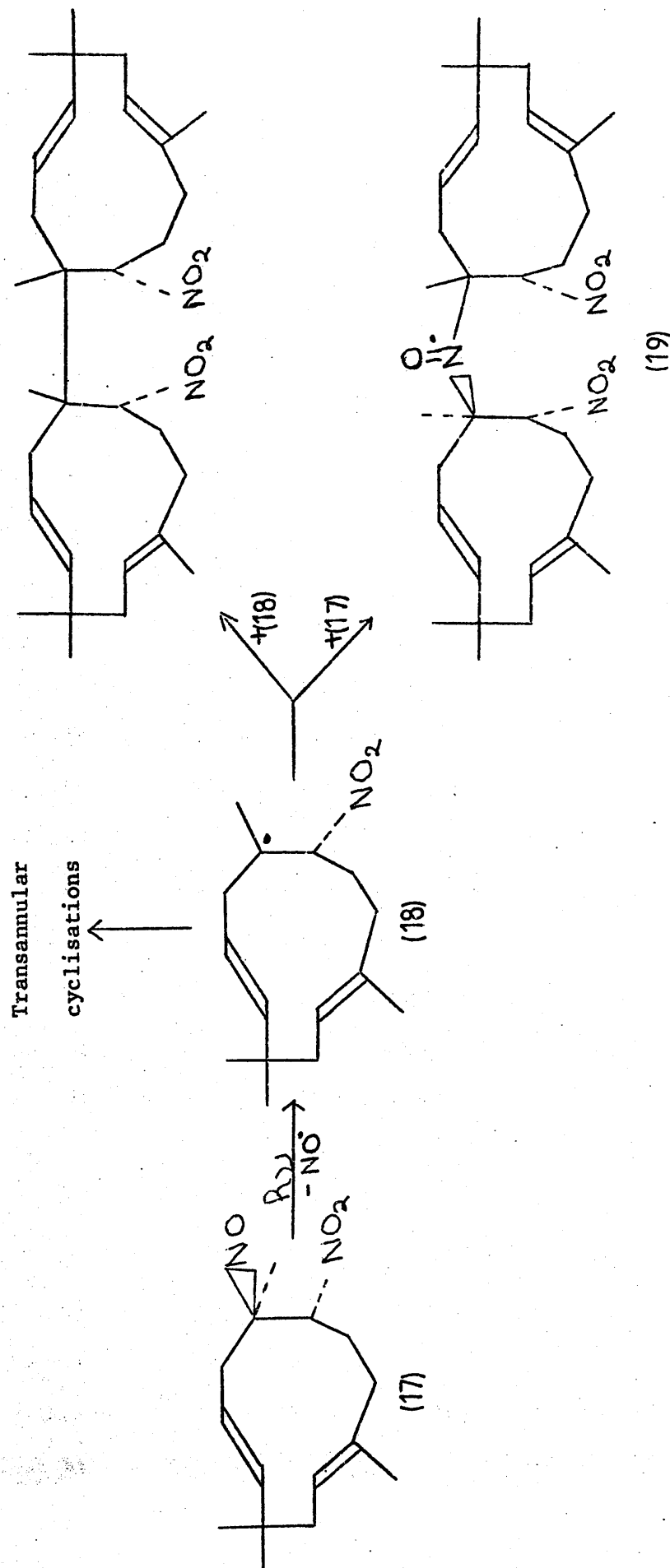


Figure 4.6 Dilute solutions of humulene nitrosite (17) in chloroform or toluene at 77°K, irradiated for a short period with red light, and the temperature allowed to rise to 295°K.

by photolysis scheme I, or by a closely analogous mechanism and the following two processes are involved.

- 1) The first possible mode of behaviour, involves the cleavage of the C-N bond of the nitroso group. The aliphatic radical (18) formed, reacts with humulene nitrosite producing the diastereomeric nitroxide radicals  $I_A$  and  $I_B$ , of structure (19).
- 2) An alternative mode of reaction, involves the displacement of  $\dot{N}O$  or  $\dot{N}O_2$  from neighbouring molecules of humulene nitrosite or dinitro-humulene by the red excited nitroso group of a molecule of humulene nitrosite. This produces nitroxide radicals of structure  $I_A$  and  $I_B$  (19), II (21), III(20) and  $\overline{IV}$  (29).

No evidence was obtained to support the transannular attack of a red excited nitroso group at the  $\pi$ -system of humulene nitrosite, which was postulated in scheme II, figure 2.9.

The paramagnetic species observed when caryophyllene nitrosite, its solutions in aprotic solvents, and its solid solutions in dinitro-caryophyllene are irradiated with red light, form by the mechanisms shown in figures 2.8, and 4.2. These are completely analogous to the corresponding reactions of humulene nitrosite. The existence of all the nitroxide radicals postulated in figures 2.8, and 4.2, had been demonstrated either by McConnell, Porte, et.al.<sup>70</sup> or in this present investigation, with the exception of nitroxide radical III' (13).

Figure 2.8 illustrates the mechanism by which nitroxide radical III' was postulated to form. In an attempt to detect this radical, the irradiation of polycrystalline samples of caryophyllene nitrosite with red light was monitored in an e.p.r. spectrometer. The transient nitroxide radical III' was not however detected, and only the nitroxide radicals I' of structure (10), and II' of structure (11), which had been previously detected by McConnell,

Porte, et. al., were observed. Nitroxide radical III' contains a nitroso chromophore and would decompose as the irradiation proceeds, forming nitroxide radical II'. The relative proportions of radicals I', II' and III' present at any time would depend on the following two factors.

- 1) First the relative rates of formation of radicals I' and III' are dependent amongst other factors, on the geometry within the crystal.
- 2) Second the relative proportions must depend on the rates of formation and decomposition of radical III'.

In this particular case, the concentration of radicals I' and II', may always be in excess of the concentration of radical III', which as a result was not observed.

One small postscript had to be added to the photolysis reactions described above, as a result of the observation that nitroxide radical II, of structure (21), which is formed during the irradiation with red light of humulene nitrosite, was itself a source of further nitroxide radicals.

#### 4.5. The irradiation with white light, of solutions of nitroxide radicals $I_A$ , $I_B$ (19) and II (21) in chloroform.

Figure 2.6 shows the e.p.r. spectrum obtained from a dilute degassed solution of humulene nitrosite dissolved in chloroform and irradiated with red light. When this solution, which contains radicals  $I_A$ ,  $I_B$  (19) and II (21), was further irradiated with the white light from a tungsten filament lamp, the e.p.r. spectrum was observed to slowly change to that shown in figure 4.7. Nitroxide radicals  $I_A$ ,  $I_B$  and II slowly disappear and are replaced by another nitroxide radical, radical V, the e.p.r.

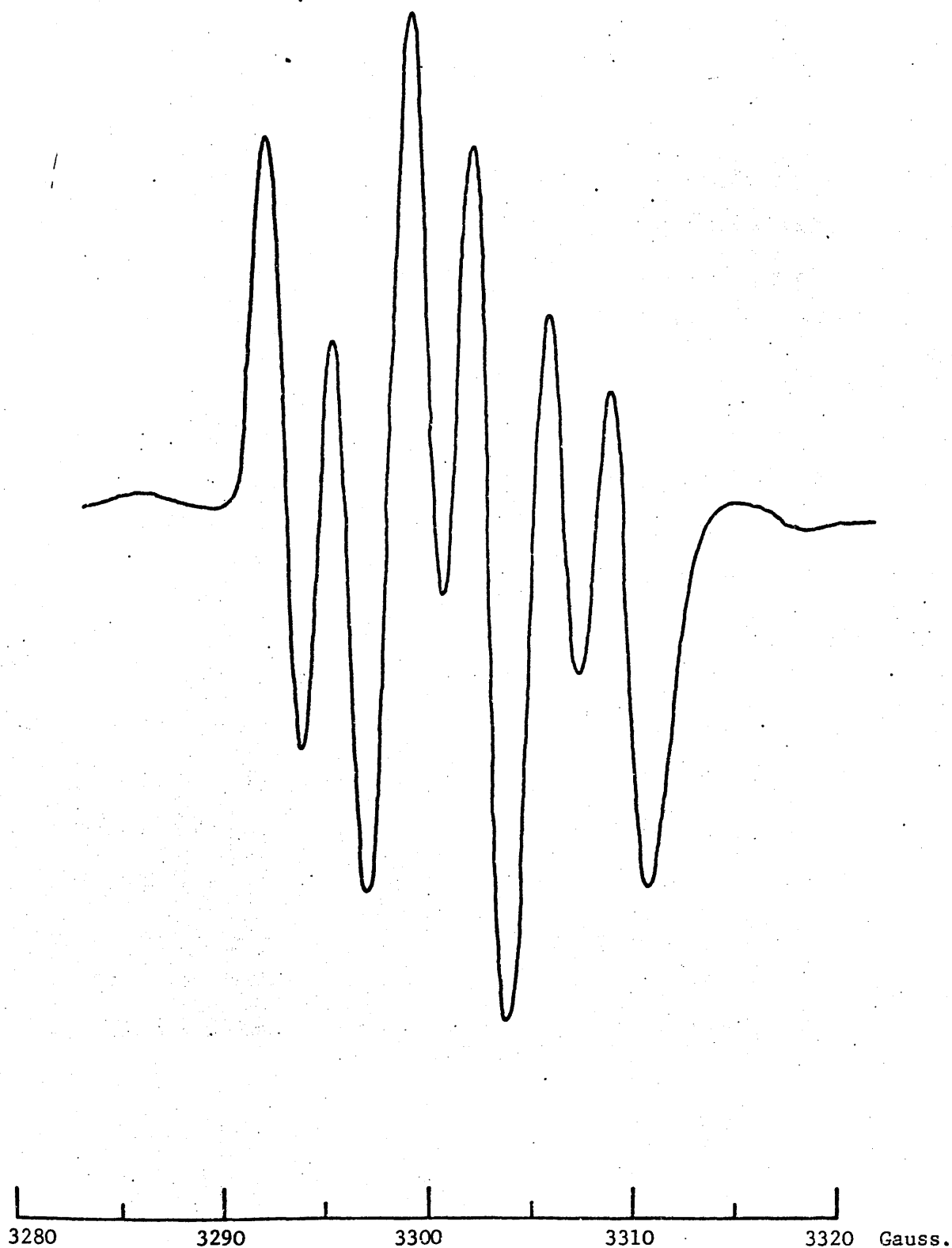


Figure 4.7 The e.p.r. spectrum of nitroxide radical V obtained by irradiating a dilute degassed solution of nitroxide radicals I<sub>A</sub>, I<sub>B</sub>, and II, in chloroform, with white light. The spectrum was recorded at 295°K.

spectrum of which, consists of a 1:1:1 triplet, split further into doublets, by the interaction with a proton. The isotropic coupling to the  $^{14}\text{N}$  nucleus in this radical is reduced in a manner consistent with increased conjugation to the nitroxide fragment.

The isotropic spin Hamiltonian parameters for nitroxide radical  $\text{V}$ , are as follows  $\left[ \text{isotropic } \langle g \rangle = 2.0064 \pm 0.0003; \text{ isotropic } a(^{14}\text{N}) = 6.8 \pm 0.2\text{G}; \text{ isotropic } a(^1\text{H}) = 2.9 \pm 0.2\text{G}; \right]$ .

In solution, radical  $\text{V}$  slowly decomposes to diamagnetic species by a process which is not photo-induced.

Nitroxide radicals  $\text{I}_\text{A}$  and  $\text{I}_\text{B}$  of structure (19), were thought to be extremely unlikely precursors of radical  $\text{V}$ , as they had a "di-tertiarybutyl-nitroxide" like structure. To confirm this, solutions containing solely nitroxide radicals  $\text{I}_\text{A}$  and  $\text{I}_\text{B}$ , obtained chromatographically as described in chapter 2, section 2.2.2, were irradiated with white light, and no changes were observed in their e.p.r. spectra. Unfortunately the irradiation could not be repeated using solutions which contained solely nitroxide radical II (21), as this radical was never isolated because of its instability; the presence of a proton on the carbon adjacent to the nitroxide grouping allows it to disproportionate to the nitron (31) and the hydroxylamine (30). Nitroxide radical II seems however, the most likely precursor and the two photo-initiated reaction mechanisms shown in figures 4.8 and 4.9 are postulated to explain a rearrangement of radical II to an extensively conjugated radical whose structure is consistent with the experimental observations made on radical  $\text{V}$ .

Scheme A shown in figure 4.8 is based on the postulate that the nitron (31) obtained from the disproportionation of radical II, could on irradiation with white light, produce an

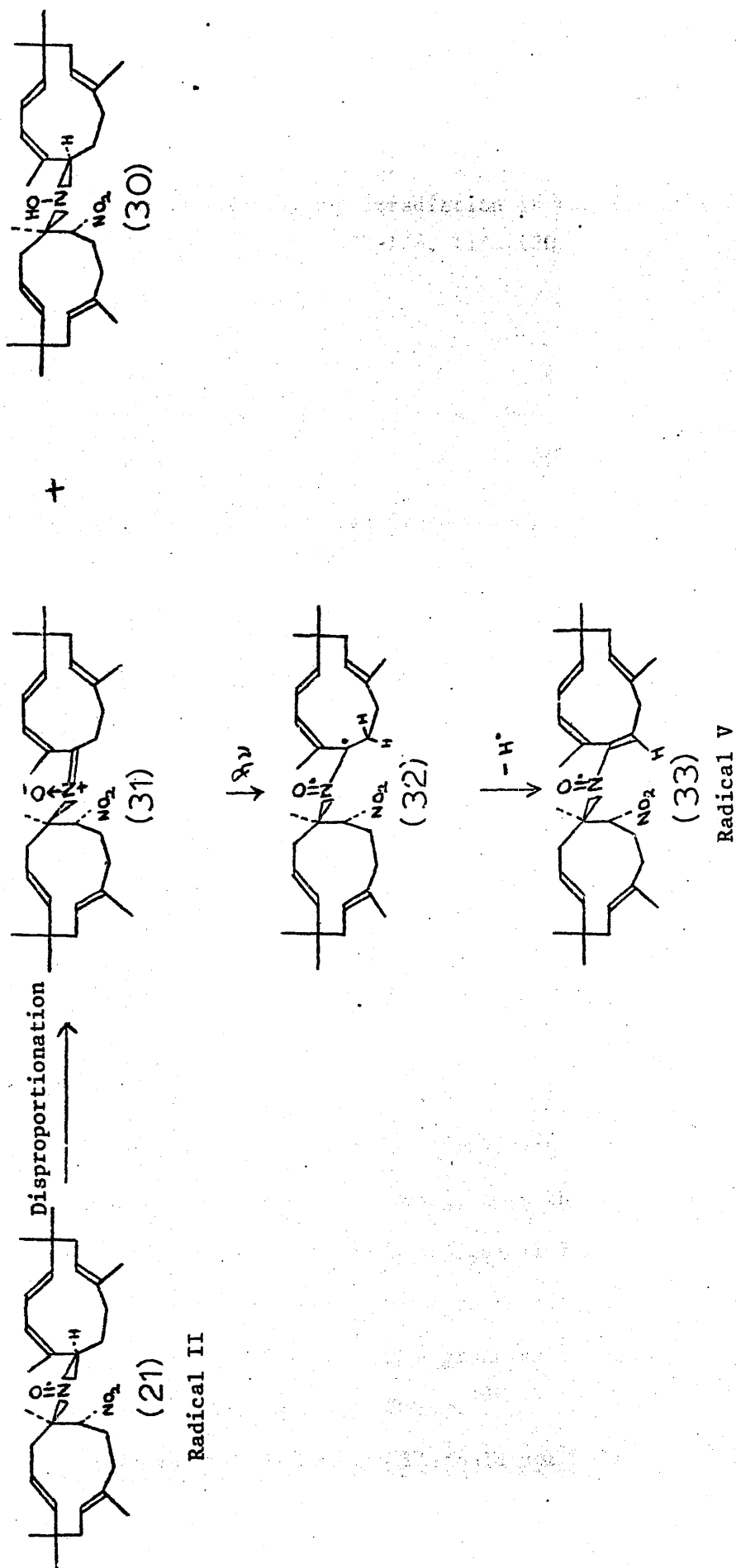
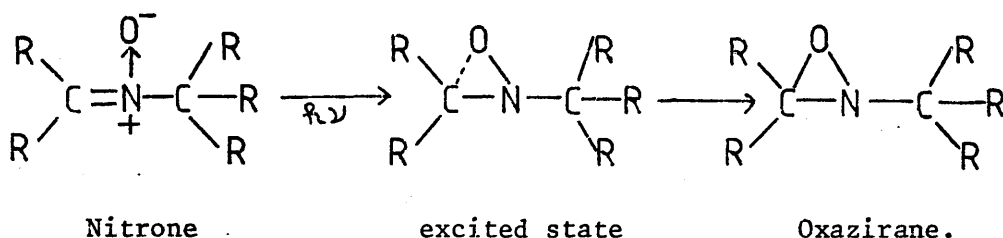


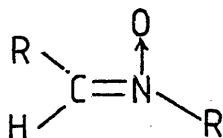
Figure 4.8 Photolysis scheme A, a mechanism postulated to explain the formation of the nitroxide radical V, observed when solutions containing nitroxide radical II (21) are irradiated with white light.



excited intermediate (32), which by the loss of a proton could form a nitroxide radical  $\bar{\text{V}}$  of structure (33). A study of the available literature on the photochemistry of nitrones, reveals that the primary step in any irradiation is the formation of oxaziranes, as shown below.<sup>103-106, 119, 120.</sup>



There are reports of nitroxide radicals having been generated when nitrones are irradiated<sup>107</sup> but only from nitrones containing the structural unit



and the nitron (31) does not have an  $\alpha$  proton. Moreover the generation of oxaziranes from nitrones requires ultra-violet radiation of approximately 360 n.m. Nitroxide radical  $\bar{\text{V}}$  was generated using visible light of wavelength greater than 400 n.m.

Scheme B is shown in figure 4.9 and is based on the postulate that if the irradiation stimulates an  $n \rightarrow \pi^*$  transition in the nitroxide grouping, then this might facilitate the abstraction of a proton from radical II forming intermediate (32) which by a further loss of a proton forms nitroxide  $\bar{\text{V}}$  (33). The  $n \rightarrow \pi^*$  transition of a nitroxide grouping involves visible wavelengths of approximately 450 n.m.<sup>108</sup>

As nitroxide radicals II could not be isolated in a pure state, the formation of the conjugated ring of nitroxide radical  $\bar{\text{V}}$ ,

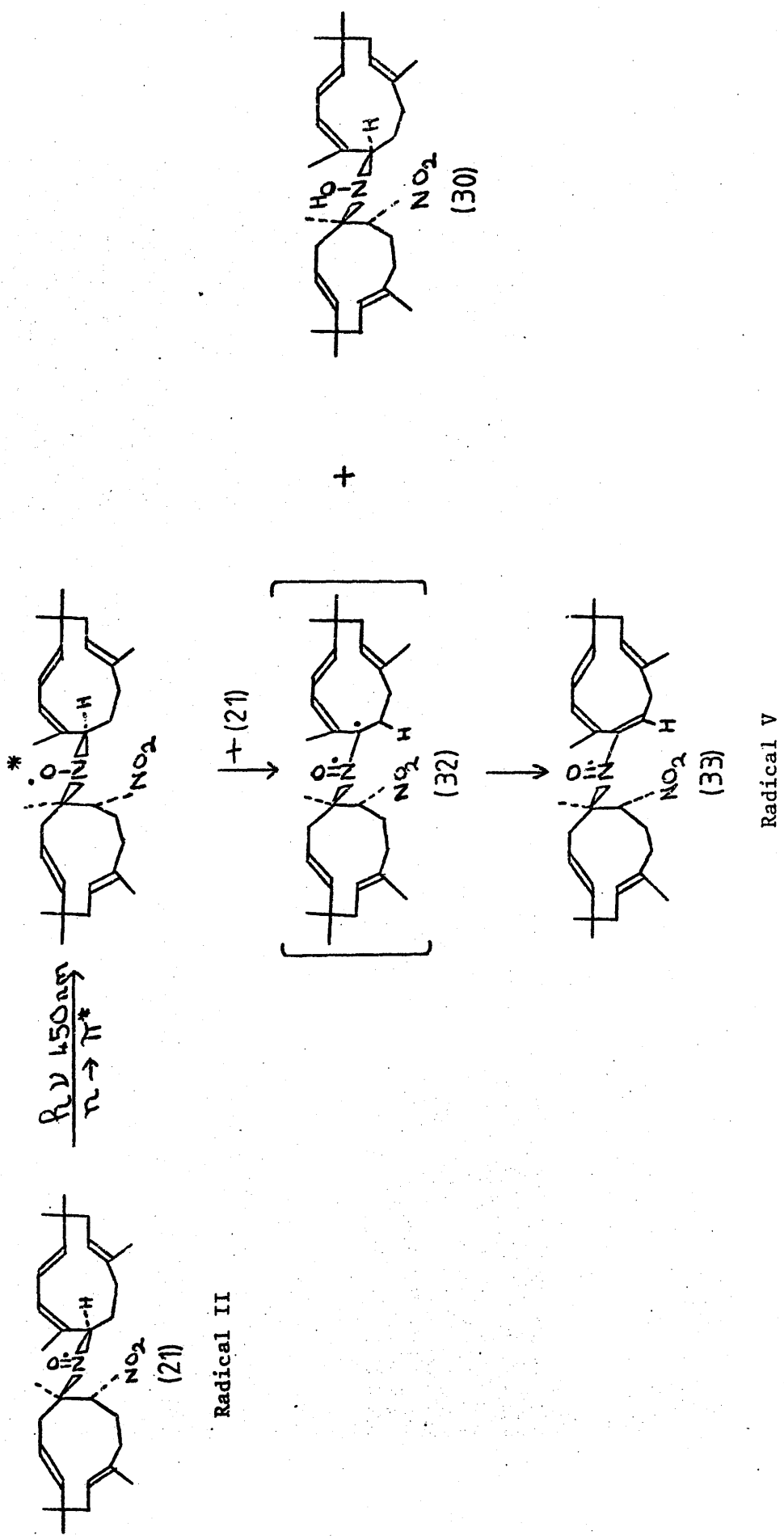


Figure 4.9 Photolysis scheme B, a mechanism postulated to explain the formation of the nitroxide radical V, observed when solutions containing nitroxide radical II (21) are irradiated with white light.

could not be accurately monitored in an ultra-violet spectrometer.

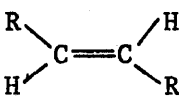
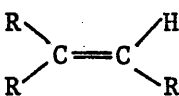
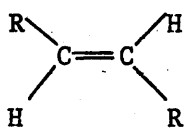
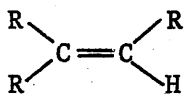
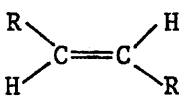
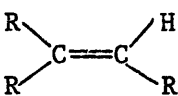
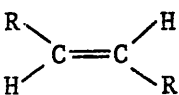
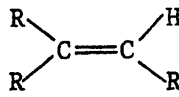
As the irradiation proceeds, the other materials present mask the change in the spectra.

APPENDIX 44'.1' Monitoring by means of infra-red spectroscopy the irradiation of humulene nitrosite with red light

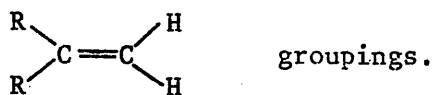
A chromatographically purified sample of humulene nitrosite was incorporated into a KBr disc at a concentration level of 1.1 mg/300 mg. The irradiation of this sample with red light was then followed in an infra-red spectrometer. During the course of the irradiation the disc became opaque, and had to be reground prior to recording each spectrum. This unavoidably led to the incorporation of some  $H_2O$  into the disc, the infra-red absorptions of which obscured the region  $4,000 - 3,200\text{ cm}^{-1}$ . Table 4.1 lists the main changes observed in the infra-red spectrum as the irradiation proceeds.

Table 4.1

The changes observed in the infra-red spectrum of humulene nitrosite as it is irradiated with red light

Humulene nitrosite (17)	Changes observed as the irradiation proceeds
<p>a) </p> <p>and </p> <p>1) <math>\nu_{C-H}</math> str. <math>3,015\text{ cm}^{-1}</math> <math>3,010\text{ cm}^{-1}</math></p> <p>2) <math>\nu_{C=C}</math> str. <math>1,660\text{ cm}^{-1}</math> <math>1,665\text{ cm}^{-1}</math></p> <p>3)  <math>\nu_{o.o.p. \text{ def.}}\ 980\text{ cm}^{-1}</math></p> <p>4)  <math>\nu_{o.o.p. \text{ def.}}\ 840\text{ cm}^{-1}</math></p>	<p>a)  </p> <p>1) The <math>\nu_{C-H}</math> str. widens and becomes less well defined.</p> <p>2) Other <math>C = C</math> stretching frequencies appear between <math>1,630 - 1,645\text{ cm}^{-1}</math></p> <p>3) As the irradiation proceeds the  out of plane deformation at <math>980\text{ cm}^{-1}</math> decreases in intensity. On completing the irradiation this loss of intensity is <math>\sim 20\%</math>. However the absorption has increased in width and more than one absorption may be present.</p> <p>4)  <math>\nu_{o.o.p. \text{ def.}}\ 840\text{ cm}^{-1}</math></p> <p>On irradiation this absorption appears to remain unchanged.</p>

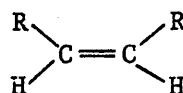
- 5) New absorptions were observed. These might indicate the presence of



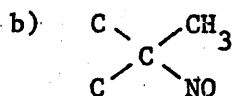
$\nu\text{C-H str.} \quad \sim \quad 3,080 \text{ cm}^{-1}$

$\nu\text{o.o.p. def.} \quad \sim \quad 910 \text{ cm}^{-1}$

- 6) No absorptions consistent with the formation of the structure



were observed.



$\nu\text{N=O str.} \quad 1,570 \text{ cm}^{-1}$

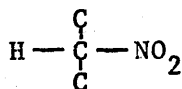
- b) The nitroso stretching frequency at  $1,570 \text{ cm}^{-1}$  decreases in intensity as the irradiation proceeds and eventually disappears.

c)

c)  $\nu\text{N=O str.} \quad \sim 1,380 \text{ cm}^{-1}$

A wide absorption ascribed to a nitroxide stretch appears at  $1,380 \text{ cm}^{-1}$  and increases in intensity until the irradiation is complete. More than one absorption may be present.

d)

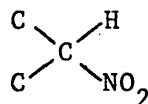


$\nu\text{NO}_2 \text{ asym.} \quad 1,560 \text{ cm}^{-1}$

$\nu\text{NO}_2 \text{ sym.} \quad 1,360 \text{ cm}^{-1}$

$\nu\text{C-N bend} \quad 872 \text{ cm}^{-1}$

d)

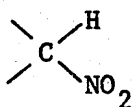


The asymmetric nitro stretch shows a small decrease in intensity as the irradiation proceeds,

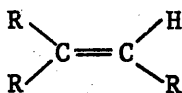
and on completing the irradiation more than one such absorption is present. The symmetric nitro stretch also decreases slightly in intensity and develops a shoulder.

e) The region

840 - 880  $\text{cm}^{-1}$



$\nu\text{C-N bend } 872 \text{ cm}^{-1}$

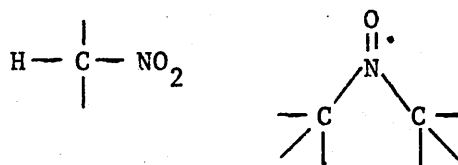


$\nu\text{o.o.p. def. } 840 \text{ cm}^{-1}$

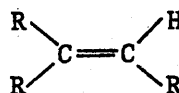
The C-N bend of the nitroso group was not identified.

e) In the region 840 - 880  $\text{cm}^{-1}$

two new absorptions appear as the irradiation proceeds. These are either additional C-N bends due to the following structures.



or the out of plane deformations of the structural unit



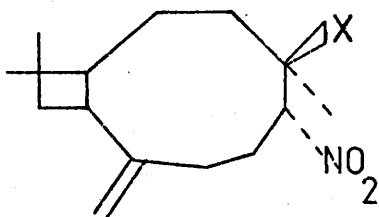
4'.2' Following by means of infra-red spectroscopy the irradiation with red light, of a solid solution of caryophyllene nitrosite (2) in dinitro-caryophyllene(27)

A solid solution of caryophyllene nitrosite in dinitro-caryophyllene (10:90) was incorporated into a KBr disc at a concentration level of 1.2 mg/300 mg. On following the irradiation of this sample in an infra-red spectrometer, no significant changes could be observed in the spectra. The experiment was repeated using a solid solution of caryophyllene nitrosite in dinitro-caryophyllene (20:80) and table 4.3 lists the main changes observed in the infra-red spectrum.



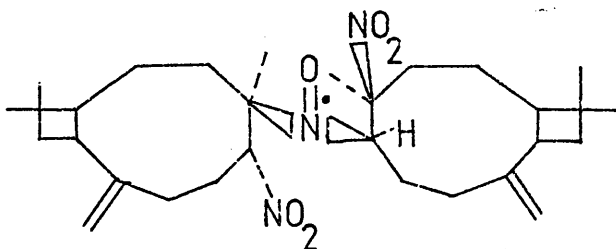
Table 4.3

The changes observed in the infra-red spectrum of a solid solution of caryophyllene nitrosite in dinitro-caryophyllene (20:80) as it is irradiated with red light



X = NO caryophyllene  
nitrosite

X = NO<sub>2</sub> dinitro-  
caryophyllene



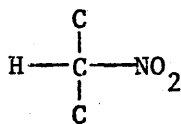
Postulated structure of radical IV' (28)

Changes observed as the irradiation proceeds.

a)  
Caryophyllene nitrosite  
 $\nu_{\text{N}} = 0$  str.  $1,570 \text{ cm}^{-1}$

a) The nitroso absorption of caryophyllene nitrosite slowly disappears and a new absorption at  $1,387 \text{ cm}^{-1}$  which is ascribed to a nitroxide stretching frequency increases in intensity.

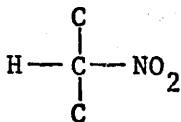
b)  
Caryophyllene nitrosite



$\nu_{\text{NO}_2}$  asym.  $1,550 \text{ cm}^{-1}$   
 $\nu_{\text{NO}_2}$  sym.  $1,360 \text{ cm}^{-1}$   
 $\nu_{\text{C-N}}$  bend  $870 \text{ cm}^{-1}$

b) There is a slight decrease in the width and intensity of the asymmetric stretches of the nitro groups. There is also a small decrease in the intensity of the symmetric nitro stretch at  $1,365 \text{ cm}^{-1}$ . It was not possible to determine with certainty the position from which the NO<sub>2</sub> was being lost.

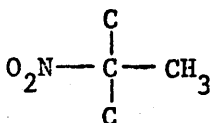
## Dinitro-caryophyllene



$\nu\text{NO}_2$  asym. 1,560  $\text{cm}^{-1}$

$\nu\text{NO}_2$  sym. 1,365  $\text{cm}^{-1}$

$\nu\text{C-N}$  bend 850  $\text{cm}^{-1}$



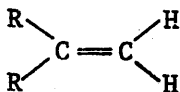
$\nu\text{NO}_2$  asym. 1,550  $\text{cm}^{-1}$

$\nu\text{NO}_2$  sym. 1,340  $\text{cm}^{-1}$

$\nu\text{C-N}$  bend 850  $\text{cm}^{-1}$

c)

## Caryophyllene nitrosite



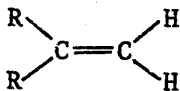
$\nu\text{C-H}$  str. 3,085  $\text{cm}^{-1}$

$\nu\text{C=C}$  str. 1,640  $\text{cm}^{-1}$

$\nu\text{o.o.p. def.}$  900  $\text{cm}^{-1}$

c) There is no apparent change in the absorptions due to carbon to carbon double bonds, but a new absorption appears at 1,640  $\text{cm}^{-1}$ .

## Dinitro-caryophyllene



$\nu\text{C-H}$  str. 3,087  $\text{cm}^{-1}$

$\nu\text{C=C}$  str. 1,635-1,645  $\text{cm}^{-1}$

$\nu\text{o.o.p. def.}$  910  $\text{cm}^{-1}$

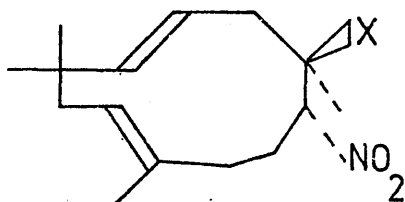
d) All the remaining absorptions in the infra-red spectrum remain unchanged.

4'.3' Following by means of infra-red spectroscopy, the irradiation with red light, of a solid solution of humulene nitrosite (17) in dinitro-humulene (24) (30:70)

A solid solution of humulene nitrosite in dinitro-humulene (30:70) was incorporated into a KBr disc at a concentration level of 1.0 mg/300 mg. The irradiation of this sample with red light, was then followed in an infra-red spectrometer. Table 4.5 lists the main changes observed in the infra-red spectrum as the irradiation proceeds.

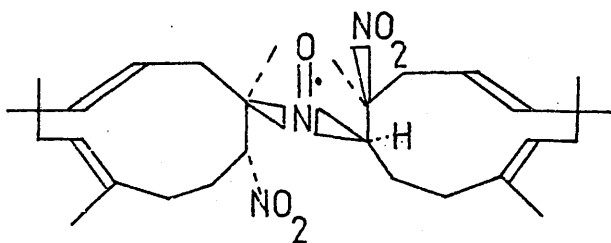
Table 4.5

The changes observed in the infra-red spectrum of a solid solution of humulene nitrosite, in dinitro-humulene (30:70) as it is irradiated with red light



X = NO - humulene  
nitrosite

X = NO<sub>2</sub> - dinitro-  
humulene



Postulated structure of radical IV (29)

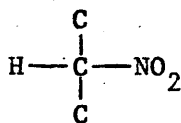
Changes observed as the irradiation proceeds.

a) Humulene nitrosite

$\nu\text{N=O str.}$        $1,570 \text{ cm}^{-1}$

a) The nitroso absorption slowly disappears, and a strong absorption at  $1,380 \text{ cm}^{-1}$  increases in intensity. This absorption is ascribed to nitroxide stretch.

b) Humulene nitrosite



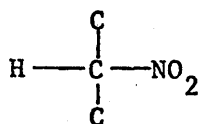
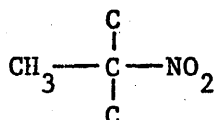
$\nu\text{NO}_2 \text{ asym.}$        $1,560 \text{ cm}^{-1}$

$\nu\text{NO}_2 \text{ sym.}$        $1,360 \text{ cm}^{-1}$

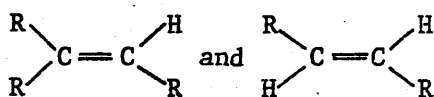
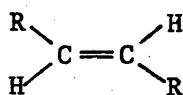
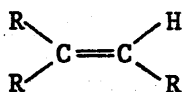
$\nu\text{C-N bend}$        $872 \text{ cm}^{-1}$

b) The overall width of the absorptions, due to the asymmetric nitro stretches, decreases. In particular the absorptions at  $1,555 \text{ cm}^{-1}$  due to the nitro group attached to the secondary carbon atom on dinitro-humulene, decreases in intensity. A decrease in the intensity of the symmetric stretch of the nitro group at  $1,360 \text{ cm}^{-1}$  is also observed.

## Dinitro-humulene

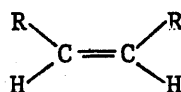
 $\nu\text{NO}_2$  asym. 1,550  $\text{cm}^{-1}$  $\nu\text{NO}_2$  sym. 1,360  $\text{cm}^{-1}$  $\nu\text{C-N}$  bend — $\nu\text{NO}_2$  asym. 1,545  $\text{cm}^{-1}$  $\nu\text{NO}_2$  sym. 1,355  $\text{cm}^{-1}$  $\nu\text{C-N}$  bend 872  $\text{cm}^{-1}$ 

c) Humulene nitrosite  
and dinitro-humulene

 $\nu\text{C-H}$  str. 3,015  $\text{cm}^{-1}$ 3,010  $\text{cm}^{-1}$  $\nu\text{C=C}$  str. 1,660  $\text{cm}^{-1}$ 1,665  $\text{cm}^{-1}$ vo.o.p. def, 980  $\text{cm}^{-1}$ vo.o.p. def, 840  $\text{cm}^{-1}$ 

c) There is no apparent change in the absorptions due to the carbon to carbon double bonds, except for a slight decrease, <5%, in the intensity of the out of plane deformations at 980  $\text{cm}^{-1}$  and 840  $\text{cm}^{-1}$ , and a slight increase in the intensity of the absorption at 1,665  $\text{cm}^{-1}$ .

No new absorptions from the out of plane deformations of the cis double bond structure shown below, were observed in the range 730-665  $\text{cm}^{-1}$



d) New absorptions, which are very weak, appear at  $1,630\text{ cm}^{-1}$ , and  $1,280\text{ cm}^{-1}$  and these may be due to nitrones.

---

e) All the remaining peaks in the infra-red spectrum remain unchanged.

---

4'.4' The irradiation, with red light, of a dilute solution of humulene nitrosite in chloroform, or toluene, at  $77^{\circ}\text{K}$

A solution of 0.1M humulene nitrosite in chloroform, was cooled under liquid  $\text{N}_2$ , in a long tailed dewar flask, to a glass at  $77^{\circ}\text{K}$ . This glass was irradiated with red light for several hours, and figure 4.5, shows the e.p.r. spectrum of this irradiated solution recorded at  $77^{\circ}\text{K}$ . On raising the temperature, and allowing the glass to liquify, most of the paramagnetic species disappear. The weak remaining e.p.r. spectrum shows the presence of two nitroxide radicals which contain the molecular fragment  $\text{R}_1\text{R}_2\text{R}_3\text{C}-\dot{\text{N}}\text{O}-\text{CR}_4\text{R}_5\text{R}_6$ , and whose isotropic spin Hamiltonian parameters are as follows

$\left[ \text{isotropic } \langle g \rangle = 2.0061 \pm 0.0003; \text{ isotropic } a(^{14}\text{N}) = 14.9 \pm 0.5\text{G}; \right], \left[ \text{isotropic } \langle g \rangle = 2.0059 \pm 0.0003; \text{ isotropic } a(^{14}\text{N}) = 14.7 \pm 0.5\text{G}; \right].$

On crystallising the products of the above irradiation from hot ethanol, white needle shaped crystals of  $\text{m.pt.} = 168 \pm 0.5^{\circ}\text{C}$  were isolated. The infra-red and  $^1\text{H}$  n.m.r. spectra identified the crystals as dinitro-humulene (24). On repeating the above reaction using a solution of humulene nitrosite, which had been thoroughly

degassed to remove oxygen, the results were exactly as described above, except that dinitro-humulene was not found in the reaction products. Similar results are obtained if toluene, rather than chloroform, is used as solvent in this experiment.

4'.5' The irradiation with red light, of a dilute solution of caryophyllene nitrosite in chloroform, or toluene at 77°K

A thoroughly degassed solution of 0.1M caryophyllene nitrosite in chloroform, was cooled under liquid N<sub>2</sub> in a long tailed dewar, to a glass at 77°K. This glass was irradiated with red light for several hours, and the e.p.r. spectrum recorded at 77°K is the same as that shown in figure 4.5.

On raising the temperature to 295°K, most of the paramagnetic species disappear, leaving a weak e.p.r. spectrum, attributable to a single nitroxide radical containing the structural unit  $R_1R_2R_3\dot{C}-NO-CR_4R_5R_6$ .

## CHAPTER 5

### THE REACTIONS OF HUMULENE NITROSITE WITH THE OXIDES OF NITROGEN

At this point in the investigations, the mechanisms involved in the production of the paramagnetic species observed when humulene nitrosite is irradiated with red light were fully determined. However the nature of the diamagnetic species formed during the photolysis reactions was not understood. The direction of the research was temporarily changed in order to study the reactions of humulene nitrosite with the oxides of nitrogen. These reactions were briefly discussed in chapter 3.

Figure 3.3 shows the e.p.r. spectrum obtained from a dilute degassed solution in chloroform, of the yellow oil formed when humulene nitrosite reacts with the oxides of nitrogen. At least three nitroxide radicals are present, two of which, radicals  $A_1$  and  $A_2$ , contain the structural unit  $R_1R_2R_3C-\dot{N}O-CR_4R_5R_6$  and the remaining radical B contains the structural unit  $R_1R_2R_3C-\dot{N}O-CHR_4R_5$ . Figure 3.4 shows the e.p.r. spectrum of a solution of radicals  $A_1$ ,  $A_2$  and B, allowed to stand until radical B disproportionated to diamagnetic species.

Preliminary silica t.l.c. experiments showed that the product of the reaction of humulene nitrosite with  $N_2O_3$  contained a minimum of four components, three of which were diamagnetic. In studying this reaction further, it was felt important to characterise and understand the mechanism by which radicals  $A_1$ ,  $A_2$ , and B were formed, and to isolate and characterise the



diamagnetic components, and hence determine if any of the products formed by a process involving transannular cyclisations.

Full details of the experimental procedures involved in reacting humulene nitrosite with  $N_2O_3$  have been outlined previously, in appendix 3, section 3'.2' (d). It should be noted however, that all experiments were performed using chloroform, from which the ethanol had been removed, as the reaction of  $\dot{N}O$  with nitroso compounds is altered if protic solvents are present.

#### 5.1 Investigation of the paramagnetic species formed during the reaction of humulene nitrosite with $N_2O_3$

The following two mechanisms were postulated as possible routes to the formation of nitroxide radicals  $A_1$ ,  $A_2$  and B.

- 1) The first scheme considered, is shown in figure 5.1, and involves the addition of  $\dot{N}O_2$ , or  $\dot{N}O$ , or  $\dot{O}NO$ , or perhaps more than one of these radicals, to either of the carbon to carbon  $\pi$  bonds in humulene nitrosite, producing an intermediate aliphatic radical, which undergoes a transannular addition to the nitroso group. This mechanism would produce two nitroxide radicals, one of structure (34) consistent with radical B, the other of structure (35) consistent with either of  $A_1$  and  $A_2$ . It should be noted, that attack of the oxides of nitrogen at the ends of the carbon to carbon  $\pi$  bonds of humulene nitrosite, other than those indicated in figure 5.1, produces aliphatic radicals, to which the nitroso groups could not cyclise, the structures produced being very strained. This first mechanism is analogous to the reaction shown in figure 1.1, which illustrates the reaction of caryophyllene with iodine to form  
NITROSITE.

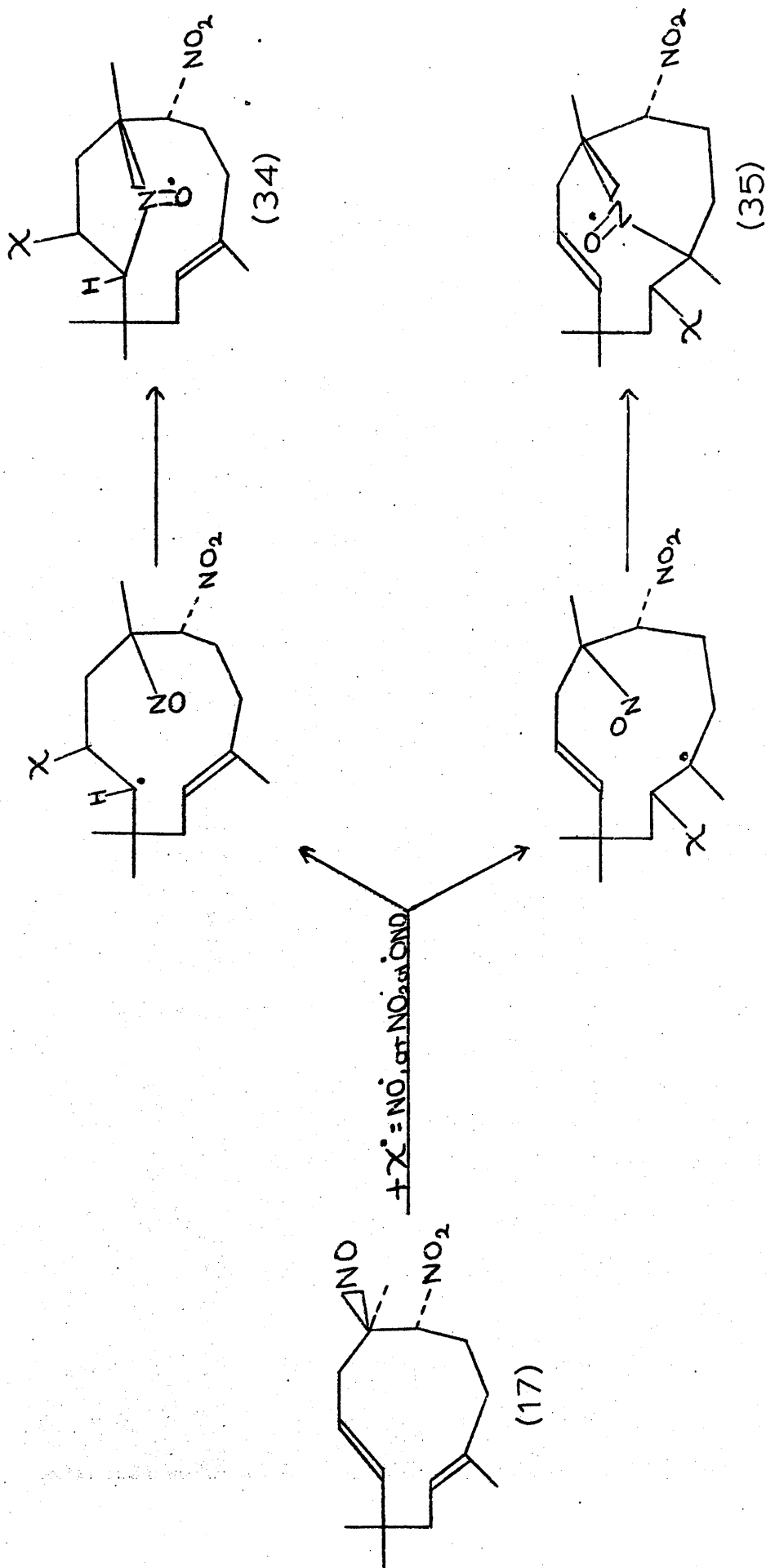


Figure 5.1 A mechanism postulated to explain the formation of the paramagnetic species observed when solutions of humulene nitrosite (17) in aprotic solvents are reacted with the oxides of nitrogen.

the iodonitrosite (3), which was discussed in chapter 1.

- 2) The second scheme is based on the well documented reaction of nitric oxide with C-nitroso compounds.<sup>24,25,27,109,110</sup> Figure 5.2 illustrates how the general scheme could be adapted to explain the reaction of humulene nitrosite with nitric oxide. The nitrosite reacts with two molecules of nitric oxide, forming complex (36), which rearranges to the diazonium structure (37). Loss of  $N_2$  from this, then produces an aliphatic radical (18). This aliphatic radical (18), can interact with the unreacted humulene nitrosite molecules, forming nitroxide radicals, which are the diastereomeric forms of structure (19), namely radicals  $I_A$  and  $I_B$ . Nitroxide radicals  $I_A$  and  $I_B$  were previously observed when humulene nitrosite was irradiated with red light. The spin Hamiltonian parameters of nitroxide radicals  $A_1$  and  $A_2$  were found to be the same as the spin Hamiltonian parameters of radicals  $I_A$  and  $I_B$  respectively, and radicals  $A_1$  and  $A_2$  may therefore be identical to radicals  $I_A$  and  $I_B$ , having formed as shown in figure 5.2.

- a) Attempts to isolate, by using chromatographic techniques, the paramagnetic species formed in the reaction of humulene nitrosite with  $N_2O_3$

When the products of the reaction of humulene nitrosite with  $N_2O_3$ , were chromatographed on silica plates, using a solvent of ether: pet.ether, (50:50), four major components were isolated at  $R_f = 0, 0.29, 0.37, \text{ and } 0.83$ . The products of  $R_f > 0$ , were extracted using analar chloroform, and were all diamagnetic. Acetone

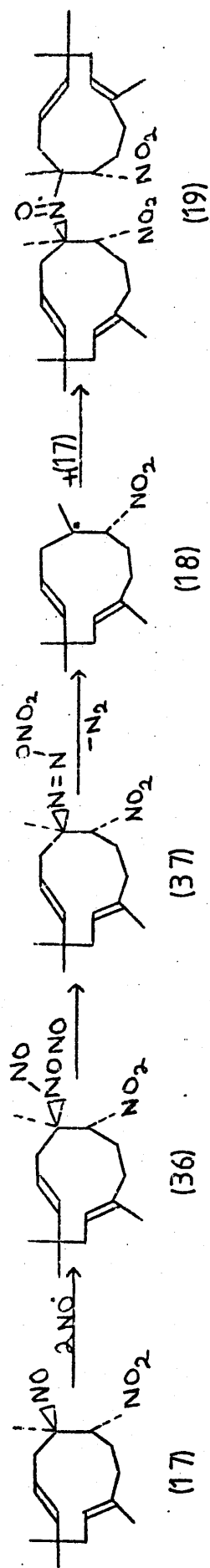


Figure 5.2 The reaction of dilute solutions of humulene nitrosite (17) in the aprotic solvent chloroform with nitric oxide.

was found to be the only solvent suitable for the extraction of the materials of  $R_{f.} = 0$ . The products of  $R_{f.} = 0$  contain all the paramagnetic species present. However only radicals  $A_1$  and  $A_2$  are observed, as radical B decomposes on the silica surface.

b) Attempted purification of nitroxide radicals  $A_1$  and  $A_2$ , using chromatographic techniques

The yellow solid of  $R_{f.} = 0$ , which contained nitroxide radicals  $A_1$  and  $A_2$ , accounted for approximately 8% by weight of the total product. The infra-red spectrum of this yellow solid is consistent with the presence of only small amounts of nitroxide radicals  $A_1$  and  $A_2$ , and the  $^1\text{H}$  n.m.r. spectrum shows only slight broadening, the majority of the species present being diamagnetic. The line shape of the e.p.r. spectrum obtained from a polycrystalline sample of this solid, indicated, that it is magnetically dilute. Attempts were made to isolate pure samples of nitroxide radicals  $A_1$  and  $A_2$ , by using all the following chromatographic techniques, which were previously used to isolate radicals  $I_A$  and  $I_B$  from the photolysis products of humulene nitrosite.

- 1) The period of chromatographic separation was extended, and various solvents were tried.
- 2) Silica column chromatography was used.
- 3) Alumina and cellulose t.l.c. were used.

All such experiments were however unsuccessful and the longer the nitroxide radicals  $A_1$  and  $A_2$  were kept on the activated surfaces, the more impure they became, because of decomposition.

c) Attempted purification of nitroxide radicals  $A_1$ ,  $A_2$  and B using techniques which do not involve chromatography

It was observed that the product of the reaction of humulene nitrosite with  $N_2O_3$  could be separated into two fractions, according to whether or not they could dissolve in the mixture ether: pet. ether, (50:50). Those fractions soluble in the mixture, corresponded to the diamagnetic species of  $R_f > 0$  which were isolated chromatographically as described earlier in this section. The insoluble fractions contained nitroxide radicals  $A_1$ ,  $A_2$  and B. The infra-red,  $^1H$  n.m.r., and polycrystalline e.p.r. spectra of the fraction containing radicals  $A_1$ ,  $A_2$  and B all indicated that the solid was magnetically dilute, diamagnetic species being the major products present.

In attempts to extract pure samples of radicals  $A_1$ ,  $A_2$  and B, the two following techniques were employed.

- 1) Efforts were made to extract basic components of the mixture into a dilute aqueous acid phase, with which nitroxides do not react. This achieved little success however and on making the acid phase more concentrated the nitroxides formed hydroxylamines and oxammonium salts, which hydrolyse and further decompose to  $\cdot OH$  radicals and the parent nitroxides.<sup>101</sup>
- 2) The reduction of nitroxide radicals  $A_1$ ,  $A_2$  and B to hydroxylamines was attempted, with the hope that these could then be chromatographically separated, and the parent nitroxides regenerated by oxidation. Unfortunately no reducing agent could be found which would selectively reduce the nitroxide group without at the same time affecting the C=C bonds, and the nitro groups.

It was thus not possible to confirm that nitroxide radicals  $A_1$  and  $A_2$ , formed by the mechanism shown in figure 5.2, were identical to radicals  $I_A$  and  $I_B$ .

## 5.2 The reaction of humulene nitrosite with nitrogen dioxide

Figure 5.1 illustrates a mechanism which involves attack of the oxides of nitrogen at the  $\pi$  system of humulene nitrosite, forming aliphatic radicals to which the nitroso group can cyclise and hence form nitroxide radicals which were earlier postulated as possible structures for  $A_1$ ,  $A_2$  and B. Nitric oxide can not be involved in the initial attack as its addition to a secondary carbon position would lead to rearrangements, forming oximes, and no such species were detected.

To determine if  $\dot{NO}_2$  was the initiating radical, solutions of humulene nitrosite were reacted with  $\dot{NO}_2$ . The experimental details of this reaction, including the isolation and characterisation of the species produced, are contained in appendix 5, section 5'.1'. The reaction did not proceed as shown in figure 5.1, and no appreciable amounts of nitroxide radicals were produced. Instead the reaction involved a slow replacement of the nitroso group of humulene nitrosite with  $\dot{NO}_2$  forming dinitro-humulene, with a subsequent addition of  $\dot{NO}_2$  and  $\dot{ONO}_2$ , over the remaining double bonds of the dinitro-humulene. The presence of  $\dot{ONO}_2$  radicals, may either arise from the interaction of  $\dot{NO}_2$  and NO with molecular oxygen, or in rearrangements resulting from the initial attack of  $\dot{NO}_2$  at the nitroso group of humulene nitrosite.

Amongst the products isolated, were structures (38) and (39) as well as dinitro-humulene (24) in what appears to be both

the cis and trans isomeric forms. A summary of the pertinent data from the  $^1\text{H}$  n.m.r. and infra-red spectra of the cis and trans forms of dinitro-humulene, is contained in tables 5.1 and 5.2 respectively.

It has also been demonstrated by the author of this thesis, that unlike caryophyllene nitrosite, see figure 1.1, chloroform solutions of humulene nitrosite do not react with iodine to produce nitroxide radicals.

### 5.3 Investigation of the diamagnetic species formed during the reaction of humulene nitrosite with $\text{N}_2\text{O}_3$

It has previously been observed that the products obtained from the reaction of humulene nitrosite with  $\text{N}_2\text{O}_3$ , can be considered in two groups according to whether they do, or do not, dissolve in a mixture of ether: pet.ether, (50:50).

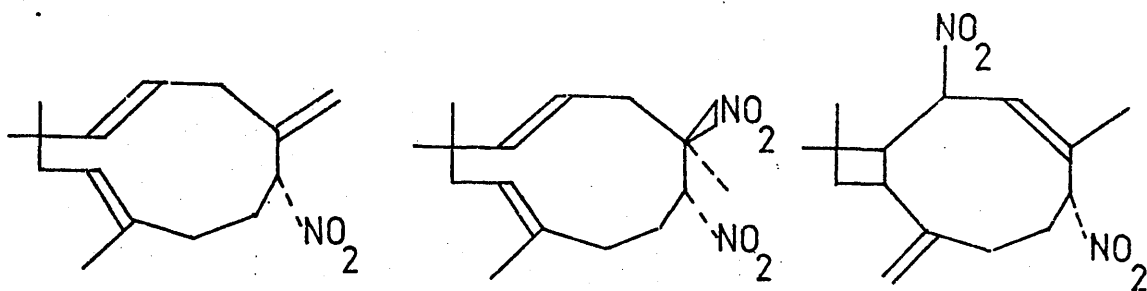
#### a) The diamagnetic components soluble in ether: pet.ether. (50:50)

By chromatographing the soluble fractions on silica plates, three major products have been isolated in a pure state from the  $R_f$  regions 0.29, 0.39, and 0.82, respectively.

The infra-red,  $^1\text{H}$  n.m.r., and mass spectra of these species, have been compared with the corresponding spectra of humulene nitrosite (17), dinitro-humulene (24), nitro-nitrato-humulene (26), caryophyllene nitrosite (2), and dinitro-caryophyllene (27). These spectra were used as standards, representing the type of structures which might be present in a humulene derivative, or in a caryophyllene based rearrangement of the humulene structure.

The three species of  $R_f$  value 0.29, 0.39, and 0.82, have been characterised to have the structures shown below.





$R_{f.} = 0.83$  (41)

Dinitro-humulene (24)

$R_{f.} = 0.29$  (40)

1) The component of  $R_{f.} = 0.83$

The material extracted from the region of  $R_{f.} = 0.83$  was an oil. This oil was further chromatographed using silica plates and carbon tetrachloride and figure 5.6 shows the  $^1\text{H}$  n.m.r. and infra-red spectra of a solid extracted from the region of  $R_{f.} = 0.29$ . By comparing these spectra with the standard humulene derivatives mentioned earlier, this material was characterised as structure (41). A summary of the pertinent data obtained from the  $^1\text{H}$  n.m.r. and infra-red spectra of (41), are contained in table 5.7, and 5.8, respectively in appendix 5. The mass spectrum of this species contains the parent molecular ion, and has a very similar breakdown pattern to that observed for humulene nitrosite. A comparison of the major peaks present in the mass spectrum of component (41) and humulene nitrosite, is contained in table 5.9, appendix 5.

During the chromatographic purification of this material (41), the infra-red, and  $^1\text{H}$  n.m.r. spectra showed traces of additional allylic methyls, trans double bonds, and geminal-dimethyls, and in particular, infra-red absorptions were observed at  $1,510\text{ cm}^{-1}$  and  $1,325\text{ cm}^{-1}$ , which appear to be due to the asymmetric and symmetric

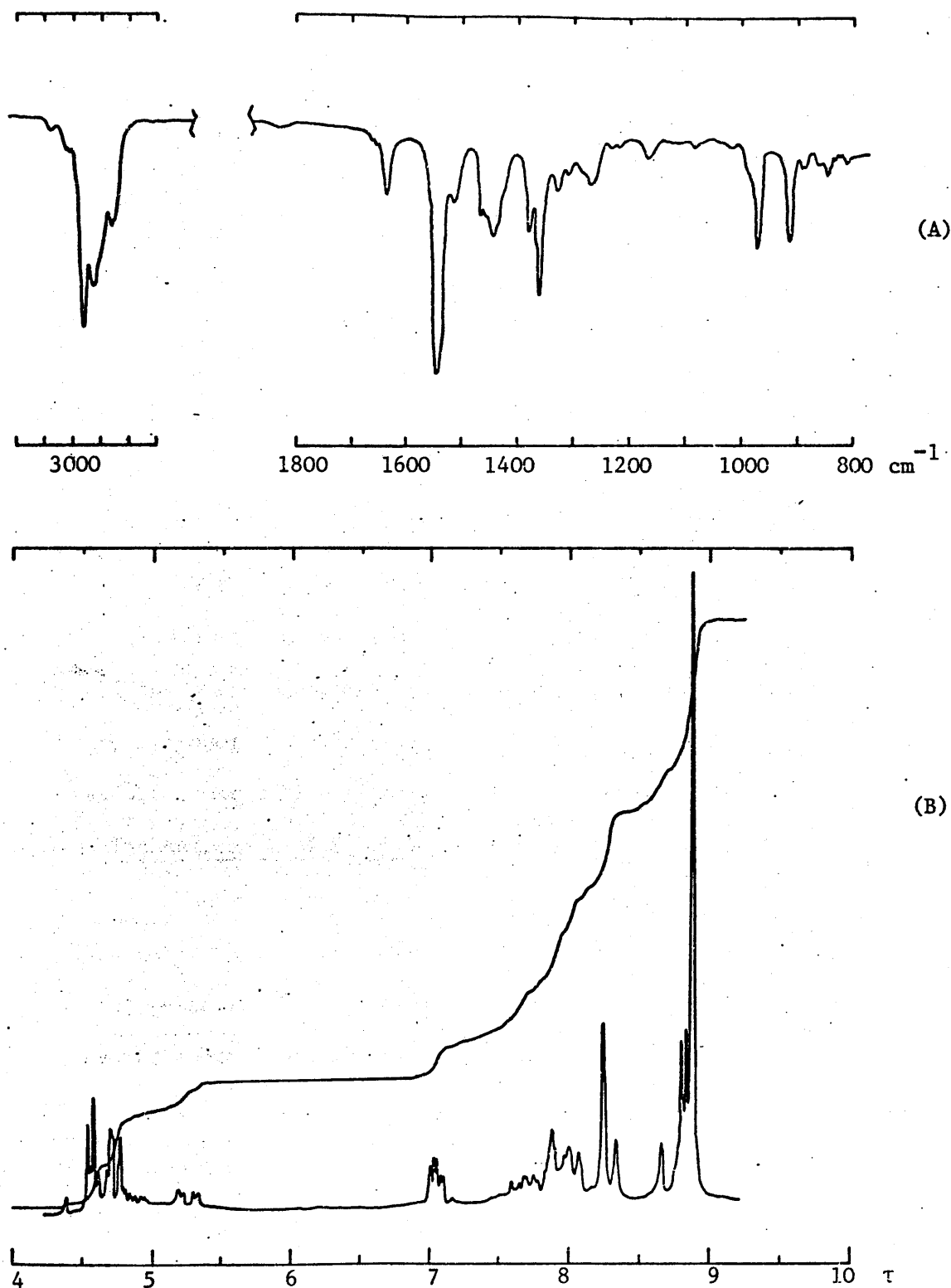
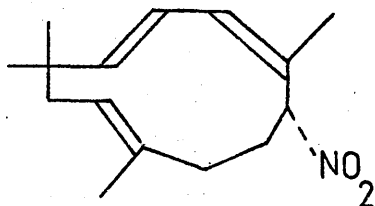
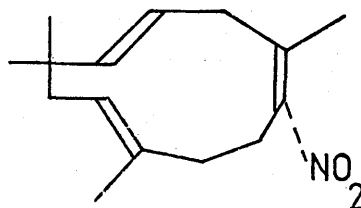


Figure 5.6 (A) The infra-red spectrum recorded in a  $\text{CCl}_4$  solution in the range  $3,200\text{--}800\text{ cm}^{-1}$ , and (B) the  $^1\text{H}$  n.m.r. spectrum recorded in a  $\text{CDCl}_3$  solution in the  $\tau$  range 4 to 10, of the component of  $R_f = 0.83$ , namely (41), isolated from the product of the reaction of humulene nitrosite with  $\text{N}_2\text{O}_3$ .

absorptions of a conjugated nitro grouping. It is probable that in addition to compound (41) small amounts of the isomeric species (42) and (43) are also present.



(42)



(43)

2) The component of  $R_f = 0.39$

This material, when crystallised from ethanol, produced clear needle shaped crystals of m.pt. =  $168.5 \pm 0.5^\circ\text{C}$ . A comparison of all the spectroscopic evidence available for this compound with the corresponding spectra of dinitro-humulene (24) showed that this crystalline material was pure dinitro-humulene.

3) The component of  $R_f = 0.29$

The material extracted from the region of  $R_f = 0.29$  was an oil. This oil was further chromatographed using silica plates and carbon tetrachloride, and figure 5.7 shows the  $^1\text{H}$ .n.m.r. and infra-red spectra of the solid extracted from the region of  $R_f = 0.12$ . This material was characterised as structure (40), and in forming has undergone a rearrangement to a caryophyllene like structure. A summary of the pertinent data from the  $^1\text{H}$  n.m.r. and infra-red spectra of (40) are contained in tables 5.10 and 5.11 respectively, in appendix 5.

During the chromatographic purification of component (40) small amounts of other species were detected. In particular,

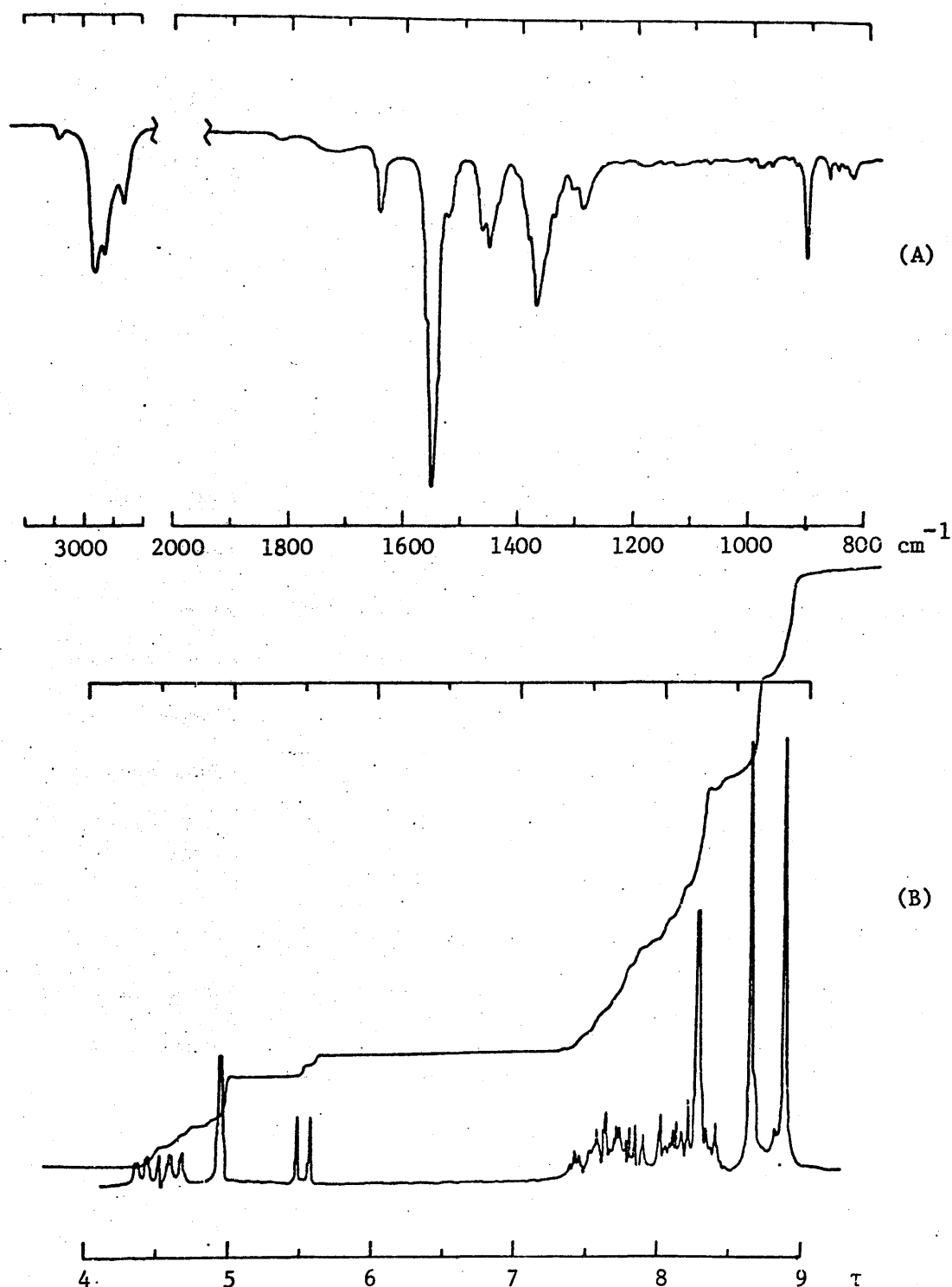


Figure 5.7 (A) The infra-red spectrum recorded in a  $\text{CCl}_4$  solution in the range  $3,200 - 800 \text{ cm}^{-1}$ , and (B) the  $^1\text{H}$  n.m.r. spectrum recorded in a  $\text{CDCl}_3$  solution in the  $\tau$  range 4 to 9, of the component of  $R_f = 0.29$  namely (40), isolated from the product of the reaction of humulene nitrosite, with  $\text{N}_2\text{O}_3$ .

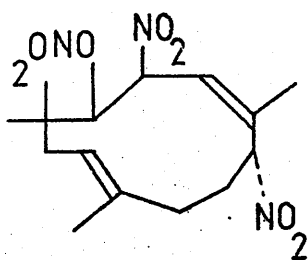
additional absorptions were observed in the infra-red spectra, for the exomethylene group, and traces of nitrates were also observed.

By a quantitative study of the absorbance, of the nitro absorptions, present in the infra-red spectra of the standard humulene and caryophyllene derivatives listed earlier, it was possible to confirm, that the component (41) contained one nitro group per molecule, and that component (40), contained two nitro groups.

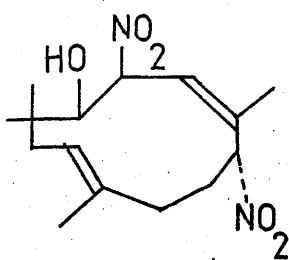
b) The diamagnetic components insoluble in ether: pet.ether, (50:50)

Those products of the reaction of humulene nitrosite with  $N_2O_3$  which were insoluble in ether: pet.ether, (50:50), were a mixture of diamagnetic species, and the nitroxide radicals  $A_1$ ,  $A_2$ , and B. Figure 5.8 shows the  $^1H$  n.m.r., and infra-red spectra of some diamagnetic species extracted from this fraction, using carbon tetrachloride.

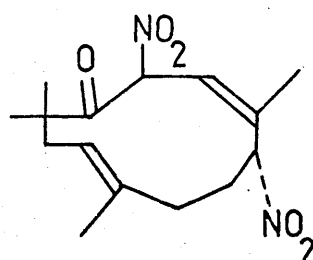
There was clearly more than one component present, however, all further attempts to purify this material were unsuccessful. A detailed examination of the  $^1H$  n.m.r., infra-red, and mass spectra of the mixture, indicated that the following species might be present.



(44)

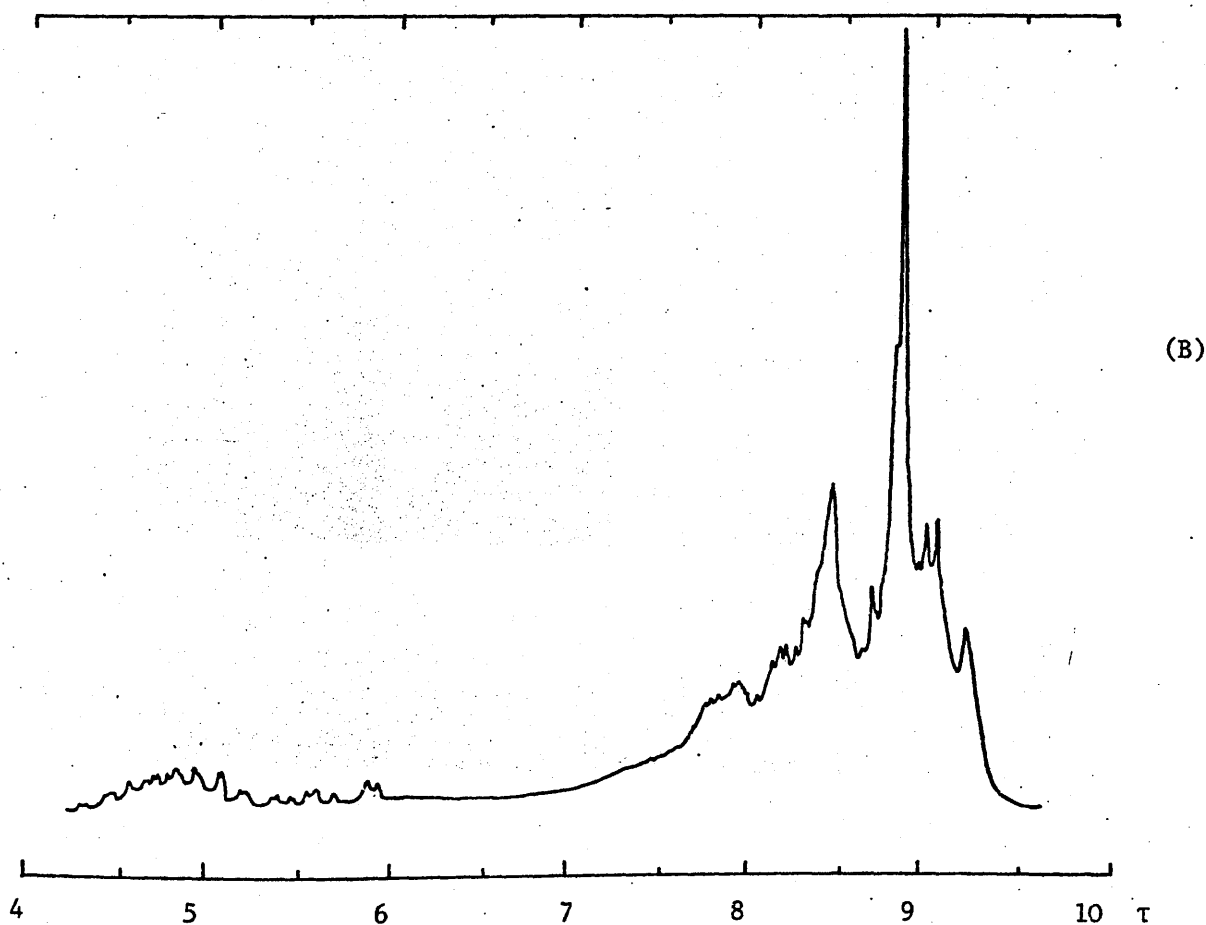
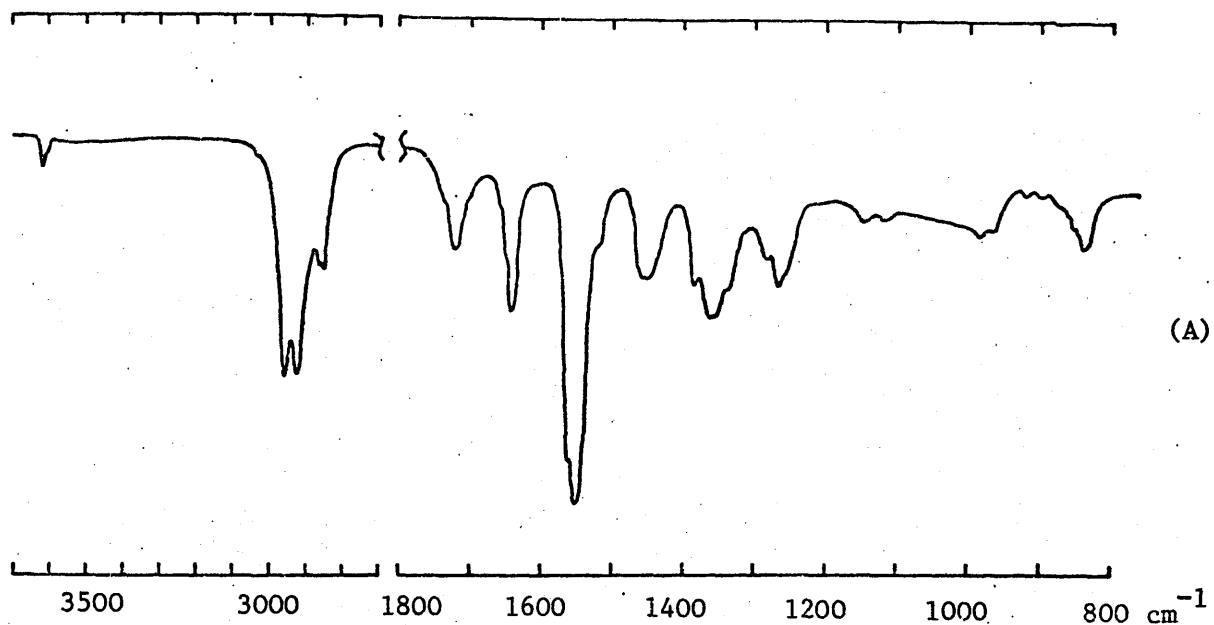


(45)



(46)

Figure 5.8 (A) The infra-red spectrum recorded in a  $\text{CCl}_4$  solution in the range  $3,700\text{--}800\text{ cm}^{-1}$  and (B) the  $^1\text{H}$  n.m.r. spectrum recorded in  $\text{CDCl}_3$  in the  $\tau$  range 4 to 10 of compounds (44-46) isolated from the product of humulene nitrosite reacted with  $\text{N}_2\text{O}_3$ .

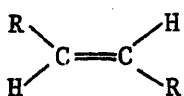


It must be emphasised however, that structures (44-46) are proposed in a very tentative manner since they are based solely on the following observations.

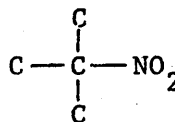
- 1) The infra-red spectrum is consistent with the presence of the structural units listed below.

Structural unit	Infra-red absorptions	
a) $\begin{array}{c} \text{R} \quad \text{CH}_3 \\ \diagdown \quad / \\ \text{C} = \text{C} \\ / \quad \diagdown \\ \text{H} \quad \text{R} \end{array}$	$\nu\text{C-H str.}$	$3,015 \text{ cm}^{-1}$
	$\nu\text{o.o.p. def.}$	$840 \text{ cm}^{-1}$
b) $\begin{array}{c}   \\ \text{H} - \text{C} - \text{NO}_2 \\   \end{array}$	$\nu\text{NO}_2 \text{ asym. str. (1,540-1,565) cm}^{-1}$	
	$\nu\text{NO}_2 \text{ sym. str. (1,355-1,365) cm}^{-1}$	
	In each case several nitro absorptions are present.	
c) $\begin{array}{c}   \\ \text{H} - \text{C} - \text{ONO}_2 \\   \end{array}$	$\nu\text{asym NO}_2 \text{ str.}$	$1,645 \text{ cm}^{-1}$
	$\nu\text{sym. NO}_2 \text{ str}$	$1,280 \text{ cm}^{-1}$
	$\nu\text{N-O str.}$	$850 \text{ cm}^{-1}$
d) $\begin{array}{c} \text{R} \\   \\ \text{HO} - \text{C} - \text{R} \\   \\ \text{R} \end{array}$	$\nu\text{O-H str.}$	$3,610 \text{ cm}^{-1}$
	This hydroxyl stretching absorption is weak.	
e) $\begin{array}{c} \text{O} \\    \\ \text{C} \\ / \quad \backslash \end{array}$	$\nu\text{C=O str.}$	$1,720 \text{ cm}^{-1}$

- 2) A comparison of the absorbance of the nitro absorptions in this sample, with the standard humulene and caryophyllene species indicated that two nitro groups are present per molecule. A comparison of the nitrate absorptions, relative to the nitro absorptions, in nitro-nitrato-humulene (26), and in this mixture, indicated that 39% of the species also contain a nitrate grouping.
- 3) The  $^1\text{H}$  n.m.r. spectrum shows a series of resonances in the  $\tau$  range 8.34 to 8.46 which are compatible with the presence of a number of allylic methyls.
- 4) The  $^1\text{H}$  n.m.r. and infra-red spectra, show no evidence of the following structural units.



and



- 5) The mass spectrum is consistent with the postulated structures. The main peaks present in the mass spectrum are summarised in table 5.12, appendix 5.

#### 5.4 The mechanism by which humulene nitrosite reacts with $\text{N}_2\text{O}_3$

The diamagnetic species formed when humulene nitrosite reacts with  $\text{N}_2\text{O}_3$  appear at first sight to have very diverse structures. They are, however, very interesting, having a common mechanistic origin, and demonstrating for the first time in this present study, species which have formed, by a transannular cyclisation of the humulene ring.

A complete mechanistic flow chart is shown in figure S.1 of the summary, which outlines the production of the species observed when solutions of humulene in an aprotic solvent, and solutions of



humulene nitrosite in an aprotic solvent, are reacted with the oxides of nitrogen.

The reaction of humulene nitrosite with the oxides of nitrogen proceeds by the scheme previously postulated in figure 5.2, and involves the attack of  $\dot{\text{N}}\text{O}$  at the nitroso group forming the diazonium complex (37), which eliminates  $\text{N}_2$ , forming the aliphatic radical (18). This aliphatic radical (18), can be stabilised in the following five ways.

- 1) First, the  $\dot{\text{O}}\text{NO}_2$  radical can abstract a proton from (18), producing structures (41), (42), (43), and nitric acid.
- 2) Alternatively the  $\dot{\text{O}}\text{NO}_2$  radical could add to (18), producing nitro-nitrato-humulene (26). As no significant traces of nitro-nitrato-humulene were observed, the  $\dot{\text{O}}\text{NO}_2$  radical would appear to prefer to abstract a proton. This preference may have its origins in steric considerations.
- 3) Third  $\dot{\text{N}}\text{O}_2$  can add to (18), producing dinitro-humulene (24).
- 4) In its fourth mode of behaviour radical (18) can interact with molecules of unreacted humulene nitrosite, producing nitroxide radicals  $\text{A}_1$  and  $\text{A}_2$ , which are thus diastereomeric forms of structure (19), and identical to nitroxide radicals  $\text{I}_\text{A}$  and  $\text{I}_\text{B}$ .
- 5) Finally, radical (18) can undergo the transannular cyclisation shown in figure S.1. The first products of this cyclisation, (48), (50) and (52), contain a cyclopropyl ring. These compounds were not detected. This is not surprising, as the cyclopropyl ring, would be susceptible to further attack by  $\dot{\text{N}}\text{O}_2$  and  $\dot{\text{O}}\text{NO}_2$ , which would result in the ring opening.

Compound (40), found to be a product of the reaction of humulene

nitrosite with  $N_2O_3$ , may have been produced by this mechanism. Compounds (44), (45) and (46), may also have formed as shown in figure S.1, from cyclised products containing a cyclopropyl ring, which were not detected prior to their further reactions with  $\dot{NO}_2$ .

The transannular cyclisation of radical (18) also produces the aliphatic radicals (47) and (49), which may react with humulene nitrosite, to produce nitroxide radicals containing the structural units  $R_1R_2R_3C-\dot{NO}-CHR_4R_5$  and  $R_1R_2R_3C-\dot{NO}-CR_4R_5R_6$ . This provides a possible explanation for the formation of nitroxide radical B, containing the structural unit  $R_1R_2R_3C-\dot{NO}-CHR_4R_5$  which is observed when humulene nitrosite reacts with  $N_2O_3$ .

#### 5.5 The paramagnetic species formed during the reaction of caryophyllene nitrosite with $N_2O_3$

Figure 3.6 shows the e.p.r. spectrum obtained from a dilute solution in chloroform, of the yellow oil formed during the reaction of caryophyllene nitrosite with  $N_2O_3$ . The single nitroxide radical present, contains the structural unit  $R_1R_2R_3C-\dot{NO}-C R_4R_5R_6$  and most probably forms when caryophyllene nitrosite reacts with nitric oxide forming a diazonium nitrate complex which decomposes with the evolution of  $N_2$  to aliphatic radical (12), which interacts with caryophyllene nitrosite to form the nitroxide radical I' of structure (10). This mechanism is completely analogous to that shown in figure 5.2 which describes the reaction of humulene nitrosite with  $\dot{NO}$ .

Attempts to isolate this nitroxide radical I' using chromatography, and sublimation at low pressures, have proved unsuccessful. Figure 5.9 shows the e.p.r. spectrum obtained from

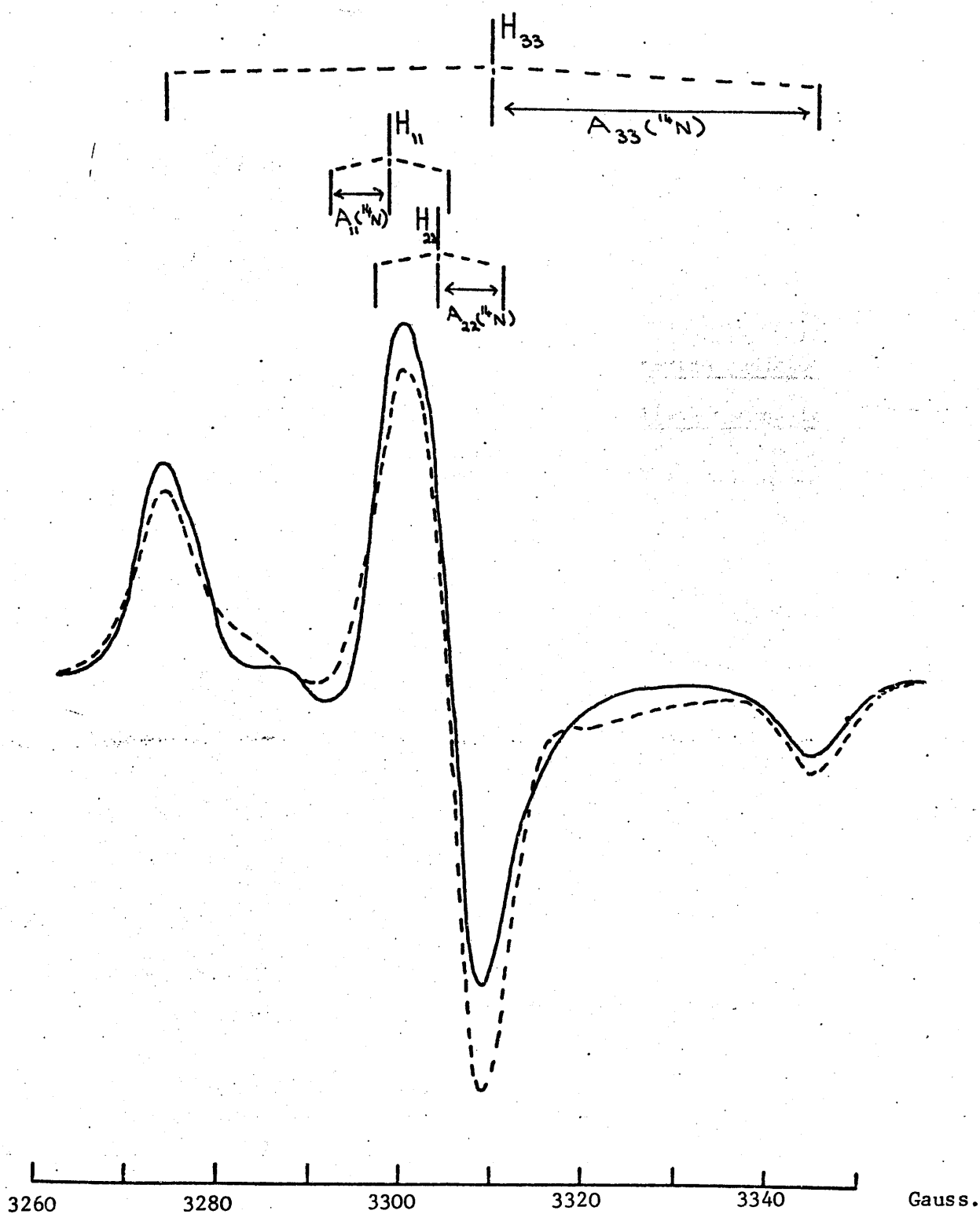


Figure 5.9 The e.p.r. spectrum recorded at 295°K, of a dilute polycrystalline sample of nitroxide radical I', obtained from the reaction of caryophyllene nitrosite (2) with  $\text{N}_2\text{O}_3$ .

a polycrystalline sample of the products of the reaction of caryophyllene nitrosite with  $N_2O_3$ . The spin Hamiltonian parameters of nitroxide radical I' obtained from an analysis of this spectrum are contained in table 5.13.

Table 5.13

The spin Hamiltonian parameters of nitroxide radical I'  
obtained from the reaction of caryophyllene nitrosite  
with  $N_2O_3$

$g_{11}$	$g_{22}$	$g_{33}$	$\langle g \rangle$	
2.0087	2.0053	2.0021	2.0054	
$A_{11}(^{14}N)$	$A_{22}(^{14}N)$	$A_{33}(^{14}N)$	$a(^{14}N)$	$\beta$
6.5G	7.0G	35.5G	16.3G	3.0G

The limits of error for  $g_{11}$ ,  $g_{22}$ ,  $g_{33}$ ,  $\langle g \rangle$ ,  $A_{11}(^{14}N)$ ,  $A_{22}(^{14}N)$ ,  $A_{33}(^{14}N)$ , and  $a(^{14}N)$ , are respectively  $\pm 0.0003$ ,  $\pm 0.0003$ ,  $\pm 0.0002$ ,  $\pm 0.0003$ ,  $\pm 0.3G$ ,  $\pm 0.3G$ ,  $\pm 0.1G$ , and  $\pm 0.3G$ .

## APPENDIX 5

### 5'.1' The reaction of humulene nitrosite with nitrogen dioxide

A dilute solution of humulene nitrosite in petroleum ether was placed in a flask, and partially degassed. The theoretical volume of nitrogen dioxide required to introduce one molecule of  $\dot{\text{N}}\text{O}_2$  for each molecule of humulene nitrosite, was then injected into the flask. Over a period of a few days, a white precipitate settled out, and the material remaining in the petroleum ether layer retained the blue colour of humulene nitrosite. All the products of this reaction were found to be diamagnetic.

#### a) Products of the reaction of humulene nitrosite with $\dot{\text{N}}\text{O}_2$ which are soluble in pet.ether

The  $^1\text{H}$  n.m.r. and infra-red spectra of the material remaining in the petroleum ether, showed the presence of unreacted humulene nitrosite, and a mixture of derivatives containing numerous nitro, and nitrate groupings. These products were chromatographed on silica t.l.c. plates using ether: pet.ether, (60:40). A series of components were present, mostly in small quantities. The two major products were present at  $R_f = 0.57$ , and  $0.5$ , and were purified by crystallising from hot ethanol. The component of  $R_f = 0.5$  was characterised as dinitro-humulene (24). A comparison of the  $^1\text{H}$  n.m.r. spectrum of the component of  $R_f = 0.57$  with the corresponding spectrum of dinitro-humulene (24) is shown in figure 5.3.

The spectra of the two species are very similar, and they appear to be the cis and trans isomers of dinitro-humulene. The cis isomer contains a small amount of a nitrate derivative, the absorptions of which were detected in the infra-red spectrum.

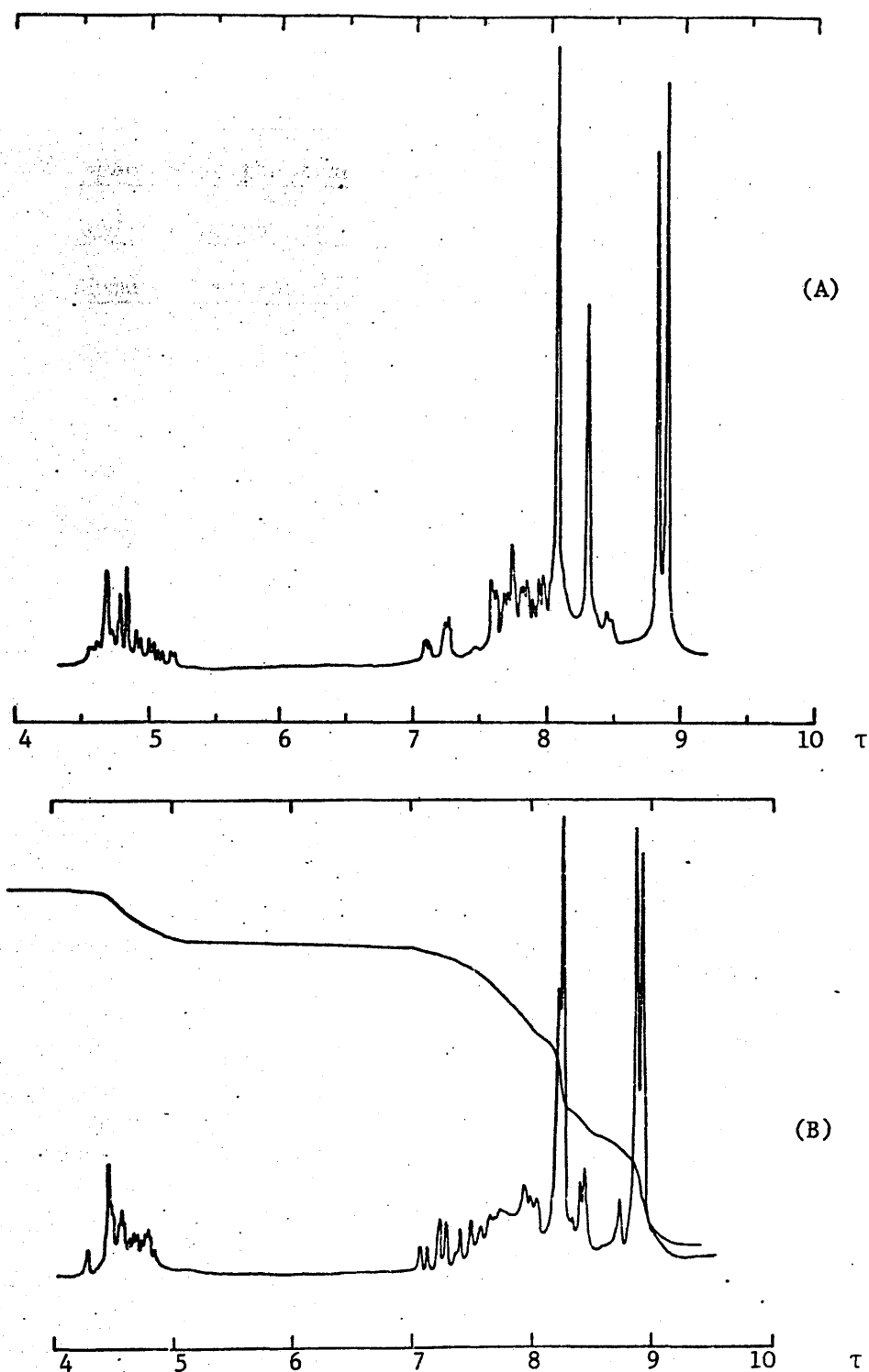
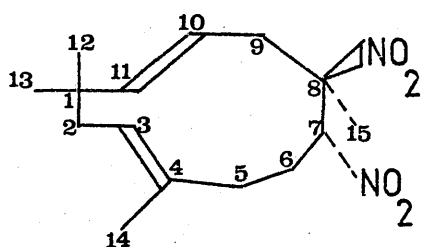


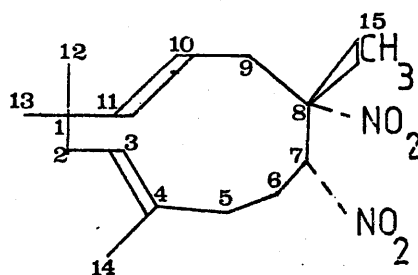
Figure 5.3 The  $^1\text{H}$  n.m.r. spectra of solutions of (A) trans-dinitro-humulene (24), and (B) cis-dinitro-humulene, in  $\text{CDCl}_3$  in the  $\tau$  range 4 to 10.

Table 5.1

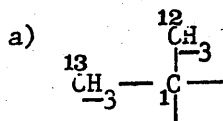
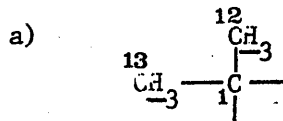
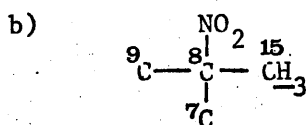
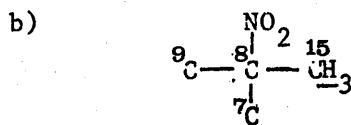
A comparison of the data obtained from the  $^1\text{H}$  n.m.r. spectra of the trans isomer of dinitro-humulene (24) and the component of  $R_f = 0.57$ , of the reaction of humulene nitrosite with  $\text{NO}_2$ , which appears to be the cis isomer of dinitro-humulene

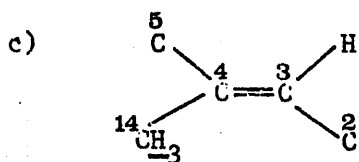


Trans dinitro-humulene

 $R_f = 0.5$ 

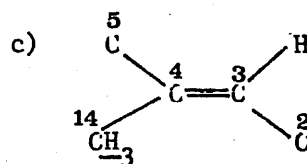
Cis dinitro-humulene

 $R_f = 0.57$ S  $\tau = 8.89$       I = 3HS  $\tau = 8.84$       I = 3HS  $\tau = 8.92$       I = 3HS  $\tau = 8.87$       I = 3HS  $\tau = 8.08$       I = 3HS  $\tau = 8.26$       I = 3H



S  $\tau = 8.29$  I = 3H

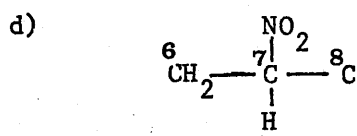
small coupling  $J < 1\text{Hz}$ .



S  $\tau = 8.23$

I = 3H

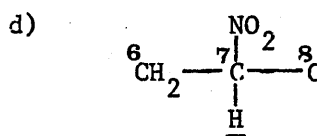
small coupling  $J < 1\text{Hz}$ .



Multiplet  $\tau = 4.74$ , I = 1H.

X part of an ABX system

$J = 0\text{Hz}$ ,  $J = 8.8\text{Hz}$ .



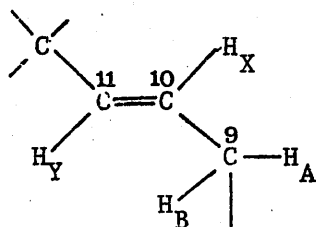
Multiplet  $\tau = 4.76$ , I = 1H.

X part of an ABX spectrum

$J = 4.5\text{Hz}$ ,  $J = 8.0\text{Hz}$ .

e) Ethylenic protons

1)



$H_X$  is the X part of an ABXY

system, and consists of a

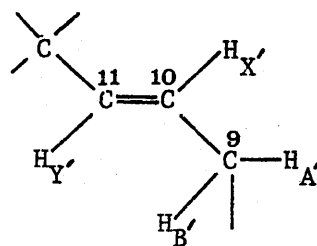
group of 8 peaks  $\tau = 5.04$

$J_{XY} = 15.9\text{Hz}$ ,  $J_{AX} = 8.8\text{Hz}$ ,

$J_{BX} = 3.0\text{Hz}$ .

e) Ethylenic protons

1)



$H_{X'}$  is the X part of an ABXY system

and consists of a group of

8 peaks  $\tau = 4.64$   $J_{XY'} = 16.5\text{Hz}$ ,

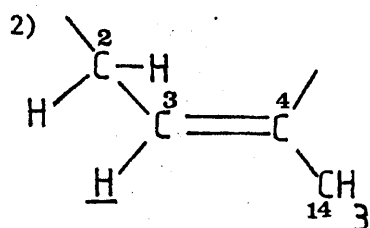
$J_{AX'} = 9.0\text{Hz}$ ,  $J_{BX'} = 4.5\text{Hz}$ .



$H_Y$  Doublet  $\tau$  4.68

$$J_{YX} = 15.9\text{Hz.}$$

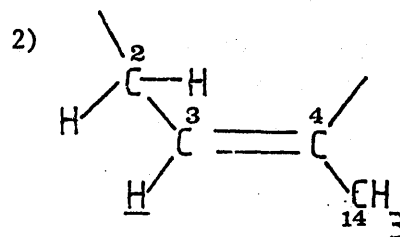
shows a small additional  
coupling of  $\approx 1\text{Hz.}$



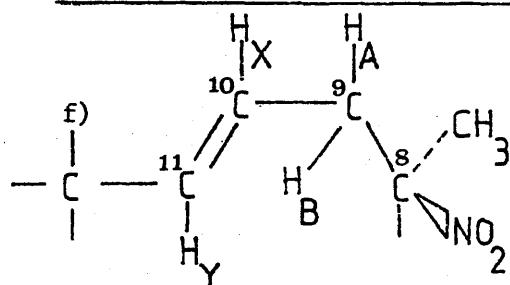
The underlined proton is  
the X part of an ABX system.  
Multiplet  $\tau = 4.64$   $I = 1H$   
 $J = 5.0\text{Hz.}$  and  $J = 9.0\text{Hz.}$

$H_{Y'}$  Doublet  $\tau$  4.64

$$J_{Y'X'} = 16.5\text{Hz.}$$



The underlined proton is  
the X part of an ABX system.  
Multiplet  $\tau = 4.52$   $I = 1H$   
 $J = 3\text{Hz.}$  and  $J = 10\text{Hz.}$



8 peaks are observed for  $H_A$

$$\tau = 7.28 \quad I = 1H$$

$$J_{AB} = 15\text{Hz.}, \quad J_{AX} = 3\text{Hz.},$$

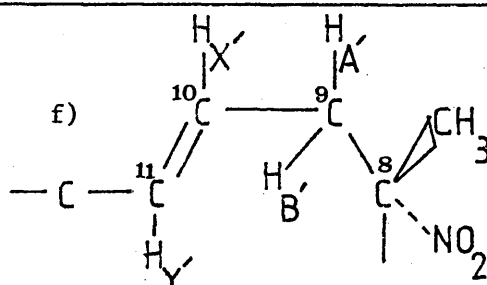
$$J_{AY} = 1\text{Hz.}$$

8 peaks are observed for

$$H_B \quad \tau 7.72 \quad I = 1H$$

$$J_{AB} = 15\text{Hz.}, \quad J_{BX} = 8.8\text{Hz.},$$

$$J_{BY} = 2\text{Hz.}$$



8 peaks are observed for  $H_B$

$$\tau = 7.18 \quad I = 1H$$

$$J_{A'B'} = 16\text{Hz.}, \quad J_{B'X'} = 4.5\text{Hz.},$$

$$J_{B'Y'} < 1\text{Hz.}$$

8 peaks are observed for

$$H_{A'} \quad \tau = 7.53 \quad I = 1H$$

$$J_{A'B'} = 6\text{Hz.}, \quad J_{A'X'} = 9\text{Hz.},$$

$$J_{A'Y'} < 1\text{Hz.}$$

## g) Allylic protons

The  $\tau$  region 7.06 to 8.52 contains 14 protons, namely 4  $\text{CH}_2$ 's, the allylic methyl, and the methyl on the carbon adjacent to  $\text{NO}_2$ .

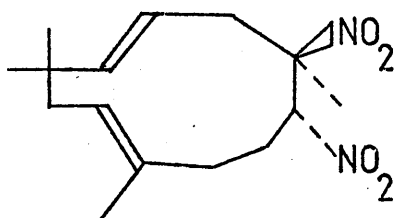
## g) Allylic protons

The  $\tau$  region 7.02 to 8.54 contains 14 protons, namely 4  $\text{CH}_2$ 's, the allylic methyl, and the methyl on the carbon adjacent to  $\text{NO}_2$ .

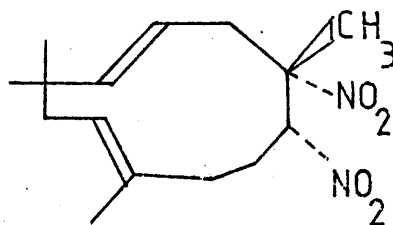
---

Table 5.2

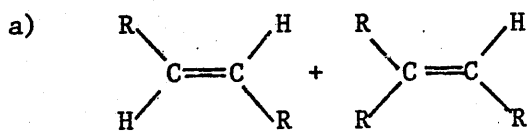
A comparison of the data obtained from the infra-red spectra of the trans isomer of dinitro-humulene (24), and the component of  $R_f = 0.57$ , of the reaction of humulene nitrosite with  $\dot{\text{NO}}_2$ , which appears to be the cis isomer of dinitro-humulene



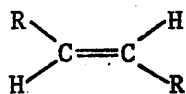
Trans dinitro-humulene

 $R_f = 0.5$ 

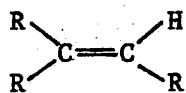
Cis dinitro-humulene

 $R_f = 0.57$ 

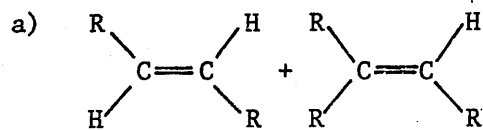
νC-H str.	3,015 $\text{cm}^{-1}$
	3,010 $\text{cm}^{-1}$
νC=C str.	1,660 $\text{cm}^{-1}$
	1,665 $\text{cm}^{-1}$



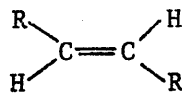
νo.o.p. def.	980 $\text{cm}^{-1}$
--------------	----------------------



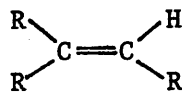
νo.o.p. def.	840 $\text{cm}^{-1}$
--------------	----------------------



νC-H str.	3,015 $\text{cm}^{-1}$
	3,010 $\text{cm}^{-1}$
νC=C str.	1,660 $\text{cm}^{-1}$
	1,665 $\text{cm}^{-1}$

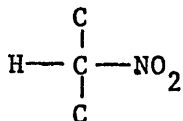


νo.o.p. def.	990 $\text{cm}^{-1}$
--------------	----------------------



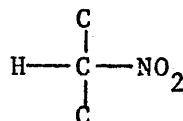
νo.o.p. def.	840 $\text{cm}^{-1}$
--------------	----------------------

b)



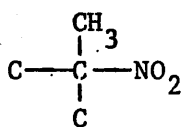
$\nu\text{NO}_2$ asym.	$1,560 \text{ cm}^{-1}$
$\nu\text{NO}_2$ sym.	$1,360 \text{ cm}^{-1}$
$\nu\text{C-N}$ bend	$872 \text{ cm}^{-1}$

b)



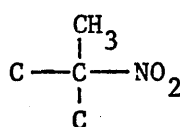
$\nu\text{NO}_2$ asym.	$1,562 \text{ cm}^{-1}$
$\nu\text{NO}_2$ sym.	$1,364 \text{ cm}^{-1}$
$\nu\text{C-N}$ bend	$870 \text{ cm}^{-1}$

c)



$\nu\text{NO}_2$ asym.	$1,545 \text{ cm}^{-1}$
$\nu\text{NO}_2$ sym.	$1,355 \text{ cm}^{-1}$

c)



$\nu\text{NO}_2$ asym.	$1,555 \text{ cm}^{-1}$
$\nu\text{NO}_2$ sym.	$1,355 \text{ cm}^{-1}$

b) Products of the reaction of humulene nitrosite with  
 $\dot{\text{N}}\text{O}_2$  which are insoluble in pet.ether

A comparison of the  $^1\text{H}$  n.m.r. and infra-red spectra of the species which precipitated from pet.ether, with the corresponding spectra of humulene nitrosite, indicated that the species formed by the replacement of the nitroso group by  $\dot{\text{N}}\text{O}_2$ , followed by a subsequent further addition of  $\dot{\text{N}}\text{O}_2$  and  $\dot{\text{O}}\text{NO}_2$  over the remaining double bonds. The species retained on average four protons in the ethylenic region of the  $^1\text{H}$  n.m.r. spectrum, and showed no signs of having formed by a process involving cyclisation. An elemental analysis of the precipitate gave the composition as 46.3%C, 6.62%H and 12.9%N, indicating that on average the empirical formula is  $\text{C}_{15}\text{H}_{24}\text{N}_{3.7}\text{O}_{8.3}$ . This material was chromatographed using silica plates, with ether: pet.ether, (60:40) as solvent. Three major product bands were present at  $R_{f.} = 0.24$ , 0.33, and 0.44, but each contained a mixture of derivatives. Crystallising the components of  $R_{f.} = 0.24$ , and 0.44, from hot ethanol, yielded small amounts of pure crystalline species. Figure 5.4 shows the  $^1\text{H}$  n.m.r., and infra-red spectra of the crystals obtained from the band of  $R_{f.} = 0.24$ , and figure 5.5 shows the  $^1\text{H}$  n.m.r., and infra-red spectra of the crystals obtained from the band of  $R_{f.} = 0.44$ . A comparison of these spectra with the corresponding spectra of the parent molecule, humulene nitrosite, indicated that the species had the respective structures (38) and (39). The pertinent data obtained from the  $^1\text{H}$  n.m.r. and infra-red spectra of species (38) and (39) are summarised in tables 5.3, 5.4, 5.5, and 5.6, respectively.

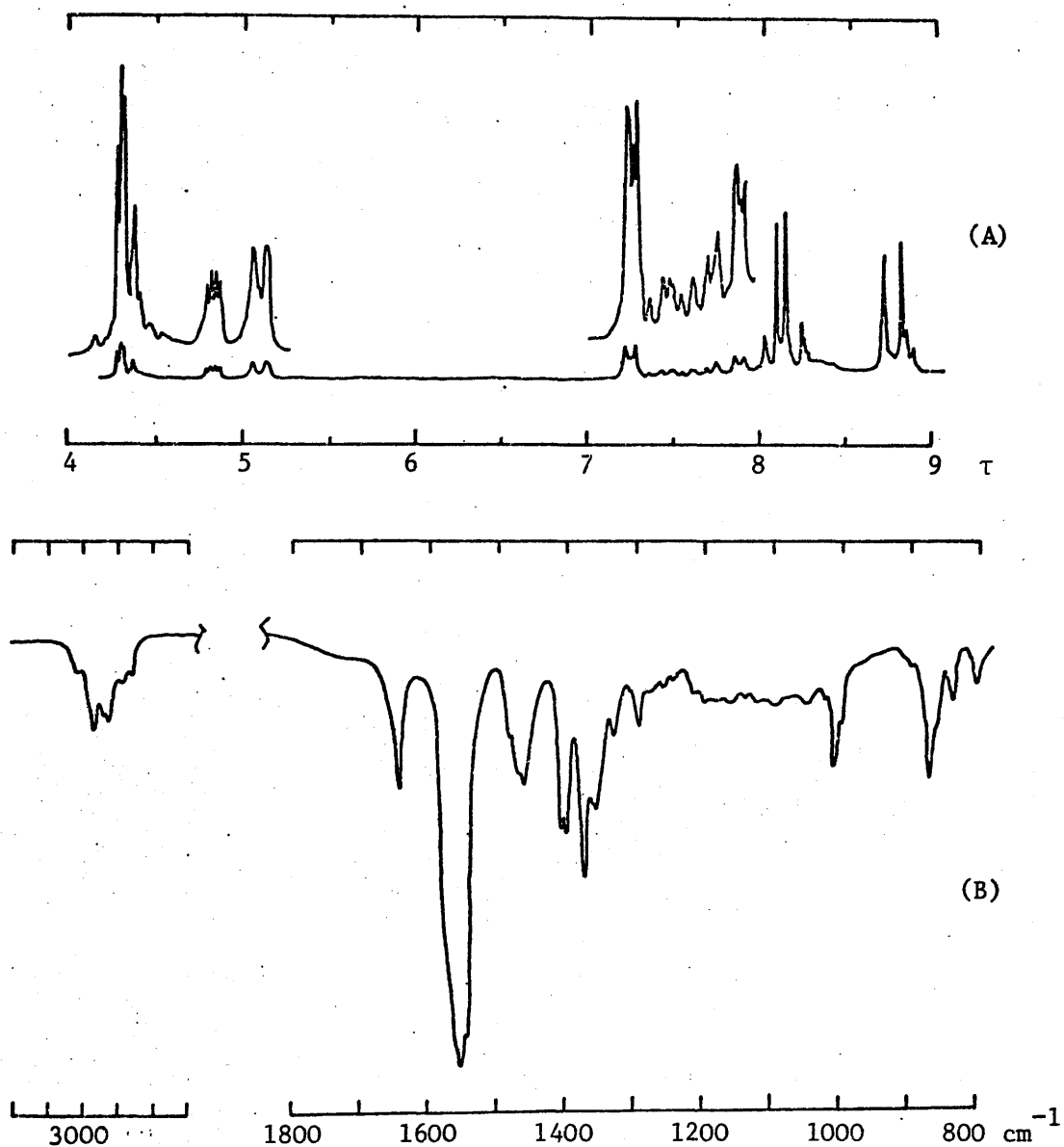


Figure 5.4 (A) The  $^1\text{H}$  n.m.r. spectrum recorded in a  $\text{CDCl}_3$  solution in the  $\tau$  range 4 to 9, and (B) the infra-red spectrum recorded in a KBr disc in the range 3,200–800  $\text{cm}^{-1}$  of the component of  $R_f = 0.24$ , namely (38), isolated from the product of the reaction of humulene nitrosite (17) with  $\dot{\text{N}}\text{O}_2$ .

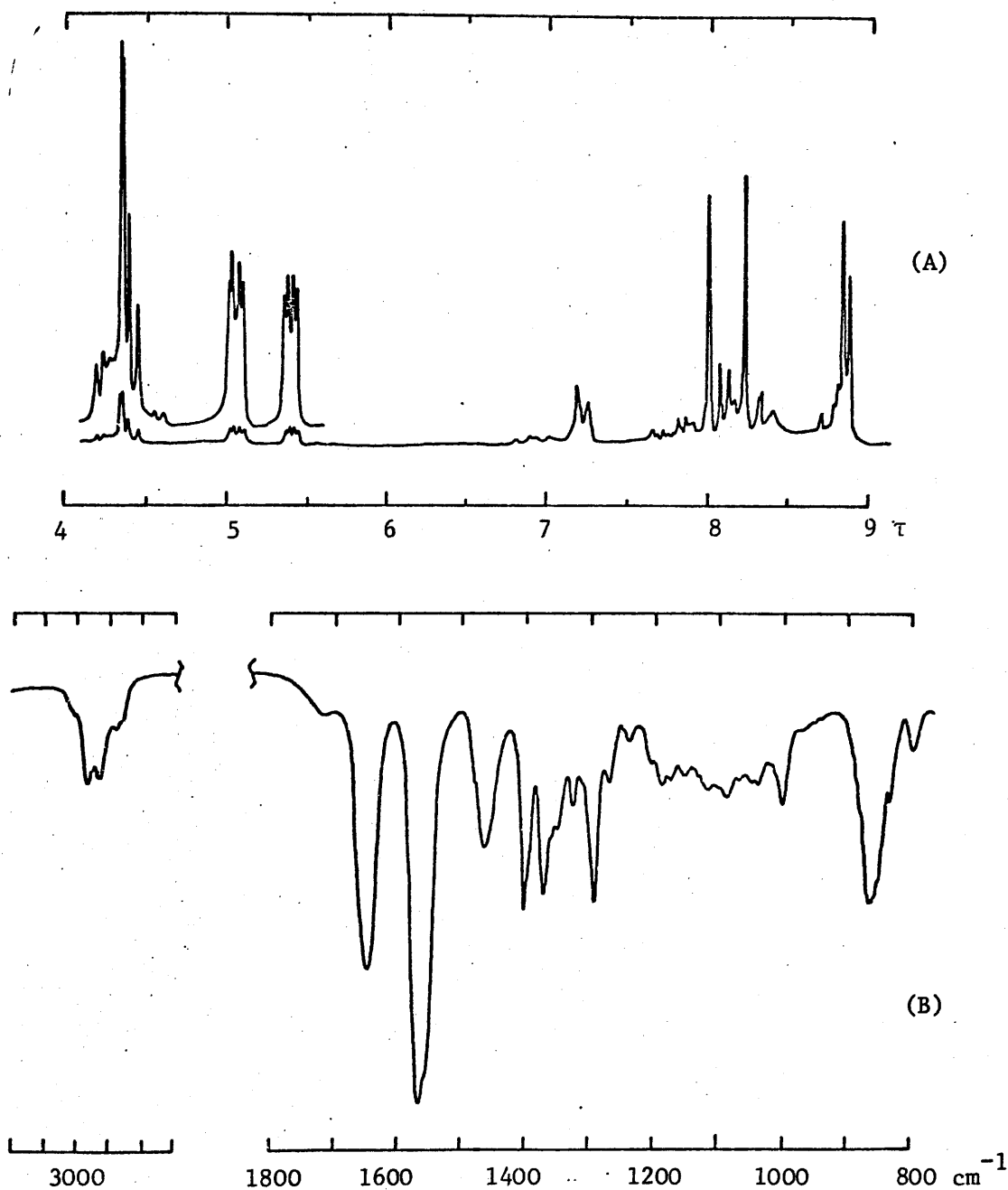
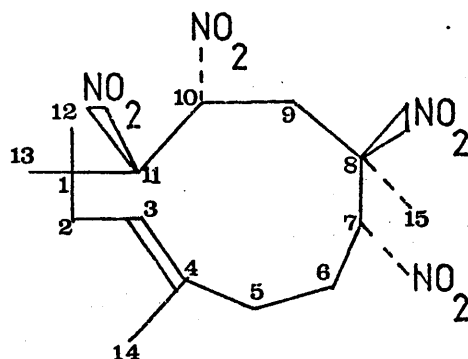


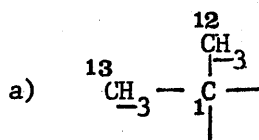
Figure 5.5 (A) The  $^1\text{H}$  n.m.r. spectrum recorded in a  $\text{CDCl}_3$  solution in the  $\tau$  range 4 to 9, and (B) the infra-red spectrum recorded in a KBr disc in the range 3,200–800  $\text{cm}^{-1}$  of the component of  $R_f = 0.44$ , namely (39), isolated from the product of the reaction of humulene nitrosite (17) with  $\text{NO}_2$ .

Table 5.3

Pertinent data from the  $^1\text{H}$  n.m.r. spectrum of compound (38)



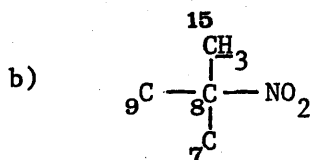
(38)



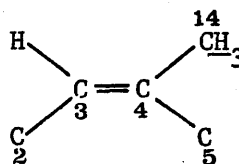
S  $\tau$  = 8.82 , I = 3H.

S  $\tau$  = 8.72 , I = 3H.

The  $\text{CH}_3$  of  $\text{C}_{12}$  lies adjacent to the nitro group on  $\text{C}_{11}$  and is shifted to lower field.



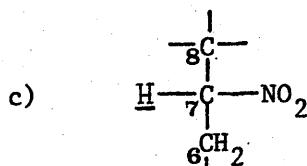
and



S  $\tau$  = 8.10, I = 3H.

and

S  $\tau$  = 8.15, I = 3H.

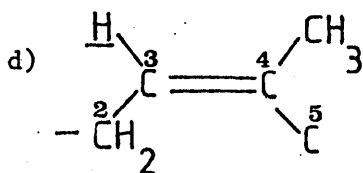


Doublet  $\tau$  = 5.10, I = 1H.

The underlined proton should be the X part of an ABX system, but it is coupling to only one proton. The proton on  $\text{C}_7$  of humulene nitrosite (17) and the proton on  $\text{C}_7$  of



nitro-nitrato-humulene (26) also coupled to only one of the protons on C<sub>6</sub>.

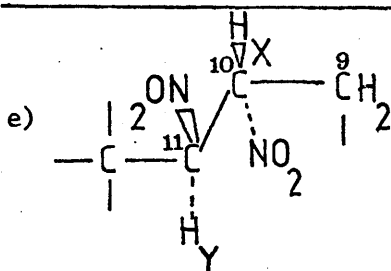


Multiplet  $\tau = 4.83$ ,  $I = 1H$ .

The underlined proton is  
the X part of an ABX system,

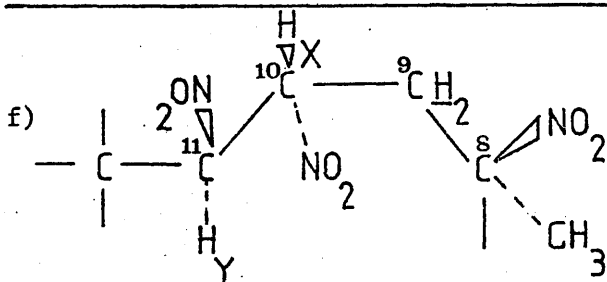
$$J_{AX} = 5.8\text{Hz.}$$

$$J_{BX} = 3\text{Hz.}$$



H<sub>Y</sub> Doublet  $\tau = 4.31$ ,  $I = 1H$ ,  $J < 1\text{Hz}$ .

H<sub>X</sub> 1:2:1 triplet  $\tau = 4.32$ ,  $I = 1H$   $J = 6.0\text{Hz}$ , shows a small  
additional coupling to H<sub>Y</sub> of  $< 1\text{Hz}$ .



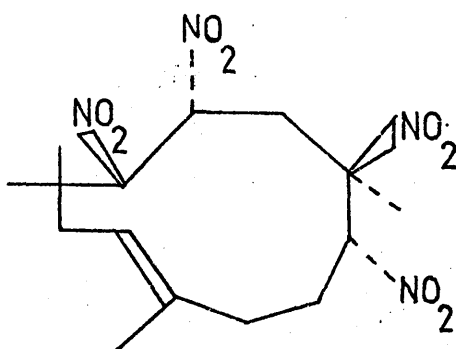
Doublet  $\tau = 7.25$ ,  $I = 2H$ ,  $J = 6.0\text{Hz}$ .

The nitro groups on C<sub>8</sub> and C<sub>10</sub> lie symmetrically on either side  
of the CH<sub>2</sub> group and the protons have almost identical chemical  
shifts.

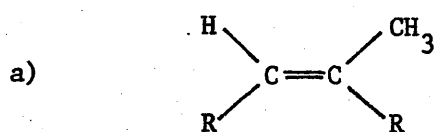
g) The remaining CH<sub>2</sub> resonances were difficult to analyse.

Table 5.4

Pertinent data from the infra-red spectrum of compound (38)



(38)



$\nu\text{C-H str.}$	$3,010\text{ cm}^{-1}$
$\nu\text{C=C str.}$	$1,660\text{ cm}^{-1}$
$\nu\text{o.o.p. def.}$	$850\text{ cm}^{-1}$

b)

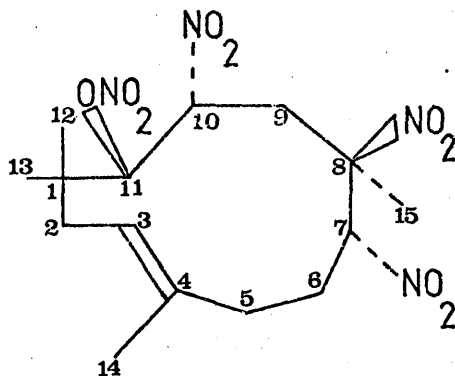
	$\nu\text{NO}_2\text{ asym.}$	$1,550\text{ cm}^{-1}$
		$1,557\text{ cm}^{-1}$
		$1,560\text{ cm}^{-1}$
	$\nu\text{NO}_2\text{ sym.}$	$1,355\text{ cm}^{-1}$
		$1,360\text{ cm}^{-1}$
		$1,365\text{ cm}^{-1}$

c)

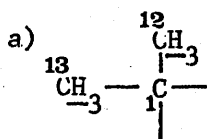
	$\nu\text{NO}_2\text{ asym.}$	$1,540\text{ cm}^{-1}$
	$\nu\text{NO}_2\text{ sym.}$	$1,347\text{ cm}^{-1}$

Table 5.5

Pertinent data from the  $^1\text{H}$  n.m.r. spectrum of compound (39)

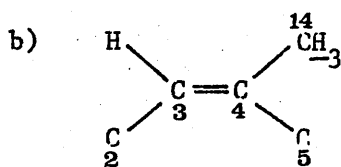


(39)

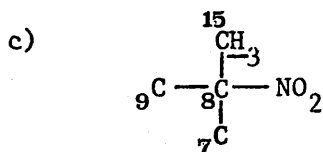


S  $\tau = 8.88$  I = 3H

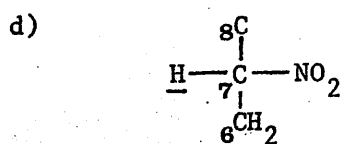
S  $\tau = 8.84$  I = 3H



S  $\tau = 8.23$  I = 3H



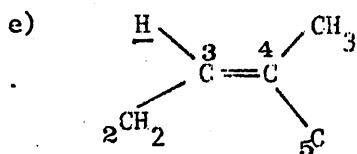
S  $\tau = 8.01$  I = 3H



The underlined proton is the X part of an

ABX system. Multiplet  $\tau$  5.06. I = 1H

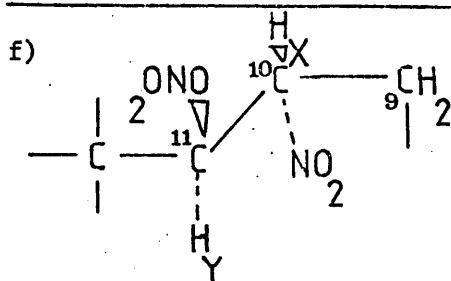
$J_{AX} = 6.0\text{Hz.}$   $J_{BX} = 2\text{Hz.}$



The underlined proton is the X part of an ABX system.

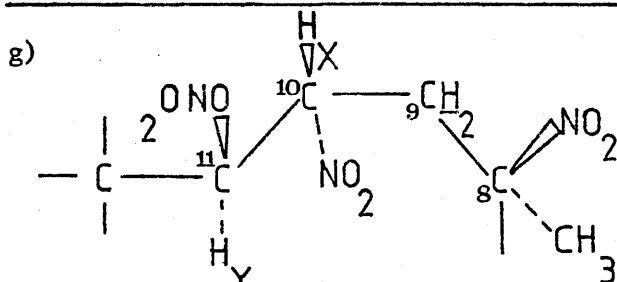
Multiplet  $\tau = 5.41$   $I = 1H$ .

$J_{AX} = 6.0Hz$ ,  $J_{BX} = 2.8Hz$ .



$H_Y$  Doublet  $\tau = 4.37$ ,  $I = 1H$ ,  $J < 1Hz$ .

$H_X$  1:2:1 triplet  $\tau = 4.4$ ,  $I = 1H$ ,  $J = 6Hz$ . shows a small additional coupling to  $H_Y$  of  $< 1Hz$ .



Doublet  $\tau = 7.23$ ,  $I = 2H$ ,  $J = 6Hz$ .

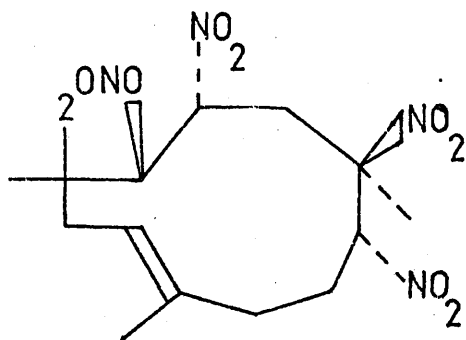
The nitro groups on  $C_8$  and  $C_{10}$  lie symmetrically on either side of the  $\underline{CH}_2$  group and the protons have almost identical chemical shifts.

h) The remaining  $CH_2$  resonances were difficult to analyse.

i) Additional resonances are present in the  $\tau$  regions 6.7 to 7.15 and 4.2 to 4.4. These may arise from the presence of small amounts of species isomeric to structure (39).

Table 5.6

The pertinent data from the infra-red spectrum of compound (39)



(39)

a)		$\nu\text{C-H str.}$	$3,010\text{ cm}^{-1}$
		$\nu\text{C=C str.}$	—
		$\nu\text{o.o.p. def.}$	$842\text{ cm}^{-1}$

b)		$\nu\text{NO}_2\text{ asym.}$	$1,560\text{ cm}^{-1}$
			$1,570\text{ cm}^{-1}$
		$\nu\text{NO}_2\text{ sym.}$	$1,370\text{ cm}^{-1}$
			$1,375\text{ cm}^{-1}$

c)		$\nu\text{NO}_2\text{ asym.}$	$1,545\text{ cm}^{-1}$
		$\nu\text{NO}_2\text{ sym.}$	$1,350\text{ cm}^{-1}$

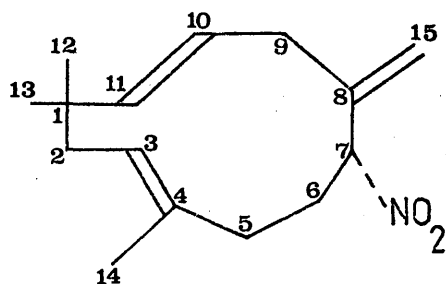
d)	$\text{R-ONO}_2$	$\nu\text{NO}_2\text{ asym.}$	$1,646\text{ cm}^{-1}$
		$\nu\text{NO}_2\text{ sym.}$	$1,290\text{ cm}^{-1}$
		$\nu\text{NO str.}$	$860\text{ cm}^{-1}$

5'.2'      Spectroscopic data obtained from the compounds  
(41), (40) and (44-46)

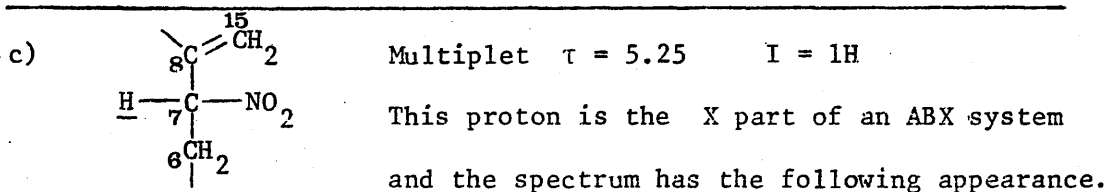
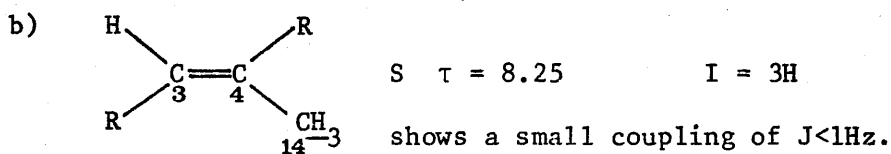
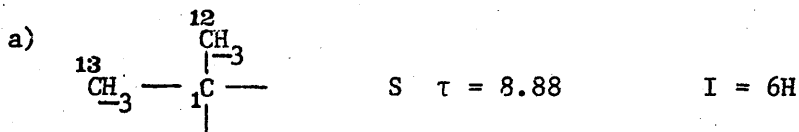
a)      Component (41)

Table 5.7

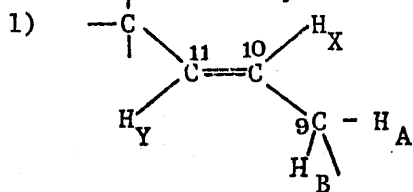
Pertinent data from the  $^1\text{H}$  n.m.r. spectrum of compound (41)



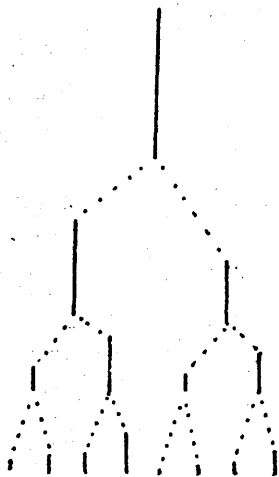
(41)



d) Ethylenic protons



$H_X$  is the X part of an ABXY system. The spectrum consists of 8 peaks with the following intensities.



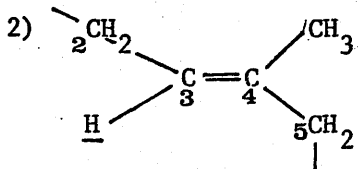
$$\tau = 4.83 \quad I = 1H$$

$$J_{XY} = 16.5\text{Hz.}$$

$$J_{XA} = 8\text{Hz.}$$

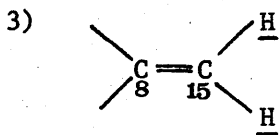
$$J_{XB} = 4\text{Hz.}$$

$H_Y$  Doublet  $\tau = 4.5$   $I = 1H$   $J_{XY} = 16.5\text{Hz.}$



1:2:1 triplet  $\tau = 4.62$   $I = 1H$

$$J = 4.5\text{Hz.}$$

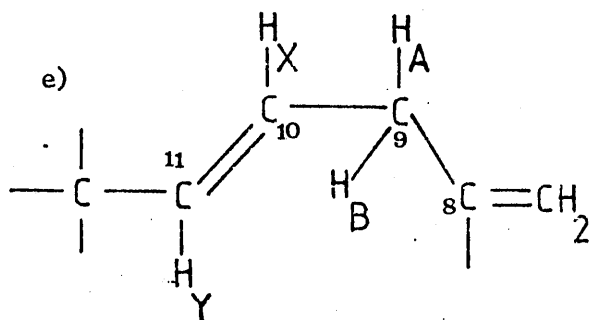


Two peaks are present

at  $\tau = 4.70$   $I = 1H$

and  $\tau = 4.77$   $I = 1H$

Each shows a small coupling of  $J < 1\text{Hz.}$



8 peaks are observed for

$$H_A \quad \tau = 7.0, \quad I = 1H.$$

$$J_{AB} = 14.0\text{Hz.} \quad J_{AX} = 6.0\text{Hz.}$$

$$J_{AY} = 1\text{Hz.}$$

8 peaks are observed for  $H_B \quad \tau = 7.18, \quad I = 1H.$

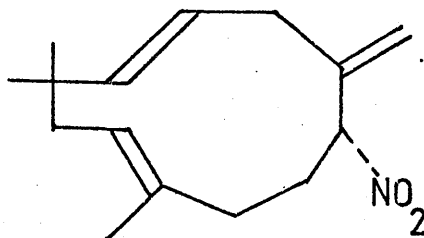
$$J_{AB} = 14.0\text{Hz.} \quad J_{BX} = 7\text{Hz.} \quad J_{BY} \approx 1\text{Hz.}$$

f) The  $\text{CH}_2$  region of the spectrum is difficult to analyse.



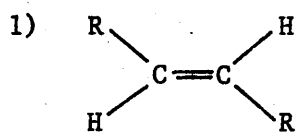
Table 5.8

Pertinent data from the infra-red spectrum of compound (41)



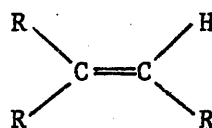
(41)

## a) Ethylenic groups

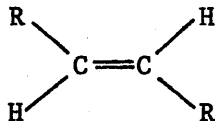


$\nu\text{C-H str.}$        $3,015\text{ cm}^{-1}$   
                           $3,010\text{ cm}^{-1}$

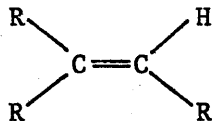
and



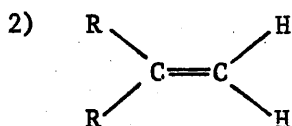
$\nu\text{C=C str.}$        $1,657\text{ cm}^{-1}$   
                           $1,665\text{ cm}^{-1}$



$\nu\text{o.o.p. def.}$        $975\text{ cm}^{-1}$

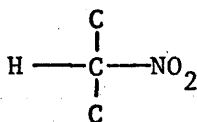


$\nu\text{o.o.p. def.}$        $845\text{ cm}^{-1}$



$\nu\text{C-H str.}$        $3,082\text{ cm}^{-1}$   
 $\nu\text{C=C str.}$        $1,635\text{ cm}^{-1}$   
 $\nu\text{o.o.p. def.}$        $915\text{ cm}^{-1}$

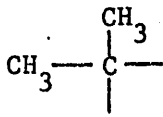
## b)



$\nu\text{NO}_2\text{ asym.}$        $1,550\text{ cm}^{-1}$   
 $\nu\text{NO}_2\text{ sym.}$        $1,360\text{ cm}^{-1}$   
 $\nu\text{C-N bend}$        $865\text{ cm}^{-1}$

These absorptions are characteristic of a nitro group attached to a secondary carbon atom.

c)

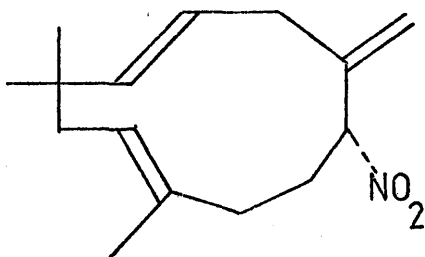


		vsym. def.	1,380 cm <sup>-1</sup>
vasym str.	2,960 cm <sup>-1</sup>	v skeletal	1,365 cm <sup>-1</sup>
vsym. str.	2,860 cm <sup>-1</sup>	v skeletal	1,170 cm <sup>-1</sup>
vasym. def. ~	1,445 cm <sup>-1</sup>	v skeletal	810 cm <sup>-1</sup>

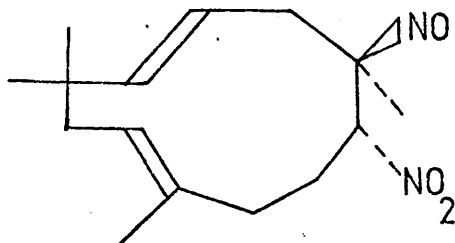
---

Table 5.9

A comparison of the main peaks in the mass spectra of compound (41), and humulene nitrosite



(41) mass = 249

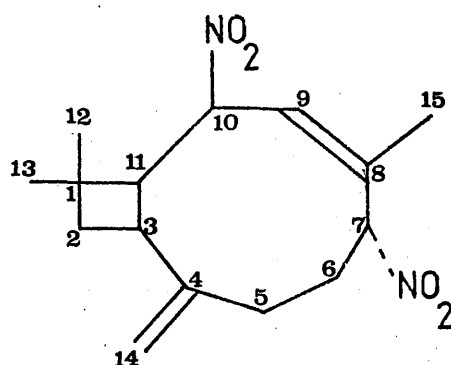


Humulene nitrosite mass = 280

---

279	} very small amounts of impurities		
265			
256			NO parent ion present
249	Parent species	250	loss of NO
233	loss of O		
217	loss of O <sub>2</sub>	220	loss of N <sub>2</sub> O <sub>2</sub>
203	loss of NO <sub>2</sub>	203	loss of N <sub>2</sub> O <sub>3</sub> + H
189		189	
175		175, 177	
159, 161		161	
147		147	
133, 135		133, 135	
119, 121		121	
107		105, 107	
93, 95		91, 93	
78		77, 79	
69		65	
55		53	
43		41	

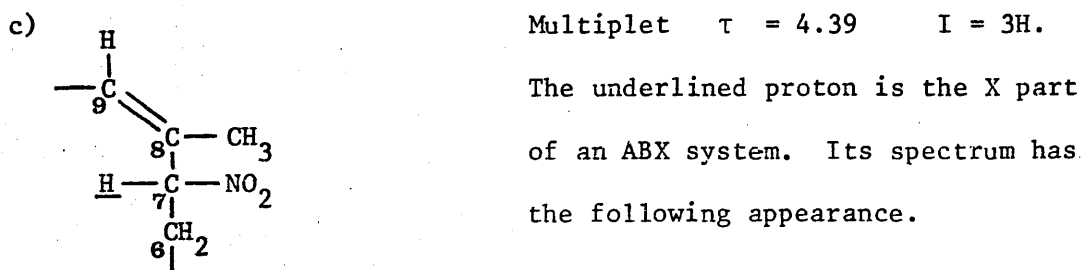
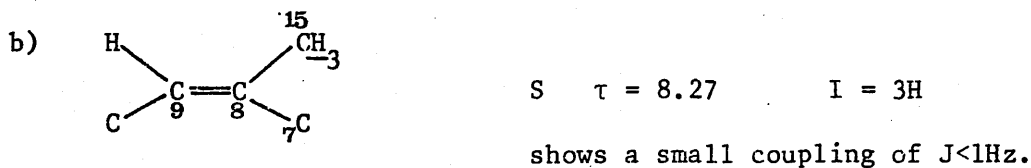
---

b) Component (40)Table 5.10Pertinent data from the  $^1\text{H}$  n.m.r. spectrum of compound (40)

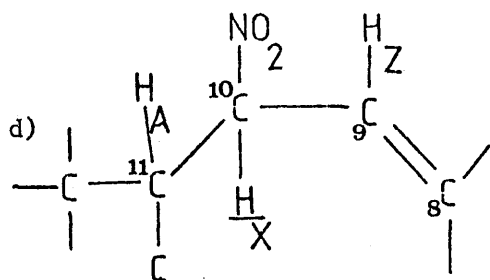
(40)



The proximity of the protons on  $\text{C}_{12}$  to the ring currents of the nitro group have caused a displacement of this resonance to lower field.



$J_{\text{AX}} = 7.5\text{Hz.}$ ,  $J_{\text{BX}} = 4\text{Hz.}$  There is a small coupling of  $< 1\text{Hz.}$  perhaps to the proton on  $\text{C}_9$ .



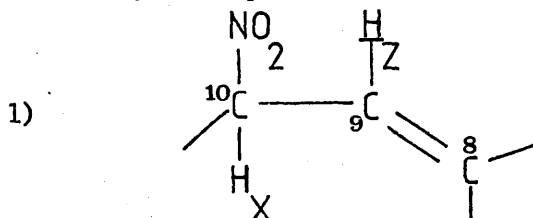
Multiplet  $\tau = 4.59$   $I = 1H$ .

The resonance of  $H_X$  is split into doublets by interaction with  $H_Z$

and then further split into doublets by interaction with  $H_A$ ,

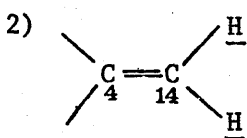
$$E_{XZ} = 9\text{Hz. } J_{XA} = 7\text{Hz.}$$

e) Ethylenic protons



$H_Z$ , doublet  $\tau = 5.55$ ,  $I = 1H$ ,  $J_{ZX} = 9\text{Hz}$ .

A small additional splitting of  $<1\text{Hz}$  is also present. This may be due to a weak interaction with the proton on  $C_7$ .



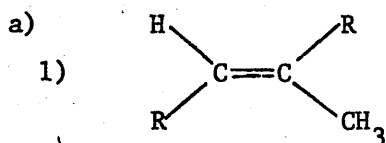
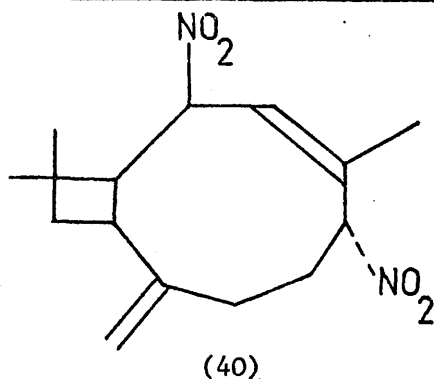
S  $\tau = 4.94$   $I = 2H$

Small splitting  $J < 1\text{Hz}$ .

f) The remaining resonances are difficult to analyse. In the  $\tau$  region 7.36 to 7.94 there are four protons. These are probably the allylic  $\text{CH}_2$ , and the two protons on the cyclobutane ring. The  $\tau$  region 7.96 to 8.48 integrates as seven protons, and these are probably the allylic methyl, and the remaining two  $\text{CH}_2$  groups.

Table 5.11

Pertinent data from the infra-red spectrum of compound (40)



$\nu_{C-H}$  str. 3,010  $\text{cm}^{-1}$

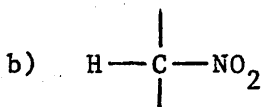
$\nu_{C-H}$  str. 3,080  $\text{cm}^{-1}$

$\nu_{C=C}$  str. 1,665  $\text{cm}^{-1}$

$\nu_{C=C}$  str. 1,630  $\text{cm}^{-1}$

$\nu_{o.o.p.}$  def. 840  $\text{cm}^{-1}$

$\nu_{o.o.p.}$  def. 900  $\text{cm}^{-1}$



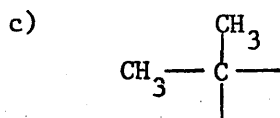
There are two sets of absorptions characteristic of a nitro group

attached to a secondary carbon atom.

$\nu_{NO_2}$  asym. 1,550  $\text{cm}^{-1}$  and 1,550  $\text{cm}^{-1}$

$\nu_{NO_2}$  sym. 1,360  $\text{cm}^{-1}$  and 1,370  $\text{cm}^{-1}$

$\nu_{C-N}$  bend 865  $\text{cm}^{-1}$  and 865  $\text{cm}^{-1}$



$\nu_{sym.}$  def. 1,390  $\text{cm}^{-1}$

$\nu_{asym.}$  str. 2,960  $\text{cm}^{-1}$

$\nu$  skeletal 1,180  $\text{cm}^{-1}$

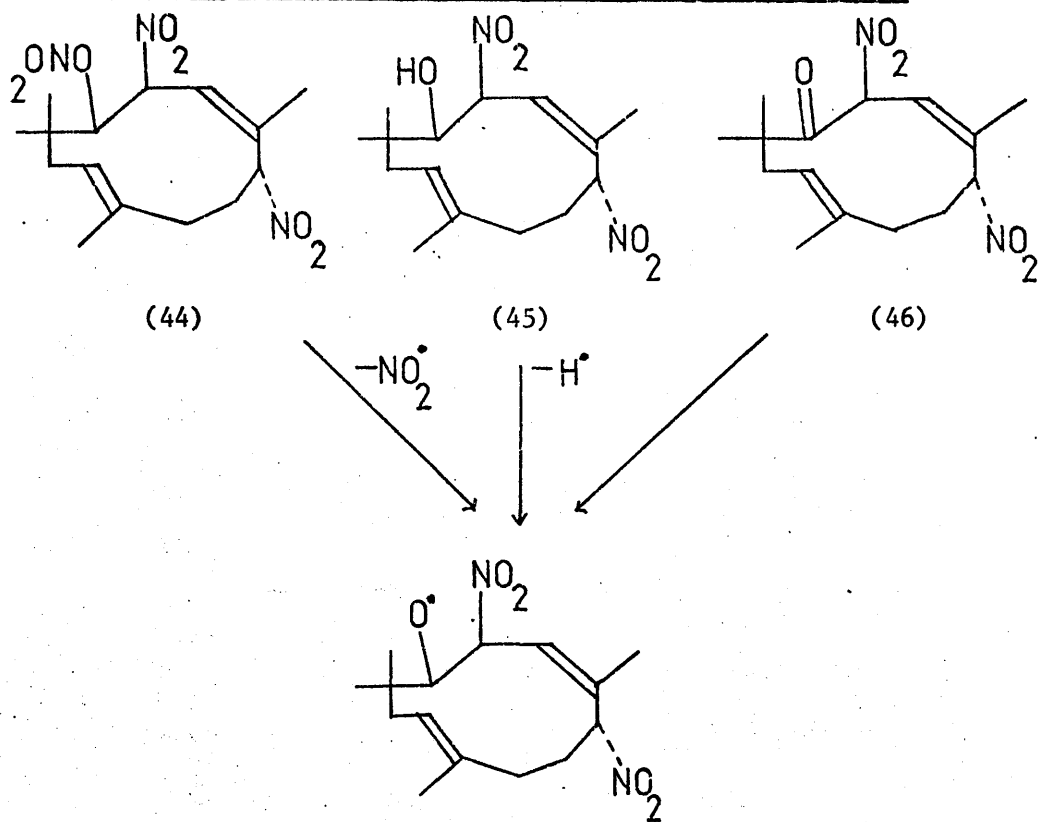
$\nu_{sym.}$  str. 2,865  $\text{cm}^{-1}$

$\nu$  skeletal 805  $\text{cm}^{-1}$

$\nu_{asym.}$  def.  $\approx$  1,450  $\text{cm}^{-1}$

c) Components (44), (45), and (46)Table 5.12

The main peaks present in the mass spectrum of the diamagnetic material postulated to contain compounds (44 - 46)



Mass = 310

Peaks observed

310

293 loss of OH

233

278 loss of O<sub>2</sub>218 loss of N<sub>2</sub>O<sub>4</sub>264 loss of NO<sub>2</sub>202 loss of N<sub>2</sub>O<sub>5</sub>247 loss of NO<sub>2</sub> + OH

CHAPTER 6AN EXAMINATION OF THE MECHANISMS GOVERNINGTHE PRODUCTION OF THE DIAMAGNETIC SPECIESOBSERVED WHEN HUMULENE NITROSITE ISIRRADIATED WITH RED LIGHT

In the initial investigations into the photochemistry of humulene nitrosite described in chapter 2, the major diamagnetic species formed on irradiating humulene nitrosite with red light were isolated. One of the products was characterised as dinitro-humulene (24), the structures of the other species present were not however determined, and the mechanism involved in their formation was not understood. At this point the study of these diamagnetic species was shelved, in favour of pursuing the investigation in the following two areas.

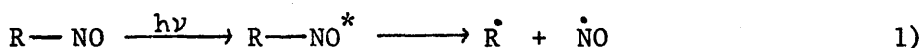
- 1) First the mechanisms governing the production of the paramagnetic species observed, when humulene nitrosite is irradiated with red light were determined. This work is summarised in figures 2.7, 4.4, and 4.6.
- 2) Second the reactions of humulene nitrosite with  $N_2O_3$  were studied and are summarised in figure S.1.

The mechanism by which the paramagnetic species form when humulene nitrosite is irradiated with red light, see figure 2.7, leads to the evolution of  $\dot{N}O$  and  $\dot{N}O_2$ . The possibility therefore existed, that the diamagnetic species observed when humulene nitrosite is irradiated with red light form by the interaction of the oxides of nitrogen with humulene nitrosite in reactions analogous to those shown in figure S.1. Before re-examining these

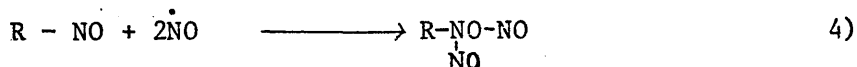
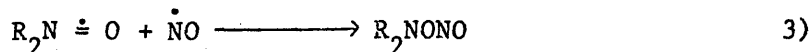


diamagnetic products of the irradiation of humulene nitrosite with red light a detailed examination of the literature available on the photolysis of C-nitroso compounds was undertaken, to determine if any of the reported photolysis mechanisms involved reaction of the nitroso compounds with liberated oxides of nitrogen.

Various studies into the photolysis reactions of C-nitroso compounds have shown that the product distribution is markedly dependent on whether the solvent used was protic, or aprotic.<sup>24-27</sup> The formation of nitroxide radicals does however appear to be general to the photolysis of C-nitroso compounds, being produced as shown below.<sup>24-28</sup>



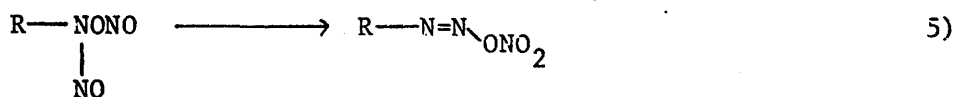
The nitric oxide released during the formation of these radicals, has been shown to further react, both with the unreacted nitroso compound,<sup>24-27,111,112</sup> and with the product nitroxide radicals,<sup>24,25,113,114,115</sup> producing the complexes shown below.



The complexes shown in equations 3) and 4) can react with protic solvents, producing nitrones, oximes, and nitrated solvent molecules.<sup>24,25,27,116</sup> Schemes for the photolysis of gem-substituted aliphatic nitroso compounds  $RR'CXNO$ , where  $X = Cl, Br, NO_2, OAc$  and  $CN$ , in protic solvents such as methanol, have been published by Gowenlock, Kresze, and Pfab.<sup>24-27</sup>

This solvation reaction in protic solvents bears no relevance to the present studies, as both the irradiations of humulene nitrosite with red light, and the reactions of humulene

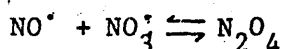
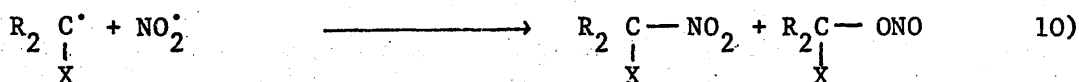
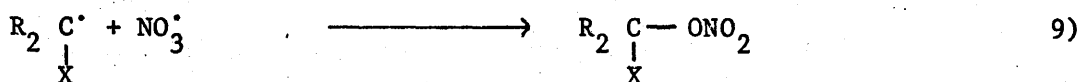
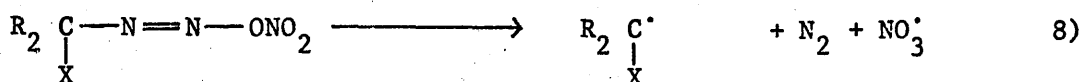
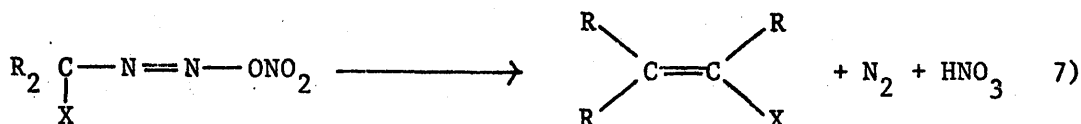
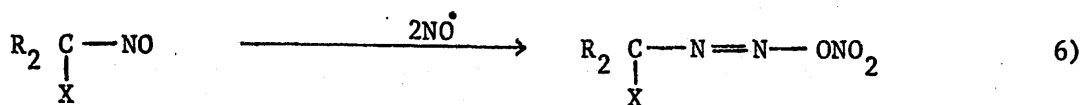
nitrosite with  $N_2O_3$  were performed, either in the solid state, or in the aprotic solvent chloroform, from which all traces of ethanol had been removed. The complex shown in equation 4), can readily rearrange to the diazonium salt as shown below.



This diazonium salt readily decomposes, and many workers have demonstrated the evolution of  $N_2$ , consistent with such a decomposition,<sup>24,25,27,111,112</sup> during the irradiation of nitroso compounds. One observation of direct relevance to the present studies, being that caryophyllene nitrosite, on irradiation with red light, evolves gaseous products, the nitrogen containing components having the composition 86.1%  $N_2$ , and 13.9%  $N_2O_3$ .<sup>76</sup>

This observation of a diazonium nitrate derivative formed on irradiating C-nitroso compounds, is directly analogous to the reaction of humulene nitrosite with  $N_2O_3$ , in the dark, which also involves a diazonium intermediate. No relevant information is available on the product distribution obtained from the photolysis reactions of nitroso compounds in which the nitroso group is attached to a carbon containing no other functional groups, ( $RR'R''CNO$ ,  $R, R', R'' = \text{alkyl}$ ). Studies of the photolysis of 2 nitro-2nitroso-propane, 1 chloro- 1 nitroso-cyclohexane and other geminal - chloro-nitroso-compounds, and finally 1 cyano- 1 nitroso-cyclohexane, by Gowenlock, Kresze, and Pfab,<sup>24-27</sup> have shown that these irradiations do not proceed by the mechanisms reported in earlier studies, which were respectively, photo-oxidation and elimination of  $HNO$ ,<sup>117</sup> by C-Cl bond fission, with the elimination of  $HCl$ , or by C-CN bond fission with elimination of  $HCN$ , but instead, the product distribution is consistent with the reaction scheme shown below.

X = NO<sub>2</sub>, Cl, or CN.



This scheme is analogous to that shown in figure S.1; illustrating the reaction of humulene nitrosite with N<sub>2</sub>O<sub>3</sub>. The irradiation of the compounds  $\text{RR}'\underset{\text{X}}{\text{C}}-\text{NO}$ , also produces diamagnetic products by mechanisms involving the abstraction of the group X,<sup>24,25,27</sup> such products have no particular relevance to the photolysis of humulene nitrosite.

Having observed from the available literature, that C-nitroso compounds can on photolysis react with liberated  $\dot{\text{NO}}$ , the diamagnetic species formed on irradiating humulene nitrosite were re-examined, to determine if a similar mechanism was in operation. In addition to the reactions in the photolysis scheme proposed by Gowenlock, humulene nitrosite when irradiated might produce species by a process of transannular cyclisation, similar to those observed in the products obtained from the reaction of humulene nitrosite with  $\text{N}_2\text{O}_3$  in the dark.

#### 6.1 Characterisation of the diamagnetic species formed on irradiating humulene nitrosite with red light

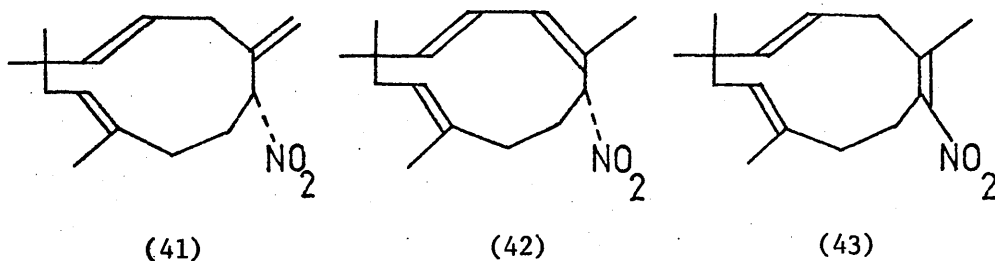
Humulene nitrosite, when crystallised rapidly from ethanol, produces needle shaped crystals, m.pt. =  $118 \pm 1^\circ\text{C}$ . If however, the crystallisation is allowed to proceed very slowly, platelets are also produced. When these different crystal types are irradiated with red light, the paramagnetic species observed are the same in each case, their production being governed by the mechanisms shown in figure 2.7. The diamagnetic species produced on irradiating the different crystal types were however, not the same.

##### 6.1.1 The diamagnetic species observed on irradiating needle shaped crystals of humulene nitrosite with red light

The diamagnetic species formed by irradiating the needle shaped crystals of humulene nitrosite with red light, were isolated using the chromatographic techniques described in chapter 2, section 2.2.2. The species obtained, were the same as those described in chapter 2, namely dinitro-humulene (24), and an oil.

The  $R_f$  value of the oil was 0.8, when chromatographed on silica plates, using ether: pet. ether, (50:50), as solvent. This is the same  $R_f$  value as compounds (41), (42) and (43), isolated from the reaction of humulene nitrosite with  $N_2O_3$ , as described in chapter 5.

Figure 2.18 shows the  $^1H$  n.m.r. and infra-red spectra obtained from this oil. These spectra were previously discussed in appendix 2 section 2'.2'.2'. (d), at which point it was suggested that the oil contained a mixture of isomeric compounds containing a single nitro group attached to either a humulene based structure or to a simple rearrangement of it. The  $^1H$  n.m.r. spectrum shown in figure 2.18, was too complex for a meaningful and complete analysis of all the resonances present. The oil is believed however to be a mixture of the following isomeric structures.



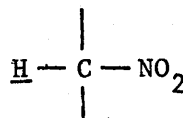
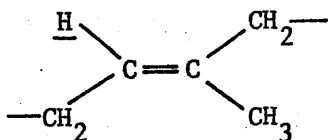
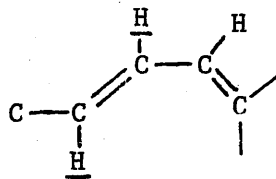
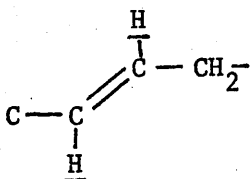
These structures are based on the following observations.

- 1) Comparison of the  $^1H$  n.m.r. spectrum shown in figure 2.18, with the  $^1H$  n.m.r. spectrum of a pure sample of compound (41), obtained from the reaction of humulene nitrosite with  $N_2O_3$  showed clearly that all the resonances associated with compound (41) were present in the spectrum of the oil.
- 2) Comparison of the absorbance of the infra-red nitro absorptions, of the species present in the oil, with those of the standard

humulene and caryophyllene derivatives indicated that one nitro group was present per molecule.

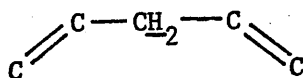
- 3) Those resonances in the  $^1\text{H}$  n.m.r. spectrum of the oil, which were not attributed to compound (41), were examined, and groups of resonances were found, compatible with the following structures, which are present in compounds (42) and (43).

- a) The  $\tau$  region 8.6 to 8.88 contained at least four resonances attributable to gem-dimethyl structures.
- b) The  $\tau$  region 8.2 to 8.4 contained five methyl resonances thought to be allylic methyls.
- c) The  $\tau$  region 3.92 to 5.69 is very complex, but appears to be consistent with the presence of the following structures.

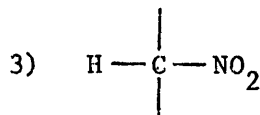
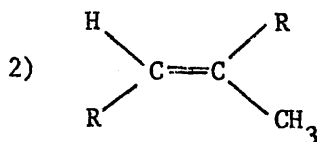
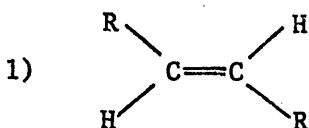


The resonances are so closely spaced that it is not possible to assign them with any degree of certainty, but some assignments, consistent with the structures shown above are detailed in appendix 6, section 6'.1'.

- d) Several groups of resonances overlap in the  $\tau$  region 6.94 to 7.24, and these may be due to structures based on the following unit.



- 4) The infra-red spectrum of the oil shows a widening of the absorptions associated with the following groups.



Absorptions are also present at  $1,520 \text{ cm}^{-1}$  and  $1,330 \text{ cm}^{-1}$  and have been assigned to the asymmetric, and symmetric absorptions of a conjugated nitro species. The pertinent data obtained from the infra-red spectrum of the oil are summarised in table 6.1, appendix 6.

6.1.2 The mechanism involved in the production of the diamagnetic species observed when needle like crystals of humulene nitrosite are irradiated with red light

Figure 6.1 shows a mechanistic flow chart postulated to explain the formation of the diamagnetic species observed when needle shaped crystals of humulene nitrosite are irradiated with red light. The mechanism is analogous to the schemes proposed by Gowenlock, and co-workers, and involves the photolytic cleavage of the C-N bond of the nitroso group, the NO released attacking humulene nitrosite and forming the diazonium complex (37) which decomposes with the evolution of  $\text{N}_2$ , to the aliphatic radical (18). This aliphatic radical (18) is stabilised in the following three ways.

- 1) First,  $\dot{\text{ONO}}_2$  can abstract a proton from (18) forming compounds (41), (42) or (43) and nitric acid.
- 2) Second,  $\dot{\text{NO}}_2$  can add to (18), producing dinitro-humulene (24).
- 3) In its last mode of behaviour (18) reacts with humulene nitrosite, forming the diastereomeric nitroxide radicals  $\text{I}_\text{A}$ , and  $\text{I}_\text{B}$ , of structure (19).

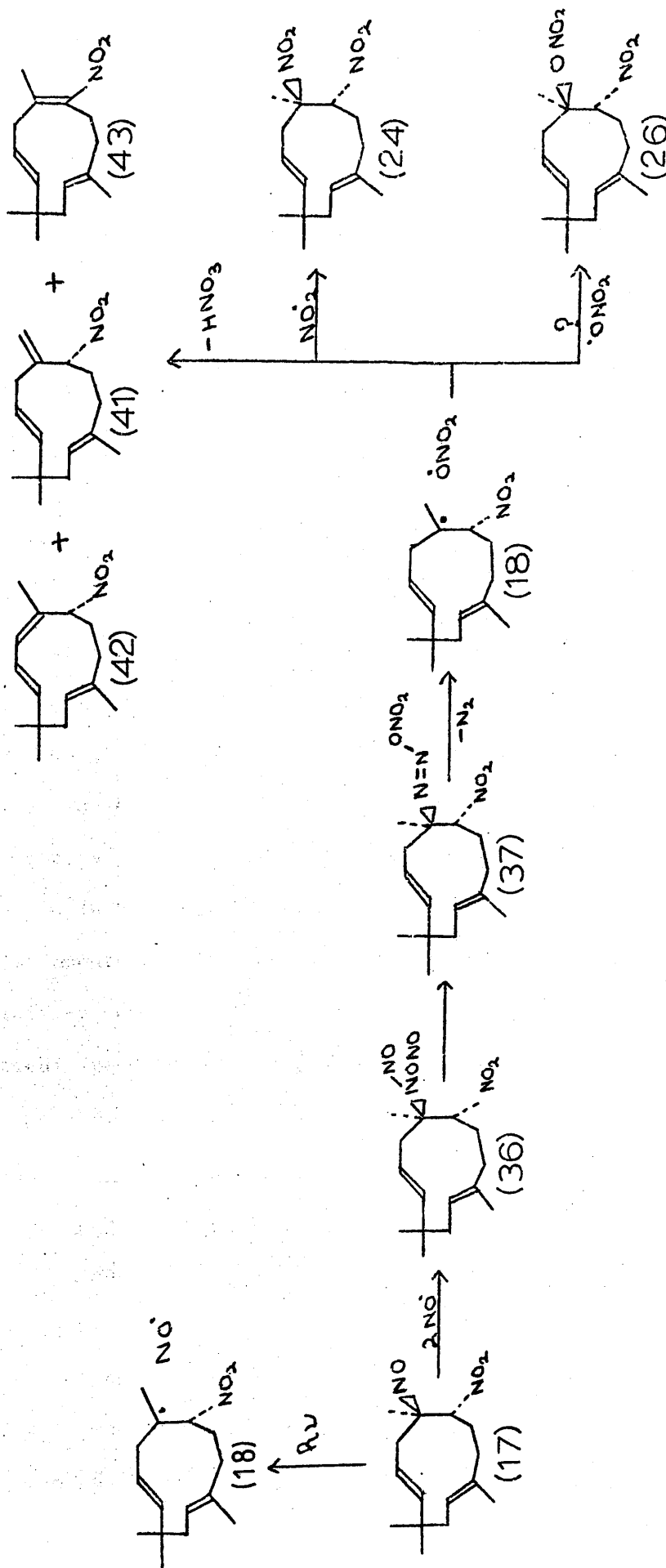


Figure 6.1 The mechanism involved in the production of the diamagnetic species observed when the needle-like crystals of humulene nitrosite are irradiated with red light.



This photolysis scheme is essentially identical to the reactions of humulene nitrosite in an aprotic solvent, with  $\text{N}_2\text{O}_3$  in the dark. In neither case does the  $\dot{\text{O}}\text{NO}_2$  radical directly add to aliphatic radical (18) producing nitro-nitrato-humulene (26), preferring to abstract a proton and form compounds (41), (42), (43) and nitric acid. One significant difference between the two reactions, was that when the needle shaped crystals of humulene nitrosite were irradiated with red light, none of the products observed had formed by a mechanism involving a transannular cyclisation of the ring, of the type postulated to account for compounds (40), (44), (45), and (46), observed when humulene nitrosite was reacted in the dark with  $\text{N}_2\text{O}_3$ , in an aprotic solvent. It is possible that the conformation of the humulene nitrosite molecules within the needle shaped crystals is not suitable for such a transannular cyclisation. Alternatively species may have formed by a process of transannular cyclisation, and then isomerised as shown in figure 6.2 to structures (54), (55), and (56). If small amounts of these species were present in the oil  $R_f = 0.8$ , containing compounds (41), (42), and (43), then it would be very difficult to detect their presence.

#### 6.1.3 The diamagnetic species observed on irradiating platelets of humulene nitrosite with red light

When the products obtained by irradiating platelets of humulene nitrosite with red light, were chromatographed on silica plates, using ether: pet.ether (50:50) as solvent, only a small amount of dinitro-humulene (24) was observed, the main components being an oil of  $R_f = 0.8$ , and three previously unobserved bands of products

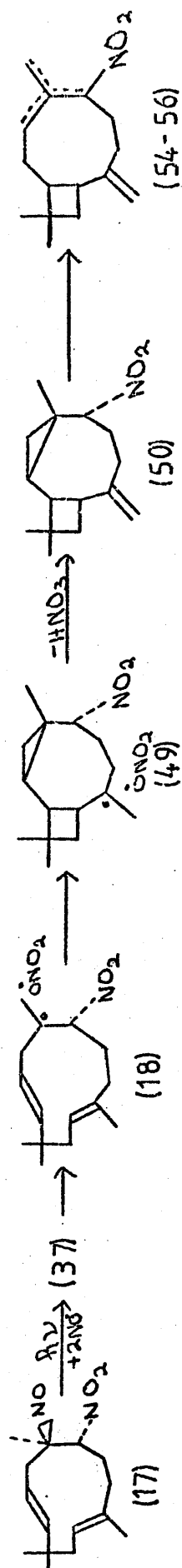


Figure 6.2 Isomerisation of the cyclopropyl ring present in intermediate (50) resulting in the formation of isomers (54-56).

at  $R_f = 0.15, 0.2, \text{ and } 0.3$ . The  $^1\text{H}$  n.m.r. and infra-red spectra obtained from the materials whose  $R_f$  values are 0.15, and 0.2, respectively are shown in figures 6.3 and 6.4. A full analysis of these spectra was not possible because of their complexity, several compounds of a similar type being present in each band. Attempts to further purify these materials and isolate individual species were unsuccessful.

The change in the diamagnetic product distribution when platelets of humulene nitrosite, rather than needle shaped crystals, were irradiated with red light, was felt to be a function of the conformations of the humulene nitrosite molecules within the two crystal systems. If the conformation of the molecules in the platelets is such that transannular cyclisation of the humulene based ring is able to take place then the decrease in the yield of dinitro-humulene (24), and the appearance of new derivatives are explained. The components of  $R_f$  value 0.15, 0.2, 0.3, and 0.8, were therefore examined to determine if the structures present resulted from transannular cyclisation.

Figure 6.5 illustrates the mechanism believed to operate when platelets of humulene nitrosite are irradiated with red light. It incorporates all the processes involved in the irradiation of the needle shaped crystals of humulene nitrosite, see figure 6.1, the aliphatic radical (18), formed by the attack of nitric oxide at humulene nitrosite being stabilised in the three ways previously described. In the platelet crystals, however, this aliphatic radical (18) can undergo a transannular cyclisation producing the aliphatic radical (49). This radical (49) can react further in the following three ways.

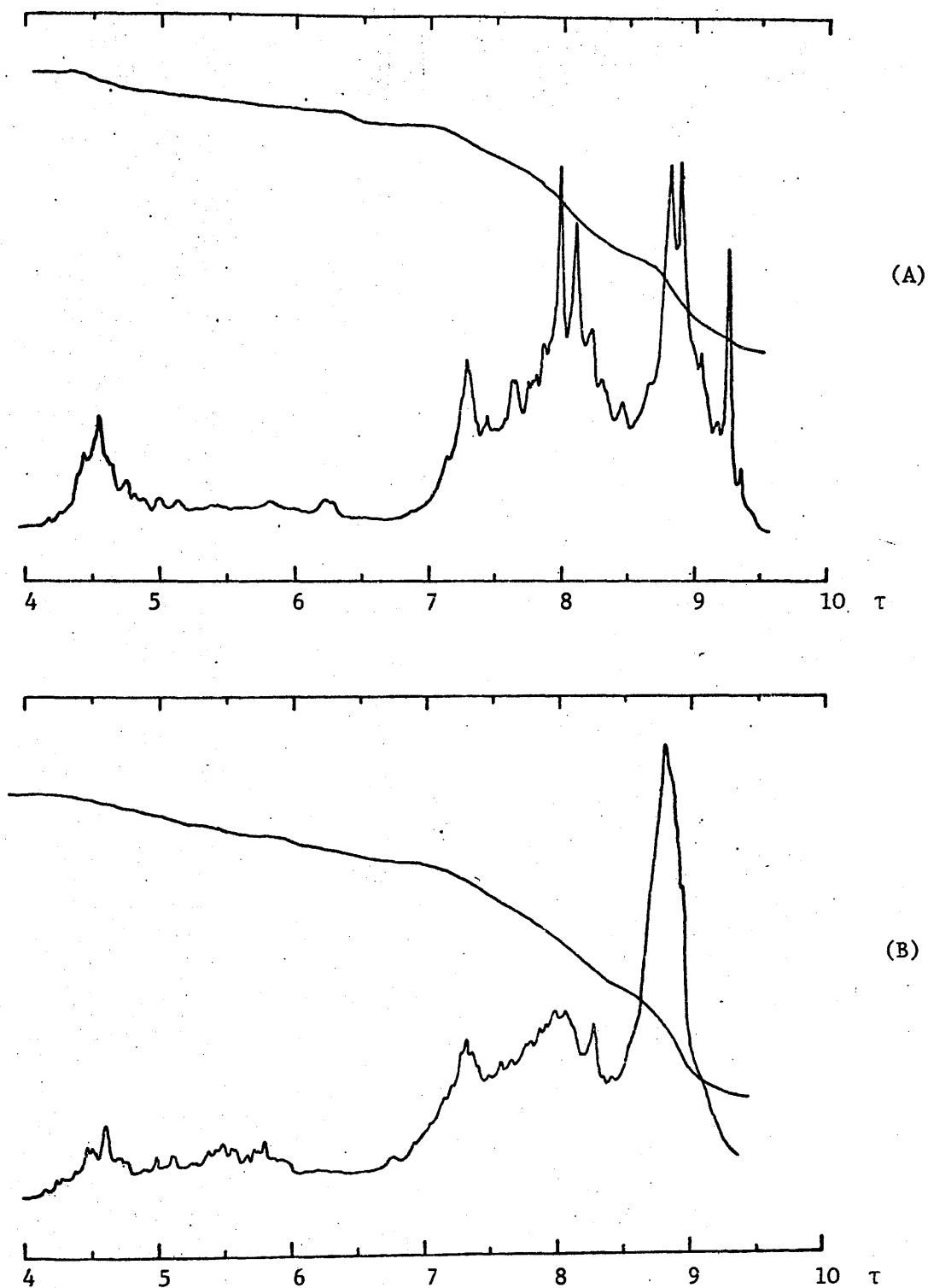


Figure 6.3 The  $^1\text{H}$  n.m.r. spectra recorded in  $\text{CDCl}_3$  solutions in the  $\tau$  range 4 to 10 of (A) the components of  $R_f = 0.15$  and (B) the components of  $R_f = 0.2$  isolated from the product of platelet crystals of humulene nitrosite irradiated with red light.

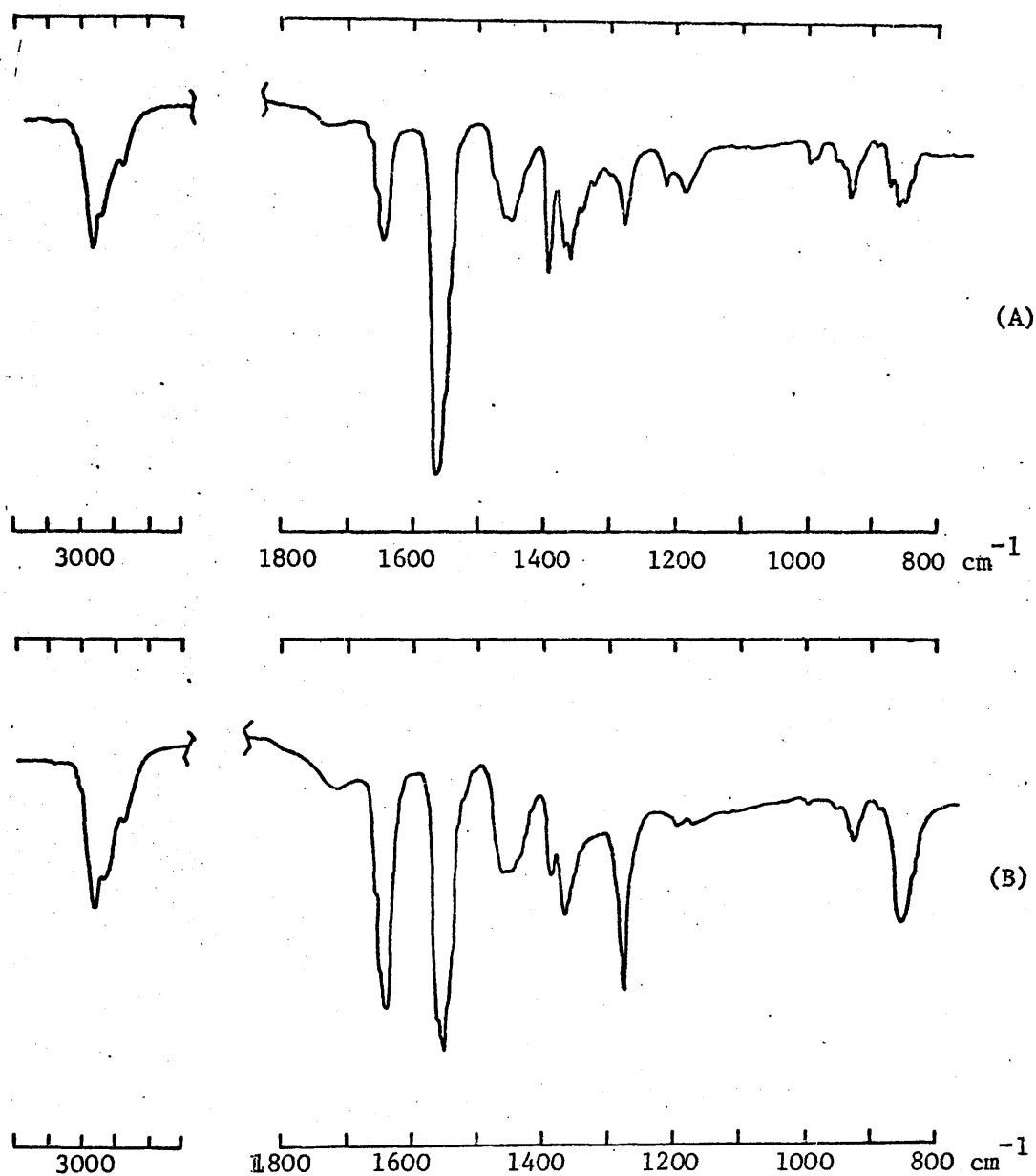


Figure 6.4. The infra-red spectra recorded in KBr discs in the range 3,200-800  $\text{cm}^{-1}$  of (A) the components of  $R_f = 0.15$ , and (B) the components of  $R_f = 0.2$ , isolated from the product of platelet crystals of humulene nitrosite (17) irradiated with red light.

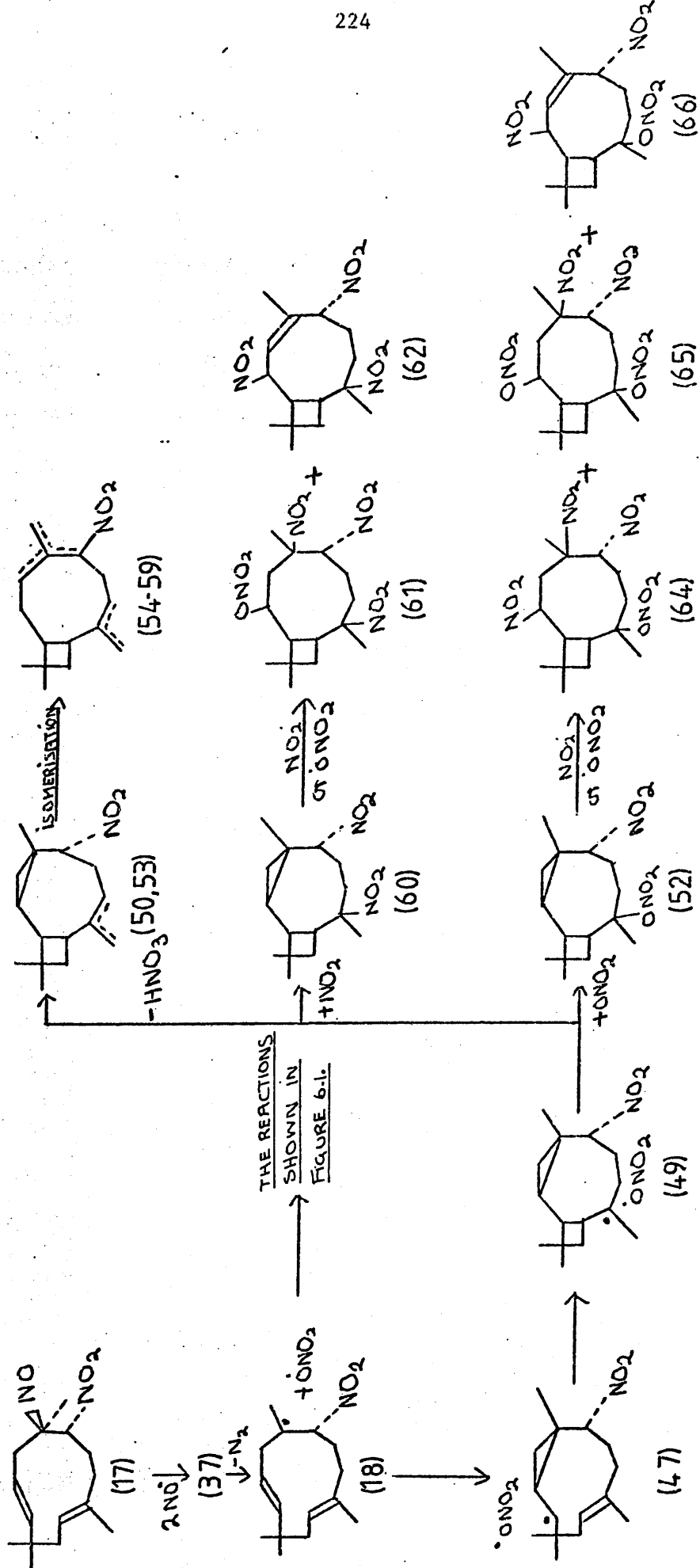


Figure 6.5 The mechanism involved in the production of the diamagnetic species observed when the platelet crystals of humulene nitrosite are irradiated with red light.

- 1) First radical (49), can be stabilised by the addition of  $\dot{\text{O}}\text{NO}_2$  or  $\dot{\text{N}}\text{O}_2$ , forming compounds (52) and (60) respectively.
- 2) Alternatively the  $\dot{\text{O}}\text{NO}_2$  radical can abstract a proton, forming the isomers (50) and (53).
- 3) Finally the cyclisation, by moving the unpaired electron out onto accessible parts of the molecule, may induce further reactions with the  $\pi$  systems of neighbouring molecules.

The products formed by such cyclisations (50), (52), (53), and (60), contain cyclopropyl rings. No species containing cyclopropyl rings have been directly detected. However, several products which appear to have been derived from them have been observed as shown in figure 6.5.

The components of  $R_f = 0.8$

The  $^1\text{H}$  n.m.r. spectrum of the products of  $R_f = 0.8$ , obtained from the photolysis of the platelets, contains all the resonances associated with compounds (41), (42), and (43), which were also observed when the needle crystals were irradiated, and it also contains many more resonances besides. The additional resonances indicate the presence of structures containing exomethylene groups and allylic methyls, and the infra-red spectrum also indicates the presence of these additional structures. The additional species are probably isomers (54-56), and (57-59), formed by an isomerisation of the cyclised, cyclopropyl compounds (50), and (53).

The components of  $R_f = 0.15, 0.2, \text{ and } 0.3$

The compounds (52) and (60), formed by transannular cyclisation, would readily react with  $\dot{\text{N}}\text{O}_2$  or  $\dot{\text{O}}\text{NO}_2$  resulting in the cyclopropyl ring being opened, thereby producing a series of compounds with structures similar to (61-66) as shown in figure 6.5. There are a large number of possible sequences and geometries in which the oxides of nitrogen could add, and numerous species with many similarities in structure would result. The  $^1\text{H}$  n.m.r. and infra-red spectra of the components of  $R_f = 0.15$ , 0.2 and 0.3 are discussed in appendix 6, section 6'.2'. They indicate the presence of cyclopropyl compounds formed by transannular cyclisation, which then react further with the oxides of nitrogen, giving species similar to (61-66). Some of the species present in the band of  $R_f = 0.2$  may not have fully cyclised, and are derived from the reaction of compounds similar to (48) with the oxides of nitrogen. In the reaction of chloroform solutions of humulene nitrosite with  $\text{N}_2\text{O}_3$ , described in chapter 5, species (44-46) were observed. These can also be derived from the partially cyclised product (48).

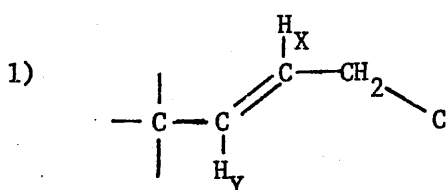
A complete flow chart outlining the photolysis reactions of humulene nitrosite is illustrated in figure S.2 of the summary. The summary also includes a concise account of the mechanisms governing the photolysis reactions of humulene nitrosite and its reactions with the oxides of nitrogen.



## APPENDIX 6

6'.1' Interpretation of the spectroscopic data for the components of  $R_f = 0.8$ , obtained by irradiating the needle - like crystals of humulene nitrosite with red light

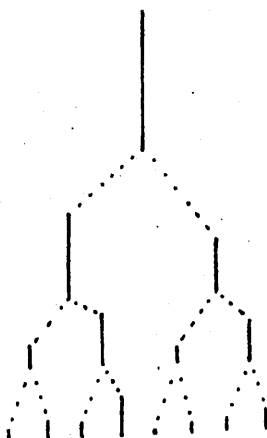
Figure 2.18 shows the  $^1\text{H}$  n.m.r. and infra-red spectra of the components of  $R_f = 0.8$ , obtained by irradiating the needle - shaped crystals of humulene nitrosite with red light, and these were discussed in chapter 6, section 6.1.1. All the resonances associated with compound (41) are present in the  $^1\text{H}$  n.m.r. spectrum. The assignment of the remaining resonances in the  $\tau$  region 3.92 to 5.69, are discussed below, and they are consistent with many of the functional groups present in compounds (42) and (43).



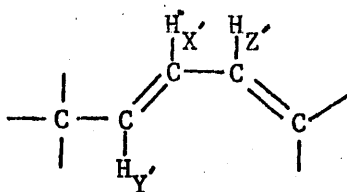
$\text{H}_Y$  doublet  $\tau = 4.74$ ,  $J_{XY} = 16\text{Hz}$ . The weighting of the spectrum suggests that  $\text{H}_Y$  is coupling to an upfield  $\text{H}_X$ .

$\text{H}_X$  is the X part of an ABXY system.  $J_{XY} = 16\text{Hz}$ . being the strongest coupling. A multiplet consisting of 8 peaks with the following intensity distribution is observed at  $\tau = 5.40$ ,  $J_{XY} = 16\text{Hz}$ .,

$J_{AX} = 9\text{Hz}$ ,  $J_{BX} = 4\text{Hz}$ .



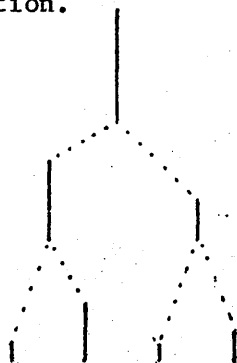
2)



$H_Y'$  doublet  $\tau = 4.67$   $J_{XY'} = 17\text{Hz}$ .

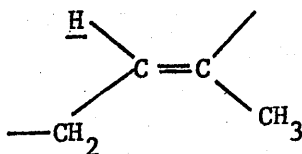
The weighting suggests that  $H_Y'$  couples to an upfield  $H_X'$

$H_X'$  A multiplet is observed at  $\tau = 5.46$ , with the following intensity distribution.

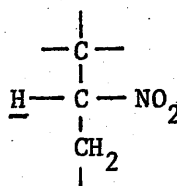


$J_{X'Y'} = 17\text{Hz}$ .  $J_{X'Z'} = 9\text{Hz}$ .

3)



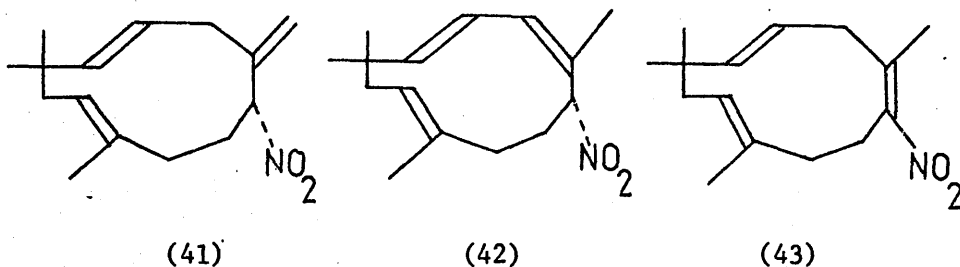
and



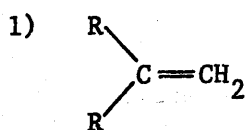
There remains many resonances which can be interpreted as ABX systems and which are consistent with the structures shown above.

Table 6.1

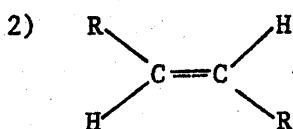
Pertinent data from the infra-red spectrum of the  
components of  $R_f = 0.8$ , obtained by irradiating the  
needle - like crystals of humulene nitrosite with  
red light



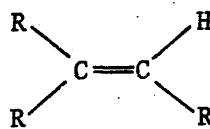
## a) Ethylenic absorptions



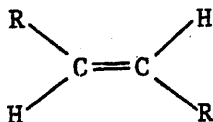
$\nu\text{C-H str.}$	$3,080\text{ cm}^{-1}$
$\nu\text{C=C str.}$	$1,640\text{ cm}^{-1}$
$\nu\text{o.o.p. def.}$	$917\text{ cm}^{-1}$
overtone	$1,835\text{ cm}^{-1}$



and

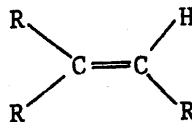


$\nu\text{C-H str.}$	$(3,005 - 3,020)\text{ cm}^{-1}$	$\nu\text{C=C str.}$	$(1,650 - 1,665)\text{ cm}^{-1}$
several absorptions present		several absorptions present	



$\nu\text{o.o.p. def.}$   $(975 - 980)\text{ cm}^{-1}$

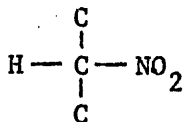
wide absorption



$\nu\text{o.o.p. def.}$   $(835 - 845)\text{ cm}^{-1}$

several absorptions are present

b)

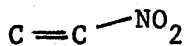
 $\nu\text{NO}_2$  asym. 1,540  $\text{cm}^{-1}$ 1,550  $\text{cm}^{-1}$  $\nu\text{NO}_2$  sym. 1,360  $\text{cm}^{-1}$ 

broad absorption.

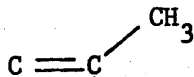
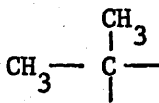
 $\nu\text{C-N}$  bend  $\sim$  865  $\text{cm}^{-1}$ 

broad series of absorptions.

c)

 $\nu\text{NO}_2$  asym. 1,520  $\text{cm}^{-1}$  $\nu\text{NO}_2$  sym. 1,330  $\text{cm}^{-1}$ 

d) All the absorptions associated with the following structures show duplications.

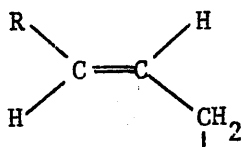


6'2' Interpretation of the spectroscopic data for the fractions of  $R_f = 0.15$ ,  $0.2$ , and  $0.3$ , obtained by irradiating platelets of humulene nitrosite with red light

The component of  $R_f = 0.15$

Figures 6.3 and 6.4 show the  $^1\text{H}$  n.m.r. and infra-red spectra of the material of  $R_f = 0.15$ . Several species are present and the spectra could not be completely analysed, however based on the observations listed below, it is proposed that either structures (61-64) or similar compounds are present.

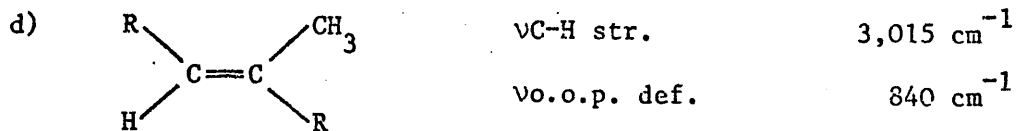
- 1) The  $^1\text{H}$  n.m.r. and infra-red spectra show no evidence of a nitroso group, or a trans double bond of structure



- 2) Absorptions consistent with the following structural units are present in the infra-red spectrum.

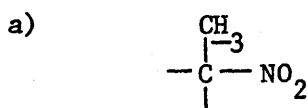
a)	$\begin{array}{c} \text{C} \\   \\ \text{C} - \text{C} - \text{NO}_2 \\   \\ \text{C} \end{array}$	$\nu\text{NO}_2$ asym.	$1,550 \text{ cm}^{-1}$
			$1,545 \text{ cm}^{-1}$
		$\nu\text{NO}_2$ sym.	$1,347 \text{ cm}^{-1}$
b)	$\begin{array}{c} \text{C} \\   \\ \text{H} - \text{C} - \text{NO}_2 \\   \\ \text{C} \end{array}$	$\nu\text{NO}_2$ asym.	$1,565 \text{ cm}^{-1}$
		$\nu\text{NO}_2$ sym.	$1,370 \text{ cm}^{-1}$
c)	$\text{R-ONO}_2$	$\nu$ asym. $\text{NO}_2$	$1,645 \text{ cm}^{-1}$
		$\nu$ sym. $\text{NO}_2$	$1,280 \text{ cm}^{-1}$
		$\nu\text{N=O}$ str.	$855 \text{ cm}^{-1}$

These absorptions show considerable splitting.



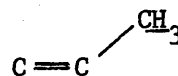
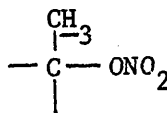
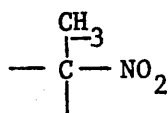
A comparison of the absorbance of the nitrate and nitro groups of the components of  $R_f = 0.15$ , with those of the standard humulene and caryophyllene derivatives, indicated, that 0.9 nitrate groups, and 2.7 nitro groups were on average present per molecule.

- 3) The <sup>1</sup>H n.m.r spectrum contains resonances consistent with the presence of the following structural units.

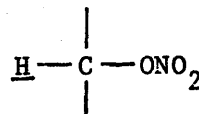
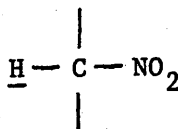
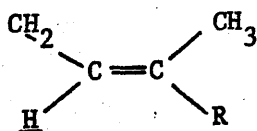


Two strong single resonances are observed at  $\tau = 7.97$  and  $\tau = 8.1$

- b) The  $\tau$  region 7.8 to 8.5 contains a broad series of resonances, compatible with the following structures.

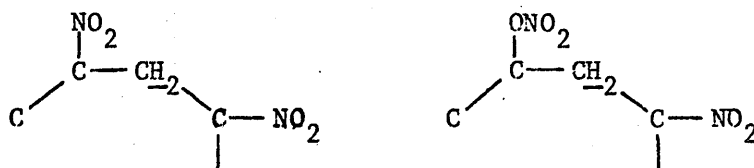


- c) The ethylenic region of the spectrum in the  $\tau$  region 4.2 to 5.7, integrates as 2.4 protons. The resonances are not well enough defined to be analysed, but are not inconsistent with the presence of the following structures.

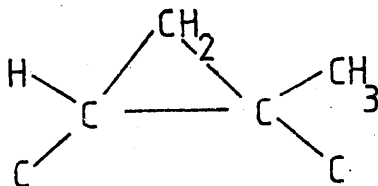


Humulene nitrosite contains four protons in this region and it should be noted, that the direct addition of the oxides of nitrogen over the double bonds, would produce structures still containing four protons in the ethylenic region. Thus the detection of only 2.4 protons indicates a cyclisation of the product molecules.

- d) A group of resonances are present in the  $\tau$  region 7.05 to 7.40, which could arise from the following types of structural units.



- e) Resonances are present in the  $\tau$  region 9.0 to 9.3. They do not appear to be consistent with the presence of the cyclopropyl structure shown below.



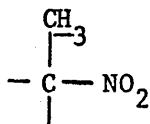
These resonances may arise as a result of an unusual shielding effect, due to the ring currents in the various nitro and nitrate groups.

The component of  $R_{f.} = 0.2$

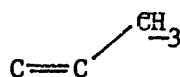
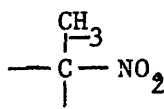
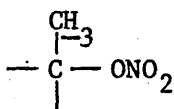
The  $^1\text{H}$  n.m.r. and infra-red spectra of the material of  $R_{f.} = 0.2$  are shown in figures 6.3 and 6.4 respectively. These spectra are similar to those obtained from the components of  $R_{f.} = 0.15$ ,

differing only on the following points.

- 1) The absorbances of the infra-red absorptions of the nitro and nitrate groups, indicate that more nitrate groupings are present, approximately 1.6 -  $\text{ONO}_2$  groups, and 1.8  $\text{NO}_2$  groups being present for each molecule.
- 2) No sharp methyl resonances were observed for the structure



however the  $\tau$  region 7.8 to 8.5, contains a broad series of resonances consistent with the presence of the following structures.



- 3) There are not as many resonances at  $\tau > 9.0$ .
- 4) There are more than three protons present in the ethylenic region of the  $^1\text{H}$  n.m.r. spectrum.

The structures present in the band of  $R_{f.} = 0.2$  are similar to those present in the band of  $R_{f.} = 0.15$  but contain relatively more nitrate groupings. Some of the species present may be based on structures (65) and (66), however the presence of more than three protons in the ethylenic region of the  $^1\text{H}$  n.m.r. suggests that some of the species present may only have partially cyclised. These latter species may be derived from compounds similar to (48) which have reacted further with  $\dot{\text{ONO}}_2$  and  $\dot{\text{NO}}_2$  removing the cyclopropyl ring.

The component of  $R_{f.} = 0.3$

Insufficient material was extracted from the band of  $R_{f.} = 0.3$  to obtain a meaningful  $^1\text{H}$  n.m.r. spectrum, however the



infra-red spectrum was recorded. As in the two previous bands the compounds present contain nitro and nitrate groups, and have lost the trans double bond and nitroso group which were present in humulene nitrosite.

APPENDIX 7ELECTRON PARAMAGNETIC RESONANCE SPECTROSCOPY7'.1' INTRODUCTION

Charged particles which possess angular momentum generate an associated magnetic dipole moment. One of the fundamental postulates of quantum theory is that electrons and nucleons can possess angular momentum only in integral multiples of a basic unit. The angular momentum of an electron originates in its intrinsic spin,  $\underline{S}$  for which  $= \frac{1}{2}$  and in its orbital motion,  $\underline{L}$  for which  $l$  takes integral values. The spin and orbital angular momenta, may be coupled by way of the magnetic moment associated with each, giving a total angular momentum,  $\underline{J}$  where  $j = l + s$ . Similarly the angular momentum  $\underline{I}$  associated with a nucleus, arises from a combination of the angular momenta of its constituent nucleons.

Eigenvalues can be obtained for the square of the angular momentum, and for its component along one axis, which is usually chosen as the  $Z$  axis. For a particle whose angular momentum is  $G$ , these eigenvalues are

$$\underline{G}^2 = G(G + 1)\hbar^2 \quad 7.1$$

and

$$G_z = m_G \hbar \quad 7.2$$

respectively, where  $m_G = G, G - 1, \dots, -G$ .

The magnetic moment  $\mu$  for an electron in an isolated atom is related to the angular momentum by the expression

$$\mu = - \gamma_e \frac{G}{c} \quad \text{where } \gamma_e \text{ is} \quad 7.3$$

the magnetogyric ratio of the electron, and is defined by

$$\gamma_e = \frac{g_e e}{2 mc} \quad 7.4$$

In expression 7.4  $e$  and  $m$  are respectively the charge and mass of the electron,  $c$  is the velocity of light, and  $g_e$  is the electronic  $g$  factor, which equals 1 and 2.00232 for the orbital and spin angular momenta respectively.

Electron paramagnetic resonance spectroscopy is a valuable tool in examining systems which contain an unpaired electron, since the interaction of the magnetic moment of the unpaired electron, with the magnetic fields generated by its surroundings yields the following two important pieces of information.

- 1) First the distribution of the neighbouring magnetic nuclei relative to the unpaired electrons is obtained.
- 2) Second the relative proportions of spin and orbital angular momenta displayed by the unpaired electron give an indication of which orbital it occupies.

In the following sections the interaction of the magnetic moment of an electron with a magnetic field is considered, and in particular a method of transforming the Hamiltonian for this interaction into a Hamiltonian containing only spin operators is discussed. Throughout, the major emphasis will be on systems in which one unpaired electron interacts with one magnetic nucleus in the molecule.

#### 7'.2' The Zeeman interaction

The energy involved in the interaction of the magnetic moment of the unpaired electron with a magnetic field  $H$  can be

represented by the following Hamiltonian,

$$\begin{aligned}\mathcal{H} &= - \underline{\mu} \cdot \underline{H} \\ &= - \mu_z H\end{aligned}\tag{7.5}$$

where the field  $\underline{H}$  lies along the  $z$  axis direction. Kramers theorem states, that in a molecule with one unpaired electron, the ground state is a spin doublet, in the absence of an applied magnetic field. If the effects of spin-orbit coupling are ignored, these ground state wavefunctions can be represented by the real wavefunctions  $\phi_0\alpha$  and  $\phi_0\beta$  with no orbital contribution to the magnetic moment. Under such conditions, the Hamiltonian shown in 7.5 would become

$$\mathcal{H} = g_e \beta_e S_z H\tag{7.6}$$

where  $\beta_e$ , the electronic Bohr magneton, is a constant equal to  $e\hbar (2mc)^{-1}$ , and  $S_z$  is the spin operator, which defines the  $z$ -axis component of the electron angular momentum. Hamiltonian 7.6. has two eigenvalues,  $-\frac{1}{2} g_e \beta_e H$ , and  $+\frac{1}{2} g_e \beta_e H$  corresponding respectively to  $S_z$  of  $-\frac{1}{2}$  and  $+\frac{1}{2}$ .

In the presence of spin-orbit coupling, a small amount of orbital paramagnetism can be reinstated, the perturbation of the ground state wavefunctions,  $\phi_0\alpha$ , and  $\phi_0\beta$ , by spin-orbit coupling mixing in the excited states  $\phi_n\alpha$ , and  $\phi_n\beta$ . The interaction of the magnetic moment of the unpaired electron with the field  $\underline{H}$  now involves both spin and orbital angular momentum operators, and is given by,

$$\begin{aligned}\mathcal{H}_z &= \beta_e \underline{H} \cdot (g_e \underline{S} + \underline{L}) \\ &= \beta_e H_z (g_e S_z + L_z) + \beta_e H_y (g_e S_y + L_y) + \beta_e H_x (g_e S_x + L_x)\end{aligned}\tag{7.7}$$

The data which can be obtained from e.p.r. spectra, can be presented in a more convenient form if 7.7, is replaced by a

Hamiltonian involving spin and not orbital operators. This artificial concept of a spin-Hamiltonian can be developed as follows:

### 7'.3' The spin-Hamiltonian

The Hamiltonian which defines spin-orbit coupling can be represented as,

$$\begin{aligned} \mathcal{H}_{LS} &= \xi \underline{L} \cdot \underline{S} = \xi (L_z S_z + L_x S_x + L_y S_y) \\ &= \xi \left[ L_z S_z + \frac{1}{2} (L_+ S_- + L_- S_+) \right] \end{aligned} \quad 7.8$$

where  $\xi$  is the spin-orbit coupling constant. The perturbation of the ground state wavefunctions  $\phi_o^\alpha$  and  $\phi_o^\beta$  which involves this spin-orbit Hamiltonian, forms new ground state wavefunctions, which can be found from first order perturbation theory to be,

$$\begin{aligned} |+\rangle &= |\phi_o^\alpha\rangle - \frac{1}{2} \xi \sum_n \frac{\langle \phi_n | L_z | \phi_o \rangle}{E_n - E_o} |\phi_n^\alpha\rangle \\ &\quad - \frac{1}{2} \xi \sum_n \frac{\langle \phi_n | L_x + i L_y | \phi_o \rangle}{E_n - E_o} |\phi_n^\beta\rangle \\ |-\rangle &= |\phi_o^\beta\rangle + \frac{1}{2} \xi \sum_n \frac{\langle \phi_n | L_z | \phi_o \rangle}{E_n - E_o} |\phi_n^\beta\rangle \\ &\quad - \frac{1}{2} \xi \sum_n \frac{\langle \phi_n | L_x - i L_y | \phi_o \rangle}{E_n - E_o} |\phi_n^\alpha\rangle \end{aligned} \quad 7.9$$

These new basis wavefunctions  $|+\rangle$  and  $|-\rangle$  are still degenerate. A magnetic field however, resolves this degeneracy,

and the interaction of the magnetic moment of the unpaired electron with the field, can be described by the Zeeman Hamiltonian 7.7. The matrix elements obtained by the operation of 7.7 on the basis wavefunctions  $| + \rangle$  and  $| - \rangle$  are as follows,

$$\begin{aligned}
 \langle + | \mathcal{H}_z | + \rangle &= \beta_e \left[ \langle + | g_e S_z + L_z | + \rangle H_z + \langle + | g_e S_y + L_y | + \rangle H_y \right. \\
 &\quad \left. + \langle + | g_e S_x + L_x | + \rangle H_x \right] \\
 \langle + | \mathcal{H}_z | - \rangle &= \beta_e \left[ \langle + | g_e S_z + L_z | - \rangle H_z + \langle + | g_e S_y + L_y | - \rangle H_y \right. \\
 &\quad \left. + \langle + | g_e S_x + L_x | - \rangle H_x \right] \\
 \langle - | \mathcal{H}_z | + \rangle &= \beta_e \left[ \langle - | g_e S_z + L_z | + \rangle H_z + \langle - | g_e S_y + L_y | + \rangle H_y \right. \\
 &\quad \left. + \langle - | g_e S_x + L_x | + \rangle H_x \right] \\
 \langle - | \mathcal{H}_z | - \rangle &= \beta_e \left[ \langle - | g_e S_z + L_z | - \rangle H_z + \langle - | g_e S_y + L_y | - \rangle H_y \right. \\
 &\quad \left. + \langle - | g_e S_x + L_x | - \rangle H_x \right]
 \end{aligned} \tag{7.10}$$

An evaluation and comparison of these matrix elements, which takes into account the Hermitian properties of angular momentum operators, shows that the following relationships hold,

$$\begin{aligned}
 \langle + | g_e S_j + L_j | + \rangle &= - \langle - | g_e S_j + L_j | - \rangle \\
 \langle + | g_e S_j + L_j | - \rangle &= \langle - | g_e S_j + L_j | + \rangle^*
 \end{aligned} \tag{7.11}$$

The following substitutions are now made,

$$\begin{aligned}
 \langle + | g_e S_j + L_j | + \rangle &= - \langle - | g_e S_j + L_j | - \rangle = \frac{1}{2} g_{jz} \\
 \langle + | g_e S_j + L_j | - \rangle &= \langle - | g_e S_j + L_j | + \rangle^* = \frac{1}{2} (g_{jx} + i g_{jy})
 \end{aligned}
 \tag{7.12}$$

These substitutions comply with the requirement that diagonal matrix elements represent the expectation values of real variables, and so must be real, whereas the off-diagonal matrix elements may be imaginary.

The matrix elements of the Hamiltonian now become,

$$\begin{aligned}
 \langle + | \mathcal{H}_z | + \rangle &= \frac{1}{2} g_{zz} \beta_e H_z + \frac{1}{2} g_{yz} \beta_e H_y + \frac{1}{2} g_{xz} \beta_e H_x \\
 \langle + | \mathcal{H}_z | - \rangle &= \frac{1}{2} (g_{zx} - i g_{zy}) \beta_e H_z + \frac{1}{2} (g_{yx} - i g_{yy}) \beta_e H_y \\
 &\quad + \frac{1}{2} (g_{xx} - i g_{xy}) \beta_e H_x \\
 \langle - | \mathcal{H}_z | + \rangle &= \frac{1}{2} (g_{zx} + i g_{zy}) \beta_e H_z + \frac{1}{2} (g_{yx} + i g_{yy}) \beta_e H_y \\
 &\quad + \frac{1}{2} (g_{xx} + i g_{xy}) \beta_e H_x \\
 \langle - | \mathcal{H}_z | - \rangle &= - \frac{1}{2} g_{zz} \beta_e H_z - \frac{1}{2} g_{yz} \beta_e H_y - \frac{1}{2} g_{xz} \beta_e H_x
 \end{aligned}
 \tag{7.13}$$

As a result of the above substitutions the matrix elements assume a form which is the same as those which would be obtained by defining a fictitious spin operator  $S$ , which would act on the states  $| + \rangle$  and  $| - \rangle$  in the same way in which the true spin operator acts on the  $\alpha$ , and  $\beta$  states, and by using a Hamiltonian of the form,

$$\mathcal{H} = \beta_e \underline{H} \cdot g \cdot \underline{S}
 \tag{7.14}$$

where  $g$  is a second rank tensor.

An expression for the Zeeman energy of the system can thus be obtained by considering the starting states to be pure spin states, and by using a Hamiltonian containing only spin operators, which is known as the spin Hamiltonian. Using this spin Hamiltonian, the orbital contribution to paramagnetism is incorporated into the g-tensor, and is reflected in the deviation of its values from the spin-only value. By comparing the elements of the spin Hamiltonian with those of the true Hamiltonian it can be shown that in general,

$$g_{ij} = g_e \delta_{ij} - 2 \xi \sum_n \frac{\langle \phi_0 | L_i | \phi_n \rangle \langle \phi_n | L_j | \phi_0 \rangle}{E_n - E_0} \quad 7.15$$

and it follows from the Hermitian properties of the angular momentum operators, that the g-tensor is symmetric.

#### 7'.4' The hyperfine interaction

The magnetic moment associated with an unpaired electron, interacts with the magnetic field generated by the magnetic moment of any nucleus in the vicinity. There are three quite distinct contributions to this interaction.

The first of these contributions arises from the presence of unpaired electron spin density at the magnetic nucleus, in cases where the wave function of the unpaired electron has a finite value at the nucleus, or where the unpaired electron can effect a polarisation of the paired S electrons about the nucleus. This is the so-called Fermi contact interaction, which is isotropic, and may be represented by a Hamiltonian of the form,

$$\mathcal{H} = \frac{8\pi}{3} g_e g_N \beta_e \beta_N \delta(r_N) \underline{I} \cdot \underline{S} \quad 7.16$$



where  $\delta(r_N)$  is the Dirac delta function which, integrated over the electronic wavefunction, gives the square of the value of the wavefunction at the nucleus.

The second contribution to the hyperfine interaction is a direct dipolar coupling between the spin magnetic moments of the electron and the nucleus. This is essentially the classical interaction of two dipoles  $\underline{\mu}_e$  and  $\underline{\mu}_N$  separated by a distance  $\underline{r}$ . This spin-dipolar interaction is anisotropic and can be represented by the following Hamiltonian,

$$\mathcal{H}_{SI} = -g_e g_N \beta_e \beta_N \left[ r^2 \underline{S} \cdot \underline{I} - 3 (\underline{S} \cdot \underline{r}) (\underline{r} \cdot \underline{I}) \right] r^{-5} \quad 7.17$$

$\mathcal{H}_{SI}$  can be usefully rewritten as,

$$\mathcal{H}_{SI} = g_e \beta_e g_N \beta_N \left\langle \frac{1 - 3 \cos^2 \theta}{r^3} \right\rangle_{av.} \underline{I} \cdot \underline{S} \quad 7.18$$

where  $\theta$  is the angle between the vector  $\underline{r}$ , which connects the dipoles, and the magnetic field direction. The orientation dependent term  $(1 - 3 \cos^2 \theta) r^{-3}$  includes a spatial average over the orbital occupied by the unpaired electron.

The final contribution to hyperfine coupling is also anisotropic, arising from the interaction between the nuclear magnetic moment, and the electronic orbital magnetic moment, and is represented by the Hamiltonian

$$\mathcal{H}_{LI} = 2g_N \beta_e \beta_N r^{-3} \underline{L} \cdot \underline{I} \quad 7.19$$

As the hyperfine Hamiltonian contains nuclear spin

operators, the basis wavefunctions now take the form  $|+, M_I\rangle$  and  $|- , M_I\rangle$ . Matrix elements can be obtained for the operation of the complete hyperfine Hamiltonian, which consists of 7.16, 7.17, and 7.19, on the basis wavefunctions  $|+, M_I\rangle$  and  $|- , M_I\rangle$ . These matrix elements, by the use of algebraic manipulations and substitutions similar to those shown in 7.12, can be made to assume a form identical to the matrix elements which would be obtained if a fictitious spin operator  $S$  was allowed to operate on  $|+, M_I\rangle$  and  $|- , M_I\rangle$ , in the same way as the true spin operator acts on  $|\alpha, M_I\rangle$  and  $|\beta, M_I\rangle$ , and using a spin Hamiltonian of the form,

$$\mathcal{H}_{SI} = \underline{S} \cdot \underline{A} \cdot \underline{I} \quad 7.20$$

where  $A$  is a second rank tensor. Thus the energy of the system including both Zeeman and hyperfine interactions, can be expressed in the form,

$$\mathcal{H} = \beta_e \underline{H} \cdot \underline{g} \cdot \underline{S} + \underline{S} \cdot \underline{A} \cdot \underline{I} \quad 7.21$$

#### 7'.5' The quadrupolar interaction

Nuclei with  $I \geq 1$  possess an electric quadrupole moment, which can interact with the gradient of the electric field at the nucleus resulting in a mixing of the nuclear spin states. The quadrupole moment does not interact directly with the magnetic moment of the unpaired electron, but it can affect the e.p.r spectrum, producing second order shifts in the energy levels, and making formally forbidden transitions involving  $\Delta m_s = \pm 1$ ,  $\Delta m_I = \pm 2$ , become weakly allowed. This interaction can thus change the positions of the resonance lines, and cause the hyperfine

lines to be unequally spaced, but only if the steady magnetic field does not lie parallel to the symmetry axis of the paramagnetic species.

The quadrupolar interaction can be represented by a spin Hamiltonian of the form,

$$\mathcal{H}_Q = \underline{I} \cdot \underline{P} \cdot \underline{I} \quad 7.22$$

where  $\underline{P}$  is the quadrupolar coupling tensor, whose components are of the form,

$$P_{ij} = \frac{e Q V_{ij}}{2I(2I-1)} \quad 7.23$$

where  $Q$  is called the quadrupole moment of the nucleus, and is defined by,

$$Q = \langle M_I = I | \sum (3z^2 - r^2) | M_I = I \rangle \quad 7.24$$

the summation being taken over the protons in the nucleus, and  $V_{ij}$  represents the  $ij$  th. component of the electric field gradient tensor.

The total spin Hamiltonian for a complex in which one unpaired electron interacts with one nucleus can now be written as,

$$\mathcal{H} = B_e \underline{H} \cdot \underline{S} + \underline{S} \cdot \underline{A} \cdot \underline{I} + \underline{I} \cdot \underline{P} \cdot \underline{I} \quad 7.25$$

#### 7'.6' Solution of the spin Hamiltonian

It is relatively simple to determine the energy levels associated with the interaction of a single unpaired electron with

one magnetic nucleus, if the paramagnetic species are in solution, since the rotation of the system averages out the anisotropic contributions to the various tensors, and the spin Hamiltonian becomes,

$$\mathcal{H} = g_o \beta_e \underline{H} \cdot \underline{S} + A_o \underline{S} \cdot \underline{I} \quad 7.26$$

$$\text{where } g_o = \frac{1}{3} \sum_i g_{ii} \quad \text{and } A_o = \frac{1}{3} \sum_i A_{ii} \quad 7.27$$

The quadrupolar tensor is traceless and there is thus no quadrupolar contribution. The eigenvalues of the Hamiltonian 7.26 are given by the equation.

$$E_{m_s, m_I} = g_o \beta_e m_s H + A_o m_s m_I + \frac{A_o^2 m_s}{2g_o \beta_e H} \left[ I(I+1) - m_I^2 \right] \quad 7.28$$

and the  $2I + 1$  transitions obey the selection rules  $\Delta m_s = \pm 1$ ,  $\Delta m_I = 0$ .

In the solid state the situation is more complex. It is possible, however, to choose a co-ordinate system which diagonalises the g-tensor, and if the principal axes of the A and P tensors coincide then the spin Hamiltonian 7.25 simplifies to,

$$\mathcal{H} = \sum_i (\beta_e g_{ii} H_i S_i + A_{ii} S_i I_i + P_{ii} I_i^2) \quad 7.29$$

If it is assumed that the magnetic field H has direction cosines l, m, and n, with respect to the principal axes of the g-tensor, and that the same set of axes diagonalise the A and P

tensors, then 7.29 can be rewritten as,

$$\mathcal{H} = \beta_e (g_{xx} 1S_x + g_{yy} mS_y + g_{zz} nS_z) H + \sum_i (A_{ii} S_i I_i + P_{ii} I_i^2) \quad 7.30$$

The energy levels and transition energies can now be found by considering the operation of the Zeeman part of the Hamiltonian on the basis wavefunctions  $|\alpha, m_I\rangle$  and  $|\beta, m_I\rangle$ , and then treating the hyperfine and quadrupolar terms as successive perturbations.

The Zeeman component of the Hamiltonian 7.30 can be written,

$$\mathcal{H} = g\beta_e (l'S_x + m'S_y + n'S_z) \quad 7.31$$

where  $gl' = g_{xx}l$ ,  $gm' = g_{yy}m$ , and  $gn' = g_{zz}n$ ,

where  $l'$ ,  $m'$ , and  $n'$ , are normalised and  $l'^2 + m'^2 + n'^2 = 1$ .

The energy matrix can now be diagonalised with respect to the Zeeman term by carrying out the following transformations.

$$S_x = a_{11} S_{x'} + a_{12} S_{y'} + a_{13} S_{z'} \quad 7.32$$

$$S_y = a_{21} S_{x'} + a_{22} S_{y'} + a_{23} S_{z'}$$

$$S_z = a_{31} S_{x'} + a_{32} S_{y'} + a_{33} S_{z'}$$

where  $Z'$  has the direction cosines  $l'$ ,  $m'$ , and  $n'$  with respect to the principal axes. Under such a transformation the Zeeman term becomes,

$$\mathcal{H}_Z = g\beta_e H S_{z'} \quad 7.33$$

and from the properties of the direction cosines,

$$g^2 = g_{xx}^2 l^2 + g_{yy}^2 m^2 + g_{zz}^2 n^2 \quad 7.34$$

If the Z-axis is chosen as the axis of quantisation for the electron spin functions  $\alpha$  and  $\beta$ , then these states are eigenfunctions of the transformed Zeeman, with energies of  $\pm \frac{1}{2} g\beta_e H$ .

The transformed hyperfine term in the Hamiltonian now becomes,

$$\begin{aligned} \mathcal{H}_{SI} = & S_x (a_{11} A_{xx} I_x + a_{21} A_{yy} I_y + a_{31} A_{zz} I_z) \\ & + S_y (a_{12} A_{xx} I_x + a_{22} A_{yy} I_y + a_{32} A_{zz} I_z) \\ & + S_z (a_{13} A_{xx} I_x + a_{23} A_{yy} I_y + a_{33} A_{zz} I_z) \end{aligned} \quad 7.35$$

The hyperfine term can now be treated using non-degenerate perturbation theory, providing it has no off-diagonal matrix elements between states which are degenerate in zero order. The diagonalisation of the energy matrix with respect to the hyperfine term is achieved by a transformation of the same type as that shown in 7.33 and the first order contribution to the perturbation energy is  $A m_s m_I$ , where

$$A^2 = (g_{xx}^2 l^2 A_{xx}^2 + g_{yy}^2 m^2 A_{yy}^2 + g_{zz}^2 n^2 A_{zz}^2) g^{-2} \quad 7.36$$

The remaining hyperfine and quadrupolar terms in the Hamiltonian, can be treated using second order perturbation theory, and the energies of the  $|\alpha, m_I\rangle$ , and  $|\beta, m_I\rangle$  states, and the allowed transitions for which  $\Delta m_s = \pm 1$ ,  $\Delta m_I = 0$ , can be evaluated.

For the special case in which the field lies along a principal axis direction, the transition energies are found to be,

$$\Delta E = g_{ii} \beta_e H + A_{ii} m_I + \frac{(A_{jj}^2 + A_{kk}^2)}{4g_{ii} \beta_e H} \left[ I(I+1) - m_I^2 \right] + \frac{(P_{kk} - P_{jj})^2}{2A_{ii}} \left[ 2I(I+1) - 2m_I^2 - 1 \right] m_I \quad 7.37$$

### '7'.7' Spin relaxation and line shapes

The spin states  $|+\frac{1}{2}\rangle$  and  $|-\frac{1}{2}\rangle$  in the absence of hyperfine coupling, and any external magnetic fields, are degenerate and are equally populated. If a steady field  $H$  is applied to the system, the populations of the two levels are governed at thermal equilibrium by a Boltzmann expression of the form,

$$\frac{N - \frac{1}{2}}{N + \frac{1}{2}} = \exp \left( \frac{\Delta E}{kT} \right) \quad 7.38$$

The microwave frequencies involved in a transition from  $|+\frac{1}{2}\rangle$  to  $|-\frac{1}{2}\rangle$  are such, that the spontaneous emission of radiation can be neglected, indicating that the excess energy is dissipated by non radiative relaxation processes.

The spin Hamiltonian 7.30 would predict infinitely sharp transitions between the allowed energy levels. This is not observed experimentally, and the width of the observed spectral lines, can be accounted for by considering the dynamics of the relaxation processes.

A collection of spins, which are allowed to interact with a magnetic field  $H_0$ , applied along the Z-axis, will at thermal equilibrium have components of the bulk magnetisation  $M$  along the three axis directions, where  $M_z$  is equal to some value  $M_0$  and  $M_x$  and  $M_y$  are both zero. If the system is removed from equilibrium,

it will relax back to the equilibrium values of the components of  $\underline{M}$  at a rate defined by,

$$\frac{dM_z}{dt} = \frac{-(M_z - M_0)}{T_1} \quad 7.39$$

$$\frac{dM_x}{dt} = \frac{-M_x}{T_2}$$

$$\frac{dM_y}{dt} = \frac{-M_y}{T_2}$$

The constant  $T_1$  is called the spin-lattice relaxation time, because for  $M_z$  to relax back to its equilibrium value, the spins have to exchange energy with the lattice, which is here defined to be the medium in which the spins find themselves. The constant  $T_2$  is called the spin-spin relaxation time. The relaxation of  $M_x$  and  $M_y$  does not involve exchange of energy with the lattice, but is concerned with a redistribution of the total energy of the system amongst the various spins.

The applied field  $\underline{H}_0$  exerts a torque on  $\underline{M}$ , causing it to precess about  $\underline{H}_0$  according to the equation,

$$\frac{d\underline{M}}{dt} = \gamma_e (\underline{M} \times \underline{H}_0) \quad 7.40$$

This precessional motion is damped by the relaxation effects, and the dynamics of the system are described by the Bloch equations, obtained by combining 7.39 and 7.40 to yield,



$$\frac{d\mathbf{M}}{dt} = \gamma_e (\mathbf{M} \times \mathbf{H}_0) - \frac{(\mathbf{i} M_x + \mathbf{j} M_y)}{T_2} - \frac{\mathbf{k} (M_z - M_0)}{T_1} \quad 7.41$$

where  $\mathbf{i}$ ,  $\mathbf{j}$ , and  $\mathbf{k}$  are unit vectors directed along the x, y, and z axes.

If a circularly polarised magnetic field  $\mathbf{H}_1$ , rotating in the xy plane with an angular velocity  $\omega$  in the same direction as the Larmor precession, is applied to the system, the Bloch equations become,

$$\frac{d\mathbf{M}}{dt} = \gamma_e (\mathbf{M} \times \mathbf{H}_0) + \gamma_e (\mathbf{M} \times \mathbf{H}_1) - \frac{(\mathbf{i} M_x + \mathbf{j} M_y)}{T_2} - \frac{\mathbf{k} (M_z - M_0)}{T_1} \quad 7.42$$

The operator  $S_z$  can only connect states with  $\Delta m_s = 0$ , whereas  $S_x$  and  $S_y$  can connect only states with  $\Delta m_s = \pm 1$ . Thus if  $\omega$  is made to approach the Larmor precession frequency  $\omega_0$ , a resonance situation arises and transitions are induced according to the selection rule  $\Delta m_s = \pm 1$ .

The equation 7.42 can be solved to yield expressions for the equilibrium values of the components u and v of the magnetisation  $\mathbf{M}$ , which lie parallel to and at right angles to  $\mathbf{H}_1$  in the xy plane, and for  $M_z$ . For a particular transition the v mode reflects the absorption of energy from the field  $\mathbf{H}_1$ , and the rate of work done by  $\mathbf{H}_1$  is given by  $\mathbf{M} \times \mathbf{H}_1 \cdot \omega$  which in this case reduces to  $\omega v H_1$ . If equation 7.42 is solved for v, then it can be shown that the line shape  $g(\omega)$  is given by

$$g(\omega) = \chi_0 \omega_0 \omega H_1^2 \frac{T_2}{1 + T_2^2 (\omega_0 - \omega)^2 + \gamma_e^2 H_1^2 T_1 T_2} \quad 7.43$$

where  $\chi_0$  is the equilibrium value of the magnetic susceptibility and  $M_0 = \chi_0 H_0$ . In cases where  $\chi_e^2 H_1^2 T_1 T_2$  is small, the line is Lorentzian in shape and has the classical normalised form,

$$g(\omega) = \frac{T_2}{\sqrt{\pi}} \frac{1}{1 + T_2^2 (\omega_0 - \omega)^2} \quad 7.44$$

If  $H_1$  or  $T_1$  is large, the term  $\chi_e^2 H_1^2 T_1 T_2$  may become important and the line shape is no longer Lorentzian. This effect is called saturation and results when the system cannot relax fast enough to maintain the population difference between the upper and lower states. Saturation causes an apparent broadening by weakening the centre of the line. The Lorentzian lineshape does not apply in situations where magnetic dipolar interactions define the broadening, and in such circumstances if the distribution of the magnetic dipoles is random with respect to the electron undergoing resonance, then the resultant line shape is Gaussian, having the form,

$$g(\omega) = \frac{T_2}{\sqrt{2\pi}} \exp \left[ -\frac{1}{2} (T_2)^2 (\omega - \omega_0)^2 \right] \quad 7.45$$

### 7'.8' Sources of line broadening

In most cases the line width is governed by  $T_2$ , and the relative importance of the various effects, which may contribute to this, depends on the particular system being studied.

For systems in which the neighbouring paramagnetic species are very close together, the unpaired electron can jump from one molecule to another, resulting in an averaging out of the hyperfine

interactions in the species, and often producing a very broad line. To avoid this, e.p.r. studies are usually carried out in solution, or on crystals of a diamagnetic host into which the paramagnetic species are doped, creating a magnetically dilute system.

In species where there is little orbital contribution to paramagnetism, the main contributions to the line widths are listed below.

- a) The anisotropic contributions to the  $g$  and  $A$ -tensors may not be completely averaged out by the rotation of the species in solution, and the resulting fluctuating magnetic fields cause broadening.
- b) When a molecule rotates in solution, the random motions of its constituent electrons and nuclei generate magnetic fields, the magnitude and direction of which fluctuates with time. The interaction of the magnetic moment of the unpaired electrons with these fields results in broadening.
- c) Some of the hyperfine interactions may not be large enough to cause splitting of the spectral lines, resulting only in a contribution to the line width.

The above effects apply to species containing one unpaired electron and little orbital paramagnetism, and in other systems other types of effect may be dominant.

#### 7'.9' Line shapes of electron paramagnetic resonance spectra of magnetically dilute glasses or polycrystalline samples

A glass or magnetically dilute polycrystalline sample can be treated as a large number of crystallites, which are randomly oriented with respect to an applied magnetic field. Under such

circumstances the experimentally observed e.p.r. spectrum arises from the summation of the spectra from all the different crystallites each one weighted by the probability of the crystallite being in that particular orientation.

The expected line shape can be computed by considering the transition probabilities as a function of orientation, together with the probability of the molecule having a given orientation relative to the magnetic field direction. For certain molecules e.g. the copper chelates, and nitroxides, where the g-tensor values are all close to 2, it is a reasonable approximation to assume that the transition probability is independent of the orientation of the crystallite in the magnetic field, but this is not a valid assumption in general.

Kneubühl has treated the case of a molecule with  $S = \frac{1}{2}$ ,  $I = 0$ . In the general case, where the molecule has orthorhombic symmetry, the principal values of the g-tensor all differ, with  $g_{11} \neq g_{22} \neq g_{33}$  and the Hamiltonian has the form.

$$\mathcal{H} = \beta_e H (g_{11} \cos \theta_1 S_x + g_{22} \cos \theta_2 S_y + g_{33} \cos \theta_3 S_z) \quad 7.46$$

where  $\theta_1$ ,  $\theta_2$ , and  $\theta_3$ , are the angles the field  $\underline{H}$  makes with the principal axes directions, and

$$g = (g_{11}^2 \cos^2 \theta_1 + g_{22}^2 \cos^2 \theta_2 + g_{33}^2 \cos^2 \theta_3)^{\frac{1}{2}} \quad 7.47$$

Only two of these three angles can be independent, and the resonant field thus depends on two orientation angles, and as a result there is a range of combinations of the two orientation angles which lead to resonance at a particular field. If the probability

that the crystallite lies in an orientation such that it gives an absorption in the range of the spectrum from  $H$  to  $H + dH$  is computed, then it can be equated to  $g(H) dH$ , where  $g(H)$  is the normalised line shape function. The lineshape function  $g(H)$  can then be expressed, in terms of the resonant fields  $H_{11}$ ,  $H_{22}$ , and  $H_{33}$  which correspond to the principal values of the  $g$ -tensor,  $g_{11}$ ,  $g_{22}$ , and  $g_{33}$  respectively. Assuming that  $H_{33} > H_{22} > H_{11}$ , then in the interval  $H_{11} \geq H \geq H_{22}$ ,  $g(H)$  is given by

$$g(H) = \frac{2H_{11} H_{22} H_{33}}{\pi H^2 (H_{11}^2 - H_{22}^2)^{1/2} (H^2 - H_{33}^2)^{1/2}} K(\lambda') \quad 7.48$$

and in the interval  $H_{22} \geq H \geq H_{33}$

$$g(H) = \frac{2H_{11} H_{22} H_{33}}{\pi H^2 (H_{22}^2 - H_{33}^2)^{1/2} (H_{11}^2 - H^2)^{1/2}} K(\lambda) \quad 7.49$$

where  $K(\lambda)$  is the standard elliptical integral given by,

$$\begin{aligned} K(\lambda) &= \frac{\pi}{2} \int_0^{\pi/2} \frac{dx}{(1 - \lambda^2 \sin^2 x)^{1/2}} \\ &= \frac{\pi}{2} \left[ 1 + \left(\frac{1}{2}\right)^2 \lambda^2 + \left(\frac{1.3}{2.4}\right) \lambda^4 + \dots \right] \end{aligned} \quad 7.50$$

and

$$(\lambda')^2 = \frac{1}{\lambda^2} = \frac{(H_{11}^2 - H_{22}^2)(H^2 - H_{33}^2)}{(H_{11}^2 - H^2)(H_{22}^2 - H_{33}^2)} \quad 7.51$$

The function of  $g(H)$  has discontinuities at  $H = H_{11}$  and  $H = H_{33}$  and becomes infinite at  $H = H_{22}$ , where  $\lambda$  and  $\lambda'$  both equal one,

and the elliptical integrals expand to infinity.

In the discussion so far, the e.p.r. transitions have been assumed to be infinitely sharp. This has been previously shown not to be the case experimentally. The broadening which occurs is best described if the individual line shapes are assumed to be described by a Gaussian function and the broadened line shape has the form,

$$g(H') = \int_{H=H_{11}}^{H=H_{33}} g(H) Y(H - H') dH \quad 7.52$$

where  $Y(H - H')$  the Gaussian line shape function is given by,

$$Y(H - H') = (2\pi)^{-1/2} \beta^{-1} \exp \left[ - (H - H')^2 (2\beta)^{-2} \right] \quad 7.53$$

and the line width is controlled by the broadening parameter  $\beta$ . The functions  $g(H)$ ,  $g(H')$  and the first derivative of  $g(H')$  are plotted in figure 7.1.

The  $g$ - tensor components can be readily obtained from the first derivative polycrystalline spectrum by measuring  $H_{11}$ , and  $H_{22}$  and  $H_{33}$ . If the electron interacts with a nucleus of spin quantum number  $I$ , then the observed spectrum can be interpreted as a superposition of  $2I + 1$  curves of the type shown in figure 7.1. Figure 7.2 illustrates the broadened first derivative curve for a molecule with  $S = \frac{1}{2}$ ,  $I = \frac{1}{2}$ , and in such cases if the peaks are well resolved, the principal components of the hyperfine tensor can be obtained. Unfortunately the orientation of the principal axes of the  $g$  and  $A$ -tensors with respect to the experimental axes, cannot be determined using this technique.

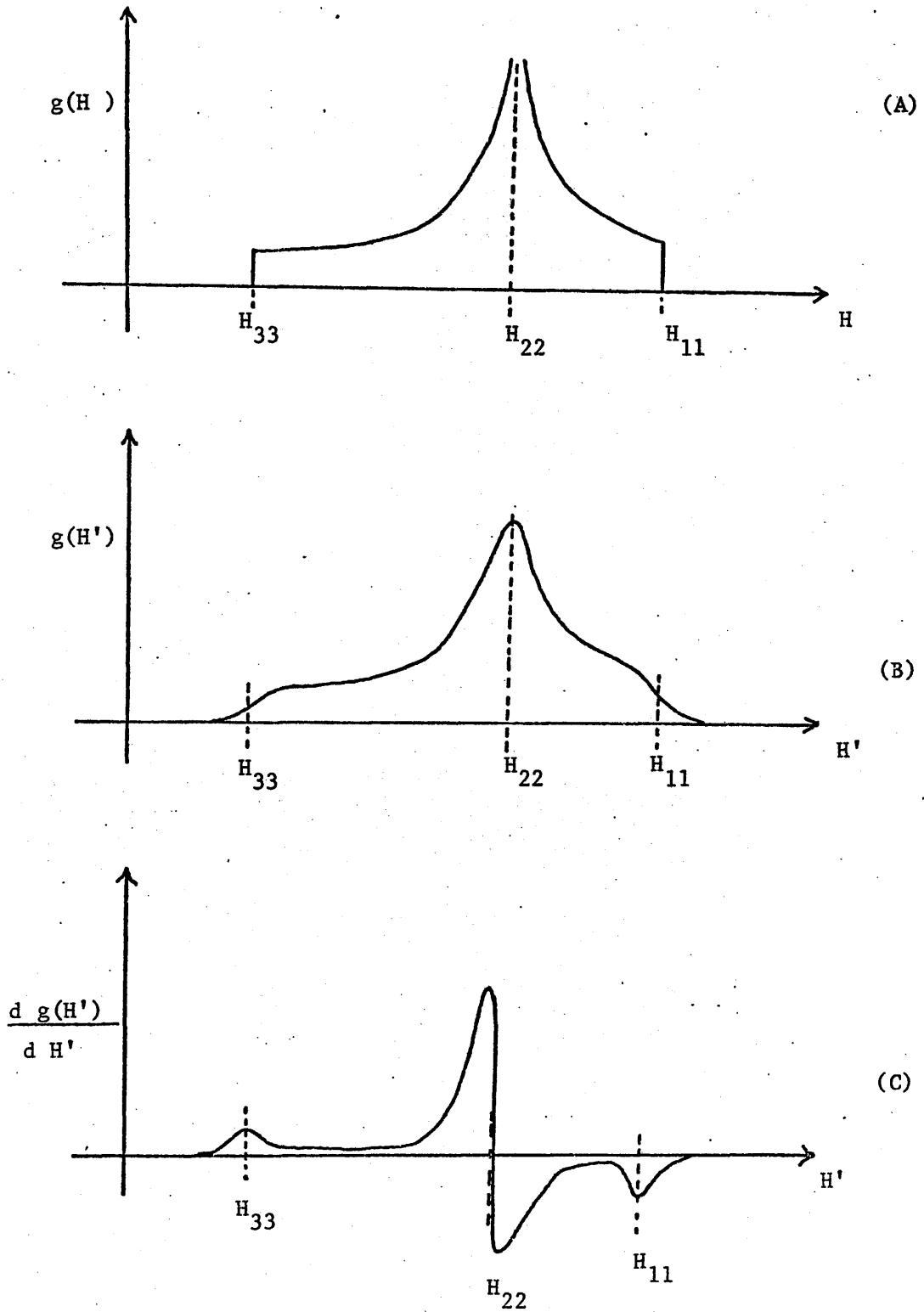


Figure 7.1 (A) The unbroadened line shape curve, (B) the broadened line shape curve, and (C) the broadened first derivative curve, for a molecule with  $S = \frac{1}{2}$ ,  $I = 0$ .

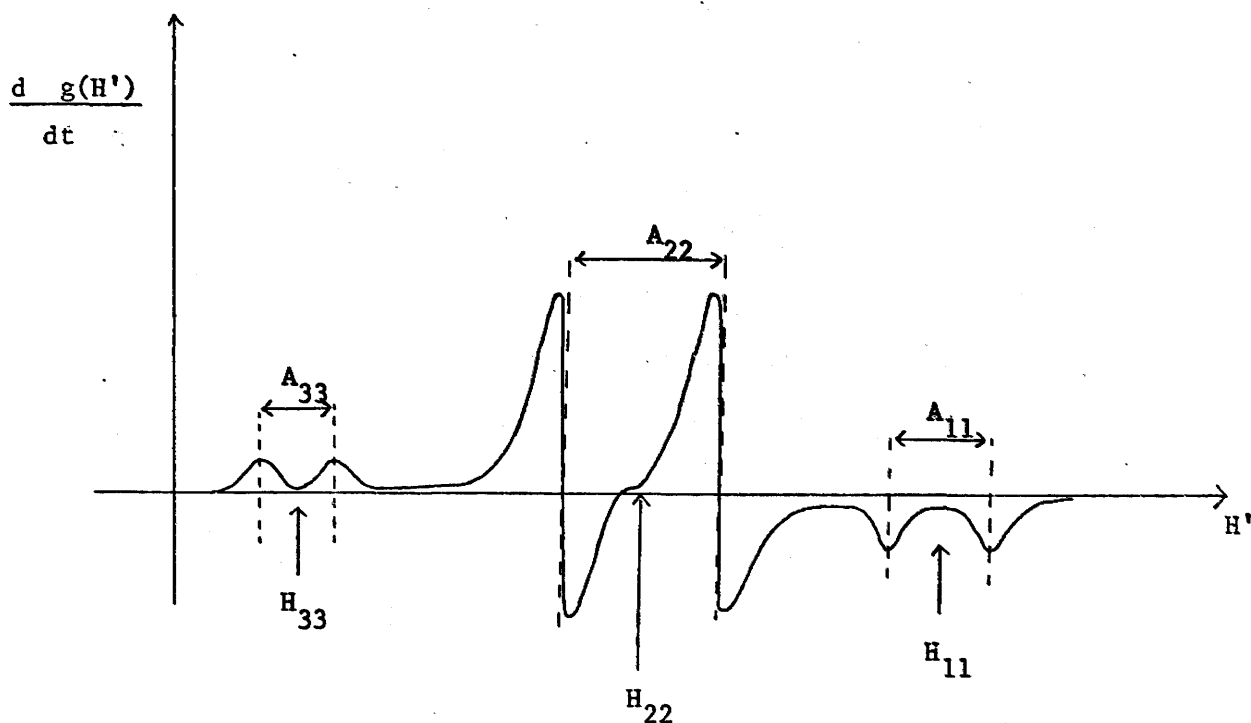


Figure 7.2 The broadened first derivative curve for a molecule with  $S = \frac{1}{2}$ ,  $I = \frac{1}{2}$ .

The above treatment was the mathematical basis of a computer program used to simulate the magnetically dilute polycrystalline e.p.r. spectra, obtained from the nitroxide radicals discussed in this thesis; and the spin Hamiltonian parameters reported for these radicals were extracted by means of this program.



REFERENCESChapters 1 - 6

1. M. Gomberg, J. Amer. Chem. Soc., 1900, 22, 757.
2. O. Piloty, B. Graf, Schwerin, Ber., 1901, 34, 1870.
3. A.R. Forrester, J.M. Hay, and R.H. Thomson, "Organic Chemistry of stable free radicals", Academic Press, London, New York, 1968, P192.
4. M. Iwamura, and I. Inamoto, Bull. Chem. Soc. Japan, 1967, 40, 703.
5. B.G. Gowenlock, and W. Lüttke, Quart. Rev., 1958, 12, 321.
6. H. Mausser, and H.H. Heitzer, Z. Naturforsch, 1965, 20b, 200.
7. A. Mackor, Th. A.J.W. Wajer, and Th. J. de Boer, Tet. Letters, 1966, 19, 2115.
8. A. Mackor, Th. A.J.W. Wajer, and Th. J. de Boer, Tet. Letters, 1967, 29, 2757.
9. R. Hoffmann, R. Gleiter, and F.B. Mallory, J. Amer. Chem. Soc., 1970, 92(2), 1460-6.
10. W. Theilacker, A. Knap, and H. Uffmann, Angew Chem., 1965, 77, 717.
11. E. Th. Strom, and A.L. Bluhm, Chem. Comm., 1966, 115.
12. Th. A.J.W. Wajer, A. Mackor, Th. J. de Boer, and J.D.W. van Voorst, Tetrahedron, 1967, 23, 4021.
13. K. Maruyama, R. Tanikaga, and R. Goto, Bull. Chem. Soc. Japan, 1964, 37, 1893.

14. P.B. Ayscough, F.P. Sargent, and R. Wilson.  
J. Chem. Soc. B, 1966, 900.
15. P.B. Ayscough, R.C. Sealy, and D.E. Woods,  
J. Phys. Chem., 1971, 75 22, 3454-61.
16. J. Mason, J. Chem. Soc., 1957, 3904.
17. E.F.J. Duynstee, Miss M.E.A.H. Mevis, H.K.  
Ostendorf, and R.J. de Kock, Rec. Trav. Chim.,  
1968, 87, 945.
18. J. Heicklen, J. Phys. Chem., 1966, 70, 618.
19. A.K. Hoffmann, A.M. Feldman, E. Gelblum, and  
W.G. Hodgson, J. Amer. Chem. Soc., 1963, 4357.
20. A. Mackor, Th. A.J.W. Wajer, and Th. J. de Boer,  
Tetrahedron, 1968, 24(2), 1623-31.
21. C. Lagercrantz, and S. Forschult, Acta. Chem.  
Scand., 1969, 23, 811.
22. C. Lagercrantz, J. Phys. Chem., 1971, 75(22)  
3466-75. (Eng).
23. I.H. Leaver, and G.G. Ramsay, Aust. J. Chem.,  
1969, 22, 1899.
24. B.G. Gowenlock, G. Kresze, and J. Pfab,  
Tetrahedron, 1973, 29, 3587-3593.
25. B.G. Gowenlock, J. Pfab, and G. Kresze,  
J. Chem. Soc., Perkins Transactions II,  
1974, 511.
26. B.G. Gowenlock, G. Kresze, and J. Pfab,  
Tetrahedron Letters, 1972, 593.
27. B.G. Gowenlock, G. Kresze, and J. Pfab,  
Justus Liebigs, Ann. Chem., 1975, 10,  
1903-13.

28. J. Pfab, Tetrahedron Letters, 1976, 12, 943.
29. J.A. Maassen, H. Hittenhaussen, and Th. J. de Boer, Tetrahedron Lett., 1971, 3213.
30. J.R. Thomas, J. Amer. Chem. Soc., 1960, 82, 5955.
31. A.K. Hoffmann, and A.T. Henderson, J. Amer. Chem. Soc., 1961, 83, 4675.
32. J.C. Baird, J.R. Thomas, J. Chem. Phys., 1961, 35, 1507.
33. G.M. Coppinger, J.D. Swalen, J. Amer. Chem. Soc., 1961, 83, 4900.
34. J.C. Baird, J. Chem. Phys., 1962, 37, 1879.
35. R. Brière, H. Lemaire, A. Rassat, Bull. Soc. Chim. France, 1965, 3273.
36. G. Chapelet-Letourneaux, H. Lemaire, and A. Rassat, Bull. Soc. Chim. France, 1965, 3283.
37. R. Brière, R. Dupeyre, H. Lemaire, C. Morat, A. Rassat, and P. Rey, Bull. Soc. Chim. France, 1965, 3290.
38. H. Lemaire, Bull. Soc. Chim. France, 1966, 559.
39. A.M. Vasserman, A.L. Buchachenko, Zhur. Strukt. Khim., 1966, 7, 673.
40. J.Q. Adams, S.W. Nicksic, and J.R. Thomas, J. Chem. Phys., 1966, 45, 654.
41. E.G. Rozantsev, Russ. Chem. Rev., 1966, 35, 658.
42. R. Brière, H. Lemaire, A. Rassat, P. Rey, A. Rousseau, Bull. Soc. Chim. France, 1967, 4479.
43. A. Calder, and A.R. Forrester, Chem. Comm., 1967, 682.

44. A. Rassat, "Molecular Spectroscopy",  
The Institute of Petroleum, London, 1968, P. 145.
45. G. Chapelet-Letourneaux, H. Lemaire, R. Lenk,  
M.A. Marechal, A. Rassat, Bull. Soc. Chim.France,  
1968, 3963.
46. R.M. Dupeyre, H. Lemaire, A. Rassat, Tet. Letters,  
1964, 1781.
47. R.H. Hoskins, J. Chem. Phys., 1956, 25, 788.
48. K.H. Schulte-Elte, and G. Ohloff, Helv. Chim.  
Acta., 1968, 51, 548.
49. K.H. Schulte-Elte, and G. Ohloff, Helv. Chim.  
Acta., 1968, 51, 494.
50. G. Gollnick, and G. Schade, Tet. Letters, 1968,  
1, 689.
51. J.M. Robertson, "Chemistry and Crystallography of  
Caryophyllene", International Review of Science,  
Chemical Crystallography, Physical Chemistry,  
Series 2, volume 11, Consultant editor A.D. Buckingham,  
Volume editor J.M. Robertson, Butterworths, London and  
Boston, 1975.
52. D.H.R. Barton, and A.S. Lindsey, J. Chem. Soc.,  
1951, 2988.
53. D.H.R. Barton, T. Bruin, and A.S. Lindsey, J. Chem.  
Soc., 1952, 2210.
54. A. Aebi, D.H.R. Barton, and A.S. Lindsey, J. Chem.  
Soc., 1953, 3124.
55. A. Aebi, D.H.R. Barton, A.W. Burgstahler, and  
A.S. Lindsey, J. Chem. Soc., 1954, 4659.

56. D.H.R. Barton, and A. Nickon, J. Chem. Soc., 1954, 4659.
57. F. Šorm, L. Dolejš, and J. Plíva, Collect. Czech. Chem. Commun., 1950, 15, 186.
58. F. Šorm, V. Jarolim, M. Streibl, and L. Dolejš, Chem. Ind. (London), 1956, 154.
59. J.M. Robertson, and G. Todd, Chem. and Ind., 1953, 437.
60. J.M. Robertson, and G. Todd, J. Chem. Soc., 1955, 1254.
61. A.W. Lutz, and E.B. Reid, J. Chem. Soc., 1954, 2265.
62. P. Doyle, I.R. Maclean, R.D.H. Murray, W. Parker, and R.A. Raphael, J. Chem. Soc., 1965, 1344.
63. W. Parker, R.A. Raphael, and J.S. Roberts, J. Chem. Soc. (C), 1969, 2634.
64. A.C. Chapman, J. Chem. Soc., 1895, 67, 54.
65. A.C. Chapman, J. Chem. Soc., 1895, 67, 780.
66. E. Deussen, J. Prakt. Chem., 1926, 114, 63.
67. D.M. Hawley, G. Ferguson, and J.M. Robertson, J. Chem. Soc. (B), 1968, 1255.
68. J.M. Bijvoet, Proc. Ned. Akad. Wetenschap., 1949, 52, 313.
69. D. M. Hawley, J.S. Roberts, G. Ferguson, and A.L. Porte, Chem. Commun., 1967, 942.
70. A.A. McConnell, S. Mitchell, A.L. Porte, J.S. Roberts, and C. Thomson, J. Chem. Soc. (B), 1970, 833.

71. S. Mitchell, J. Chem. Soc., 1928, 3258.
72. S. Mitchell, J. Chem. Soc. (A), 1930, 34, 1829.
73. O. Schreiner, and E. Kremers, Pharm. Arch., 1899, 2, 273.
74. J. Simonsen, "The Terpenes", Cambridge University Press, 1953, vol. 3, p. 41. Sec. Edit.
75. E. Deussen, Annalen, 1909, 369, 44.
76. R.M. Hoffman, J. Amer. Chem. Soc., 1934, 56, 1894.
77. O. Schreiner, "The Sesquiterpenes", Pharm. Rev. Pub. Co., Milwaukee, 1904, p. 74.
78. F. Šorm, J. Mleziva, A. Arnold, and J. Plíva, Collect. Czech. Chem. Commun., 1949, 14, 699.
79. V. Herout, M. Streibl, J. Mleziva, and F. Šorm, Collect. Czech. Chem. Commun., 1949, 14, 76.
80. F. Šorm, M. Streibl, J. Plíva, and V. Herout, Collect. Czech. Chem. Commun., 1952, 16, 639.
81. F. Šorm, M. Streibl, V. Jarolim, L. Novotný, L. Dolejš, and V. Herout, Collect. Czech. Chem. Commun., 1954, 19, 570.
82. G.R. Clemo, and J.O. Harris, J. Chem. Soc., 1951, 22.
83. G.R. Clemo, and J.O. Harris, J. Chem. Soc., 1952, 665.
84. J.O. Harris, J. Chem. Soc., 1953, 184.
85. R.W. Fawcett and J.O. Harris, J. Chem. Soc., 1954, 2673.
86. P. Clarke, and G.R. Ramage, J. Chem. Soc., 1954, 4345.

87. R.P. Hildebrand, M.D. Sutherland, and O.J. Waters,  
Chem. Ind. (London), 1959, 489.
88. S. Dev, Tetrahedron, 1960, 9, 1.
89. J.B. Hendrickson, Tetrahedron, 1959, 7, 82.
90. M.D. Sutherland, and O.J. Waters, Aust. J. Chem.,  
1961, 14, 596.
91. A.T. McPhail, R.I. Reed and G.A. Sim, Chem. Ind.  
(London), 1964, 976.
92. A.T. McPhail, and G.A. Sim, J. Chem. Soc. (B),  
1966, 112.
93. J.A. Hartsuck, and I.C. Paul, Chem. Ind. (London),  
1964, 977.
94. K.W. Gemmell, W. Parker, J.S. Roberts, J.M. Robertson,  
and G.A. Sim, J. Chem. Soc. (B), 1970, 947.
95. J.M. Robertson, and G. Todd, Chem. and Ind.,  
1953, 437.
96. J.M. Robertson, and G. Todd, J. Chem. Soc.,  
1955, 1254.
97. J.M. Greenwood, J.K. Sutherland, and A. Torre,  
Chem. Commun., 1965, 410.
98. F.H. Allen, and D. Rogers, J. Chem. Soc. (B),  
1968, 1047.
99. "Sidgwick's Organic Chemistry of Nitrogen", 3rd Edit.  
Ian T. Millar, and H.D. Springall, Claredon Press,  
Oxford, 1966. P. 341, 342.
100. M.E. Cradwick, P.D. Cradwick, and G.A. Sim, J. Chem.  
Soc. (Perkin Trans. II), 1973, 404.

101. A.R. Forester, J.M. Hay, and R.H. Thomson,  
"Organic chemistry of stable free radicals",  
Academic Press, London and New York, 1968, p. 225.
102. R.P. Hildebrand, and M.D. Sutherland, Aust. J.  
Chem., 1961, 14, 272.
103. S. Dev, J.E. Anderson, V. Cormier, N.P. Damodoran,  
and J.D. Roberts, J. Amer. Chem. Soc., 1968,  
19(5), 1246.
104. R. Bonnett, V.M. Clark, and A. Todd, J. Chem.  
Soc., 1959, 2102.
105. H. Shindo, and B. Umezawa, Chem. Pharm. Bull.,  
1962, 10, 492.
106. K. Koyano, H. Suzuki, Y. Muri, and I. Tanaka,  
Bull. Chem. Soc. Jap., 1970, 43(11), 3582.
107. A.L. Bluhm, and J. Weinstein, J. Amer. Chem.  
Soc., 1970, 92(5), 144.
108. H.H. Jaffe, and M. Orchin, "Theory and Applications  
of U.V. Spectroscopy ", J. Wiley and Sons, N.Y.,  
1962, P. 179.
109. L. Donaruma, and D. Carmody, J. Org. Chem. 1957, 22, 635.
110. E. Bamberger, Ber. Deut. Chem. Ges., 1897,  
30, 506.
111. L. Creagh and I. Trachtenberg, J. Org. Chem.,  
1969, 34, 1307.
112. E.F. Duynstee, and M.E.A.H. Mevis, Rec. Trav.  
Chim., 1971, 90, 932.
113. J. Mason, J. Chem. Soc. 1963, 4531.



114. R.N. Haszeldine, and H.H. Mattinson, J. Chem. Soc., 1957, 1741.
115. A.R. Forrester, J.M. Hay, and R.H. Thomson, "Organic Chemistry of Stable Free Radicals", Academic Press, London and New York, 1968, P. 221-222.
116. V.A. Ginsburg, L.L. Martinova and M.N. Vasilova, Zh. Obshch. Khim., 1967, 37, 1083.
117. D. H. Hammick and M.W. Lister, J. Chem. Soc., 1937, 489.
118. S. Mitchell, and J. Cameron, J. Chem. Soc., 1938, 1964.
119. J.S. Splitter, and M. Calvin, J. Org. Chem., 1958, 23, 657.
120. M.J. Kamlet, L.A. Kaplan, J. Org. Chem., 1957, 22, 576.

#### APPENDIX 7

The treatment of the theory in appendix 7 of this thesis was based on the following sources.

1. A. Carrington and A.D. McLachlan, "Introduction to Magnetic resonance", Harper and Row, New York, N.Y., 1967.
2. A. Abragam and B. Bleaney, "Electron Paramagnetic Resonance of Transition Ions", Clarendon Press, Oxford, 1970.

3. C.P. Slichter, "Principles of Magnetic Resonance",  
Harper and Row, New York. N.Y., 1967.
4. N.M. Atherton, "Electron Spin Resonance",  
Ellis Horwood, London, 1973.
5. F.K. Kneubühl, J. Chem. Phys., 1960, 33, 1974.
6. F.K. Kneubühl, Helv. Phys. Acta., 1962, 35, 259.

